Investigating Cooling Performance and Energy Utilization of Refrigerated Shipping Container Packed with Fresh Fruit using Computational Fluid Dynamics Modelling

by

Samuel Tenaw Getahun

Dissertation presented for the degree of Doctor of Philosophy in the Faculty of Engineering at the University of Stellenbosch

Supervisors:

Prof. Umezuruike Linus Opara

Prof. Chris J. Meyer

March 2017

Stellenbosch University https://scholar.sun.ac.za

Declaration

By submitting this thesis electronically, I declare that the entirety of the work contained therein is my own, original work, that I am the sole author thereof (save to the extent explicitly otherwise stated), that reproduction and publication thereof by Stellenbosch University will not infringe any third party rights and that I have not previously in its entirety or in part submitted it for obtaining any qualification.

Date: March 2017

Copyright ©2017 Stellenbosch University
All rights reserved

Stellenbosch University https://scholar.sun.ac.za

Abstract

This dissertation addresses a number of topics that arise from the use of a refrigerated shipping containers (reefers) during transportation of fresh produce. The work contributes to (i) development of a computational fluid dynamics (CFD) model of a reefer packed with fresh produce, (ii) simultaneous estimation of produce quality and energy consumption to maintain product value and minimize wastage in the cold chain system. The work presented herein is concerned primarily with three topics: the airflow distribution in reefers (empty and packed), **c**ooling operation of apple fruit, and energy use with respect to packaging designs and fan operation. Additionally, a chapter is presented that focuses on the impact of environmental conditions on the performance of fruit packed reefer during transportation.

First, a numerical and experimental investigation of airflow and temperature distribution inside two types of empty reefers (T-bar floor and flat floor) used for fresh fruit handling was conducted to establish the fundamental characteristics of transport phenomena. Then, a CFD model of a fully loaded reefer was developed using porous medium approach. Fruit stacked pallets were modelled as porous media, in which volume average transport equations were employed, to avoid complex geometries inside packed pallet and minimize computational cost. Wind tunnel tests were used to obtain the pressure drop characteristics of palletized stack of apple fruit and the viscous and inertia coefficients in Darcy-Forchheimer equation. The detailed structure of the T-bar floor of the reefer and resistance-to-airflow of wooden pallets that were previously overlooked, were incorporated in the model. Airflow, pulp temperature and, energy consumption data obtained from a fully loaded, full-scale reefer were used to validate the model. The validated model was used to further investigate airflow

Stellenbosch University https://scholar.sun.ac.za

distribution and fruit cooling performance of packaging designs used for handling apples and vertical airflow resistance or addition of bottom vent-holes.

Energy consumption of reefers packed with apple fruit during shipping was examined experimentally and numerically using the validated model. The energy consumption of reefers packed with different apple packaging designs was evaluated with respect to seven-eighth cooling time, which confirmed the influence of ventilation area on energy use and the trade-off between the energy savings that can be achieved by employing packaging designs with low and high fruit packing density. In addition, the effect of evaporator fan on energy consumption was studied by simulating fruit packed reefers operating at low, medium, high and variable evaporator fan speeds. The study demonstrated significance of optimal fan speed operation on energy use of reefers packed with stacked load of fresh produce.

Finally, the impact of climate on cooling performance and energy consumption of reefer during shipping was studied. The study showed an increase in fruit temperature and energy consumption due to heat conduction through the walls when the reefer operate in high temperature region. Overall, the CFD model developed predicted airflow, heat transfer and energy use with satisfactory accuracy. The model and research approach can be applied to a wide range of horticultural products and cold chains with slight modification.

Stellenbosch University https://scholar.sun.ac.za

Opsomming

In hierdie tesis word verskeie onderwerpe i.v.m. die gebruik van verkoelde skeepshouers gedurende die vervoer van vars produkte, behandel. Die navorsing dra by tot (i) ontwikkeling van ’n berekeningsvloeidinamika (BVD) model van ’n skeepshouer gepak met vars produkte, (ii) gelyktydige skatting van produk gehalte en energieverbruik om sodoende die waarde van die produk te behou en vermorsing van energie in die koue-ketting sisteem te verminder. Daar word veral op drie onderwerpe gefokus: die lugvloeiverspreiding in die skeepshouers (leeg en volgepak), die verkoeling van die appels, en die gebruik van energie deur die verkoelings- en waaierontwerpe. Daar is ook ’n hoofstuk wat fokus oor die impak van omgewingstoestande op die prestasie van vrugte verpak in die skeepshouer tydens vervoer.

Daar is eerstens ’n numeriese en eksperimentele ondersoek gedoen na lugvloei en temperatuurverspreiding binne die twee tipes leë skeepshouers (T-vorm vloer en plat vloer) om die fundamentele kenmerke van die vervoerverskynsels te verstaan. Toe is ’n BVD model van ’n volle gelaaide skeepshouer met die gebruik van die poreuse medium benadering ontwikkel. Vrugte-verpakte houtpalette is gemodelleer as poreuse media, waarin gemiddelde volume vervoer vegelykings gebruik is om komplekse geometrie binne-in die gepakte houtpalet te vermy en om berekende koste tot die minimum te beperk. Windtonnel toetse is gebruik om die val-in-druk kenmerke van die gepakte appels en die taaiheids- en traagheidskoëffisiente van die Darcy-Forchheimer vergelyking te verkry. Die gedetailleerde struktuur van die T-vorm vloer van die skeepshouer en die weerstand tot lugvloei van houtpalette wat voorheen misgekyk is, word ook in die model geïnkorporeer. Die lugvloei, temperatuur van die vleisgedeelte

Stellenbosch University https://scholar.sun.ac.za

van die vrugte, en die data oor energie-verbruik wat verkry is vanaf ’n volgelaaide, volskaal skeepshouer is gebruik om die model te valideer. Die gevalideerde model is gebruik om lugvloeiverspreiding en vrugte-verkoeling van verpakkingsontwerpe wat gebruik word vir die hantering van appels en die vertikale lugvloei weerstand of die byvoeging van ventilasie gaatjies verder te ondersoek.

Die energieverbruik van skeepshouers gepak met appels is gedurende verskeping eksperimenteel en numeries met die gebruik van die gevalideerde model ondersoek. Die energieverbruik van skeepshouers met verskillende tipes appelverpakking is vir sewe-agstes verkoeling evalueer, wat die invloed van ventilasie area op energieverbruik en die kompromie met energiebesparing bevestig het, en verkry word deur die gebruik van verpakkingsontwerpe met lae-en hoë vrugte verpakkingsdigtheid. Verder is die effek van ’n verdampingswaaier op die energieverbruik bestudeer deur vrugteverpakte skeepshouers met waaiers wat teen lae-, middel- en hoë spoede loop, te simuleer. Die studie het die belangrikheid van optimale waaierspoed operasie op die energieverbruik van skeepshouers volgepak met vars produkte getoon.

Laastens is die impak van klimaat op die verkoelingsdoeltreffendheid en die energieverbruik van skeepshouers tydens verskeping bestudeer. Daar is bevind dat die temperatuur van die vrugte asook die energieverbruik van die skeepshouer in streke met hoë temperature weens die geleiding van hitte deur die mure, verhoog. Oor die algemeen het die BVD model die lugvloei, hitte-oordrag en energieverbruik akkuraat voorspel. Hierdie model en navorsingsbenadering kan op ’n wye reeks tuinbou produkte en koue kettings, met klein aanpassings, toegepas word.

Stellenbosch University https://scholar.sun.ac.za

Acknowledgements

Firstly, I would like to acknowledge the support and guidance of my supervisors: Prof U.L. Opara and Prof C.J. Meyer. Their knowledge and advice was shared without reservation and was invaluable throughout the PhD experience. The supervisor-student relationship was relaxed and open; it would be difficult to find a better group to work with. Chris you are a great source of interesting conversation and academic guidance. Opara thank you for the financial support and, you have been a decisive influence in my life for the last few years and, certainly, the foremost influence in my academic career.

I would like to extend a special thanks to Dr. Alemayehu Ambaw and Dr. Mulugeta Delele who gave me constructive comments and uninterrupted support throughout my study. I would also like to acknowledge all my friends at SARChI Postharvest Technology Research Lab for their support and friendship, I am grateful for that.

Financial assistance from the National Research Foundation (NRF), South African Postharvest Innovation Programme (PHI) and Hortgro^{science} is gratefully acknowledged. I would also like to thank the following people for their technical, administrative and logistical support: Mr. Cobus Zietsman and Ms. Welma Liebenberg from Department of Mechanical Engineering, Ms. Nazneen Ebrahim at SARChI Postharvest, Mr. Henk Griessel from Tru-Cape and, Mr. Con Louw from Ceres Fruit Growers.

Finally, I wish to express my gratitude to my family, my friends and my parents for their help and encouragement. Especially my wife Yenatfanta and daughter Rediet for their endless support, understanding, and love.

Stellenbosch University https://scholar.sun.ac.za

Contents

Abstract ii
Opsomming iv
Acknowledgements vi
Contents vii
List of Figures xii
List of Tables xxiii
1. General introduction 1
1.1. Background and motivation 1
1.2. Research objective and scope 5
1.3. Thesis outline 6
2. Literature review on refrigerated shipping container modeling and energy use 7
2.1. Introduction 7
2.2. Reefers 8
2.2.1. Types of reefers 8
2.2.2. Working principle and packaging/stuffing of reefer 11
2.3. Modelling airflow and heat transfer in reefer 12
2.3.1. Resistance network modelling 13
2.3.2. Computational fluid dynamics (CFD) modelling 15
2.4. Factors that affect energy consumption in cold chain systems and quantification of energy in reefer container 29
2.4.1. Insulation 30

Stellenbosch University https://scholar.sun.ac.za

2.4.2. Infiltration 31
2.4.3. Product property 31
2.4.4. Packaging design and alignment 33
2.4.5. Fans 35
2.4.6. Defrost load 36
2.4.7. Forklift loads 37
2.5. Quantification of energy consumption: Experimental, analytical and mathematical approaches 37
2.5.1. Experimental and analytical approaches 37
2.5.2. Mathematical approaches 43
2.6. Conclusion 47
3. Experimental and numerical investigation of airflow and heat transfer inside empty reefer 50
3.1. Introduction 51
3.2. Materials and methods 53
3.2.1. Reefer 53
3.2.2. Measurements 56
3.2.3. Airflow 56
3.2.4. Temperature 56
3.3. Model formulation 57
3.3.1. Assumptions 57
3.3.2. Governing equations 58
3.3.3. Geometry, boundary and initial conditions 59
3.3.4. Mesh generation, sensitivity analysis and simulation 63
3.4. Result and discussion 64

Stellenbosch University https://scholar.sun.ac.za

3.4.1. Inlet air flow 64
3.4.2. Air velocity distribution inside the reefer 65
3.4.3. Temperature distribution inside the reefer 68
3.4.4. Airflow characteristics under high evaporator fan speed 69
3.4.5. Airflow characteristics under low evaporator fan speed 74
3.5. Conclusion 78
4. Airflow and heat transfer inside refrigerated shipping container packed with stacked load of apples: Numerical model development and validation 80
4.1. Introduction 81
4.2. Materials and methods 83
4.2.1. Fruit and packaging box 83
4.2.2. Reefer 84
4.2.3. Measurements 85
4.2.4. Pressure drop characteristics 85
4.2.5. Airflow 86
4.2.6. Temperature 87
4.2.7. Model equations 88
4.2.8. Geometry, boundary and initial conditions 92
4.2.9. Simulation procedure 93
4.3. Result and discussion 94
4.3.1. Pallet pressure drop characterization 94
4.3.2. Model validations 96
4.4. Conclusion 103
5. Numerical evaluation of airflow, heat transfer, and effects of vertical flow inside apple packed refrigerated shipping container fruit packed inside commonly used packaging designs 104

Stellenbosch University https://scholar.sun.ac.za

5.1. Introduction 105
5.2. Materials and methods 107
5.2.1. Packaging boxes 107
5.2.2. Wind-tunnel experiment 112
5.3. Mathematical modelling 112
5.3.1. Governing equations 112
5.3.2. Model parameters 113
5.3.3. Boundary and initial condition 113
5.3.4. Simulation setups 113
5.3.5. Simulations 114
5.4. Result and discussion 115
5.4.1. Characterizing the airflow resistances 115
5.4.2. Analysis of the airflow distribution inside the reefer 117
5.4.3. Analysis of the temperature distribution and the cooling rate 123
5.4.4. Influence of the vertical airflow resistance 127
5.4.5. Cooling rate and temperature profile 130
5.5. Conclusion 136
6. Numerical and experimental study of energy consumption in apple packed reefers 137
6.1. Introduction 138
6.2. Materials and methods 140
6.2.1. Reefer 140
6.2.2. Packaging boxes 141
6.2.3. Experimental study 143
6.2.4. Set-up and measurements 143
6.2.5. Model 145

Stellenbosch University https://scholar.sun.ac.za

6.2.6. Simulation 148

6.3. Result and discussion 149

6.3.1. Total and component-specific electricity usage of the refrigeration system 149

6.3.2. Ventilated packaging design 155

6.3.3. Vertical airflow resistance 157

6.3.4. Evaporator fan speed 159

6.4. Conclusion 161

7. Effects of climatic conditions on cooling characteristics and energy consumption of apple packed reefer during marine transport 163

7.1. Introduction 163

7.2. Materials and methods 165

7.2.1. Reefer and fruit load 165

7.2.2. Numerical model and assumptions 167

7.2.3. Numerical simulation 168

7.2.4. Initial and boundary conditions 168

7.3. Result and discussion 171

7.3.1. Fruit cooling characteristic and temperature profile 171

7.3.2. Heat load and environmental effect 174

7.3.3. Energy consumption 175

7.4. Conclusion 177

8. General summary and conclusions 178

8.1. Summary and conclusions 178

8.2. Future prospects 181

References 182

Stellenbosch University https://scholar.sun.ac.za

List of Figures

Figure 1-1: Comparative graph of major products from 2013 and 2012 showing gross national income from major food products in South Africa (SADAFF, 2014)..... 3

Figure 2-1: Sketch showing the basic structure of partially packed T-bar reefer container..... 10

Figure 2-2: Influence of the load on the airflow pattern. (a) Streamlines in unloaded configuration, Laser–Doppler measurements (1100 points). (b) Streamlines in unloaded configuration, RSM model. (c) Streamlines in loaded configuration, RSM model. (d) Air velocity scale (Moureh et al., 2002). 27

Figure 2-3: Respiration process 32

Figure 2-4: Effect of vent area on airflow characteristics: (a) air velocity vector, 3% vent area (left), 11% vent area (right); (b) pressure drop, 3% vent area (left), 11% vent area (right); (c) turbulence kinetic energy, 3% vent area (left), 11% vent area (right); for superficial velocity of 0.5 m s−1 (Delele et al., 2013b)..... 34

Figure 2-5: Geometry of the boxes evaluated: standard and Supervent corrugated fibreboard containers (CFC) and the Ecopack reusable plastic container (RPC) (Defraeye et al., 2014) 45

Stellenbosch University https://scholar.sun.ac.za

Figure 2-6: Energy required for maintaining the airflow through one layer of CFCs and two layers of RPC containers modelled until the seven-eighth cooling time is reached (Defraeye et al., 2014) 46

Figure 3-1: Schematic showing the Carrier Transicold bottom-air delivery T-bar reefer (Models 69NT-40-541-306, 314 & 328) (a), closer view of the T-bar floor structure (b) and the cross sectional view showing the dimensions of the T-bar (c)..... 54

Figure 3-2: Schematics showing the position of the velocity and temperature sensors inside the T-bar reefer (a) and the candlestick sensors (b). A total of ninety-nine measurement points were used..... 57

Figure 3-3: Schematics of the model geometry corresponding to a reefer at high evaporator performance. The model explicitly incorporated the detailed structure of the reefer floor..... 60

Figure 3-4: Velocity decay of the air jet from the cooling unit into the T-bar floor container at high evaporator performance. Numerical and experimental results 65

Figure 3-5: The experimental (symbols) and simulated (solid curves) magnitudes of air velocities as a function of vertical and axial locations inside the T-bar floor reefer. The locations are 1m from the inlet face (a), 3 m (b), 6 m (c), 8 m (d), 9 m (e) and 11 m (f) 67

Figure 3-6: Air velocity magnitude on a line one meter above the floor at 0.5 of the width (a) and two third of the width (b)..... 68

Figure 3-7: The measured and simulated characteristics of the air cooling inside a T-bar floor reefer under high evaporator performance operation (at

Stellenbosch University https://scholar.sun.ac.za

air exchange rate of ≈ 80 h^{-1}) were compared. Temperature was measured were averaged over the volume of the reefer..... 69

Figure 3-8: Simulated airflow pattern on a section plane bisecting the reefers. Simulation results corresponds to, a) T-bar floor model and, b) Flat floor model reefers operating at high evaporator performance (c) airflow pattern for empty slot ventilated enclosure (Moureh et al, 2002) at Inlet velocity=11.5 m s^{-1} (comparable to high evaporator performance) 70

Figure 3-9: Contours of magnitudes of vertical air velocity on section plan bisecting the T-bar floor reefer (a) and flat floor reefer (b). Simulation corresponds to the reefers working at high evaporator performance with an air flow rate of 5400 $m^3 h^{-1}$ (air exchange rate of ≈ 80 h^{-1})..... 72

Figure 3-10: Jet flow characteristics of T-bar floor and flat floor models at high evaporator performance numerical study (a) and, static pressure distribution in the domain (b) 73

Figure 3-11: Simulated airflow pattern on a section plane bisecting the reefers. Simulation results corresponds to, (a) T-bar floor model, (b) Flat floor model reefers operating at low evaporator performance. 75

Figure 3-12: Contours of magnitudes of vertical air velocity on section plan bisecting the T-bar floor reefer (a) and flat floor reefer (b). Simulation corresponds to the reefers working at low evaporator performance with an air flow rate of 2500 $m^3 h^{-1}$ (air exchange rate of ≈ 36 h^{-1})..... 76

Stellenbosch University https://scholar.sun.ac.za

Figure 3-13: Jet flow characteristics of T-bar floor and flat floor models (a) and, Static pressure distribution (1 m above the floor) along the length of the reefer (b) at low evaporator performance numerical study 77

Figure 4-1: Components of the palletized Econo-D box analysed in this study. (a) a bag of apple fruit each containing approximately 1.5 kg top red apples, (b) corrugated fibre carton (Econo-D) to contain eight bags of fruit, (c) pallet formed from 8 layers of boxes with 8 boxes per layer and, (d) standard wooden pallet on which stacking was formed. 84

Figure 4-2: Schematic showing partially packed bottom-air delivery T-bar reefer (a) and, closer view of the T-bar floor structure 85

Figure 4-3: Schematics showing setup of the wind tunnel experiment to measure the vertical direction (y-direction) pressure drop characteristic of palletized fruit stack. Measurements were taken across half a pallet: (a) top half of a pallet (without wooden pallet) and (b) bottom half of a pallet with wooden pallet (WWP). (c) Isometric view of the bottoms half of a pallet. 86

Figure 4-4: Schematics of the position of pulp temperature sensors (red circle) and air velocity sensors (blue circle). (a) Showing the positions of the temperature and air velocity sensors as seen from top, (b) position of temperature and air velocity sensors as seen from side of a pallet, (c) position of airflow sensors in the overhead space and, (d) a snapshot (door side) of a fully packed reefer wired with the sensors. 88

Figure 4-5: Pallet arrangement and porous media zonal representation of packed pallets inside a fully loaded reefer. Top view (a), dimensions of the

Stellenbosch University https://scholar.sun.ac.za

stack shown on isomeric view of the porous pallet zones and, front view of the porous zones from the door side of the reefer (c). 93

Figure 4-6: Experimental pressure drop versus superficial air velocity plot for air flow horizontally and vertically through half a pallet (see Figure 4.3). The vertical airflow for the bottom half included the flow resistance of the wooden pallet. 95

Figure 4-7 Measured and simulated air velocities in the free region between the two rows inside reefer (a) and in the region above the pallet (in the region between stack and the reefer ceiling) (b). 97

Figure 4-8 Simulated profile of airflow inside a fully loaded reefer. Colour contours show magnitude of air velocity and arrows (vector) show the local airflow direction on vertical plane bisecting pallets in row 1 (a), the air gap between the two rows (b) and pallets in row 2 (c). 98

Figure 4-9 Measured (dashed line) and simulated (solid lines) evolution of pulp temperatures (pallet averages) inside a fully loaded reefer. Pallets(p) in row one (R1) p1 to p4 (a), p5 to 9(b) and (c) p9 to p11and, Pallets(p) in row two (R2) p1 to p3 (d) p4 to p6(e) and p7 to p9(f). The reefer was loaded with 15 tons of fruit (twenty pallets each holding 768 kg apple fruit). The reefer was operating at cooling flow rate of 5400 m^3 h^{-1} 100

Figure 4-10: Average cooling rate of fruit in row 1 (blue) and row 2 (red). The dashed line curves show the measured (experimental) fruit temperature evolution and the solid line curves show the numerical predictions. The horizontal lines show half cooling times (dashed lines) and 7/8th cooling time (solid line) 101

Stellenbosch University https://scholar.sun.ac.za

Figure 4-11 Simulated profile of produce temperature at 24 hour on vertical plane (YZ-plane) bisecting row 1 (a) and row 2 (2) inside reefer. 102

Figure 4-12: Experimental (red) and numerical (blue) average pallet temperatures at 24 hours of cooling. (a) Pallets in row 1 and, (b) pallets in row 2. Vertical lines in Figure 4.12 show standard deviations calculated based on temperatures at bottom, middle and top of a pallet..... 102

Figure 5-1: Schematics of the three package designs examined in this study. Isometric view of Econo D (a), double layer display carton box (Mk9) (b) and Telescopic packaging box (Mk6) (c). The right column depicts the bottom side of the Econo D (d), Mk9 (e) and Mk6 (f) boxes. Sizes shown correspond to the external dimensions. 109

Figure 5-2: Stacking of the packaging boxes in to a pallet. The top row shows the palletized Econo-D (a) Mk9 (b) and Mk6 (c) packaging designs. The bottom row shows the corresponding box arrangement of an individual layer forming the pallet. Notice that pallet of the Mk6 packaging box is stacked in a staggered manner in the top half to ensure stability 111

Figure 5-3: Experimentally obtained pressure loss vs. flow rate profiles of palletized Mk6 and Mk9 boxes. Pressure loss profiles for horizontal airflow perpendicular to the width (Mk6-L and Mk9-L) and, perpendicular to the length (Mk6-W and Mk9-W). The profiles of the pressure loss along the vertical direction were obtained for the bottom half of the pallet (Mk6-V-B and Mk9-V-B) and for the top half of the pallet (Mk6-V-T and Mk9-V-T). The bottom half incorporated the airflow resistance due the wooden pallets. 117

Stellenbosch University https://scholar.sun.ac.za

Figure 5-4: Vertical airflow velocity profiles in the pallets configured in row 1 and row 2 inside a reefer with the Mk 6 (a)(b), Mk9 (c)(d) and, Econo-D (e)(f). The simulations correspond to a reefer working at an inlet airflow and temperature of 5400m^3 h^{-1} and -1℃. 119

Figure 5-5: Average horizontal airflow magnitudes through row1 and row2 inside a reefer along the Z-axis. Pallets in row 1 and row 2 were configured with horizontal airflow (Z-direction) across the width and length of the pallets, respectively. The simulations correspond to a reefer working at an inlet airflow and temperature of 5400m^3 h^{-1} and -1℃. 121

Figure 5-6: Temperature contour in time on a horizontal (ZX) plan bisecting the reefer with the Mk6 (a), Mk9 (b) and Econo-D (c) packaging boxes..... 124

Figure 5-7: Temperature contour at 72 h on vertical (YZ) planes bisecting row 1(left) and row 2 (right) of the reefer with the Mk6 (a), Mk9 (b) and Econo-D (c) packaging boxes. 126

Figure 5-8: The produce temperature history (average) in row 1 (broken lines) and row 2 (solid lines) inside reefer with Mk6 (Blue), Mk9 (green) and Econo-D (red) boxes. The half cooling time and the 7/8th cooling time are marked with horizontal broken and solid lines, respectively.... 127

Figure 5-9: Average vertical airflow distribution as vertical airflow resistance in the pallets vary from the base model (100%) (Apple fruit packed in Econo-D) packaging box. Pallet row 1 (a) and, pallets row 2 (b) 128

Figure 5-10: Average horizontal airflow magnitude in Ec-25, Ec-50, Ec-75 models. The horizontal airflow magnitude was calculated from averaged magnitudes at bottom, middle and top layers of the pallets

Stellenbosch University https://scholar.sun.ac.za

in the respective row in the three models. These were compared with that of the result found for the base model in pallet row 1 (a) and pallet row 2 (b)..... 130

Figure 5-11: Average cooling rate of the produce in pallet row 1(broken curves) and pallet row 2 (full curves) of the reefers palletised with the normal Econo-D box (black curve), Econo-D with vertical airflow resistance reduced by 25% (blue curve-Ec-25), 50% (green curve-Ec-50) and 75% (red curve-Ec-75). The broken and full horizontal lines mark the half cooling time and the 7/8th cooling time, respectively..... 132

Figure 5-12: Simulated results showing the effect of the vertical airflow resistance on the cooling rate inside reefer. The spatial and temporal temperature evolution of apple fruit in a packed reefer as the vertical airflow resistance was set 25 % (Ec-25), 50% (Ec-50) and 75 % (Ec-75) of the base model (No bottom vent packaging design-Econo-D box). Representative pallets (p) from row 1(R1) a) p2 & p5 b) p8 & p11 and, from row 2(R2) c) p1& p4 and d) p6& p8 134

Figure 5-13: Simulated temperature contours on vertical plans (Z-Y planes) bisecting pallets in row 1(left) and row 2 (right). The contours correspond the instantaneous temperature distribution inside the reefer after cooling the load for 72 hours from initial temperature of 9.5 ℃ with cooling air supply at -1 ℃ (5400 $m^3 h^{-1}$). (a) Base model (b) Ec-25 (c)Ec-50 and, Ec-75 (d) 135

Figure 6-1: Schematics of the three package designs examined in this study. Isometric view of Econo D (a), double layer display carton box (Mk9) (b) and Telescopic packaging box (Mk6) (c). The right column depicts

Stellenbosch University https://scholar.sun.ac.za

the bottom side of the Econo D (d), Mk9 (e) and Mk6 (f) boxes. Sizes shown correspond to the external dimensions. 142

Figure 6-2: Simplified diagram of refrigeration system of a reefer and measurement points for power use of (a) total reefer, (b) compressor, (d) condenser motor and (d)evaporator motors 144

Figure 6-3: Configuration of fan motor and evaporator coils (ASHRAE, 2010). 146

Figure 6-4: Representation of airflow path inside a fully packed reefer (a) and, components of the refrigeration unit of a reefer (b)..... 147

Figure 6-5: Measured power consumption of reefer operating in "Normal" control mode (a) and, QUEST control mode (b) during the 72 h cooling period. Reefer loaded with 15.36 tonnes apple fruit (in Econo-D box) at 9.5 °C initial produce temperature. Cooling air at 5400 m^3 h^{-1} and -1 °C was supplied. 150

Figure 6-6: Cumulative heat load of the reefer packed with apple fruit in Econo-D packaging boxes (a) and, heat load due evaporator fan, respiration and, conduction from the environment (b). 153

Figure 6-7: Measured and predicted energy consumption of the reefer packed with apple fruit in Econo-D box design during the 72 hours cooling operation. 154

Figure 6-8: Energy consumption of reefers loaded with apple fruits inside Econo-D packaging box, Mk6 and, Mk9 packaging boxes in a reefer operating in "Normal" control mode. (a) Transient power use by each reefer, (b) cumulative energy consumption of each reefer and, (c) energy consumption per tonne of apple fruit. Solid lines show the

Stellenbosch University https://scholar.sun.ac.za

power consumption of the reefers and, broken lines show the SECT of fruit in each reefer..... 156

Figure 6-9: Reefers operating at high, medium and low fan speeds. (a) Refrigeration heat load and, (b) average temperature evolution during high, medium, low and variable speed fan. Variable speed used high speed - 8100 $m^3 h^{-1}$ (0-40 hours), medium speed - 5400 $m^3 h^{-1}$ (40-55 hours) and, low speed - 2700 $m^3 h^{-1}$ (55-72 hours)..... 160

Figure 6-10: Energy consumption associated with evaporator fan of the reefers operating at high, medium, low and variable fan speeds. High speed - 8100 $m^3 h^{-1}$ (0-40 hours), medium speed - 5400 $m^3 h^{-1}$ (40-55 hours) and, low speed - 2700 $m^3 h^{-1}$ (55-72 hours)..... 161

Figure 7-1: (a) Reefer container ship on route, (b) apple export route from South Africa to Europe and, (c) annual average wind speed map (https://www.windfinder.com/weather-maps/forecast/#3/5.79/-18.54)..... 166

Figure 7-2: Effects of climatic conditions on fruit temperature inside a reefer. (a) Reefers in different climatic conditions (20, 40, 0 ℃ and 7.2 m s^{-1} wind speed) and adiabatic condition. (b) Fruit temperature evolution in a reefer during nine days of marine transportation through successive climatic conditions (20, 40 and 0 ℃ and 7.2 m s^{-1} wind speed)..... 172

Figure 7-3: Effects of heat conduction through the walls of the reefer on fruit load adjacent the side walls of the reefer. Temperature profile on a plane bisecting the reefer horizontally at the middle (5.8 m from cooling unit) of the reefer after 3 days in (a) 20, (b) 40 and, (c) 0℃ ambient

Stellenbosch University https://scholar.sun.ac.za

temperature zones. (d) Spatial temperature variation along the length of the reefer and airflow streamlines coloured by temperature (coloured by temperature from -1 to 0 ℃). 173

Figure 7-4: Heat load due to to respiration (a) and conduction from the environemt (b) in the reeefers that were exposed to three ambient temperatuers and one under adiabatic condition. 175

Figure 7-5: Cumulative energy consumption of fruit packed reefer under three climatic conditions with 20 (blue), 40 (red) and 0 ℃ (green) temperatures and 7.2 m s^{-1} wind speed. Fruit load initial temperature was 0.75 0 ℃. 176

Figure 7-6: Reefer cumulative energy consumption of a reefer passing through climatic conditions of 20 (blue), 40 (red) and 0 ℃ (green) temperatures and 7.2 m s^{-1} wind speed. Initially, the fruit load was at 0.75 ℃ entering 20 ℃ ambient temperature region 177

Stellenbosch University https://scholar.sun.ac.za

List of Tables

Table 2-1 Best estimate of the top ten food refrigeration processes ranked in terms of their potential for total energy saving (James & James, 2011) 39

Table 2-2 Shows refrigeration capacities and power consumption for Thermo-King refrigeration units with Scroll w/R404A compressor model (Wild et al., 1999) 41

Table 2-3 Evaluated reefers energy consumption rates per twenty-foot equivalent unit (TEU), their consumption proportions and differences, relative to 2.7 kW per TEU (Fitzgerald et al., 2011) 43

Table 3-1: Reefer wall materials and corresponding thicknesses (ASHRAE, 2010) 55

Table 3-2: Boundary conditions 61

Table 3-3: Calculated overall HTC for heat flow through the container wall based on the material property (Table 3.1) and ambient condition (291.15 K) 63

Table 4-1 Pressure drop characteristics of a pallet. Values were calculated from curve fitting of the pressure drop vs. velocity data to the Darcy-Fochhaimer equation which describes the permeability and resistance of the pallet. 91

Table 4-2 Summary of HCT and SECT of each pallet inside the reefer 99

Stellenbosch University https://scholar.sun.ac.za

Table 5-1 Ventilation area ratio (VAR), loading characteristics of the Econo-D, Mk9 and Mk6 boxes 110

Table 5-2 Palletization and stacking of the three packaging boxes inside a reefer .. 111

Table 5-3 Experimentally determined coefficients of the Darcy-Forchheimer equation of the three different pallets and for the modified Econo-D boxes. 115

Table 5-4 Average HCT and SECT of the different packaging designs in the two pallet rows 127

Table 6-1 Nominal power of refrigeration unit motors 141

Table 6-2: Daily total energy consumption of reefers operating in “Normal” and QUEST control mode. For the reefer operating in “Normal” mode energy use of refrigeration sub units was measured 151

Table 6-3 Energy required to pull down fruit temperatures to the SECT temperature using different apple packaging designs (apple fruit load of 15.36 tonnes per each reefer)..... 158

Table 7-1 Calculated overall heat transfer coefficients of the walls of the reefer at three ambient temperatures 170

Stellenbosch University https://scholar.sun.ac.za

Chapter 1

1. General introduction

1.1. Background and motivation

The primary agricultural sector of South Africa contributes 3 % to the country's gross domestic product (GDP), and the entire chain of agricultural sector contributes about 12 % (South African Department of Agriculture, Forestry and Fishery (SADAFF), 2014). Perishable produce of the country is an important section of the agricultural sector and brings foreign exchange from its export. Figure 1.1 shows recent gross income from different agricultural products (2012 to 2013). The maximum income increment was exhibited by fresh fruits (19.4 %). Some of the perishable produce is consumed locally. It is part of daily nutrition in the country. The local consumption of fruits has increased by 11.4 % from 2012 to 2013; however, the price of fruit has increased by 8.9 % (SADAFF, 2014). There could be a number of factors for price increase, such as production cost, transportation cost, and rising energy price.

Fresh horticultural and agricultural products are living organisms that carry on many biological processes essential to maintain life. Energy that is needed for these life processes comes from the accumulated food reserves through a process called respiration. The final result of respiration activity is product deterioration and senescence, and hence achieving as low a respiration rate as possible is desirable to prolong the shelf life of biological materials (Brosnan, 2001). For this the product needs to be cooled to low temperature, however, during extensive transport period packed fruits are subject to heat and mass transfer with the environment. In addition, uniform cooling in bulk within shipping container is difficult to attain, owing to existence of an uneven distribution of the airflow which results in considerable temperature and humidity differences within the product. Non-uniform humidity

Stellenbosch University https://scholar.sun.ac.za

might lead to condensation of moisture where relative humidity reaches saturation or excessive dehydration where the relative humidity remains below 80 % (Goswami, 2009) and the variability of the cooling rate and resultant spatial variation in temperature of the product causes the product quality to deteriorate through either increased respiration at higher temperature or by chilling injury at lower temperature.

Refrigerated shipping containers are used in South Africa to transport fresh fruit from cold stores to abroad (global) and to different parts of the country for domestic use. Globally, Europe is the main destination of South African fruit which takes around 61% of the fruit export (Ngcobo et al., 2012). The duration for transport of fruit from South African cold store to a cold store in Europe ranges from 20 to 30 days (Fawole et al., 2013). Refrigerated shipping container is used to transport perishable produce if the duration of transportation between the cold store and the destination is more than 2 hours (Perishable Product Export Control Board; PPECB 2013:4-22).

Cold chain systems are the most important postharvest technologies that are applied to maintain the quality during handling, storage and transportation of horticultural produces. Globally, refrigerated shipping containers are an important part of the cold chain system which forms 31% of the world's food handling (Jolly et al., 2000). Refrigerated shipping containers are dominating the global fresh produce transport to distant markets. Their global usage has reached 60% by 2013 (Dodd, 2012). Locally (South Africa) they are the most common mode of transport for fresh fruit handling. The evolution of refrigerated containers' use for fresh fruit transport took a significant leap from 30% in 2000 to 90% in 2011 compared to refrigerated vessels as per the PPECB.

Stellenbosch University https://scholar.sun.ac.za

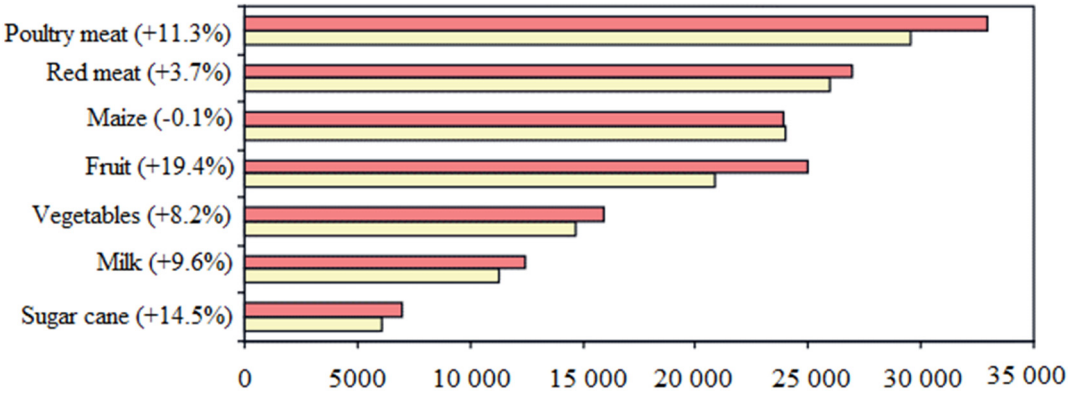

Figure 1-1: Comparative graph of major products from 2013 and 2012 showing gross national income from major food products in South Africa (SADAFF, 2014)

The world's energy demand and consumption are increasing every year. Primary energy sources (fossil fuel) are depleting and their environmental impact is raising anxiety around the world (Saidura et al., 2010). The energy demand in South Africa is increasing by around 5 % (Zhongjie, 2008). Even though different ways to address the energy shortage exist, energy saving is always an important measure. A cold chain is involved in different sectors, such as commercial, industrial, transportation and agriculture. Energy consumption in regard to refrigeration is the largest portion of total energy consumption during pre-processing, refrigerated storage, transportation, retail, and end-user's consumption of the agriculture/food products. The figure often cited being about 50% of total energy consumption in the food industry is from refrigeration related facilities, yet approximately 81 % of annual energy consumption goes to product transportation, only 19% is used for direct refrigeration of produce in refrigerated container, in case study of New Zealand import export (Fitzgerald et al., 2011). Figures published on cold store energy consumption in New Zealand by (Werner and Famarazi, 2006) shows an energy consumption between 370-560 kWh per m^2 annually and 8-120 kWh per m^3 annually for cold stores of sizes between 900 ~ 2500m^2. In general, energy is an important input in postharvest handling of perishable produce.

Stellenbosch University https://scholar.sun.ac.za

In order minimize unnecessary energy waste in refrigerated shipping container system, it needs to be designed to be energy efficient and provide high cooling capacity to ensure rapid pull down to carriage temperature and to maintain produce quality. Improper operation and design cause a significant waste of energy. This avoidable waste of energy results in unnecessary economic loss. Energy use in a shipping container is affected by the amount of heat the refrigeration equipment must remove, packaging designs, and the efficiency of the equipment. The main sources of heat in a shipping container, which are similar to cold chain facility for long-term storage, are transmission through walls, evaporator coil fans, air leakage, and respiration of the packed produce (Thomson, 2001).

Study and optimization of shipping container system requires extensive experimentation which may need considerable amount of capital. However, numerical modelling offers an economic alternative to physical experiments, although it is imperative that the reliability of the model be established through validation against experimental data. (Zou et al., 2006a,b) has developed a computational fluid dynamics (CFD) modelling system of the airflow patterns and heat transfer inside ventilated packages. If information on packaging system, cooling conditions, produce properties is used as model input data, the results obtained can predict the effects of these factors on the airflow patterns and cooling rate.

CFD is a simulation tool for the modelling of fluid flow problems based on the solution of the governing flow equations. Early applications of CFD were devoted to crucial industrial problems in aeronautic or nuclear applications. In 1970-1980's, the power of digital computers became sufficient to perform calculations within acceptable time frames and CFD was applied to a wider range of problems. CFD is becoming an extensively used design tool, thanks to the ever-growing power of affordable personal computers (Smale, et al, 2006). CFD can be successfully applied to numerous problems, not only for modelling the fluid flow but also for modelling transfer of heat, mass (transpiration or dissolution), phase change (freezing, melting or boiling), chemical reactions (combustion or rusting),

Stellenbosch University https://scholar.sun.ac.za

mechanical movements (impellers, pistons, fans or rudders) and stress or deformation of related structures (Xia, 2002).

Nowadays, cooling operation management in many refrigerated shipping containers and cold stores is difficult to consider as rational, which is always a practical problem for reducing the cost of energy and improving the homogeneity of temperature though out the packed produce. CFD knowledge is a useful tool to have a profound understanding of the process with great benefits with small cost. Validated mathematical model that take into account the physical, chemical and biological processes is viable alternative. Validated mathematical models can answer 'what if' questions in a relatively cheaper way. CFD modelling technique is the primary method of choice for modelling transport processes during postharvest handling of horticultural products.

1.2. Research objective and scope

The main aim of this research is to develop and validate a CFD model applicable to a refrigerated shipping container of fresh fruit that is capable of predicting the total energy consumption of the system and then apply the validated model for improving the operation and thermal design of shipping containers.

Specific objectives

- Development of CFD model of shipping container, taking into account produce properties, operational parameters and container and package design parameters

- Conducting model validation experiments on power consumption of commercial shipping container

- Studying the effect of different operational and design parameters on energy consumption of shipping containers

Stellenbosch University https://scholar.sun.ac.za

1.3. Thesis outline

Chapter 2 provides background knowledge necessary to support the remainder of the work presented in this literature study.

Chapter 3 Numerical model of an empty refrigerated container development and model validation using experimental work to predict airflow and heat transfer process in the domain. The validated model was also used to study two evaporator performance levels/container air recirculation rates and to evaluate the effect of the T-bar floor design on the overall airflow characteristics.

Chapter 4 addresses the model development and validation of a zonal porous medium computational fluid dynamic (CFD) model of airflow and produce cooling inside a fully loaded refrigerated shipping container (reefer). Wind tunnel test was used to obtain the pressure drop characteristics of palletized stack of apple fruit to determine coefficients in Darcy-Forchheimer equation for porous media calculation.

Chapter 5 provides numerical evaluation of the effects of apple packaging box designs and pallet stacking configuration on the airflow distribution and fruit cooling uniformity in a produce packed reefer using a validated model.

Experimental and numerical study of energy consumption in reefer loaded with stacks of apple fruit is discussed in Chapter 6. The effect of ventilated packaging designs on energy consumption inside a reefer are evaluated. In addition, the effect of evaporator fan on energy consumption was studied by simulating fruit packed reefers operating at low, medium, high and variable evaporator fan speeds were investigated.

Chapter 7 addresses the study on the impact of environmental conditions on fruit packed reefers as they are shipped and has to pass thorough different ambient temperature regions over long and extended period. Finally, chapter 8 offers concluding remarks and future prospects.

Stellenbosch University https://scholar.sun.ac.za

Chapter 2

2. Literature review on refrigerated shipping container modeling and energy use

2.1. Introduction

Refrigerated shipping containers are one of the four segments of the cold chain; cooling and storage; refrigerated transport; distribution centre and refrigerated display in super markets. The term reefer has become an established term to refer refrigerated shipping containers and we will use this term in rest of this study. Heat transfer during produce cooling in a reefer principally takes place by the convective heat transfer mechanism. Cooling air from the evaporator fans is supplied into the container where it will be forced to flow in from the bottom (for bottom delivery system reefers) then between the pallets, through packed produce, and between the pallet and the ceiling, respectively before it reaches the outlet. Energy consumption in reefers depends on its status, operational conditions and design parameters. In order to understand and quantify the energy consumption, it is imperative to understand the governing phenomena, airflow and heat transfer.

Researchers have been developing mathematical models to predict airflow and heat transfer modelling for the last 30 years (Smale et al., 2006). Previous reviews on mathematical modelling approaches in postharvest applications discussed the growth in use and acceptance of CFD for modelling transport phenomena in cold chain systems (Ambaw et al., 2013; Dehghannya et al., 2010; Defraeye et al., 2015c; James et al., 2006; Norton and Sun 2006; Redding et al., 2016; Smale et al., 2006; Wang and Sun 2003; Xia et al., 2002; Zhao et al., 2016). However, it is still difficult to develop an explicit model of huge domains, such as a packed reefer or packed cold store, therefore smart approximations are still

Stellenbosch University https://scholar.sun.ac.za

necessary. Mathematical modelling of airflow and heat transfer in refrigerated transport systems (reefers and trailers) has been conducted by several researchers (Defraeye et al., 2015a; Menia et al., 2002; Moureh et al., 2002; Moureh and Flick, 2004; Moureh and Flick, 2005; Moureh et al., 2009a, b; Rodríguez-Bermejo et al., 2007; Smale, 2004) to improve the airflow pattern in order to achieve an efficient cooling operation.

The aim of this chapter is to review airflow and heat transfer modelling approaches, such as Resistance network and Computational Fluid Dynamics (CFD) that are applicable for reefer modelling. Detail review on porous media modelling approach in postharvest handling of packed produce and previous studies conducts. In addition, reefer energy consumption quantification and factors that affect energy consumption in will be discussed reviewed based on previously conducted studies (experimental, analytical and numerical methods).

2.2. Reefers

Refrigerated transport is an important part of the cold chain system, particularly in South Africa where integration of supply chain needs improvement (Dodd, 2012). Reefers used for temperature controlled transport are basically similar in construction however they have differences in the type of insulation, structure for conditioned air circulation, and refrigeration system.

2.2.1. Types of reefers

Reefer containers are usually 2.44 m wide (8ft), 2.44 to 2.89 m high (8 to 9.5 ft) and 6 or 12.19 m long (20 or 40 ft) (ASHRAE, 2009). A reefer has hinged doors in one end for cargo loading and other access to the interior. They usually have polyurethane insulation at 7.62 cm thickness (3 in.) in walls and floors, and 10.16 cm (4 in.) in ceilings. As shown in Figure 2.1, containers have standardized corner fittings to secure them to vessels, railway cars, and highway vehicles. There are four container floor types (T-bar, Castellated Plate, Perforated and Flat floor

Stellenbosch University https://scholar.sun.ac.za

with pallet base for airflow) from which to choose from (Smale, 2004). Each of the floor designs provide different advantages and have different limitations.

T-Bar floor: - The grid running along the length of the reefer commonly known as a T-bar floor, taking its name from the T-shaped cross-section of aluminium extrusions that forms the floor. Difficult to walk on, to load pallets using machines with wheels (this can be solved by using plywood on the floor for wheels which can be removed after loading), can be damaged by forklift and difficult to keep clean are the limitations of T-bar floor. The floors have lots of different advantages regarding the refrigeration process. Its floor design helps air flow by allowing the cold air to travel around the container from the refrigeration unit underneath the pallets by channelling the flow. In addition, pallets form an additional space between container floor and cargo; also form an air flow channel. This provides the cooling process with a system to increase efficiency in terms of effectiveness. In a flat floor container pallet bases create space that facilitate airflow (Smale, 2004).

Perforated floor: - It gives less obstruction to airflow and better distribution in containers than castellated floors, but they are difficult to clean unless they are removable (Smale, 2004).

Castellated floors: - This floor type is a floor with a rectangular grooving running from inlet side to the door side. It has holes for vertical airflow distribution. It is known for its strength and to its easy to clean structure. The airflow is obstructed due to reduction in free area (Smale, 2004).

In marine transport there are three types of reefer based on their configuration. They are conventional reefer vessels, porthole containers and integral refrigerated. Conventional reefer vessels carry their cargo in large refrigerated holds. Usually porthole container is not referred as refrigerated container because it has no integral refrigeration unit. The lack of a refrigeration unit allows such containers to have a larger internal volume. It has sealable holes

Stellenbosch University https://scholar.sun.ac.za

that are located on the front and are used for refrigerated air circulation. The container is supplied with cold air via the central cooling plant. While on shore these containers need to be attached to a clip-on refrigeration system to maintain the cold environment of the inside. The use of this type of containers has decreased because the lack of clip-on refrigeration units at ports and flexibility of integral container has improved. Integral refrigerated container has a built into refrigeration unit attached to its end and it only need a power supply. These containers are the ones that are widely used in shipping industry today.

Depending on their design, integrated containers get the refrigerated air supply either at the floor (bottom air delivery) level or at the ceiling (top air delivery) level. The greater percentage of integral containers currently in service has bottom air delivery configuration. The air flows through grill on the floor and returns back to the refrigeration unit, after passing vertically through packed produce, via the space between the top of the cargo and the ceiling of the container (this headspace is called false-channel). The floor of integral containers is usually an aluminium T-bar floor running from the inlet along the length of the container.

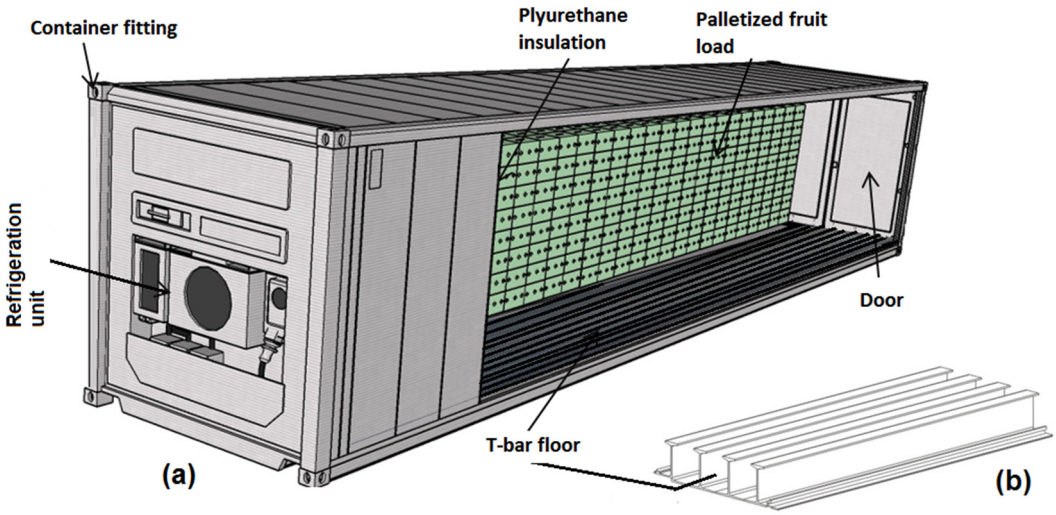

Figure 2-1: Sketch showing the basic structure of partially packed T-bar reefer container

Stellenbosch University https://scholar.sun.ac.za

2.2.2. Working principle and packaging/stuffing of reefer

Cold air is constantly circulated through the cargo space to dissipate heat. Cold air is blown at relatively high velocities through a small inlet section located adjacent to or near the ceiling the refrigeration unit through the grids in the ducted floor and then drawn off again below the container ceiling on the same side as the inlet. The circulating fans then force the air through the air cooler, which also acts as an evaporator in the cold circuit, and back through the gratings into the cargo. Ethylene and CO_2 produced from respiration of the produce in the container are regularly removed by ventilating via the fresh air exchange vents (considering the air outside is ethylene free). Air pressure caused by the fan across the vents will allow fresh air in through one vent and ethylene containing air through the other vent. Fresh air exchange rates vary widely depending on the source of the information, for example, suggested rates for apples in a 40' container ranged from 264 $m^3 h^{-1}$ (Smale, 2004) to just 10 $m^3 h^{-1}$ (Irving, 1997). However excessive fresh air exchange increases the heat and moisture load on the container unnecessarily which will eventually affect the efficiency of the container as infiltration would.

Stuffing or arranging load into a reefer container depends on the product airflow requirements. With any arrangement patterns, pallets must cover the entire T-bar floor to ensure proper distribution of refrigerated air. However, not all palletized cargo or, irregular shaped goods, can be stuffed in this way. In that case, when the load does not cover the entire T-floor, it is important to put cover where no cargo is stuffed in order to avoid short-circuiting of the circulating air (PPECB, 2013; Moureh and Flick, 2004). The height of the cargo must not exceed the red cargo load line, which shows maximum allowed cargo height, so that ample free space is left above the stow to ensure proper air circulation around the load (PPECB, 2013).

Inside a reefer container the airflow is influenced by the type of packaging and the method of arrangement used. The type of load also affects the cooling airflow rate and energy consumed. In the case of pre-cooled frozen load transport

Stellenbosch University https://scholar.sun.ac.za

(<-10 °C) small fluctuation in temperature does not affect the load significantly therefore the reefer's compressor can be switched on and off to regulate internal temperature (frozen mode operation) (Wild, 2009). Since no heat has to be dissipated from the loads themselves the cooling air flows merely to remove the heat which penetrates the insulation from outside (ASHRAE, 2009). Frozen type of load will consume less energy than chilled produce load (Fitzgerald et al., 2011). When the reefer is loaded with chilled produce, normally the fans operate at full speed since the temperature has to be kept very close to set point to maintain quality of the respiring load (chilled mode operation) (ASHRAE, 2009). However, the recent development and implementation of QUEST I&II (QUality and Energy in Storage and Transport,) programs, that have a protocol designed to reduce the energy consumption of the unit by avoiding inefficient part-load compressor operation and optimizing evaporator fan speed with heat load, showed the mechanism that avoids full speed fan operation (Lukasse et al., 2011).

2.3. Modelling airflow and heat transfer in reefer

Modelling of transport phenomena in reefer can be studied by considering the airflow or the temperature of the product. Complete models combine both and deal with the temporal features of transportation: fluctuating ambient conditions, packaging orientation, product removal/loading, etc. All long-distance transport systems, such as, trailers and reefer can be considered mobile refrigerated units and share most of the processes and mechanisms that occur in cold store facilities. Therefore, some of the modelling approaches applied for cold stores can be considered relevant to transport systems with little change being required to the inherent model. The common denominators for cold stores and reefer are climatic changes, effect of environmental condition on heat transfer with external wall, sun radiation and infiltration of air from the environment.

Modelling packed agricultural produce has evolved significantly in last few decades (Ambaw et al., 2013). However, due to computational power limitation, complicated property of produce and geometrical complexity of packed produce,

Stellenbosch University https://scholar.sun.ac.za

development of an efficient model that is capable of simulating the real phenomenon remains a challenge. This problem particularly prominent in large domains such as reefers, trailers and, cold stores. The significant improvement in computing technology made higher level of detailed modelling and simulation possible. In addition, researchers have been trying different techniques that can alleviate the problem. One method to minimize computational cost is employing porous media modelling approach (Alvarez and Flick, 2007; Ambaw et al., 2013; Delele et al., 2012; Hoang et al., 2015; Moureh et al., 2009a, b; Tapsoba et al., 2006). In this section the techniques applied in modelling reefer so far will be discussed.

2.3.1. Resistance network modelling

Resistance network models have been used by civil engineers in the design of water distribution system in which pipe network (hydraulic network) analysis is conducted using Hardy-Cross method (Cross, 1936). Before CFD application for airflow prediction inside a reefer, Van der Ree et al. (1974) developed a simple channel network model and solved using a finite element program called BERTEM but there was no validation of the model and the results were only used for qualitative observations. The airflow model did not include momentum and moisture loss also was not taken into account. The model was based on vertical air velocities in the crevices between the stacks of boxes which were calculated from the crevice sizes and the overall air circulation rate assuming equal pressure fields above and below the stack and laminar flow throughout. Similarly, Meffert and van Beek (1983) developed a resistance network model to predict airflow in the cargo space of transport equipment using electric analogy for laminar flow. The pressure drop is calculated by, equation 2.1.

$$\Delta P = Q\beta_{lam} \qquad 2.1$$

Stellenbosch University https://scholar.sun.ac.za

Where, Q is fluid volumetric flow ($m^3 s^{-1}$) and β_{lam} is laminar resistance (Pa s m^{-3}).

As computational power increase, the algorithms improved. Wood and Rayes (1981) discussed two basic approaches which solve mass and energy equations; the first approach known as solving the node equations treats the pressure at convergent/divergent points as unknowns and solves the mass balances at each point. The second approach, known as solving the loop equations, treats flow rates as the unknowns in energy equations around primary loops and again solves mass balances at convergent/divergent points. The solution for the node equations was when small error in pressure caused large error in flow rates for low resistance pipes. The authors found the loop equations were more likely to converge.

The resistance network model developed by Wang and Touble (1988) to predict mass and heat transfer resulted in a significant error but showed some level of agreement with experimental results. Later Wang (1990) used CFD code Phoenics and k-ε turbulence model to predict airflow, temperature and moisture transport. The modelling was conducted in two steps to shorten computational time; airflow modelling (steady state) followed by heat and mass transfer modelling (unsteady state) by neglecting buoyance force due to natural convection. The model was validated only on temperature measurements. Air velocity was not measured therefore the validity model cannot be confirmed. Menia et al. (2002) developed a simplified resistance network model to predict airflow inside a scaled model of top air-delivery refrigerated vehicle loaded with pallets. The vehicle was divided into four quarters as shown in Figure 2-2.

Stellenbosch University https://scholar.sun.ac.za

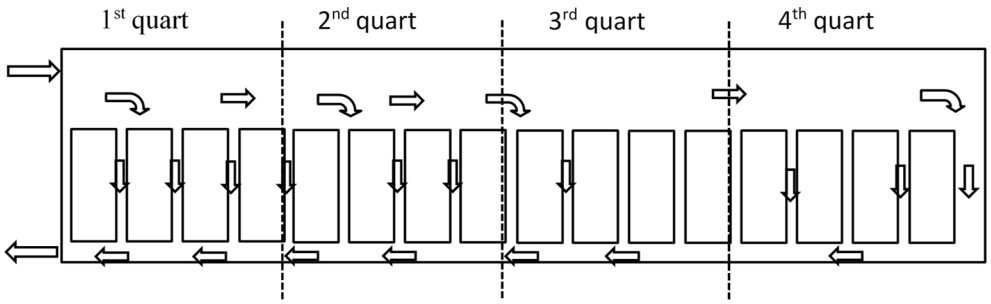

Figure 2-2: Side view of the refrigerated vehicle compartmented for hydraulic network (Menia et al., 2002)

The resistance in each quarter was combined to form 10 equations using the Hardy-Cross method. Two loading patterns were considered for simulation. The airflow was assumed either in the laminar or turbulent regime depending on the channel type and CFD (Fluent) predictions. The results of the model presented a good qualitative agreement with the experimental data of the two loading patterns. The disagreement between the two models (resistance network and CFD) were proposed to be two; the assumption of vertical flow in channels adjacent to the walls and the effect of combining flow and recirculation of air in the head space between the pallets and the ceiling which were not included in the resistance network (Smale et al., 2006).

A resistance network model has also been used by Smale (2004) to predict airflow in reefers and holds carrying palletized boxes of fruit. Large number of nodes and equations were solved using a Newton-Raphson algorithm. Fully loaded shipment was used for validation of the simulation results against air velocity and fruit temperatures and reported a reasonable agreement.

2.3.2. Computational fluid dynamics (CFD) modelling

Computational Fluid Dyanamics (CFD) is the analysis of systems of equations governing transport phenomena (continuity equation, Navier-Stokes equations and additional conservation equations) (Versteeg and Malalsekera,

Stellenbosch University https://scholar.sun.ac.za

1995). In CFD modelling the real geometry of the system is discretized and Navier-Stokes equation for mass, momentum and energy are solved using the appropriate numerical methods such as finite difference, finite element and finite volume. The application of CFD by food engineers began in the 1990s, which has become a common practice in the postharvest research areas. There are numerous commercial CFD codes that are supported on different platforms, to name a few common ones Fluent, CFX, Phoenics, Star-CD. Xia and Sun (2002) listed more commercial codes and discussed the common commercial codes in detail.

Numerical modelling techniques have been applied to study, optimize and design processes that are related to horticultural produce cooling, storage and handling (Alvarez et al., 2003; Defraeye et al., 2015b; Delele et al., 2009a, b; Delele et al., 2012; Ferrua and Singh, 2007; Hoang et al., 2003; Hoang et al., 2015; Tanner et al., 2002a, b; Verboven et al., 2006; Xie, et al., 2006; Xu and Burfoot, 1999; Zou et al., 2006a, b). The studies showed the applicability of mathematical models in predicting airflow, heat and mass transfer and were used to study the effects of different operational and design parameters in cold chain systems. However, application of numerical method such as CFD in postharvest handling systems has challenges due to the geometrical complexity and size of the produce packed systems (cold store, reefer, display cabinet) that requires high computational power to solve transport phenomena equations.

Researchers used different techniques to employ CFD in their study. For example, Xie, et al. (2006) in their study of the effects of design parameters on flow and temperature fields of a cold store considered the product load as a solid domain. The authors employed a k-ε turbulence model with wall functions to model a 2D CFD model and a relatively coarse mesh. The application of coarse mesh minimized computational power requirement but limited the accuracy of the model, whereas the simplification of the actual 3D to 2D caused loss in connectivity of air spaces and flow condition. However, the error encountered was not significant in predicting temperature field in that particular study (Ambaw et al., 2013) and

Stellenbosch University https://scholar.sun.ac.za

similar result was found in temperature profile studies in a stack using 2D models (Xie, et al., 2006; Alvarez and Flick, 2007; Dehghannya et al., 2011). In other studies, researchers used scaling (Defraeye et al., 2015b; Lovatt et al., 1993; Moureh et al., 2002; Yu and Hoff, 1999) symmetry (Moureh and Flick, 2004) and a porous media approach (Bakker-Arkema et al., 1969; Hoang et al., 2000; Mirade et al., 2005; Verboven et al., 2004; Moureh et al., 2009a, b; Delele et al., 2013a, b; Ambaw et al., 2014) to apply CFD for complex and enormous cold chain systems.

Recently CFD porous media modelling approach has become a common technique in postharvest applications due to its advantage in addressing the computational power limitation and capability of representing the dynamic flow effects on a macroscopic level, adequately (Ambaw et al., 2013; Hoang et al., 2015).

Porous media modelling concept

Fruits in cold stores or reefer are packed in bulk with boxes and stacked in a pallet. These bulk packed fruits can be treated as porous media (Bakker-Arkema et al., 1969). The porous media approximation is a common technique in postharvest applications due to its advantage in addressing the computational power limitation and adequately represents the dynamic flow effects on a macroscopic level since it relates particle size, shape, alignment with airflow and void fraction to the pressure drop over the modelled object (Zou et al., 2006a, b; Norton and Sun, 2006; Verboven et al., 2006). This assumption has become common approach in recent years in modelling of cold store and reefer stacked with fruits (Hoang et al., 2000; Mirade et al., 2005; Verboven et al., 2004; Moureh et al., 2009a, b; Delele et al., 2013a, b;Ambaw et al., 2014).

Airflow in porous media

Darcy experimentally concluded that fluid flow rate was proportional to the pressure loss and the cross-sectional area and inversely proportional to the length of the flow path. The famous Darcy's Law is written as follows:

Stellenbosch University https://scholar.sun.ac.za

$$\Delta P = \frac{\mu}{\kappa} u \qquad 2.2$$

Where μ (kg $m^{-1}s^{-1}$) is the dynamic viscosity of the fluid and κ (m^2) the permeability of the porous medium, u is the superficial velocity. Nearly all engineering calculations for porous media flow problems have originated from Darcy's Law and/or purely empirical determinations. Later Dupuit (1863) has proved empirically, that Darcy's Law is limited to very low velocity and becomes invalid when inertial forces become effective. Since then, several related theories and approaches have been developed to approximate the flow of fluid through porous media. Darcy-Forchheimer equation, which includes a quadratic term, describes flow in high velocity scenarios (equation 2.3).

$$\Delta P = -\frac{\mu}{\kappa}\vec{u} - \beta\rho|u|\vec{u} \qquad 2.3$$

The original Ergun (1952) equation which was developed for a packed bed of uniformly sized spheres has been modified for application of agricultural products on beds. The model can be considered as purely empirical since the coefficients of linear and quadratic velocity terms are directly estimated, without considering the physical characteristics such as porosity and particle size (Verboven et al., 2004). Chau et al. (1985) used a modified Ergun equation by incorporating porosity, particle diameter and fluid properties for bulk orange. They fitted two remaining empirical parameters to the measured pressure drops however, the values of this parameters change for different fruit size and stacking patterns.

Resistance of airflow has been described mathematically in the form of the Ergun equation, which is the special case of the Darcy-Forchheimer-Brinkman equation (2.4) (van der Sman, 2002; Verboven *et al.,* 2006);

Stellenbosch University https://scholar.sun.ac.za

$$\Delta P = -\frac{\mu}{\kappa}\vec{u} - \beta\rho|u|\vec{u} - \mu_{eff}\nabla^2\vec{u} \qquad 2.4$$

Where, β is Forchheimer coefficient, κ is the permeability of the porous medium and μ_{eff} is the effective dynamic viscosity in the boundary layer at the solid to porous media interface.

The Brinkman term (the third term on the right side of equation 2.4), which describes the boundary layer at solid to porous media interface, where the velocity reduces to zero exactly at the solid wall (packaging), does not have a significant influence on the pressure drop over a packed bed on a global scale (van der Sman, 2002). Hence, exclusion of the term exhibits bumps near the interface on numerical results but that is not physical (van der Sman, 2002).

Ramsin equation 2.5 is also common in postharvest applications to determine pressure drop through bulk of produce and vented packages (Haas et al., 1976; Chau et al., 1985; Has and Felsenstein, 1987; Smale, 2004; Ngcobo, 2013);

$$\frac{\Delta P}{L} = au^b \qquad 2.5$$

Where, a is resistance coefficient and b is resistance exponent that are primarily dependent on stacking pattern, particle diameter and porosity (Delele et al., 2008) and they are experimentally determined (Smale, 2004). Delele et al. (2008) employed both Ramsin and Darcy-Forchheimer equation to study the local airflow using the explicit geometry of stacked horticultural products in boxes. A combined discrete element (DE)-CFD modelling was applied. The result was fitted for both, pressure drop vs velocity, Darcy-Forchheimer equation fitted better than Ramsin equation. However, at low velocity (<0.1 m s^{-1}) the difference between the numerical prediction and those calculated from the equation increase. This was pointed out as limitation of the equations for low Reynolds number flow.

Stellenbosch University https://scholar.sun.ac.za

Based on the theory of Reynolds for resistance to fluid flow, Ergun (1952) illustrated that a pressure drop through a porous media is caused by the simultaneous viscous and kinetic energy losses. Pursuing this, he developed a general equation of fluid flow through porous media (Eqn. 2.6), which combines the Blake-Kozeny equation for laminar flow and the Burke-Plummer equation for turbulent flow (Prukwarun et al., 2013).

$$\frac{\Delta P}{L} = A\frac{(1-\varepsilon)}{\varepsilon^3}\frac{|u|\vec{u}}{{d_{eff}}^2} + B\frac{\mu(1-\varepsilon)u^2}{d_{eff}\varepsilon^3} \qquad 2.6$$

Where, ε is porosity, d_{eff} effective diameter, A is the Blake–Kozeny–Carman constant and B is Burke–Plummer constants with values 150 and 1.75 respectively. The first term on the right side represents the viscous energy loss and the second term on the right side represents the kinetic energy loss.

Heat transfer modelling in a porous media

Modelling heat transfer in a porous media is complicated. The heat transfer depends on the thermal and physical properties of the solid and fluid phases involved. Usually the thermal conductivity of the solid phase is higher than that of the fluid. Therefore, conduction heat transfer in porous media depends on the physical property such as, structure of the matrix and thermal conductivity of the phases (Dehghannya et al., 2010). Experimental studies showed that for convective heat transfer in porous media the energy equation should account the effect of both the macroscopic and microscopic velocity fields the temperature field (Kaviany, 2012). In principle Local thermal equilibrium (LTE) and local thermal non-equilibrium (LTNE) models are the two models used for heat transfer modelling in porous media.

In (LTE) heat transfer in porous media can be described by a single energy equation if thermal equilibrium between the moving fluid and the solid phase is

Stellenbosch University https://scholar.sun.ac.za

assumed (Quintard et al., 1997). This method has been investigated by several authors (Quintard and Whitaker, 1995; Nield et al., 2002). Based on this assumption the general energy equation can be written as,

$$\frac{\partial}{\partial t}\left(\phi\rho_a Cp_a T + (1-\phi)\rho_p Cp_p T\right) + \frac{\partial}{\partial x_j}(\phi\rho_a Cp_a T) = \frac{\partial}{\partial x_j}\left[\partial\lambda_{eff}\left(\frac{\partial T}{\partial x_j}\right)\right] - \phi\frac{\partial}{\partial x_j}(\rho_a Cp_a\overline{u_j'T'}) + S_e \quad 2.7$$

$$\lambda_{eff} = \lambda_a + \frac{Cp_a\mu_t}{Pr_t} \quad 2.8$$

Where ε_p is the porosity, λ_{eff} effective thermal conductivity, W (m K)$^{-1}$.

In most cases of flow in a fluid saturated porous media the assumption of local thermal equilibrium is valid (Nakayama and Kuwahara, 2005); this assumption has been used by several researchers (Nakayama and Kuwahara, 1999; Antohe and Lage, 1997; Masuoka and Takatsu, 1996; Chourasia and Goswami, 2007a). However, LTE modelling approach has limitations during transient calculations or in the presence of heat generation in solids particularly for large particle size solids and low conductivity fluids. Heat transfer under these conditions is not well verified for LTE modelling approach (Verboven et al. 2006; van der Sman 2008; Laguerre et al. 2008; Hoang et al. 2015). Van der Sman (2008) reported that the LTE assumption is valid if the fluid Stanton number, $St_a = \frac{L_x h_h a_p}{u_x \rho_a Cp_a} \gg 1$, vapour Stanton number, $St_v = \frac{L_x h_m a_p}{u_x} \approx 1$, Biot number, $Bi = \frac{h_m D_p}{\lambda_p} \ll 1$ and the particle Reynolds number, $Re_p = \frac{\rho_a u_x D_p}{\mu_a} \ll 10^3$ (Delele et al. 2012). Delele et al. (2012) reported also that irrespective of the calculated Biot number close to 1, the experimental and the simulation results were in agreement. The authors used the mixing rule to estimate the effective thermal conductivity.

Stellenbosch University https://scholar.sun.ac.za

$$\lambda_{eff} = \varepsilon\lambda_a + (1-\varepsilon)\lambda_p \qquad 2.9$$

Under circumstances where LTE is not applicable LTNE is used. Two macroscopic conservation equations are used to describe the fluid phase and the solid phase separately.

Fluid zone energy equation

$$\varepsilon_p \frac{\partial \overline{T_a}}{\partial t} + \overline{u_j}\left(\frac{\partial \overline{T_a}}{\partial x_j} + \frac{1}{\rho_a Cp_a}\frac{\partial \overline{p}}{\partial x_j}\right) = \varepsilon_p \frac{\partial}{\partial x_j}\left(\frac{\lambda_{eff}}{\rho_a Cp_a}\frac{\partial \overline{T_a}}{\partial x_j}\right)$$

$$+ \frac{A_{sfi} h}{\rho_a Cp_a}\left(\overline{T_p} - \overline{T_a}\right) \qquad 2.10$$

Where turbulent viscosity, $\mu_t = \rho_a C_\mu \frac{k^2}{\omega}$, for k-epsilon model and, $\mu_t = \rho_a \frac{k}{\omega}$, for k-omega model and Pr_t (0.85) is the turbulent Prandtl number

Solid zone energy equation

$$(1-\varepsilon_p)\frac{\partial \overline{T_p}}{\partial t} = (1-\varepsilon_p)\frac{\partial}{\partial x_j}\left(\frac{\lambda_p}{\rho_p Cp_p}\frac{\partial \overline{T_p}}{\partial x_j}\right) + \frac{A_{sf} h}{\rho_a Cp_a}\left(\overline{T_a} - \overline{T_p}\right) + S_e \qquad 2.10$$

Where, A_{sf} is specific area (interfacial area density, that is, the ratio of the area of the fluid / solid interface and the volume of the porous zone) (the total surface of apples in a pallet divided by its volume), μ_t is turbulent viscosity. The first term is the fluid energy, on the right side the first term is the convective heat transfer (CHT) between the air and the produce and the last term is the source term. Similarly, in the solid zone equation the first term is the transient term, on the right side the first term is the diffusion term, the second term is the convective term and the last term is the source term.

Stellenbosch University https://scholar.sun.ac.za

Heat transfer resistance between the cooling air and a single apple in a box are the carry bag and the convective heat transfer resistance between the cooling air and the carry bag. However, if we consider the average fruit temperature for our calculation which is located at 3/4th of the radius of the apple, then the resistance of fruit will be included (Van der Sman, 2003). Hoang et al., (2015) indicated that for a fruit with a Biot number (Bi) 0.1 < Bi < 10, the internal resistance can be calculated as R/4λ. In addition, the equivalent convective heat transfer coefficient (CHTC) can be calculated by,

$$h = \frac{1}{\left(\frac{1}{h_{pa}} + \frac{\mathrm{R}}{4\lambda}\right)} \qquad 2.11$$

The turbulent flow CHTC (h_{pa}) for a disordered pack of spheres is correlated by:

$$Nu = \frac{h_{pa}D}{k_a} = 2 + 1.1 + Re^{0.6}Pr^{1/3} \qquad 2.12$$

For a single apple located in the middle of other apples in a carry bag in a packaging box is the plastic, stationary air in the bag which acts as an insulator and the convective heat transfer. Therefore Eqn. (2.11) for the CHTC can be modified as,

$$h = \frac{1}{\left(\frac{1}{h_{pa}} + \frac{\mathrm{R}}{4\lambda} + \frac{\Delta x_{air}}{\lambda_{air}}\right)} \qquad 2.13$$

Application of the porous modelling approach in postharvest systems

In CFD modelling explicit geometry representation of is always a priority rather than as a porous medium for better accuracy. Delele et al. (2008) developed a validated numerical methodology that takes into account product geometry, box

Stellenbosch University https://scholar.sun.ac.za

design and randomness of stacking explicitly by combined discrete element (DE) and CFD for modelling airflow through a stack of packed fruits. The methodology showed the capability of the approach to give detailed flow characteristics to the level of individual pores. However, this methodology will be expensive and highly complicated when a system as big as packed reefer is the subject. Therefore, porous media approach has been applied widely applied in large cold chain systems.

Zou et al. (2006a) studied airflow and heat transfer in bulk and layered packaging systems by porous medium approach. The model was developed with volume-averaging method and the model was validated by experimental results (Zou et al., 2006b). Chourasia and Goswami (2007) developed a 3D model to predict the airflow, heat and mass transfer in a single bag of potato by assuming a porous medium using Darcy-Forchheimer momentum equation. For both transient and steady state cooling the rate of moisture loss, velocity vector and temperature contour were presented and the results were compare with experimental data. Alvarez and Flick (2007) modelled forced-air cooling of stacked food products represented by PVC spheres as a macro-porous medium using Darcy-Forchheimer momentum equation to predict the average superficial velocity. The model considered the turbulence dissipation and generation in the porous medium which was not included by other modellers (Xu and Burfoot, 1999; Hoang et al., 2003; Moureh and Flick, 2004; Moureh and Flick, 2005 Nahor et al., 2005a, b; Chourasia and Goswami, 2007a,b; Delele et al., 2009a,b).

Several studies were conducted in enclosures/mobile refrigerated transport systems such as trailers and reefers; empty and packed. The porous media approach was employed to study airflow in citrus packed shipping containers (Talbot et al., 1990). The model used the Darcy-Forchheimer and Ergun equations for the flow resistance calculations by using finite element commercial codes. Air velocity in the free space for different packaging scenarios was not considered (Dehghannya et al., 2010). Moureh et al. (2009b) developed a 3D model in reefer with and without air-duct system, loaded with two rows of slotted pallet, using the RSM turbulence

Stellenbosch University https://scholar.sun.ac.za

model to predict the airflow pattern. To calculate the pressure loss in the pallets the Ergun equation was used. The same scaled model as Moureh et al. (2004) was used for experimentation. Moureh et al. (2009a, b) investigated the airflow pattern in a reefer using a 1:3.3 scaled model and RSM turbulence CFD model. Airflow was predicted in container loaded with two rows of ventilated pallets filled with spherical objects which were considered as porous medium. Pressure loss coefficient was determined in a wind tunnel experiment. To avoid the problem of large computational capacity requirement during meshing the small gaps between the pallets were replaced by fictitious porous medium that gave aerodynamically equivalent airflow resistance (the size of the gap was increased from 0.02m to 0.06m) (Tapsoba et al., 2007). Darcy's equation governed airflow to pressure gradient relationship. The porous medium approach was proposed because the air velocity measurement showed that laminar flow was dominant in the small gaps between the pallets. Similarly, Moureh and Flick (2009a) developed a model to study airflow characteristics in an enclosure partially filled with slotted porous boxes. In the model the air gap between boxes was replaced with a fictitious porous media that imposes equivalent resistance to the actual flow in the region (Tapsoba et al., 2007). It was reported that the model prediction was in reasonable agreement with experimental result.

Recently, Hoang et al. (2015) modelled a small cold store with four apple pallets (composed of 8 layers of wooden bins) and compared two modelling approaches. In the first approach, each pallet was modelled as one porous medium and in the other approach; each layer of a pallet was modelled as solid block representing the bin (8 solid blocks in a pallet). In the solid block approach, the spherical shape of the fruits was considered by doubling area of the top side of the block area. It was reported that both models showed good agreement with experimental results of temperature evolution with air flow pattern prediction agreed well qualitatively. It was noted that the porous medium approach gives a fairly good result with nearly four times less than the number of elements. Therefore, from the above discussions it can be drawn that modelling pallets as a

Stellenbosch University https://scholar.sun.ac.za

porous medium is practicable and the quality of the result can also be enhanced by increasing the number of elements to some extent.

Porous media modelling has limitations. The continuous medium assumption break-up during cooling operation, particularly in forced air precooling process where the packaging to product diameter under 10 is the main problem (Eisfeld and Schnitzlein, 2001; Verboven et al., 2006; Dehghannya et al., 2010). In addition, when LTNE model is applied for a packed produce determination of the model parameters involves complicated calculation. Estimation of these parameters has not been successful (Ferrua et al., 2007; Dehghannya et al., 2010). The other drawback is lack of capturing detailed spatial and temporal temperature heterogeneity such as among the individual fruits (Defraeye et al., 2015b).

Alternative modelling approaches

A number of other models besides resistance network and CFD have been developed in the past to predict airflow and heat transfer in cold stores and reefer. In this compendium the models that have been employed in postharvest application, such as Lattice scheme modelling and Scaled modelling, have been considered.

a) Lattice scheme model

Lattice scheme model, in which packets of fluid was represented by qausi-particles, was used to model convection-diffusion phenomena in vented transport packaging for produce (Van der Sman, 1999). The mass and energy transfer laws where obeyed by movement and collision of this packets of particles under lattice laws. Van der Sman (1999) used three Lattice-Boltzman based models and validated against experimental results. This model has advantage over finite element and finite difference methods on relatively easy boundary condition implementation and possibility of modelling complex processes in a single framework (Smale, 2004).

Stellenbosch University https://scholar.sun.ac.za

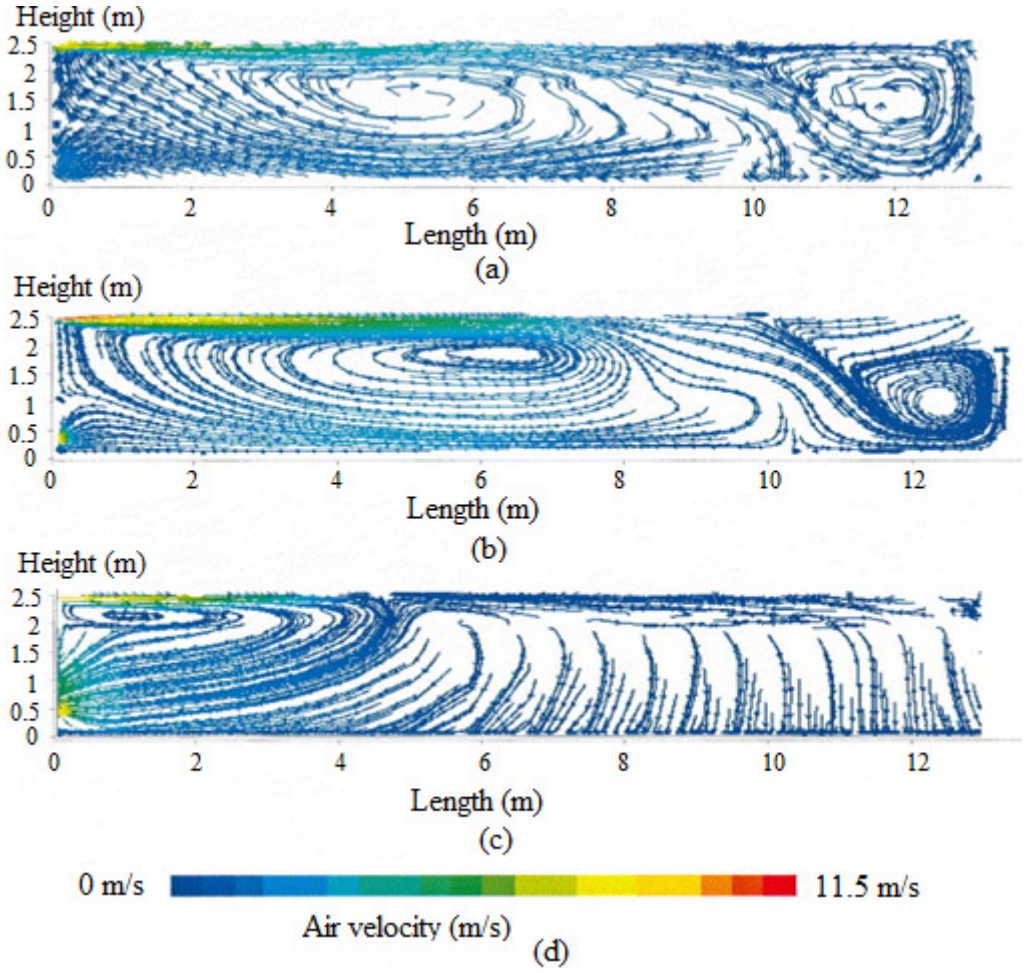

Figure 2-3: Influence of the load on the airflow pattern. (a) Streamlines in unloaded configuration, Laser–Doppler measurements (1100 points). (b) Streamlines in unloaded configuration, RSM model. (c) Streamlines in loaded configuration, RSM model. (d) Air velocity scale (Moureh et al., 2002).

b) Scaled modelling approach and symmetry boundary conditions

Scaled modelling approach is preferable when modelling large system. The objective of this approach is to eliminate the use of full scale application to reduce operating cost and increase flexibility during measurement. In scaled modelling approach a relationship criterion under different operating conditions needs to be created relevant to the full scale in order to extend the validated result to the full

Stellenbosch University https://scholar.sun.ac.za

scale system. Scaled modelling technique has been used by scientist to study airflow and species transport. Lovatt et al. (1993) used scaled model of chiller to show airflow trends and effect of turning vanes. A water filled model with an electrode to produce hydrogen bubbles for flow visualization was used. The Reynolds number was used as a similarity criterion. The model was developed for qualitative use and no validation was conducted. 1:6 and 1:3 scaled models were used to study similarity criterion for celling slot ventilated agricultural enclosures with intermediate airflow (Yu and Hoff, 1999). The study compared inlet jet momentum ratio and Reynolds number as a potential similarity criteria and showed that the Reynolds number is the best similarity criterion. Moureh et al. (2002) used scaled model (1:3) in modelling airflow in reefers. The model was constructed with glass at the front wall in order to have optical access to measure the airflow inside using Laser Doppler anemometer (Figure 2-3). The model was validated but no similarity criterion was stated.

In other studies, researchers used model scaling and symmetry boundary conditions for enormous and complicated 3D domains for simplification of CFD model. Defraeye et al. (2015b) developed a model composed of eight fruit packed boxes in vertical layers to the study fruit cooling in a low velocity vertical flow that emulate ambient cooling scenario in a reefer. The study contributed a fundamental insight of the airflow and cooling phenomena in reefers and gives the potential modelling approach for a full scale packed reefer. The following simplifications were made, only vertical flow was considered; air gaps and symmetry boundary was used in all sides. It was reported that cooling was faster than the practical study and show logical cooling pattern from the bottom layer to the top layer. However, in the experimental study of citrus cooling from an ambient condition it was reported that the cooling rates of different pallets lacks logical pattern Defraeye et al. (2015a). Moureh and Flick (2004) also shown that the temperature profile in packed enclosure (top air-delivery system) does not follow a reasonable cooling pattern in a pallet (from bottom to top) and among pallets along the flow direction.

Stellenbosch University https://scholar.sun.ac.za

Other researchers apply symmetry boundary conditions to simplify a model and reduce the computational requirement (Ambaw et al., 2014; Defraeye et al., 2013; Delele et al., 2008; Ferrua and Singh, 2009a; Kwon et al., 2015; Moureh and Flick, 2004). Moureh and Flick (2004) applied geometrical symmetry boundary condition in a palletized enclosure and modelled half the domain (one row of pallets). Although this simplification has advantages, due to the nature of airflow in the confined enclosure that involves flow recirculation, turbulent shear flows and expanding jet flow application of symmetry boundary in such systems can lead to numerical errors.

2.4. Factors that affect energy consumption in cold chain systems and quantification of energy in reefer container

Energy use in reefer containers and cold storage facilities is affected by several factors. The main sources of heat in cold chain facilities for long-term storage are transmission through walls, evaporator fans, lights, air leakage, and respiration of the stored product (Thompson, 2001). In the case of reefer the main factors that affect energy consumption are the amount of heat the refrigeration equipment must remove from the load, outside ambient air temperature and humidity, exposure to sun radiation during transport, external wall paint of the container refrigerant type, and the efficiency of the equipment (age of the container), evaporator fan motor, air leakage (infiltration), heat generated due to respiration of loaded produce (Fitzgerald et al. 2011; Jolly et al, 2000; Wild et al., 1999; Wild et al., 2008).

Energy consumption in a reefer system can be affected by different operational and design parameters. The dominant factors involved in postharvest handling of perishable produce are container design, thermal insulation, fan operation, operational malfunction, fruit packaging design, produce property, defrost load and, packaging design and alignment. Most of these factors are

Stellenbosch University https://scholar.sun.ac.za

common between reefer and cold storage (Thompson et al., 2010) and most of the literature found was on cold storage.

2.4.1. Insulation

Thermal insulation is necessary for proper control of storage conditions by reducing heat exchange with the environment. An inferior quality, old or damaged and, thinner insulation leads to high heat transfer and requires a larger compressor with more power consumption to make meet the additional cooling load. This in turn increases both energy wastage and recurring expenses. Therefore, optimum insulation quality and thickness is critical to improve energy-efficiency and maintain quality of stored produce. Heat gain from the environment varies depending on the type of the reefer. According to ISO 668-1995 (E) measurement, total maximum heat leakage rate at 20 ℃ is given as 42 W K^{-1} for TAL Starcool reefer (Maersk, 2016). Tridib (2009) reported the cold storage must be insulated in such a way that heat in-leak should not increase beyond 6 – 8 W m^{-2}, however is not so in practice.

Recently experimental study on reducing the heat transfer across the insulated walls of refrigerated truck trailers was conducted by Ahmed et al. (2010). The authors adapted well proved phase change material (PCM) from its successful practical result in building walls and structural insulated panel (SIP) by (Zhang et al., 2005) and (Medina et al., 2008), respectively. Integration of PCMs in regular building walls resulted in 11–20 % peak heat transfer rate reduction with a PCM concentration of 10 %. Peak heat transfer reduction of 37 and 62 % was found in SIPs with 10 and 20 % PCM, respectively. Ahmed et al. (2010) used two test truck trailer simulators (small scale model) with equal dimension of $1.22 \times 1.22 \times 1.22$ m, to evaluate effect of PCM. The result showed the incorporation of the PCM caused an average reduction of 29.1 % in peak heat transfer and an average of 16.3 % in total heat transfer rate.

Stellenbosch University https://scholar.sun.ac.za

2.4.2. Infiltration

Infiltration create additional refrigeration heat load due to inefficient sealing, density difference between the inside and outside air, opening and closing of doors during loading. Gosney (1975) modelled infiltration in a cold store using analytical method and was able to predict the infiltration for two experiments within experimental error. This model over predicted the infiltration for the other experiments and was worst for the 0.43 m wide door. Foster et al. (2003) showed in their CFD model that the Gosney (1975) model was the best of the analytical models and was able to predict the infiltration for two of the experiments within experimental error. Cold storage facilities apply air curtains (Foster et al., 2007), make entry to the store to be through doors that are automatically opened for 15 seconds per opening and (Stoecker, 1998), air curtain devices (Gonçalves et al., 2012). Stoecker (1998) created analytical equations to predict heat load due to natural convection through openings and in a 3-D CFD model. The maximum air leakage and heat leakage in reefers (Starcool-SCI 40 Maersk) were reported to be 0.25 m^3 h^{-1} at 500 Pa and maximum 40 W K^{-1}, respectively (Maersk, 2012).

$$Q_{inf} = C_{inf} A_d \sqrt{H} \left(\frac{\rho_i - \rho_o}{\rho_i}\right)^{1/2} \left[\frac{2}{1 + \rho_i/\rho^{1/3}}\right]^{3/2} \left(\frac{\rho_i + \rho_o}{2}\right) \qquad 2.14$$

Where, Q_{inf} is infiltration coefficient (0.692 √m/s), Ad is area of door (m2), H is height of door, ρ_i and ρ_o are density of air inside and outside, respectively.

2.4.3. Product property

High rate of respiration and moisture loss during postharvest handling of horticultural produces have an adverse effect on its quality and storability. The quality of fruits at the time of storage and during the long-term storage also has direct bearing on the electrical power consumption. The maturity, initial temperature, damage to the skin of fruits in the form of cutting, bruising, and

Stellenbosch University https://scholar.sun.ac.za

peeling are the quality attributes of the product which affect the metabolic heat of respiration as well as moisture loss (Becker et al., 1996; Mohsenin, 1968). This may add the heat load and in turn result in increased power consumption. It has been reported that respiration heat load, has low impact in forced air cooling (Tanner et al., 2002a, b).

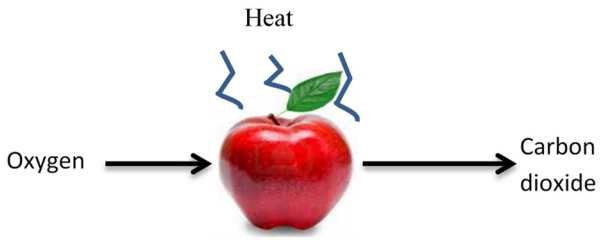

Figure 2-4: Respiration process

Respiration reaction

$$C_6H_{12}O_6 + 6O_2 \Longrightarrow 6CO_2 + 6H_2O + Heat$$

Heat generation by respiration

The correlation developed by Becker et al. (1996) relates a produce's rate of carbon dioxide $\dot{m}_{CO_2}$ $(mg\ kg^{-1}\ h^{-1})$ production to its temperature (equation 2.15).

$$\dot{m}_{CO_2} = f * \left(\frac{9T_m}{5} + 32\right)^g \qquad 2.15$$

The heat generation per unit mass of produce due to respiration Q_{resp} (J kg^{-1} h^{-1}) can then be related to carbon dioxide production rate. Where, T_m is the mass average commodity temperature (°C), f and g are respiration coefficients (given in Becker et al. (1996) for different produce).

Stellenbosch University https://scholar.sun.ac.za

$$Q_{resp} = 10.7f * \left(\frac{9T_m}{5} + 32\right)^g \quad 2.16$$

2.4.4. Packaging design and alignment

One of the basic elements of importance in postharvest storage is the product and how it is stacked and packed (Ambaw et al., 2013). The main function of packaging materials is maintaining the quality of fruits during postharvest handling and storage by providing mechanical protection against injuries, minimizing produce moisture loss and retarding microbial growth (Opara, 2011). The major factors that should be taken into consideration when designing are, type of produce, pallet construction, cooling method used, and transport methods. The sagging carton obstructs ventilation across the surface of the box and is likely to cause mechanical damage to the produce in the package under it. Packaging boxes should be designed to allow for adequate air flow, which together with cooling requirements are produce dependent. Vents alignment with adjacent cartons on the pallet are one of the main factors that affect the air flow through the bulk (Castro et al., 2005, Castro et al., 2004; Delele et al., 2013a,b; Tridib, 2009). Alvarez and Flick (1999) demonstrated that heterogeneity of the forced-air process is not only generated by an increase in the air temperature as it flows through the produce pallet, but also by the heterogeneity of the airflow behaviour within the palletized structure. The preassure drop as a result of fruit load, packaging design and alignment during cooling of products affects the product quality (Thomson, 2001) and the energy consumption (Defraeye et al., 2014). It is clear that there is a significant impact of the produce containers and their vent design on the efficiency and homogeneity of the forced-air cooling process which in turn affect energy consumption of the system.

Stellenbosch University https://scholar.sun.ac.za

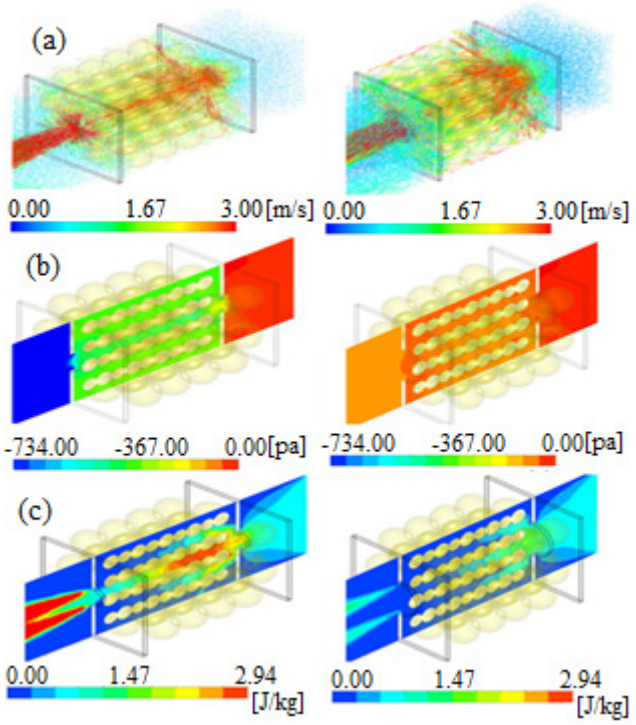

Figure 2-5: Effect of vent area on airflow characteristics: (a) air velocity vector, 3% vent area (left), 11% vent area (right); (b) pressure drop, 3% vent area (left), 11% vent area (right); (c) turbulence kinetic energy, 3% vent area (left), 11% vent area (right); for superficial velocity of 0.5 m s^{-1} (Delele et al., 2013b)

Delele et al. (2013a) applied CFD and employed SST-k-ω turbulence model, to study the effect of packaging vent design on airflow and heat transfer. In the study vent areas (1, 3, 5, 7, 9, 11, 20 and 100 %), shape (circular and rectangular), vent numbers (1, 2, 4, 6, and 9) and positions (central and peripheral) were considered (Figure 2.4). For effect of vent area on airflow was studied by varying the superficial velocities from 0.05 to 2 m s^{-1} and for the study of vent number, shape and position a superficial velocity of 0.5 m s^{-1} was applied. For the effect of vent parameters on cooling characteristics, cooling air pressure of 30 Pa and 100 Pa was applied. The simulation result showed that only up to 7 % increment of vent area increase the cooling rate significantly. The vent shape had no significant effect on cooling rate and airflow uniformity in the stack. Several

Stellenbosch University https://scholar.sun.ac.za

researchers have recommended different packaging vent area ratios (Baird et al., 1988; Castro et al., 2005). Pathare et al. (2012) also reported recommended vent areas which vary with the type of the material such as, for corrugated fireboard 4-27 %, for plastic containers 25 %, for clamshells 13 % and for polyethylene bags 0.5-2.5 %.

2.4.5. Fans

One of the high heat load source is from fixed load from the evaporator fans. Fans liberate the heat throughout the day due to their continuous operation. And in addition there is lack of seasonal control (Ambaw et al., 2016). There is a general lack of "sophistication" in the control regimes used for items such as suction pressure, defrost frequency and evaporator fans. The fan control regimes used in most of cold stores is relatively crude, either with 24/7 fan operation or some form of on/off control. Fan power consumption follows a "cubic relationship" with flow rate. This means if one slows the fan to give 80% flow it only uses 50% power. According to British Frozen Food Federation (2009, if one reduces flow further to 50%, the power usage falls to 12.5%. Thompson et al. (2010) reported that the evaporator fans in cold stores operates at maximum refrigeration design but mostly less than the maximum capacity is required to achieve the set point. The potential energy saving opportunities indicated were using variable speed fans, increasing vent area of boxes, using less lighting or efficient lamps. Hence optimizing fan operation will not only save fan power consumption but also save the compressor power needed to remove heat generated by the fan motor. The heat load from the evaporator fan motor can be calculated using Eqn. (2.17) (Evans et al., 2014).

$$Q_{fan} = \frac{N_m P_m}{\eta_{mot}} \qquad 2.17$$

Where, N_m is number of motors, η_{mot} is motor efficiency and, P_m is motor power.

Stellenbosch University https://scholar.sun.ac.za

2.4.6. Defrost load

During operation of a reefer, a layer of ice will form on the evaporator coils when the unit has a temperature SET lower than 0 °C. Therefore, during this period, the evaporator fans will turn off and heat will be produced by electrical elements and defrosting will take place. In modern reefers fans are turned off automatically in order to prevent heat from fan motor entering the cargo, however the heat produced by the elements needs to be removed by the refrigeration system.

The effects of defrost load, operating conditions (cooling mode, set point (0 °C and 6 °C), defrosting system and load level) and outer ambient temperature on performance of multi-compartment reefer containers has was studied by Rodríguez-Bermejo et al. (2007). The multi-compartment was modelled using a CFD to study the thermal characteristic of reefer containers. The result showed the significant effect of solar radiation on the indoor temperature. The authors also showed the current control strategies for off/on control refrigeration is poor for maintaining industry set point (±0.5 °C) and modulated cooling allows better temperature homogeneity. They recommended further research on cooling mode strategies to minimize energy consumption.

In experimental investigation in display cabinets Ke-zhi Yu et al (2009) compared a vertical display cabinet with central air supply (VDCCAS) with conventional vertical display cabinet (CVDC). It has been indicated that temperature fluctuation, which is caused by frosting and defrosting, was creating heterogeneity and affecting the energy consumption. The result also showed that VDCCAS can decrease the frost magnitude easier than the CVDC since it has better control of the air curtain velocity, hence decrease the product temperature rise in the defrost cycle from 3 to 2 ℃. The study showed, by optimizing air curtain velocity the temperature fluctuation can be decreased and the energy consumption by the compressor will decrease.

Stellenbosch University https://scholar.sun.ac.za

2.4.7. Forklift loads

Forklift is used to load pallets into container after the reefer has been cooled to the desired pulp temperature. Forklifts generate heat that increase refrigeration heat load in cold chain facilities (Evans et al., 2014). An estimation of the heat load due to a forklift operating within a space can be obtained from the information on the motor and assuming 80% efficiency for battery powered and 33% for internal combustion powered forklifts (ASHRAE. 2009).

$$Q = MR \text{ x } tm \text{ x } 24 \qquad 2.18$$

Where, Q is capacity (W), MR is Motor Rating (W), t is time in use per day (hr.), and m is motor efficiency (80% battery & 33% internal combustion).

2.5. Quantification of energy consumption: Experimental, analytical and mathematical approaches

2.5.1. Experimental and analytical approaches

Numerous papers are written on reefer, cold storage facilities and cooling systems performance (energy utilization) and mostly they are based on the information available at the facility's documentation (Castro et al., 2005; Evans, 2007; Fitzgerald et al., 2011; Goswami, 2009; Thompson et al., 2010; Wang & Muller, 2000; Wild et al., 1999; Wild et al., 2008). Evans (2007) and Goswami (2009) studied efficient design, operation, maintenance and management of cold storage and indicated the rise in the electrical consumption in cold chain facilities and described the possible causes as higher volume of product being cooled than before, product is entering storage hotter, infiltration, insulation being wet or missing and problems of malfunctioning refrigeration equipment. According to energy mapping conducted (based on data feed from facilities) in ten food refrigeration processes in UK, following retail display and kitchen refrigeration, energy consumption of refrigerated transport system was the highest (James &

Stellenbosch University https://scholar.sun.ac.za

James, 2011). The potential energy savings of each unit has been estimated based on the knowledge and technology at the time of the study (Table 2.1). To this end, 20-25 % energy saving per year was estimated for reefer. The authors concluded that the Coefficient of Performance (COP) of transport refrigeration systems was low, ranging from 0.5 to 1.75 and that up to 40 % of diesel consumed during transportation is used by the refrigeration system. The study gave estimation of the energy consumption but did not provide a quantified analysis of the major factors that contribute for the energy waste because of the lack of experimental data.

In another study Tassou et al. (2009) reviewed the current approaches in road food transport refrigeration. They provided estimates of the environmental impact and covered advances in the development of alternative technologies to vapour compression refrigeration systems which has a potential to reduce energy consumption. Similarly, Fitzgerald et al. (2011) estimated the fuel consumption for refrigeration to be 19 % of fuel related to its journey. However, the conclusions had to be based on theoretical and derived data due to the lack of any experimentally measured data on fuel consumption by refrigeration systems in commercial use. Thompson et al. (2010) and Castro et al. (2005) studied the energy utilization in forced air coolers for fruits in storage by applying energy coefficient (EC) and energy added ratio (EAR), respectively.

$$EC = \frac{MC_p(T_i - T_f)}{Ec} \qquad 2.19$$

$$EAR = \frac{E_r + E_v}{E_p} \qquad 2.20$$

Stellenbosch University https://scholar.sun.ac.za

Table 2-1 Best estimate of the top ten food refrigeration processes ranked in terms of their potential for total energy saving (James & James, 2011)

		Energy		Saving	
	Sector	**'000t CO_2/y**	**GWh/y**	**%**	**GWh /y**
1	Retail display	3100-6800	5800-12700	30-50	300
2	Catering – kitchen refrigeration	2100	4000	30-50	2000
3	Refrigerated Transport	1200	4820	20-25	200
4	Cold storage – generic	500	900	20-40	360
5	Blast chilling – (hot)	20-330	310-610	20-30	180
6	Blast freezing – (hot) products, ready	120-220	220-420	20-30	130
7	Milk cooling- (on farm)	50-170	100-320	20-30	100
8	Diary processing – milk/cheese	130	250	20-30	80
9	Potato storage- bulk raw potatoes	80-100	140-190	~30	60
10	Primary chilling – meat carcasses	60-80	110-140	20-30	40

Thompson et al. (2010) applied EC concept which is similar to COP of a refrigeration system except the system boundary is drawn around the entire refrigerated facility. This index accounts for the temperature drop during cooling in addition to the weight of produce cooled. The electricity consumed included the power to operate refrigeration equipment, lights, fans and battery chargers for lift trucks. Heat loads for each operation were calculated using standard procedures

Stellenbosch University https://scholar.sun.ac.za

(ASHRAE, 2009). For product load, the thermal energy load and respiration heat of the fruits will be combined. Transmission load corresponds to the heat transferred through walls, roof, and floor; internal equipment heat load is calculated by adding the loads coming from fans, lights, and fan motor heat production. EAR, considers respiration energy (E_r) (kJ), produce field heat (E_p) (kJ) and ventilation energy (E_v) (kJ), which are independent of the mechanical characteristics of the cooling system, however, it was used to evaluate the effect of packaging container opening and airflow rate on the cooling performance.

Thompson et al. (2010) showed that only 36 % of the total electrical energy was used for fruit cooling purpose and 45 % of total was used to remove the heat generated fans, lights and lift trucks. The authors indicated energy saving can be achieved using variable speed fans (evaporator operates at maximum refrigeration design but mostly less than the maximum capacity is required to achieve the set point), increasing vent area of boxes, using less lighting or efficient lamps. In this study the electricity use data was used smartly to grab on a suffice indicative scientific evidence on the potential energy saving options based on the relationship of the amount of heat load from the system and energy needed to remove that heat load. In this study the airflow pattern, produce temperature heterogeneity and factors that affect the cooling operation such as packaging strategy and design were not considered in the calculation. Castro et al. (2005) reported energy saving options during forced air cooling with respect to packaging design, as ventilation area increased to 8 % the EAR decreased but a small change was observed as opening area increased to 100%. Similarly, Delele et al. (2013) also reported up to 7 % increment of vent area increase the cooling rate significantly. The authors recommended an opening area between 8 and 16 % for energy use optimization.

After analysis of experimental and statistical data available on 2300 TEUs (Twenty-foot equivalent units), Wild et al. (1999) presented individual reefer power consumption 4 kW per TEU for 20 ft. reefer and 7 kW per TEU for 40 ft. reefer. The result shows a significant range of uncertainty. Since TEU was used for

Stellenbosch University https://scholar.sun.ac.za

analysis the mean energy consumption was 3.6 kW per TEU. This value was revised to be 2.7 kW per TEU by Wild et al. (2008). Fitzgerald et al. (2011) assumed a mean energy consumption rate of 2.7 kW per TEU but they have indicated that there is a potential of ±60 % variation. Thermo King Smart Reefer Manufactures reported cooling capacity of the refer (Table 2.2) with respect to types of compressor. The measured power consumption (while cooling banana) vary from 5.3 to 10.7 kW as the set-point temperature varied from -29 °C to 21 °C, respectively (Wild et al., 1999). In another study, using Quest II program was reported to reduce the energy consumption of an apple packed reefer by 56 %, compare to non-QUEST system (Lukasse et al., 2011).

Table 2-2 Shows refrigeration capacities and power consumption for Thermo-King refrigeration units with Scroll w/R404A compressor model (Wild et al., 1999)

Refrigeration Capacity Net cooling capacities at 37.8 °C ambient and 60 Hz electric power (Zer-O™)		
Container Temperature (°C)	Cooling capacity (W, Watt)	Power consumption (kW)
21	13771	10.7
2	9962	9.1
-18	5860	6.1
-29	3809	5.3

Fitzgerald et al. (2011) used equation (2.22) to calculate the fuel consumption resulting from maintaining the refrigerated condition of various products during their transportation. Data for calculation was obtained from concerning authorities and companies (Fitzgerald et al., 2011). The comparative compilation of the calculated energy consumption rates per TEU were presented relative to 2.7 kW per TEU (Table 2.3) as assumed from Wild et al. (2008) (Fitzgerald et al. (2011) cited the use of the assumption by McLaren et al. (2009) in calculation of carbon foot print life cycle assessment). The authors suggested that

Stellenbosch University https://scholar.sun.ac.za

the actual energy consumed by reefers may be between 63 % greater and 52 % less than values calculated in this study and pointed out the area of uncertainty in which there exists little peer-reviewed journal literature available, as most cited values are sourced from the ‘‘grey’’ literature.

$$FC = P * \frac{D}{v} \%MCR * SFOC * \frac{m_{NZ}}{M_{Total} * U} \qquad 2.21$$

Where, FC is the fuel consumption in grams (g), P is the maximum installed engine power of the main or auxiliary engine(s) in kilowatts (kW), D is the distance travelled by the vessel in nautical miles (nm), v is the mean cruise speed of the vessel in knots (nm h^{-1}), %MCR is the mean load on the main or auxiliary engine(s) as a fraction of the engines’ maximum installed engine power, SFOC is the specific fuel oil consumption rate (g kWh^{-1}), m_{NZ} is the mass of individual products imported to or exported from New Zealand on-board each vessel voyage in tonnes (tonnes), M_{Total} is the maximum cargo capacity of each vessel (tonnes) and, U is the mean utilisation fraction of each vessel’s cargo capacity, which calculated by dividing the mean total mass of all cargo on-board a vessel by its maximum cargo capacity (Fitzgerald et al., 2011).

Recently, in an experimental case study of ambient loading of warm citrus Defraeye et al. (2016) compared the standard airflow configuration with two novel airflow strategies namely, channelling and horizontal airflow configurations. The result showed standard and channelling configurations showed similar fruit to cooling behaviour, however the channelling configuration was reported to exhibit less moisture loss from the fruit and better quality. On contrary the horizontal configuration was the worst in all aspects (such as cooling rate of fruit, temperature heterogeneity, and fruit quality). The measured power use of the reefers with standard, channelling and horizontal airflow configurations were 8.9, 9.5 and 8.0 kW (on the first day), 1.7, 1.8 and 1.0 kW (at the end of day 21), respectively. The authors reported higher energy consumption of the reefer, with the channelling

Stellenbosch University https://scholar.sun.ac.za

configuration, could be due to the large amount of heat extracted on the first day but as days go by the cooling units require less energy (Lukasse et al., 2011).

Table 2-3 Evaluated reefers energy consumption rates per twenty-foot equivalent unit (TEU), their consumption proportions and differences, relative to 2.7 kW per TEU (Fitzgerald et al., 2011)

Energy consumption rate (kW/TEU)	Source	Proportion relative to 2.7 kW/TEU
2.7	Wild (2008)	1
1.3	Port Otago monthly minimum	0.48
2.3	Port Otago monthly maximum	0.85
1.7	Port Otago monthly mean	0.63
2.7	Port Otago 40 hr, 6 frozen TEU mean	1
4.4	Port Otago 18 hr, 10 TEU mean	1.63

2.5.2. Mathematical approaches

The experimental study or mathematical model development to predict detailed energy consumption of reefers is extremely difficult due to the range and complexity of the variables that can influence the performance. Some of the factors are detailed by Fitzgerald et al. (2011), such as mechanical and thermal, environmental factors, reefer specification, age of the reefer and James et al. (2006) also listed difficult to model factors such as solar radiation incident on the outside of a container and heat produced by other reefers in various stacking configurations.

Jolly et al. (2000) developed a mathematical model of reefer refrigeration system by creating sub-models for key components and coupling them by governing mass and energy transfer relationships to predict cooling performance. Power consumption, airflow to determine the volumetric flow rate, temperature and pressure were measured. The system of equations developed for the sub-models

Stellenbosch University https://scholar.sun.ac.za

were combined to form integrated system of algorism and solved by Newton-Raphson method. Simulation conducted by varying the internal set temperature while keeping ambient temperature constant (38 °C). The predicted compressor power ranged from 8.63 to 4.42 kW for temperature variation from -18 to 13.4 °C. Deviation of the model predictions from experimental result ranges from -7.8 to +0.16 % and the study did not consider defrost cycle duty, the pressure drop in the load and, heat generation in the reefer. In addition, the steady state simulation made does not represent the dynamic nature of cooling operation, however it has revealed the complexity of modelling energy consumption due to the nature of the process.

Defraeye et al. (2014) evaluated the performance of three different designs of orange packaging containers namely, Standard, Supervent and Ecopack (Figure 2.5) during precooling operation. In the study CFD was used with simplifications on the model to decrease computational cost and Reynolds-averaged Navier-Stokes (RANS) in combination with SST k-ω turbulence model was employed in combination with wall functions. They found sufficient agreement with the experimental which indicates enough accuracy of the model.

The power required for the forced airflow was calculated using equations (2.22) and (2.23) (Defraeye et al., 2014):

$$P_w = \Delta P G_a \qquad 2.22$$

$$\Delta P = \xi_1 G_a^2 + \xi_2 G_a \qquad 2.23$$

Where, P_w is the power required to force air through the computational model, ΔP is the pressure drop is the sum of Forchheimer's inertia term and Darcy's viscous term, G_a is the flow rate through the computational domain ($m^3\ s^{-1}$), ξ_1 and, ξ_1 are pressure loss coefficients.

Stellenbosch University https://scholar.sun.ac.za

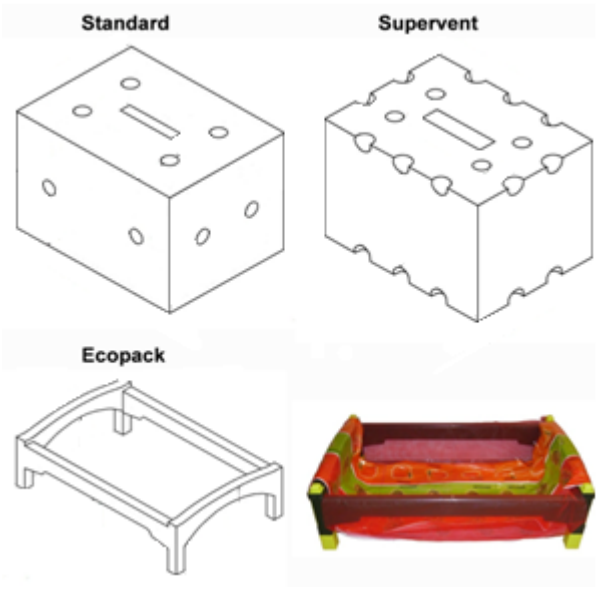

Figure 2-6: Geometry of the boxes evaluated: standard and Supervent corrugated fibreboard containers (CFC) and the Ecopack reusable plastic container (RPC) (Defraeye et al., 2014)

The normalized convective heat transfer coefficient (CHTC) was compared and found the standard container seems to have the highest CHTC followed by Suppervent. The highest CHTC in CFCs was designated to be due to the high air velocity as air pass through the vents (jet effect), however it was shown that high CHTC doesn't necessary means heat transfer operation was efficient because it has caused higher cooling heterogeneity. A container which provides the fastest cooling rate does not necessarily mean it is the best for fruit quality as potentially chilling injury occurs at low temperature operations (Defraeye et al., 2014). At a similar airflow rate fruits packed in an Ecopack container cooled slower due to lower CHTC but minimum heterogeneity. Ecopack showed the lowest pressure drop due to its superiority in open area ratio and with respect to the set temperature energy required to cool to -0.5 °C (sterilization temperature) was 28 % more than the normal cooling to 4 °C (normal treatment temperature). Figure 2.6 depicts a prospect of significant energy savings that was found in the Supervent and Ecopack packaging designs compared with the standard design. The authors recommended

Stellenbosch University https://scholar.sun.ac.za

other packaging design factors such as effect of total open are of the containers needs to be considered for optimized result (Defraeye et al., 2014).

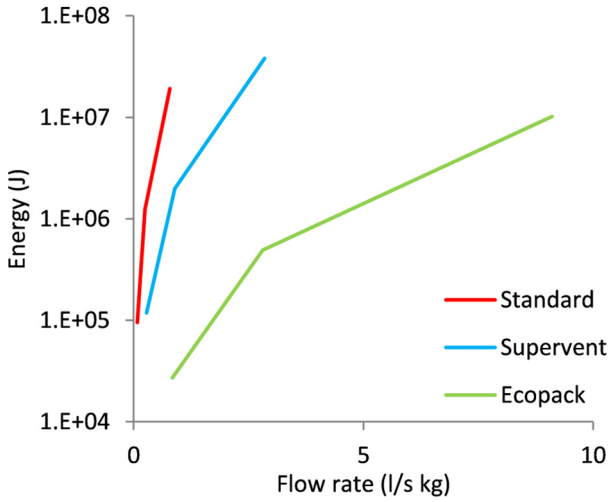

Figure 2-7: Energy required for maintaining the airflow through one layer of CFCs and two layers of RPC containers modelled until the seven-eighth cooling time is reached (Defraeye et al., 2014)

In another study, Defraeye et al. (2015b) evaluated the feasibility of ambient loading of citrus within the context of cold disinfection treatment using theoretical calculation and full-scale experimental study in a 40-foot Mark Q reefer to determine fruit cooling time (seven-eighth cooling time-SECT). In the theoretical calculation of average cooling load ($P_{AVG,7/8,s}$) losses such as heat transfer from the environment, respiration heat (34 W tonnes^{-1}), latent heat due to moisture evaporation, heat loss due to infiltration (42 W K^{-1}), ventilation and heat from evaporator fans and, 10 % safety factor on the total load were included (ASHRAE, 2010; Thompson, Mejia, & Singh, 2010). The authors used peak cooling load (P_{peak}) to account high cooling power requirements at the start of cooling operation due to exponential fruit cooling nature.

$$P_{AVG,7/8,s} = \frac{mc_p(T_{ini} - T_{7/8})}{t_{7/8}} \qquad 2.24$$

Stellenbosch University https://scholar.sun.ac.za

$$P_{peak} = mc_p \frac{\ln(8)}{t_{7/8}} (T_{ini} - T_{air}) \qquad 2.25$$

Where, m is the total mass of oranges in the reefer, c_p is the specific heat capacity of the oranges (3850 J $kg^{-1}K^{-1}$), T_{ini} is the initial temperature of the oranges (20 ℃), $T_{7/8}$ is the resulting SECT (1.2 ℃) and T_{air} is the set temperature of the cooling air (-1.5 ℃). Although experimental result of fruit cooling took 5 days, the theoretical calculation showed the reefer has cooling power (≈10.7 kW) to cool the fruit in less than 5 days. The step-down fruit cooling operation applied for the experimental study (to avoid fruit chilling injury) was suggested for this variation as fruit could not be cooled down quick enough.

2.6. Conclusion

The basic airflow and heat transfer modelling approaches have been covered in this review. Several airflow models have been used in modelling reefer and cold stores. However, in recent years CFD is the dominant modelling tool due to its flexibility and efficiency in its accuracy compared with the others. Basically there are two major modelling approaches in a packed container airflow and heat transfer modelling (Resistance network and CFD), even though there have been a number of other models (Lattice Model, Scaled model). The resistance network modelling was used by several researchers for modelling airflow and heat transfer before CFD became popular and computational power of computers was limited.

Turbulence modelling is complicated and selecting an appropriate turbulence model that is capable of predicting the transport phenomena accurately demands experience and evaluation. A number of turbulence models (such as RSM, K-ε models and, K-ω model) have been used to predict airflow pattern in reefer. RSMs' prediction was found to be closer to experimental results than K-ε model for flows in an enclosed environment such as reefer. However, recently K-ω model appears to be efficient and requires less computational time compared to RSM

Stellenbosch University https://scholar.sun.ac.za

model in postharvest applications. It is interesting to compare the two turbulence models for reefer modelling to study there efficiency, accuracy and in particular prediction capacity of flow separation and attachment in an enclosed environment which is a common problem.

A fully packed reefer has a complicated geometry that makes it very difficult during grid generation if explicit representation is the choice. This is due to the design of packaging boxes that have multi-vents with thin wall and the shape and orientation of tightly packed fruits in packaging boxes. In order to capture the airflow connectivity in the packed pallet correctly it is recommended to have fine grids around the multi-vents with a maximum of 20% growth rate of elements to the neighbouring portion of the container. However, the fine grids will lead to economically unmanageable mesh due to the high size ratio of the packaging boxes and the rest of the domain. Therefore, treating produce packed pallets as a porous medium is the most effective way to model the domain and this modelling approach offers comparatively accurate simulation of fluid flow and heat transfer phenomena in reefer with relatively less computational capacity requirement than the other modelling approaches.

In postharvest handling of perishable products, it is not only maintaining the quality of loaded produce but also the amount of energy used for cooling is important. Different approaches have been used to study energy consumption. Most of the studies conducted to quantify energy consumption are based on the data provided by cold chain facilities and port authorities. The focus of the studies was focused on the average total energy consumed by reefer container transport (not the amount of energy utilized for cooling operation in particular). The information on energy consumption of reefers is useful in maritime carbon-foot printing studies and it adds to the scarce data available. However, in order to find a way to save energy in perishable produce transport, it is essential to quantify the amount of energy utilized for refrigeration operation. The energy consumption estimated for refrigeration operation ranges from 19% to 40% which brings issues of uncertainty

Stellenbosch University https://scholar.sun.ac.za

due to lack of experimental data. The data will give some idea or can be used as guide line but it is difficult to make use of it for meaningful energy saving.

There are a number of factors in postharvest handling such as packaging design, packaging orientation and product property that have direct effect on energy consumption. Therefore, consideration of these important factors, which are critical for both conservation of produce quality and refrigeration energy consumption, in reefer energy quantification study is imperative.

Stellenbosch University https://scholar.sun.ac.za

Chapter 3

3. Experimental and numerical investigation of airflow and heat transfer inside empty reefer*

Abstract

During transportation of fruits and vegetables, factors such as temperature, air exchange, humidity levels, and packaging design and stacking arrangements in the reefer are extremely important to maintain this cold chain. In this study, the airflow and temperature distribution inside two types of refrigerated shipping containers were investigated. CFD model of airflow and heat transfer were developed and experimentally validated. Measurements of airflow velocities and temperatures were taken from 222 sample positions inside a full-size reefer. The validated model was then implemented to study the effect of container designs and operational conditions on airflow pattern and distribution. High and low evaporator fan speed scenarios of two different reefer designs (T-bar floor and flat floor) were investigated and these showed that the airflow distribution in the two container designs were markedly different. The reefer with T-bar floor design exhibited a noticeable reduction of air recirculation zone and enhanced vertical air movement

* Samuel Getahun, Alemayehu Ambaw, Mulugeta Delele, Chris J. Meyer, Umezuruike Linus Opara. 2016. Experimental and numerical investigation of airflow and heat transfer inside empty reefer. International Journal of Refrigeration (Submitted).

Stellenbosch University https://scholar.sun.ac.za

compared to the reefer with flat floor design. The temperature profile in the two reefer designs at high and low evaporator fan speed conditions were spatially uniform due to turbulent mixing of air across the length and the width of the container. Good agreement was found between measured and predicted values of air velocities and temperatures. The root-mean-square errors was between the experimental and the numerical results for vertical ariflow was 1.60. Although presence of produce load can change the flow field in a reefer significantly, the flow characteristics of the air from the inlet into the reefer, its distribution along the length and vertically will still be influenced by the operating and design parameters. The airflow simulation results provide fundamental insights on the effects of these design and operational parameters on the airflow distribution in a reefer.

3.1. Introduction

Refrigerated shipping containers (reefers) are used for long distance transport of fresh fruit from a cold store to a port or vice versa and from a cold store to a supermarket. It is crucial to control the temperature, air flow and moisture inside the reefers to avoid produce quality loss. Control of the environmental condition inside postharvest handling systems such as cold stores, reefers, display cabinets depends on many factors including the thermal insulation of the container (Laguerre et al., 2008), temperature fluctuation (Ambaw et al., 2016), rate of respiration of produce and the air circulation which depends on the design of the reefer (Fitzgerald et al., 2011) and the design and stacking of the packaging boxes (Tanner et al., 2002ab; Tanner and Amos, 2003; Delele et al., 2013ab; Defraeye et al., 2013; Berry et al., 2016).

Reefer usually come in 6.0 m or 12.20 m long (ASHRAE, 2009), with 7.62 cm thick polyurethane insulation in the walls and the floor, and 10.16 cm in the ceiling. Reefers may have different floor design structures (T-bar, castellated plate, perforated and flat with pallet base for airflow), and each floor design has its own advantages and disadvantages (Smale, 2004; Vigneault et al., 2009). The floor design may affect air exchange inside the reefer and in turn the cooling rate, the

Stellenbosch University https://scholar.sun.ac.za

temperature and humidity distributions. Understanding the effect of floor designs on the airflow and cooling characteristics of reefers is therefore very important.

Experimental study of large cooling containers like reefers is time consuming, expensive and can only provide limited information on the flow field (Foster et al., 2002). Application of computational fluid dynamics (CFD) model to study operational and design parameters has become popular in recent decades. Frequently, the actual cooling system is reduced to a realistically simple but accurate model to sufficiently capture important characteristics of the airflow with existing computational capability (Finn and Brennan, 2003). In another study, Smale (2004) compared flat floor and perforated floor reefers by applying resistance network model, however, the static pressure predictions corresponding to the perforated floor reefer showed discrepancies in the under floor region attributed to poor prediction of kinetic energy along measurement difficulties. Moureh et al. (2009 c) employed a 3D CFD model to characterize and show the effect of air duct system on the uniformity of airflow field in refrigerated trailers. The authors reported that the air duct system improved the ventilation homogeneity significantly. In another study, Xie et al. (2006) showed by use of a CFD model that the corner curves in a cool store room improves uniformity of airflow by reducing incidence of eddy formations.

Previous studies on reefer and slot-ventilated enclosures (refrigerated trailers/vehicles) generally assumed fixed working conditions (Moureh and Flick, 2002; Moureh et al., 2009 a, b; Tapsoba et al., 2009). However, reefers are frequently operated at normal or economic mode. Under normal mode, the evaporator fans operate at high speed (at air exchange rate of ≈ 79 h^{-1}) and under economic mode the evaporator fans operate at low speed (at air exchange rate of ≈ 36 h^{-1}). Hence, it is appropriate to study the airflow and heat transfers inside reefers at different operation modes. Furthermore, structure of the floor of the reefer is aerodynamically important and can profoundly affect the airflow distribution inside the reefer (Vigneault et al., 2009). Hence, a more complete knowledge of airflow,

Stellenbosch University https://scholar.sun.ac.za

temperature and moisture transports inside a reefer can be obtained by considering the effects of design and operational parameters. This information can be used in reefer design modifications, to improve packaging designs and loading pattern arrangement.

The objective of this study was to investigate the effects of design and operational conditions on the airflow and temperature distribution inside two types of reefers with different floor designs, namely, T-bar and flat floor. A 3D CFD models of the airflow and heat transfer inside a T-bar floor reefer was developed, experimentally validated and used to characterize the airflow and temperature distribution inside an empty reefer. In addition, the validated model was used to study two operating conditions of evaporator, namely high and low evaporator fan speeds in the T-bar and flat floor reefers.

3.2. Materials and methods

3.2.1. Reefer

This study used the Carrier Transicold bottom-air delivery T-bar reefer (Models 69NT-40-541-306, 314 & 328) for model validation. This reefer has internal dimension of 11.56 m in length, 2.29 m in width and 2.58 m in height. Its external dimensions are 12.19 m in length, 2.43 m in width and 2.89 m in height (Figure 3.1). There are 35 extruded T-bars on the floor that run from the air inlet side to the door side. The shape and dimensions of the T-bar structure is shown in Figure 3.1 (b) and (c). The walls of the container are composed of three different layers of materials (Table 3.1). Polyurethane insulation is used in the middle, sandwiched between stainless steel and aluminium metal sheets.

There are different operational modes for the reefer. The action taken by the operational software based on the interaction of the input variables that come from temperature and pressure sensors and temperature set point is called mode. These operation modes include perishable (>-10 °C) and frozen mode (<-10 °C) (Manufacturer's operation and Service Manual).

Stellenbosch University https://scholar.sun.ac.za

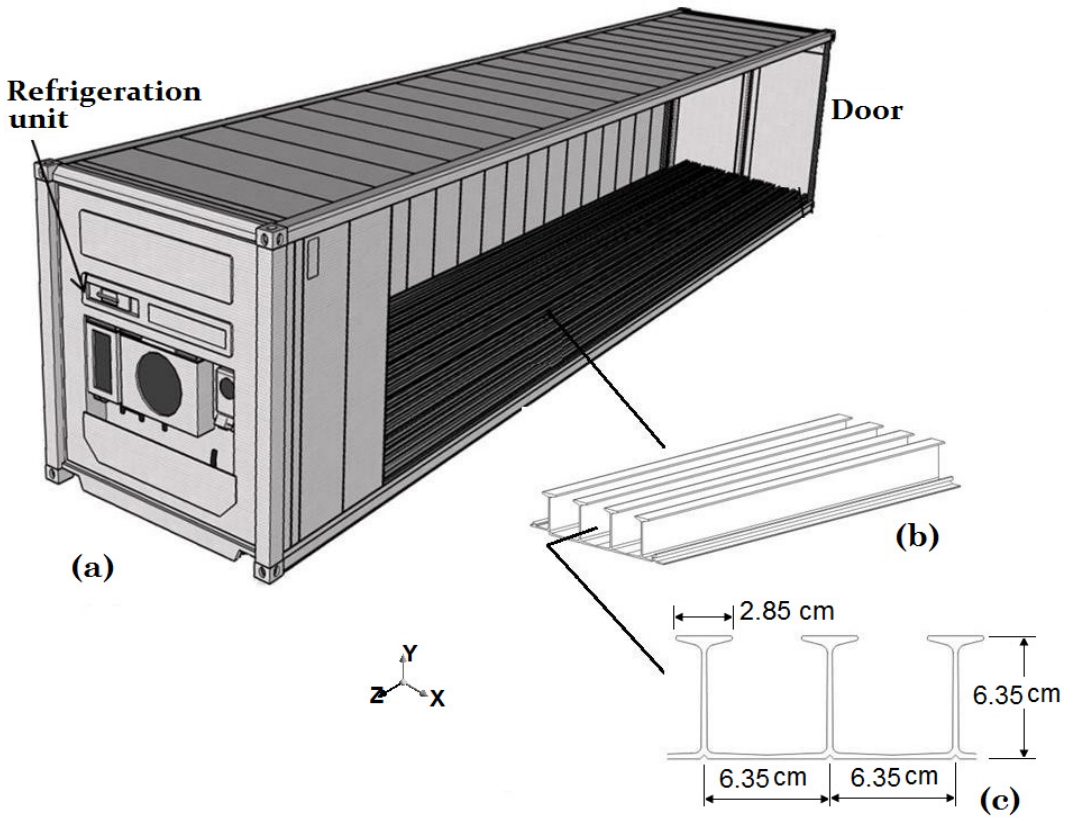

Figure 3-1: Schematic showing the Carrier Transicold bottom-air delivery T-bar reefer (Models 69NT-40-541-306, 314 & 328) (a), closer view of the T-bar floor structure (b) and the cross sectional view showing the dimensions of the T-bar (c).

Stellenbosch University https://scholar.sun.ac.za

Table 3-1: Reefer wall materials and corresponding thicknesses (ASHRAE, 2010)

Location	Surface	Material	Density (kg m^{-3})	C_p (W $(kg.K)^{-1}$)	k (W $m^{-1} K^{-1}$)	Thickness (mm)
Side Walls	Outer	Stainless steel/MGSS*	8005	425	15	1
	Middle	Polyurethane	30	1400	0.025	76
	Inner	Stainless steel/HGSS*	7600	425	15	1
Ceiling	Outer	Stainless steel/MGSS	8005	425	15	1.5
	Middle	Polyurethane	30	1400	0.025	100
	Inner	Aluminium	2702	896	167	1
Floor	Outer	Stainless steel/ Corten	8000	425	15	1.5
	Middle	Polyurethane	30	1400	0.025	76
	Inner	Aluminium	2702	896	167	1
Door	Outer	Stainless steel	8005	425	15	1.6
	Middle	Polyurethane	30	1400	0.025	78
	Inner	Stainless steel/HGSS*	7600	425	15	1
Refrigeration unit side	Outer	Stainless steel	8005	425	15	1
	Middle	Polyurethane	30	1400	0.025	85
	Inner	Aluminium	2702	896	167	1

**MGSS-muffler grade stainless steel*

***HGSS-High Grade Stainless Steel*

Stellenbosch University https://scholar.sun.ac.za

3.2.2. Measurements

3.2.3. Airflow

Airflow measurements were conducted using TVS 1100 data logger with candle stick sensors with accuracy ± 2% and measuring range 0-20 m s^{-1} as calibrated by the supplier (Advanced Thermal Solutions Inc, Norwood, USA). Cooling air enters the refrigerated container with average inlet velocity of 8.5 m s^{-1} and volumetric flow rate of 5416 m^3 h^{-1}. There were 198 measurement points in total on the three levels on grid positions as shown in Figure 3.2a. The sensors were arranged in three levels vertically (near the T-bar floor, 1 m above the floor and 2 m above the floor) and axially a row of sensors were positioned at 1 m distance from each other starting from the refrigeration unit as shown in Figure 3.2a. In addition, 12 measurement points each were used at the inlet and outlet regions.

3.2.4. Temperature

Temperature was monitored using T-type thermocouples with a 34970A data acquisition unit (± 0.1 °C; Agilent Technologies, Santa Clara CA 95051, USA) (Figure 3.2). Measurements were taken from ninety-nine grid positions as shown in Figure 3.2a. The sensors were arranged in three levels vertically (near the T-bar floor, 1 m above the floor and 2 m above the floor) and axially sensors were positioned at 1 m distance from each other starting from the refrigeration unit as shown in Figure 3.2a. The candle stick sensors were positioned at a spot by attaching them on thin bars using scotch tape to support the sensors against the air flow. Thin bars were used to minimize interference. Temperature data was logged every 30 seconds for 1h. In addition, air velocities at the inlet and outlet sections of the refrigeration unit were measured by placing sensors at 12 grid points at the inlet and outlet cross sections.

Initially, the air inside the reefer was kept at 18 °C. During the experiment the reefer was set to operate at high evaporator fan speed and the make-up air inlet was totally closed to minimize environmental effect. The set point for the cooling

Stellenbosch University https://scholar.sun.ac.za

air was then switched to -0.5 °C for the cooling experiment. The refrigeration unit circulates the air inside with an average inlet air velocity of 8.5 m s^{-1} and volumetric flow rate of 5416 m^3 h^{-1} to pool the temperature down to the set point.

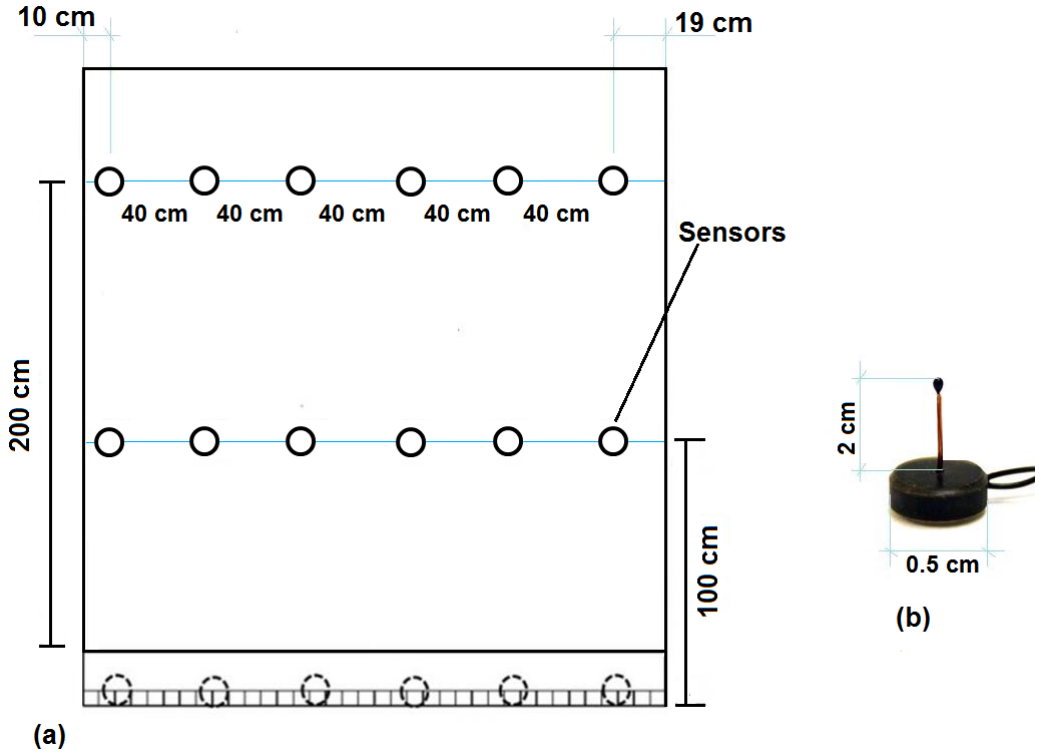

Figure 3-2: Schematics showing the position of the velocity and temperature sensors inside the T-bar reefer (a) and the candlestick sensors (b). A total of ninety-nine measurement points were used.

3.3. Model formulation

3.3.1. Assumptions

The following basic assumptions were made during the model formulation.

- The outside environment was assumed constant at an average temperature of the ambient air 18 °C, pressure of 101 kPa and relative humidity of 80 %. This ambient condition is a common daily average values during the period (winter) of the experiment which was in the month of July in Stellenbosch, South Africa.

Stellenbosch University https://scholar.sun.ac.za

- The cooling unit was accounted for in the model by using the measured conditions (temperature and air velocity) at the inlet and outlet of the cooling unit to specify the inlet and outlet boundary conditions of the CFD model.
- Thermal radiation exchange between the exterior surface and the surroundings was neglected since the outer surfaces of the walls of the reefer were painted white and the reefer was not exposed to direct sunlight.
- The physical properties of air were assumed constant for the temperature and pressure ranges of the experiment.
- The RANS k-ω shear stress (k-ω SST) model was used to model turbulence in the domain. This turbulent model perform best in postharvest CFD applications (Zhang et al., 2007b; Ambaw et al., 2013; Delele et al., 2013b).
- Heat conduction through the walls, floor, door and ceiling was calculated based on an average outside air temperature of 18 °C. The insulation on all boundaries was calculated based on the type of material and its thickness.
- Since the air circulation fans were positioned upstream of the evaporator coil (a blow-through configuration), the fan heat was assumed totally removed directly by the evaporator coil.
- Heat loads due to lighting and other activities were not considered in the model since in practice, the reefers are not opened during the experiment, and there are no lights, and activities within the reefers are minimal.

3.3.2. Governing equations

The airflow and heat transfer in the domain are governed by the mass, momentum and energy conservation equations given by Eqn. (3.1), Eqn. (3.2) and Eqn. (3.3), respectively (Versteeg and Malalsekera, 1995). Density of air was assumed constant at the cooling air temperature (≈ 272.65 K).

$$\nabla \boldsymbol{u} = \mathbf{0} \tag{3.1}$$

Stellenbosch University https://scholar.sun.ac.za

$$\frac{\partial \mathbf{u}}{\partial t} + \nabla.\left((\mathbf{u} \oplus \mathbf{u})\right)\nabla.\left(\left(\frac{\mu + \mu_t}{\rho}\right)\nabla \mathbf{u}\right) = \mathbf{s}_U - \frac{1}{\rho}\nabla p \qquad 3.2$$

Where, **u** is the vector of the velocity (m s^{-1}), t is time(s), μ is the dynamic viscosity of air (kg $m^{-1}s^{-1}$), μ_t is the turbulent eddy viscosity (kg $m^{-1}s^{-1}$), p is pressure (Pa) and $\mathbf{S}_U$ (m s^{-1}) is momentum source term.

$$\rho_a C_{p,a}\left(\frac{\partial T}{\partial t} + U.\nabla T_a\right) = \nabla.((k_a + k_t)\nabla T_a) + S_e \qquad 3.3$$

where C_{pa} (J $kg^{-1}K^{-1}$) is the heat capacity of air, , ρ_a (kg m^{-3}) is the density of air, T_a (K) is the air temperature, k_a(W $m^{-1}K^{-1}$) is the thermal conductivity of air, k_t (W $m^{-1}K^{-1}$) is the turbulent thermal conductivity and S_e (W m^{-3}) is the energy source term, $S_e = 0$. The turbulent thermal conductivity, through the empirical turbulent Prandl number (Pr), is a function of the turbulent viscosity ($k_t = \frac{\mu_t C_{Pa}}{Pr}$). To calculate this turbulent viscosity, the shear stress transport (SST) k-ω turbulence model was chosen based on Zhang et al. (2007ab), Delele et al., (2008) and Defraeye et al., (2013), that showed this model to be superior in comparison to the k-ε or k-ω turbulence models. The relevant model parameters and their values are summarized in Table 3.2.

3.3.3. Geometry, boundary and initial conditions

Figure 3.3 illustrates the model geometry and the boundary conditions for a reefer at high evaporator fan speed. The model explicitly incorporated the detailed structure of the floor structures. The model contains a fluid domain bounded by the reefer walls, door, ceiling, floor, inlet air baffle plate and the side wall of the refrigeration unit.

The inlet of the fluid domain in the computation was specified from measured velocity and temperature values at exit of the evaporator fan. The exit of

Stellenbosch University https://scholar.sun.ac.za

the fluid domain in the computation was specified by velocity boundary in such a way that the mass flow in and the mass flow out from the reefer was balanced.

For a set temperature of -0.5 °C, the supply air temperature of the cooling air entering a reefer drops until it is in-range. Therefore, measured average temperature evolution of the supply air that drops from the initial temperature of 18 °C to the set temperature was specified for the inlet temperature. The inlet air temperature was specific using UDF (user-defined function) to account for the supply temperature evolution to the set temperature. Table 3.2 summarizes the inlet and outlet boundary conditions.

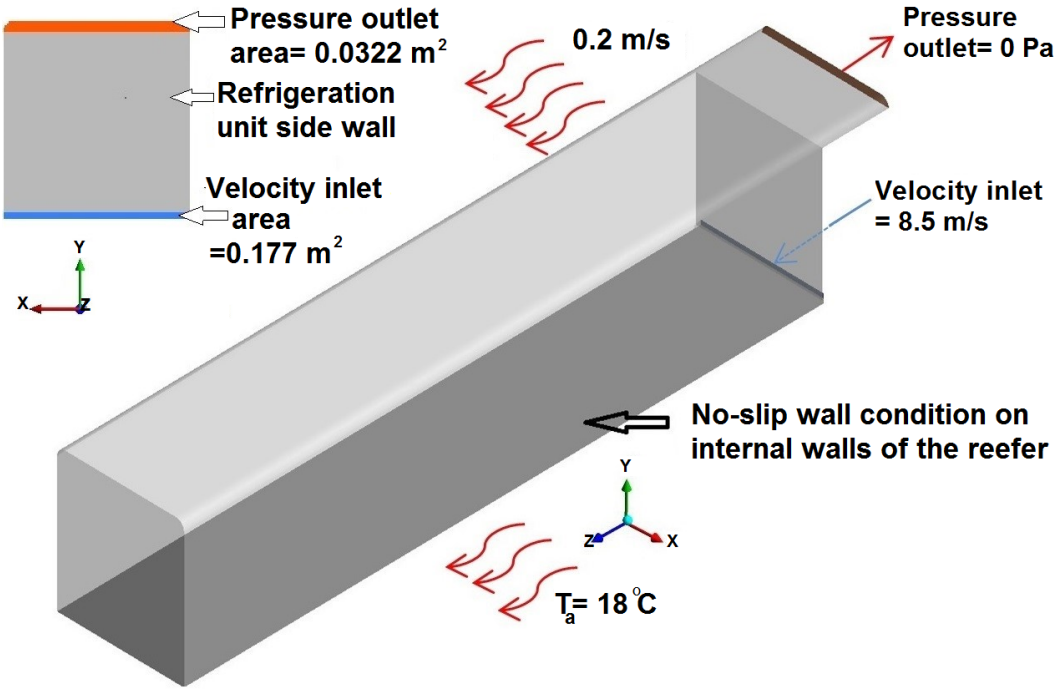

Figure 3-3: Schematics of the model geometry corresponding to a reefer at high evaporator fan speed. The model explicitly incorporated the detailed structure of the reefer floor

Turbulence intensities (I_t) at the inlet and outlet are calculated based on the air velocity measurement that were monitored at 12 equal positions on both boundaries at high evaporator fan speed. Sample data (n=200) was recorded for a

Stellenbosch University https://scholar.sun.ac.za

specified period (10 minutes) and the I_t at each position was calculated using the respective root mean square and the average velocity (Table 3.2). The I_t's at each measurement point for both boundaries are averaged to determine the average turbulent intensity for each that will be used at the inlet boundary. For low fan speed levels the I_t was calculated assuming a fully developed flow at the inlet and outlet.

Table 3-2: Boundary conditions

Boundary conditions	Evaporator fan speed	Inlet	Outlet	Remark
Velocity, v ($m\ s^{-1}$)	High Low	8.5 $m\ s^{-1}$ 4.0 $m\ s^{-1}$	-	Experimental Calculated
Turbulence intensity (I_t)	High (a) Low(b)	8.56% 3.86%	3.87% 3.87%	Experimental Calcualted
Temperature	High	Step wise decrease (T_i =291.15 to T_f=271.65 K)	Back-flow Back-flow Temperature ($T_{initial}+T_{set}$)/2=282 K	Inlet (Experimental) Outlet (Assumed)
	Low	-	-	Inlet (Experimental) (outlet) (Assumed)

(a)Calculated from experimental result. Averaged turbulence intensity, $I_t = \sum_{i=1}^{n} \frac{RMS}{\bar{v}}$ where RMS is the Root mean square given by $RSM = \sqrt{\frac{\sum(v_i-\bar{v})^2}{N}}$, where

Stellenbosch University https://scholar.sun.ac.za

v_i (m s^{-1}) is the instantaneous velocity magnitude and $\bar{v}$ is average velocity (m s^{-1}) (Versteeg and Malalasekera, 1995)

(b) Calculated from (Florez-Orrego et al., 2012): $I_t = \frac{0.16}{Re^{\frac{1}{8}}}$, where Re is the Reynolds number given by $Re = \frac{H_d v \rho_a}{\mu}$, where μ is the dynamic viscosity (kg $(ms)^{-1}$), $H_d = \frac{4 \times A}{P_w}$, where A is area ($m^2$) and P_w is wetted perimeter (m)

$$Q = \frac{\Delta T}{R_{tot}} = \frac{\Delta T}{\frac{2\Delta x_1}{k_1 A_1} + \frac{\Delta x_2}{k_2 A_2} + \frac{1}{h_o A_o}} \quad 3.4$$

The walls, ceiling, floor, door and surfaces of the cooling unit were considered as no slip boundaries. The heat fluxes at the container walls, floor and door were calculated based on Fourier's Law (Eqn. 3.4). Where, k_1 (W (m K) $^{-1}$) is thermal conductivity of the outer and inner wall material, k_2 (W (m K) $^{-1}$) is thermal conductivity of polyurethane which is sandwiched between the outer and inner wall, h_o (W $m^{-2}K^1$) is the convective heat transfer coefficient between the outside surface and ambient air, A_1 (m^2) is the area of the inner surface of a wall, A_2 (m^2) is the area of the middle (polyurethane) layer of a wall and A_0 (m^2) is the area of the outer surface of a wall.

$$Nu = 0.037 Re^{0.8} Pr^{1/3} \quad 3.5$$

The convective heat transfer coefficient was calculated assuming turbulent flow over a flat plate (Eqn. 3.5) (Bird, 2002). Where Nu is the Nusselt number, Re is the Reynold's number and Pr = 0.69 is the Prandtle number. Air velocity near the wall at the experimental site was ≈ 0.2 m s^{-1} and the average ambient temperature was 291.15 K. The airflow on the outer walls of the container was low because two of its walls were bounded by a building next to it and there is a tree that shades most of the container's body.

Stellenbosch University https://scholar.sun.ac.za

Property of air at the film temperature 281.9 K are, $\Pr = 0.707$ $\mu = 1.76 \times 10^{-5}$ kg (m s)$^{-1}$ $\rho = 1.265$ kg m^{-3} k= 0.0255 (W (m K)$^{-1}$).

Assuming $A_1 = A_2 = A_0 = A$, an overall heat transfer coefficient $U = \frac{1}{R_{tot}A}$ can be used to simplify Eqn. 3.5. Table 3.3 summarizes the calculated overall heat transfer coefficients for the walls of the reefer.

Table 3-3: Calculated overall HTC for heat flow through the container wall based on the material property (Table 3.1) and ambient condition (291.15 K)

Location	U, W m^{-2}K^{1}
Walls	0.31
Door	0.30
Ceiling	0.28
Floor	0.22

3.3.4. Mesh generation, sensitivity analysis and simulation

Model geometry was developed using ANSYS® DesignModeler™ Release 16.0 (ANSYS, Canonsburg, PA, USA). Discretization of the computational domain was based on the flow characteristics, structure of geometry and modelling approach. Fine mesh was used in the regions where large velocity gradients were expected such as the inlet and outlet of both the T-bar and flat floor reefer models. The T-bar floor design model required extra finer mesh and on narrow structures of the T-bar surfaces. Discretization of the domain was on ANSYS® Meshing™ Release 16.0 and the problem setup and simulation was on ANSYS® Fluent™ Release 16.0 (ANSYS, Canonsburg, PA, USA).

Hybrid grid was used for discretization of the computational domains of the T-bar floor and flat floor design models. Richardson extrapolation method (Franke et al., 2007; Roache 1994) was used to measure the level of grid independence. Grids of 7 million and 5 million cells, which corresponds to discretization errors of 5.2 and 5.0 % in estimating heat fluxes through boundaries of the T-bar floor and flat floor domains, respectively, were used.

Stellenbosch University https://scholar.sun.ac.za

First, the airflow inside the container was solved assuming a steady state condition. Then, the steady state airflow condition was used as an initial condition to the subsequent transient heat transfer calculation. The transient heat transfer was conducted merely for model validation purpose. SIMPLE discretization scheme was used for pressure-velocity coupling and second order upwind discretization was used for momentum, specific dissipation rate and energy calculations. The transient simulations were run for 24 hours with a time step of 1 s using a computer with 12 core Intel Xeon processor (3.30 GHz) and 40GB Ram.

3.4. Result and discussion

Model validation was conducted using the T-bar floor design reefer operating at high evaporator fan speed condition (5416 m^3 h^{-1}). Furthermore, the validated model was used to evaluate high and low evaporator fan speeds (section 3.2 and section 3.3 respectively) in T-bar and flat floor design reefer models.

3.4.1. Inlet air flow

The cooling air enters the container horizontally (perpendicular to the inlet face) with high velocity (≈ 8.5 m s^{-1}) as a jet. The jet decays along axial direction because it interacts with the surrounding air and solid surfaces and losses momentum. This characteristic is commonly expressed by a ratio of the local velocity component (u_w) in the jet direction to the inlet velocity magnitude (U) as shown in Figure 3.4 for the T-bar floor reefer. The model captured the pattern of the jet decay accurately but with a significant over predictions between 2 m and 8 m. This region was a primary air recirculation region where air velocity measurements were highly uncertain. The error bar shows the standard deviation of duplicated tests that ranges between 0 to 0.28 m s^{-1}. Both the experiment and simulation estimated the jet decay (flow separation) from the floor ≈9 m (3 L/4), assuming jet flow separation from the wall when u_w/U gets below 0.1 (Yu and Hoff, 1999).

Stellenbosch University https://scholar.sun.ac.za

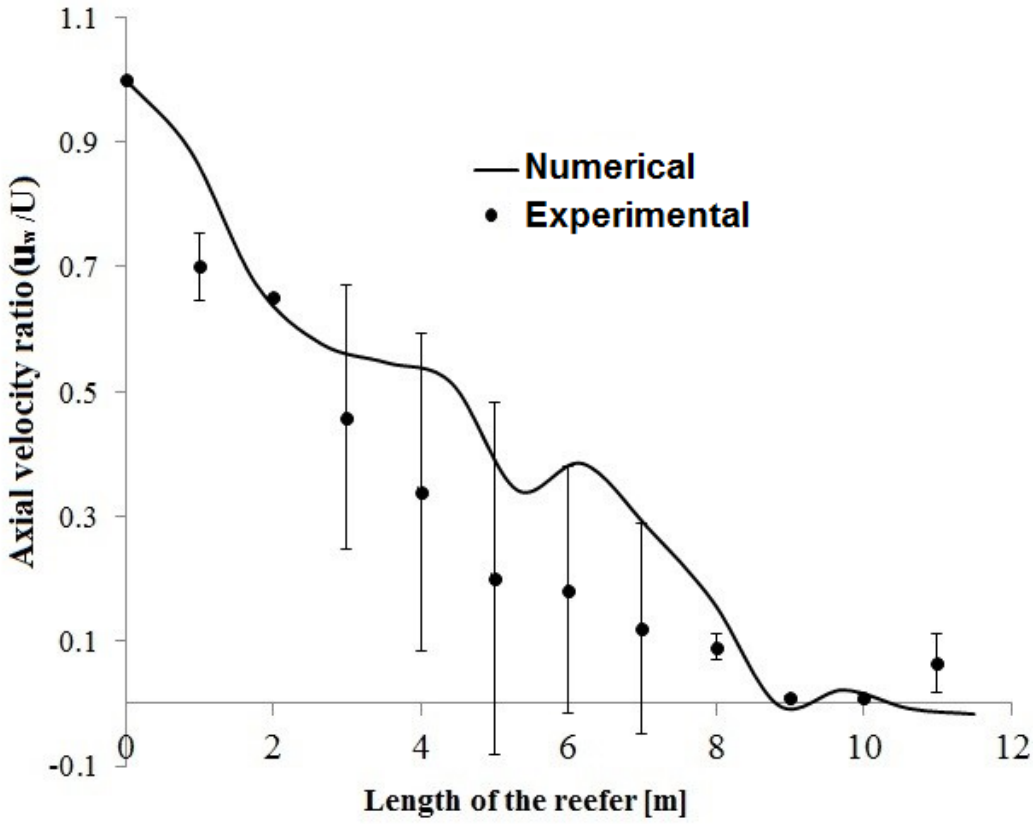

Figure 3-4: Velocity decay of the air jet from the cooling unit into the T-bar floor container at high evaporator fan speed. Numerical and experimental results

3.4.2. Air velocity distribution inside the reefer

Air velocities measured along the reefer length at a 1 m distance from each other starting from side inlet to the door side (from 1 m to 11 m) and at 3 levels (bottom (In the T-bar structure)), middle (1 m) and top (2 m)) above the floor (Figure 3.2). Such measurements taken at 1, 3, 6, 8, 9 and 11 m axially (along Z-axis) from the inlet side to the door side are presented. Figure 3.5 shows the experimental and simulated air velocity magnitudes. A good agreement between the measured and the simulated results was obtained. The root-mean-square error between the experimental and the numerical results for the positions shown in Figures 3.5 and 3.6 were 1.60 and 0.3 respectively. Near the inlet region the airflow tends to cling to the floor as it moves horizontally due to Coanda effect. Coanda effect is the phenomena in which a jet flow adheres itself to a surface and remains

Stellenbosch University https://scholar.sun.ac.za

attached even when the surface moves away from the initial jet direction (oblique contact) (McMillan and Considine, 1999). At 3 m from inlet side, air velocity in the top portion of the reefer was significant. From 3 to 6 m along Z-axis (see Figure 3.5 (a) to (c)) the airflow pattern was similar; higher near the floor, lower in the middle and higher in the top region. This was due to the high velocity of the inlet air stream at the bottom and the returning air stream at the top. Then, the air velocity was observed to be more uniform from about 6 m onward (see Figure 3.5 (c) to (f)).

Figure 3.6 shows the measured and simulated air velocities distribution at two positions across the width. Both were taken one meter above the floor, one was in the middle (0.5 width) (Figure 3.6a) and the other at two third of the reefer width (from the right side wall) (0.75 width) (Figure 3.6b). The two air velocity distributions show the variation of the air velocity magnitude across the width of the reefer. The air velocity at middle was higher due to diminishing influence of wall shear stress on the flow field compared from the wall to the middle of the reefer.

The numerical result has managed to capture the peek air velocity that was resulted from the sharp upsurge of separating flow. Unless the exact flow separation region was known already and sensor at that position was orientated in such way that it can capture the vertical flow. A small positional error in the sensor can lead to high discrepancy (Hoang et al., 2015). Therefore, in the region where separating flow has significant influence a sensor that was also positioned vertically was not well influenced by the vertical flow (V_v). Similar measurement errors were also reported by Hoang et al. (2015) in cold room loaded with pallets.

Stellenbosch University https://scholar.sun.ac.za

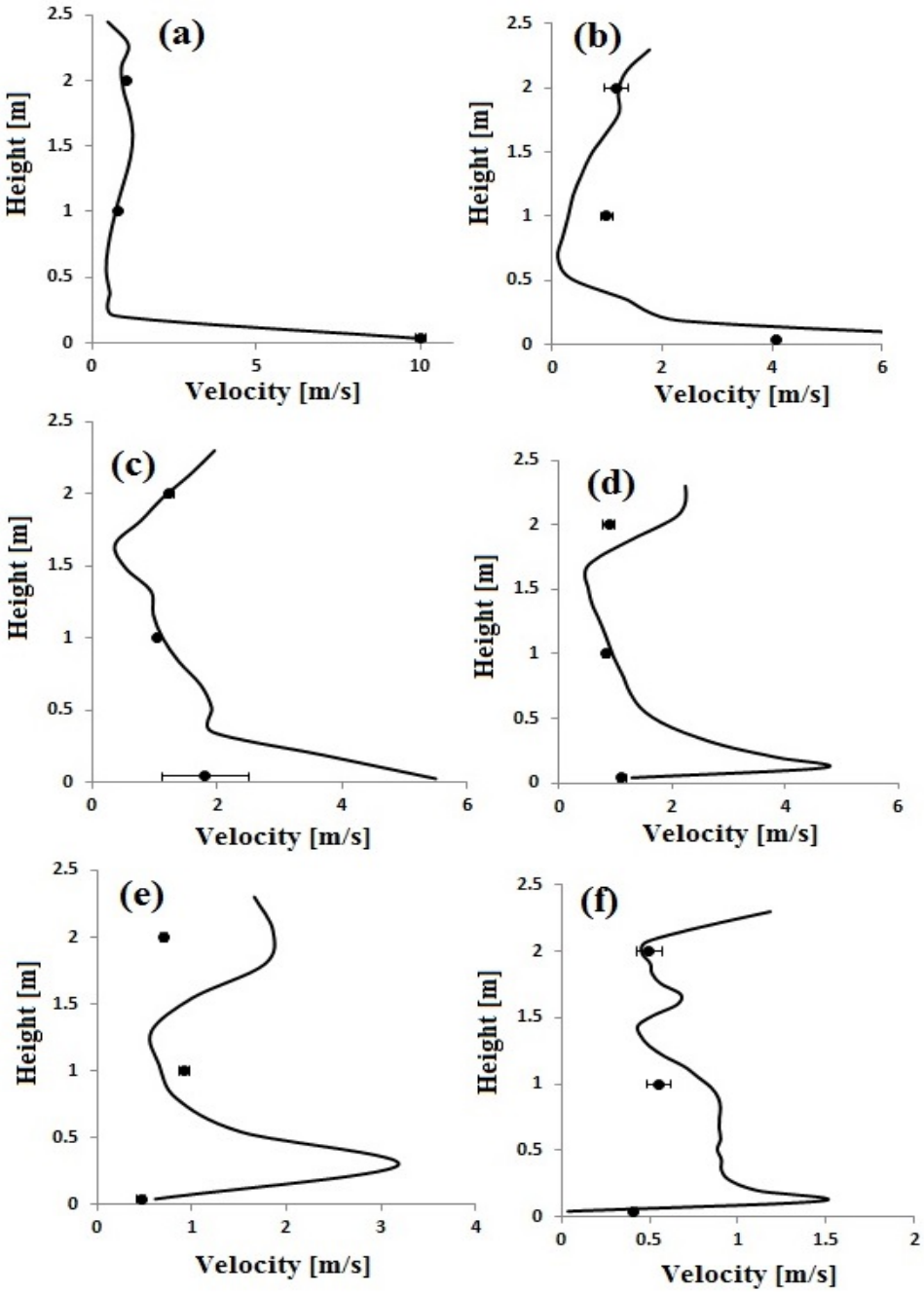

Figure 3-5: The experimental (symbols) and simulated (solid curves) magnitudes of air velocities as a function of vertical and axial locations inside the T-bar floor reefer. The locations are 1m from the inlet face (a), 3 m (b), 6 m (c), 8 m (d), 9 m (e) and 11 m (f)

Stellenbosch University https://scholar.sun.ac.za

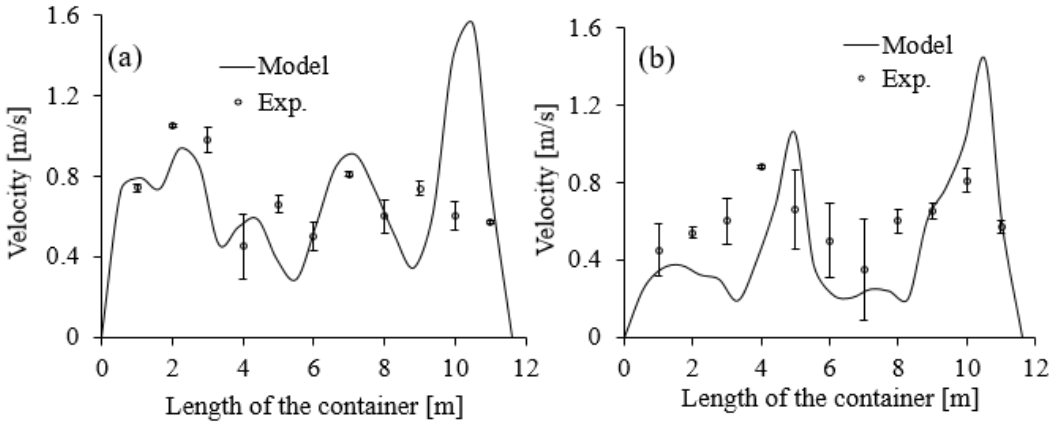

Figure 3-6: Air velocity magnitude on a line one meter above the floor at 0.5 of the width (a) and two third of the width (b)

3.4.3. Temperature distribution inside the reefer

Figure 3.7 shows the measured and simulated temperature inside the reefer under high evaporator fan speed operation (at air exchange rate of ≈86 h^{-1}) during cooling. There was good agreement between measured and simulated temperature (Figure 3.7) with a root mean square error of 0.48.

It took 26 minutes to cool the air inside the T-bar floor design reefer to the set temperature (-0.5 ℃) and the cooling rate observed was spatially uniform. Nevertheless, a marginal slower cooling of the air was noticed near the door side ≈11 m, (outermost region from the cooling air inlet) compared to other positions. This was due to low airflow distribution in the region which resulted from short circuiting of the cooling air at flow separation where majoring of the cooling air recirculates back. The temperature difference between the maximum (door side≈11 m) and the minimum temperature (inlet side) in the reefer was 0.4 ℃ during cooling period. This was due to the fact that the reefer was empty. Due to this, the same cooling characteristics were also observed in the T-bar floor design reefer at low evaporator fan speed and for flat floor design reefer (high and low evaporator fan speeds). Therefore, experimentally recorded temperature profile in the T-bar

Stellenbosch University https://scholar.sun.ac.za

floor design reefer was used for model validation and the study focussed on airflow distribution.

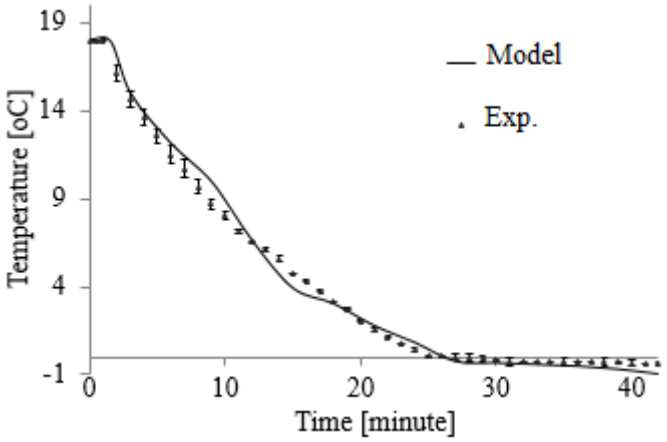

Figure 3-7: The measured and simulated temperature of the air cooling inside a T-bar floor reefer under high evaporator fan speed operation (at air exchange rate of ≈ 80 h^{-1}) were compared. Temperature was measured were averaged over the volume of the reefer

3.4.4. Airflow characteristics under high evaporator fan speed

The effect of reefer's floor design on airflow profile in a reefer was studied at high and low evaporator fan speed conditions. In this section (section 3.2) the airflow profile in the validated T-bar floor design reefer model and that of a flat floor design reefer model are compared at high evaporator fan speed. In following section (section 3.4.5) the airflow profile in these reefer models under low evaporator fan speed will be presented.

Figure 3.8 a & b depicts the air flow profiles on a vertical plan bisecting the T-bar floor and the flat floor reefers under high evaporator fan speeds, respectively. Under this condition the evaporator operates at an air flow rate of 5400 m^3 h^{-1} (air exchange rate of ≈ 80 h^{-1}). The main air stream (F1) sustained up to about 8 m in the T-bar (Figure 3.8a). For the T-bar floor 96 % of F1 separated from the floor and the remaining 4 % (in the T-bar structure (F4)) formed a small recirculation zone at the bottom corner of rear part. This recirculating flow has evidently reduced size of

Stellenbosch University https://scholar.sun.ac.za

the dead zone in the rear part of the reefer by increasing the airflow rate coming through the section z=9.5 m from 0.2 to 0.6 $m^3 h^{-1}$. In the flat floor design model F4 was absent and there was only one large, low airflow secondary recirculation.

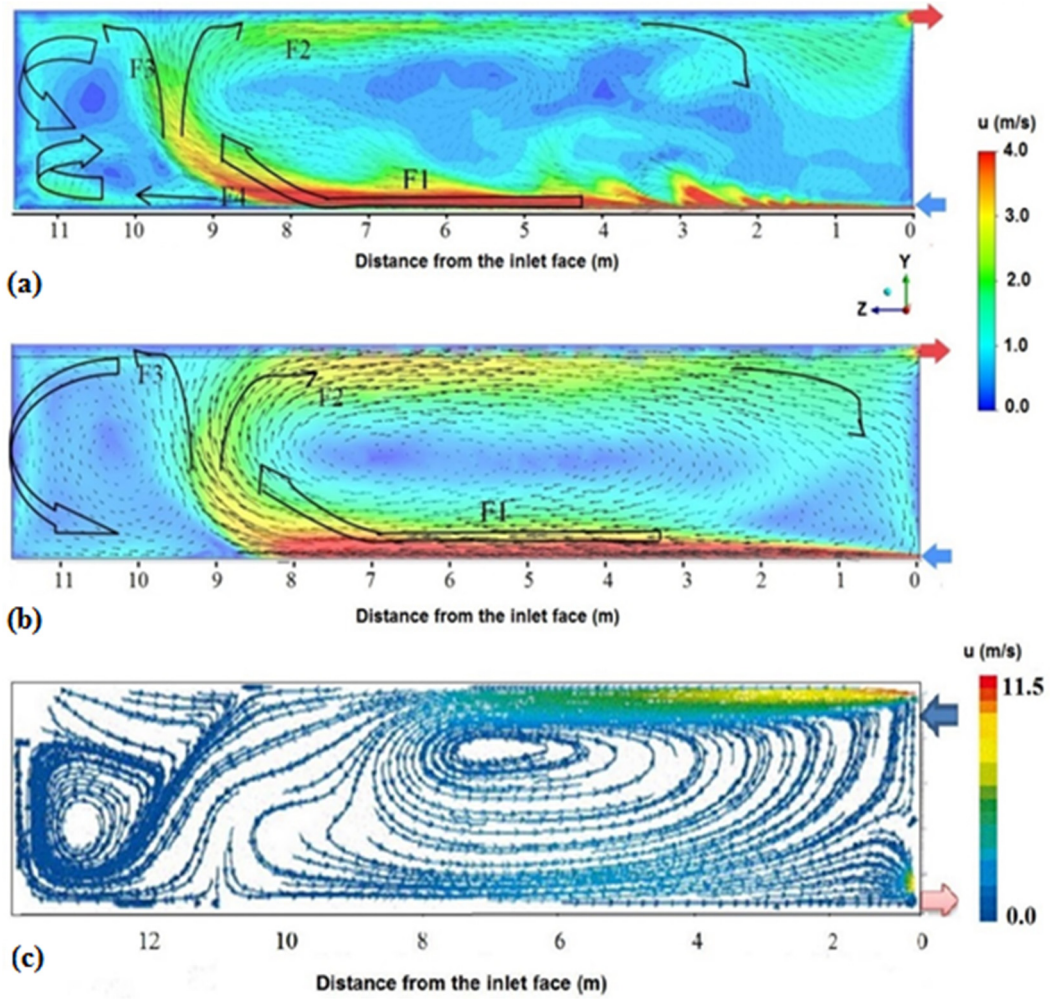

Figure 3-8: Simulated airflow pattern on a section plane bisecting the reefers. Simulation results corresponds to, a) T-bar floor model and, b) Flat floor model reefers operating at high evaporator fan speed (c) airflow pattern for empty slot ventilated enclosure (Moureh et al, 2002) at Inlet velocity =11.5 m s^{-1} (comparable to high evaporator fan speed)

The separated stream divided into two streams (F2 and F3) when it reached the ceiling. F2 formed the returning air stream with some part of it recirculated and joined the main stream (F1). This phenomenon created a primary circulation zone

Stellenbosch University https://scholar.sun.ac.za

in the middle region of the domain. On the other hand, F3 which was approximately a quarter of F2, in terms of mass flux, flew along the ceiling and down the door to form a secondary circulation zone. The primary circulation zone was stronger and covers wider region than the secondary circulation. The magnitudes of air velocities in the core of the primary circulation zone ranged from 0 to 0.85 m s^{-1}. The airflow pattern captured for the flat floor design model at high evaporator fan speed and T-bar floor at low evaporator fan speed (section 3.3.1) were found to be similar to the numerical result of found by Moureh et al. (2002) at high fan speed operation (5500 m^3 s^{-1}) for a top air delivery and flat ceiling system (Figure 3.8 c).

In both reefer models the weakest vertical flow regions were observed near the inlet region (≈1 m from the inlet) and near the door (≈ 11 m from the inlet). Also, the air velocity was essentially horizontal with a negligible vertical velocity component near the inlet region due to the Coanda effect and the inlet air baffle plate. Near the door, due to flow separations and recirculation the region was a dead air zone. Though the airflow profiles in the two reefer designs were considerable similar, there were some important differences. Particularly in the primary recirculation region, (3 to 6 m from the inlet side) the air velocity in the T-bar floor design model was 25 % higher than that in the flat floor design model. Notice also the additional small circulation zone at the bottom corner of the rear part of the T-bar reefer.

The key difference between the two reefer designs was revealed by evaluating the vertical airflow magnitude (Figure 3.9). There were distinctive successions of high vertical flow regions when going from inlet side to the door side in the T-bar floor design model (Figure 3.9a). A good deal of the cooling air flowed upward through the T-shaped structure. Vertical airflow is crucial to increase airflow uniformity and to maintain packed produce at desired temperature (Defraeye et al., 2015a, b). Such upward directed flow streams were lacking in the flat floor reefer (Figure 3.9 b). These was due to better adherence of incoming cooling air jet on the smooth surface of the flat floor by the Coanda effect than on

Stellenbosch University https://scholar.sun.ac.za

the T-bar floor (Tapsoba et al., 2007) which resulted the cooling air jet to flow axially towards the rear without appreciable vertical motion. This has impact on the cooling air distribution and cooling operation, particularly in fruit loaded reefer where cooling air mainly flows thought the packed produce from bottom to top (Defraeye et al., 2015 a,b).

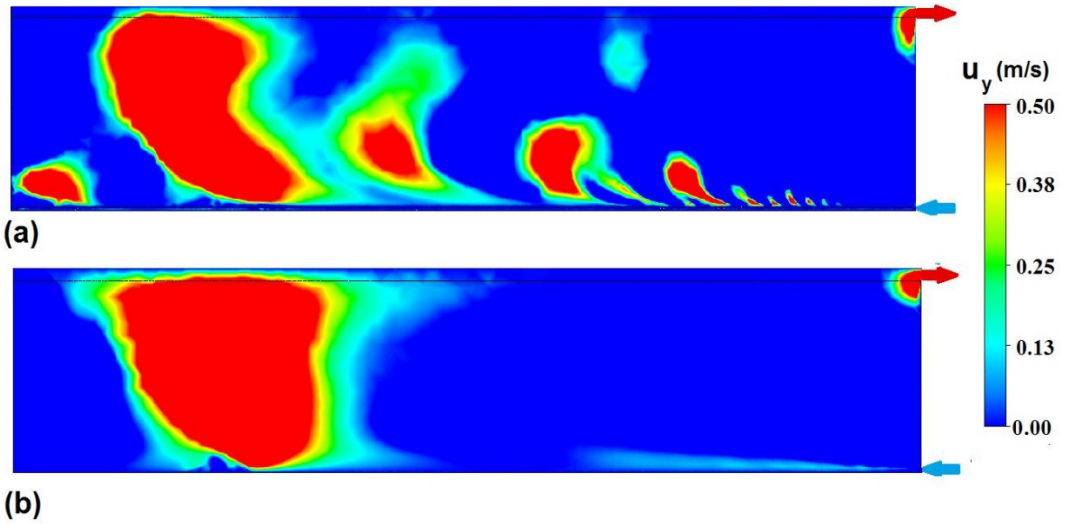

Figure 3-9: Contours of magnitudes of vertical air velocity on section plan bisecting the T-bar floor reefer (a) and flat floor reefer (b). Simulation corresponds to the reefers working at high evaporator fan speed with an air flow rate of 5400 $m^3 h^{-1}$ (air exchange rate of ≈ 80 h^{-1})

Figure 3.10a compares the jet flow characteristics of the cold air entering the reefers at high evaporator fan speed. The jet velocity of the T-bar floor design model was higher velocity up to 5.7 m. Afterwards the jet velocity in the flat floor was greater than that in the T-bar floor design model. This was due to strong primary recirculation zone in the flat floor reefer which influenced the jet flow characteristics significantly. The effect of the recirculation zone was limited in the T-bar model due to the relatively weak recirculation caused by the floor structure.

Stellenbosch University https://scholar.sun.ac.za

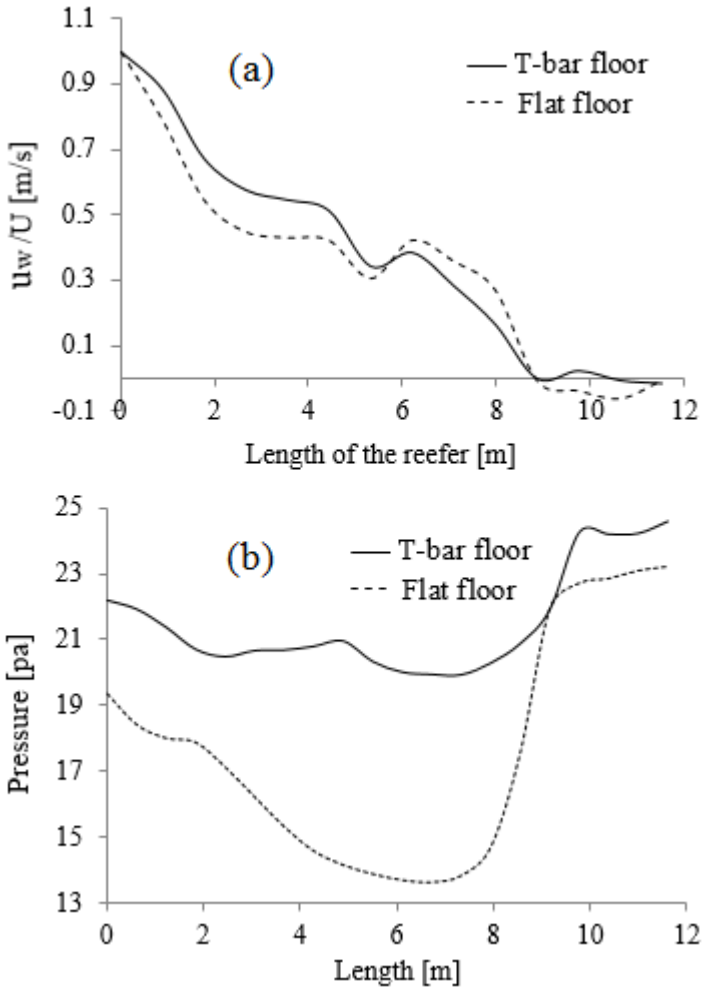

Figure 3-10: Jet flow characteristics of T-bar floor and flat floor models at high evaporator fan speed numerical study (a) and, static pressure distribution in the domain (b)

Flow separation occurred at 9 m (≈3 L/4) for both T-bar and flat floor design reefer models. This result was consistent with previous studies in similar enclosures. For instance, Moureh et al. (2002) and Moureh and Flick (2005) reported flow separation of 7 m and 10 m in a 13.3 m refrigerated truck for an air inlet flow rate of 4750 $m^3 h^{-1}$ and 5500 $m^3 h^{-1}$, respectively. Karimipanah (1998) reported that the jet flow is affected by pressure gradient at 0.7 L; however, other authors also reported 0.64 (Adre and Albright, 1994) to 0.84 L (Yu and Hoff, 1999). The flat floor design reefer showed a higher positive pressure gradient between inlet

Stellenbosch University https://scholar.sun.ac.za

side and door side ($dP/dz > 0$ or ΔP= 10 Pa) compared with the T-bar floor design reefer (ΔP= 4.5 Pa) (Figure 3.10b). This adverse pressure gradient resists the airflow to the rear region (door side). Therefore, for the flat floor design a more substantial air recirculated in the primary circulation before reaching the rear region. This also affects the jet flow characteristics. For the flat floor design model a significant amount of the primary recirculation air re-joined the jet approximately at 5.5 m. This was reflected in the jet decay curve for which the velocity ratio for the flat floor design model shows an increase from 6 to 9 m (Figure 3.10a). Similar studies were conducted by researchers for top delivery flat floor/ceiling enclosure using experimental and different turbulence models (Moureh et al., 2002; Moureh and Flick, 2003; Tapsoba et al., 2007). The jet flow characteristics and pressure gradient between the inlet and the door side (Figure 3.10 a & b) computed using our model showed good qualitative agreement. As shown in Figure 3.10b, the pressure gradient between the inlet side and the door side was adverse, which is a characteristic of flows in which the inlet and outlet are located on the same side. This pressure gradient affects the axial flow of the jet in contrast to the Coanda effect in which the jet flows adhered to the floor and was the main cause of flow separation (jet decay) (Figure 3.10b) (Moureh et al., 2005).

3.4.5. Airflow characteristics under low evaporator fan speed

Figure 3.11 a & b depicts the air flow profiles on a vertical plan bisecting the T-bar floor and the flat floor reefers under low evaporator fan speeds, respectively. The evaporator operates at an airflow rate of 2500 $m^3\ h^{-1}$ (air change rate of ≈ 36 h^{-1}).

Stellenbosch University https://scholar.sun.ac.za

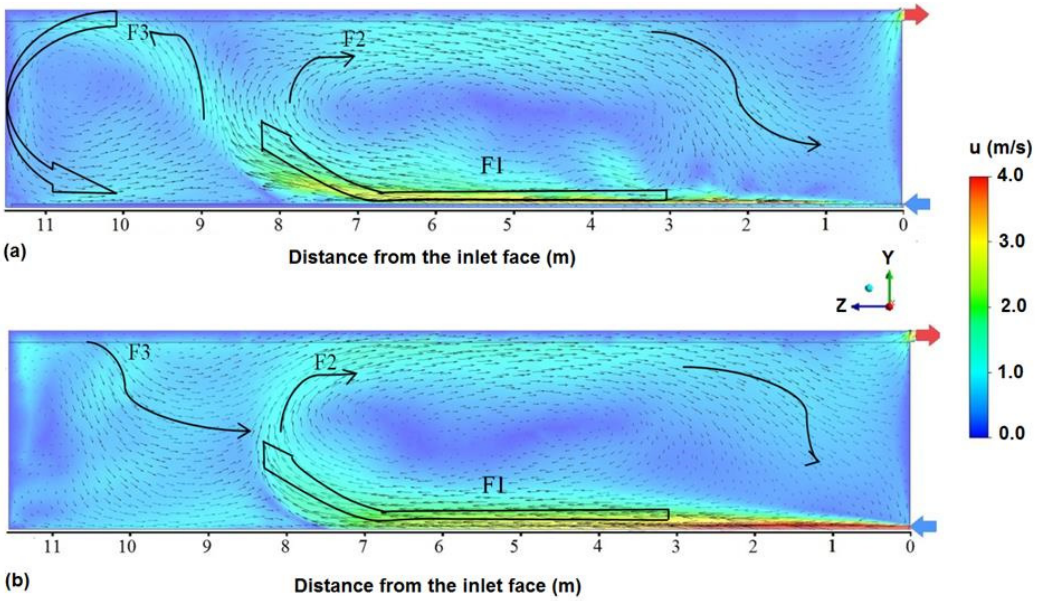

Figure 3-11: Simulated airflow pattern on a section plane bisecting the reefers. Simulation results corresponds to, (a) T-bar floor model, (b) Flat floor model reefers operating at low evaporator fan speed.

Under low evaporator fan speed, the main airflow stream (F1) sustained up to about 8 and 7.5 m for the T-bar and flat floor design reefers, respectively. This is 1 m shorter than the distance it travels under high evaporator fan speed scenario. In both reefer designs the main stream divides into two streams (F2 and F3) as it comes near the ceiling. F2 forms the returning air stream with some part of it flows down and joined the main stream (F1). This phenomenon created the primary recirculation zone in the middle region of the reefers. The primary recirculation zone for both reefer designs extend approximately from 2 m to 8 m. F3 which flows to the door side of the T-bar model forms a distinct secondary recirculation zone while such secondary recirculation zone is absent in the flat floor design under low evaporator fan speed.

Figure 3.12 depicts simulated contours of vertical air velocity magnitudes on a section plane bisecting the reefers operating at low evaporator fan speed. The improved vertical airflow streams in the T-bar floor design model were obvious at low evaporator fan speed as well.

Stellenbosch University https://scholar.sun.ac.za

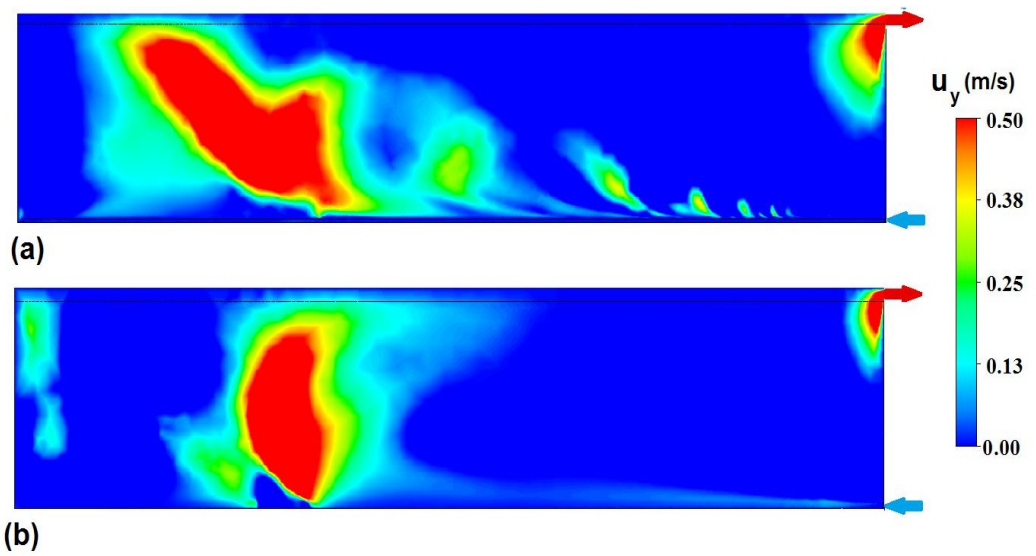

Figure 3-12: Contours of magnitudes of vertical air velocity on section plan bisecting the T-bar floor reefer (a) and flat floor reefer (b). Simulation corresponds to the reefers working at low evaporator fan speed with an air flow rate of 2500 $m^3 h^{-1}$ (air exchange rate of ≈ 36 h^{-1})

Figure 3.13 depicts the jet flow characteristics and static pressure profiel for the T-bar and flat floor designs at low evaporator fan speeds. The cooling air enters the container horizontally (perpendicular to the inlet face) at ≈4.5 m s^{-1} as a jet. The jetflow decayed at 7.4 (0.64 L) and 7.8 m (0.67 L) , which is ≈2 L /3 from the inlet face, for the T-bar and flat floor design models, respectivively. These results were in range with the previous findings, that reported wall jet penetration distance of 0.64 (Andre and Albright, 1994), 0.7 (Moureh and Flick, 2003) and 0.84 (Yu and Hoff, 1999) times the length of the encoluser. The magnitude of the jet velocity for the flat floor design model was enhanced from 6 to 8 m due to a similar effect discussed in high evaporator fan speed operation (influence of the primary recirculation of the air). The pressure profile along the jet showed a higher pressure gradient for the flat floor model than the T-bar floor

Stellenbosch University https://scholar.sun.ac.za

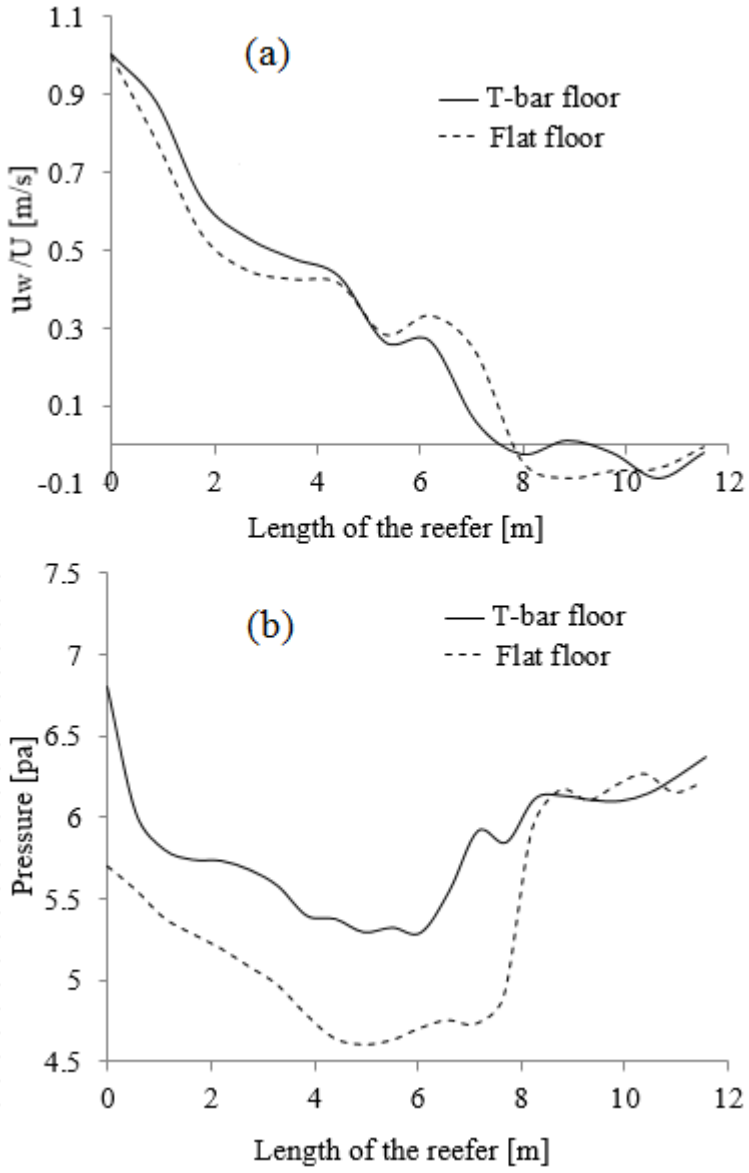

Figure 3-13: Jet flow characteristics of T-bar floor and flat floor models (a) and, Static pressure distribution (1 m above the floor) along the length of the reefer (b) at low evaporator fan speed numerical study

model (Figure 3.13 b), which was also the case at high evporator fan speed operation (Figure 3.10 b). The static pressure profiles along the length in the two models drop to their respective minimum in the primary recirculation region (2 to 8 m). However, for the T-bar floor model it was not as sever due to its vertical flow distribution characteristics that reduces the size and strength of the primary air

Stellenbosch University https://scholar.sun.ac.za

recirculation (low pressure region). This ability of the T-bar floor structure to reduce pressure gradient between the inlet and the rear region indicates energy saving oportunity.

3.5. Conclusion

The study demonstrated the importance of reefer floor design on the airflow distribution at high and low evaporator fan speed conditions. By incorporating the floor structures explicitly in the CFD model, the difference between two reefer floor designs were visualized and quantified. The T-bar floor structure is characterized by an increased proportion of vertical airflow inside the reefer compared with the flat floor structure. This is important during long distance shipping of fresh produce where cooling air has to flow from the bottom of a pallet to the packed produce in a fully loaded reefer.

The T-bar floor design reefer recorded 42 % and 51 % less pressure gradient between the inlet side and door side compared to flat floor design reefer at low and high evaporator fan speeds, respectively. This reduction in the adversity of the pressure gradient in turn reduced dead zone in the rear part of the T-bar floor design reefer by increasing the airflow rate coming through the section z=9.5 m from 0.2 to 0.6 $m^3 h^{-1}$. Presence of produce load can change the flow field in a reefer significantly. However, operational (fan speed) and design (floor structure) parameters will still influence flow characteristics of the incoming air, air distribution along the length (to the rear part) of the container and vertically (into the load). The airflow simulation results in this study provide fundamental insights on the effects of these design and operational parameters and remains relevant in study of packed reefers.

The transient temperature profile in both reefer designs was spatially uniform since they are empty and due to turbulent mixing of air. The time to cool the air inside the T-bar and flat floor design reefers to the set temperature was similar at high and low evaporator fan speed conditions.

Stellenbosch University https://scholar.sun.ac.za

The CFD model developed can be applied to study other parameters such as, airflow distribution, energy consumption and, ambient environmental conditions that affect cooling operation heat transfer inside a reefer packed with fresh produce during long shipping periods.

Stellenbosch University https://scholar.sun.ac.za

Chapter 4

4. Airflow and heat transfer inside refrigerated shipping container packed with stacked load of apples: Numerical model development and validation†

Abstract

This paper developed and validated a porous medium computational fluid dynamics (CFD) model of airflow and produce cooling inside a fully loaded refrigerated shipping container (reefer). Wind tunnel tests were used to obtain the pressure drop characteristics of a palletized stack of apple fruit. One-phase porous medium CFD model of the air flow and heat transfer was defined using the Darcy-Forchheimer equation. The detailed structure of the T-bar floor of the reefer and the resistance to airflow of wooden pallets were included in the model. Heat generation due to produce respiration and convective heat transfer with the surrounding environment were incorporated in the CFD model. Airflow and temperature data obtained from a fully loaded, full-scale reefer were used to validate the model. The model successfully reproduced the airflow and temperature profiles inside the reefer. High and low cooling regions were properly identified. The airflow path

† Samuel Getahun, Alemayehu Ambaw, Mulugeta Delele, Chris J. Meyer, Umezuruike Linus Opara. 2016. Airflow and heat transfer inside refrigerated shipping container packed with stacked load of apples: Part I – Numerical model development and validation. Journal of Food Engineering (Submitted).

Stellenbosch University https://scholar.sun.ac.za

inside the reefer was visualized using vector and contour plots. Model predictions were acceptably accurate with an average error of 26% and 18% in predicting airflow and temperature, respectively. The absence of vent holes on the bottom face of the packaging box caused non-uniform airflow leading to a highly heterogeneous cooling, demonstrating the importance of packaging design that takes into account the particulars of airflow paths inside reefers. A subsequent paper, Part II, will implement the validated model presented here to further investigate packaging boxes with respect to vertical airflow to optimize the cooling process in reefers.

4.1. Introduction

Refrigerated shipping container (reefer) is one of the key segments of the fresh produce cold chain in addition to pre-cooling, storage, handling at distribution centres and refrigerated display. Uniform distribution of air inside reefers is very important to insure uniform cooling of the produce (Tanner and Amos, 2003). Temperature, if not properly controlled, rises due to heat production by the commodity and other heat sources such as fan motors, heat infiltration from outside, solar radiation, etc. In addition, chilling injury and/or hot spots due to non-uniform cooling lead to produce quality loss (Tanner and Amos, 2003; Jedermann et al., 2013). Hence, it is very important to control temperature inside reefer to preserve quality and reduce loss (Vigneault et al., 2009).

Controlling reefer internal temperature depends upon many factors including external climatic conditions, the thermal insulation of the reefer, the product's rate of respiration and the air circulation which depends on reefer designs, package designs and package arrangements inside the reefer (Defraeye et al., 2016). These factors interact in a complex manner that understanding the effects of design and operational parameters experimentally alone is time consuming and inadequate. In the last few decades, experimentally validated numerical models has been successfully used to acquire important information on airflow and temperature distributions inside cold storage systems (Smale et al., 2006; Dehghannya et al., 2010).

Stellenbosch University https://scholar.sun.ac.za

Several previous studies used this technique to analyse airflow and heat transfers in refrigerated transport systems (refrigerated vehicles/trailer, enclosures) (Moureh et al., 2002; Tapsoba et al., 2007; Moureh and Flick, 2004; Smale, 2004; Rodríguez-Bermejo et al., 2007; Moureh et al., 2009a, b). Earlier studies applied resistance network modelling approach (Meffert and Van Beek, 1983; Wang and Touber, 1990; Ménia et al., 2002) which has limitations on capturing flow regimes near walls and flow recirculation (Samll, 2004). Computational fluid dynamics (CFD) is the primary method of choice in recent studies for its powerful visualization capabilities, high spatial and temporal resolution of airflow and temperature distributions with acceptable level of accuracy (Xia, 2002; Norton and Sun Da-Wen, 2006; Smale et al., 2006; Verboven et al., 2006; Ambaw et al., 2013).

However, application of CFD for large and complex systems, like reefers, remains a challenge due to high computational demand (James et al., 2006). Fruit inside reefers are packed in bulk in boxes and stacked on a pallet forming a complex geometry. For a reefer packed with 20 pallets, model discretization is very expensive due to the high size ratio of geometries that make up the domain (Zhao et al., 2016). For example, a typical reefer is 12 m long while the packaging box is 3 mm thick. Geometries describing contacted fruits and contact between fruit and packaging walls are very small that makes domain discretization computationally expensive. To solve this problem, actual geometry is usually simplified to porous medium (Zou et al., 2006a,b). In this approach, stacked fruit were simplified to medium consisting of a fluid phase (air) and a solid phase (apple fruit and packaging materials) with constant volume fraction in space and time (Ambaw et al., 2013, Hoang et al., 2000; Verboven et al., 2004; Liu and Masliyah, 2005; Quintard and Whitaker, 2005). This approach benefits in managing the computational power requirement and solves the airflow (air circulation in a reefer, airflow through stacked pallets) and heat transfer (such as heat conduction from the environment, fruit sensible heat and respiration heat) characteristics in a packed reefer. In the porous domain, local equilibrium between the fluid and solid phases is reasonably assumed to further simplify the problem.

Stellenbosch University https://scholar.sun.ac.za

To accommodate spatial variability of the stacking, zonal porous medium approach can be applied. In this approach, different regions of the inside of a cooling facility can be defined by a zonal porous medium (Tanner et al., 2002a, b; Hong et al., 2012; Laguerre et al., 2013). In addition to packaging design, wooden pallets (used as a base for the stack) and arrangement of stacked pallets (anisotropic airflow resistance) also affect airflow distribution (Hoang et al., 2015; Defraeye et al., 2015b). Zonal porous media approach could be used to integrate the effect of these parameters that have been omitted in previous studies and decrease some of the limitation of modelling a packed reefer.

The objective of this study was to develop and validate 3-D CFD model capable of predicting airflow and heat transfer in a reefer packed with apple fruit. Zonal porous medium CFD model was developed and validated with airflow and temperature data obtained from experimental study on a fully loaded, full-scale reefer. In part II of this study, the validated model will be used to further investigate commonly used apple packaging boxes and effect of vertical airflow resistance inside fruit packed reefers.

4.2. Materials and methods

4.2.1. Fruit and packaging box

In this study fruit were packed in a corrugated fibre cartons (CFC) packaging boxes (Econo-D), which is a display package design (open on top) normally used in local market and sometimes in export market in South Africa (Berry et al., 2015). The box contains apple fruit in plastic bags (Figure 4.1a). Each bag contains approximately 1.5 kg of apple (11 apple fruit (top red cultivar) per bag). Each box carries 8 bags (≈ 12kg apple fruit). Figure 4.1b depicts the shape and dimensions of the packaging box. The short side has a vent-hole ratio of 3.2% composed of two horizontally oriented rectangular vent holes at the bottom region and one larger horizontally oriented rectangular vent hole (is also a handle) on the top middle region. The long side has two circular vent holes positioned in the

Stellenbosch University https://scholar.sun.ac.za

middle giving this side a vent hole-ratio of 1.09 %. The bottom side of the box has no vent hole.

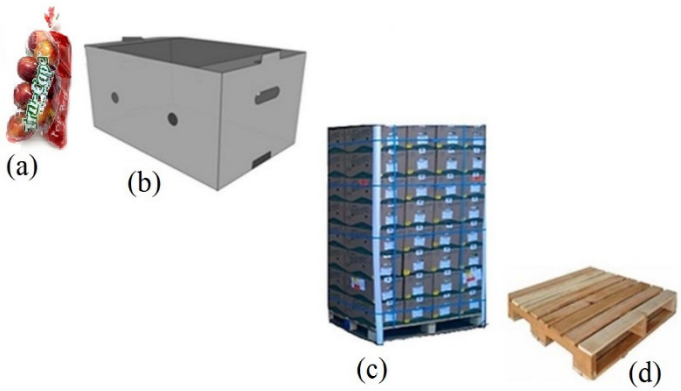

Figure 4-1: Components of the palletized Econo-D box analysed in this study. (a) a bag of apple fruit each containing approximately 1.5 kg top red apples, (b) corrugated fibre carton (Econo-D) to contain eight bags of fruit, (c) pallet formed from 8 layers of boxes with 8 boxes per layer and, (d) standard wooden pallet on which stacking was formed.

4.2.2. Reefer

Figure 4.1c shows the stack (pallet) ready for loading into the reefer. Stacks were formed on a standard wooden pallet that have a dimension of 1.2 m × 1 m × 0.15 m (Figure 4.1d). A stack contains 8 layers of 8 boxes. State-of-the-art reefer (Star cool SCI-40, Maersk reefer equipped with QUEST I control) located at Ceres Fruit Growers (Pty) Ltd, Western Cape, South Africa was used to conduct the experiment. This reefer has internal and external Length × Width × Depth of 11.59 m × 2.29 m × 2.54 m and 12.19 m × 2.44 m × 2.90 m, respectively (Figure 4.2 a). There are 35 extruded T-bars on the floor that run from the refrigeration unit side to the door side. The shape and dimensions of the T-bar structure is shown in Figure 4.2 b&c. The walls of the container are composed of three different layers of materials. Polyurethane insulation is used in the middle (ASHRAE, 2010). The reefer was a bottom air delivery unit. Cold air from the refrigeration unit enters into the reefer from bottom and the returning air leave the reefer at the top to the

Stellenbosch University https://scholar.sun.ac.za

refrigeration unit. The reefer has an inlet baffle plate that guide the horizontal flow of inlet air between the T-bars. The inlet baffle plate extends 20 cm to the reefer.

Totally, 15 tons of fruit was loaded into the reefer (twenty pallets each holding 768 kg apple fruit). The pallets were arranged in two rows that were separated by air gap. One of the rows contains 11 pallets with shortest side of pallets against the side wall while the second one contains 9 pallets with longest side against the side wall. Pallets in a row were tightly aligned with the minimum possible gap between them. The refrigeration unit was operating at cooling flow rate of 5400 m^3 h^{-1} (at an air exchange rate of ≈ 80 h^{-1}). The reefer was equilibrated to -1 °C before loading.

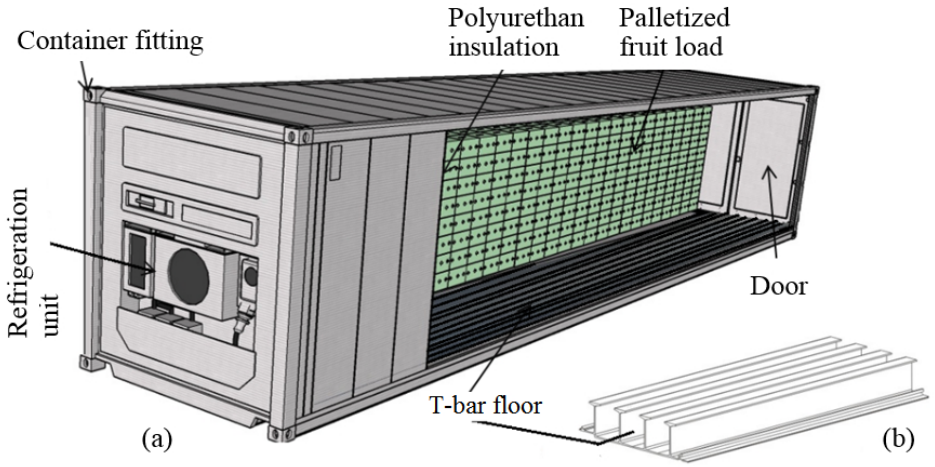

Figure 4-2: Schematic showing partially packed bottom-air delivery T-bar reefer (a) and, closer view of the T-bar floor structure

4.2.3. Measurements

4.2.4. Pressure drop characteristics

Pressure drop characteristic of a pallet (Figure 4.1c) was determined from wind tunnel experiment (Figure 4.3). Bagged water filled plastic balls of 8 cm diameter were stacked to represent the fruit. Then, a pallet was halved into two equal parts along the y-axis. Using this setup, pressure drop vs. air flow data corresponding to airflow along vertical (y-direction), horizontal (x-direction) and

Stellenbosch University https://scholar.sun.ac.za

transverse (z-direction) directions were acquired for the two halves (Figure 4.3). The bottom half (Figure 4.3c) includes the wooden pallet.

Air velocity was measured using TVS 1100 data logger with candle stick sensors (Advanced Thermal Solutions Inc, Norwood, USA). The sensors had a measurement range of 0 to 20 m s^{-1} and an accuracy of ±2 % m s^{-1}. Five points at the outlet of the wind tunnel. The pressure drop was measured using differential pressure meter (Air Flow Meter Type A2G-50, WIKA, Alexander Wiegand SE & Co. KG, Klingenberg, Germany) with data controller (WCS-13A, Shinko Technos CO LTD, Osaka, Japan) to record the total pressure drop across the stack.

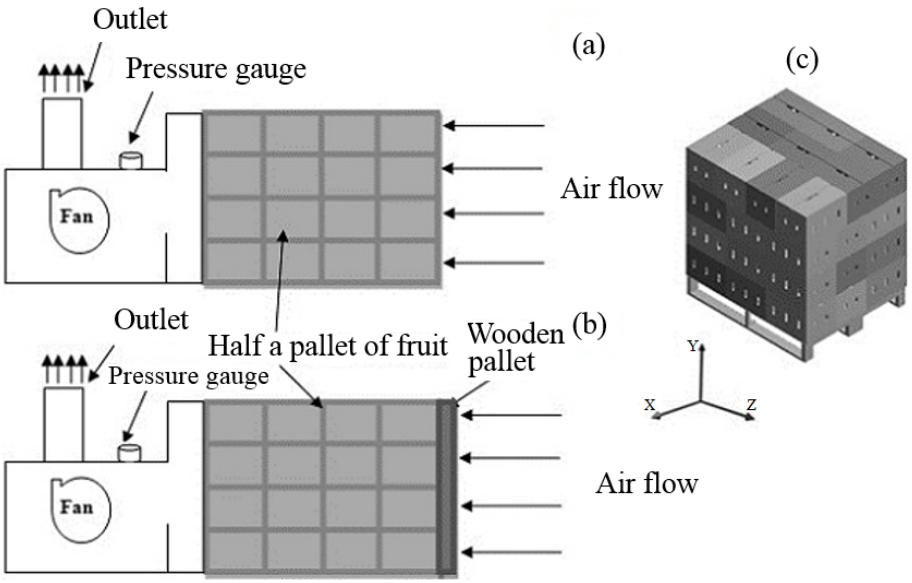

Figure 4-3: Schematics showing setup of the wind tunnel experiment to measure the vertical direction (y-direction) pressure drop characteristic of palletized fruit stack. Measurements were taken across half a pallet: (a) top half of a pallet (without wooden pallet) and (b) bottom half of a pallet with wooden pallet (WWP). (c) Isometric view of the bottoms half of a pallet.

4.2.5. Airflow

The airflow profile inside a loaded reefer was measured on sampling points as shown in Figure 4.4. Measurements were taken in the free region between the two rows, in the region between the stack and the reefer ceiling and in the region

Stellenbosch University https://scholar.sun.ac.za

between the stack and the reefer door. Airflow measurement was conducted using TVS 1100 data logger with candle stick sensors (measuring range 0-20 m s^{-1} with ±2 % m s^{-1}) (Advanced Thermal Solutions Inc, Norwood, USA). In addition, turbulent intensity (TI) at the inlet and outlet were determined from measured air velocities assuming a fully developed flow. To do this, a 10 minutes (taking measurements every 30s) sample of the velocity at 12 equally spaced positions at inlet and outlet of the tunnel were used to estimate turbulent intensities (Vesteeg and Malalasekera, 2007).

4.2.6. Temperature

Fruit pulp temperatures were measured every 30 seconds for a duration of 72 h with T-type thermocouples (Thermocouple products Ltd, Edenvale, South Africa, with operating range of −30 to 100 °C and accuracy of ± 0.025%) inserted into the core of 60 sample fruits inside the reefer. The relative positions of the pulp temperature sensors are shown in Figure 4.4. Sampling was from three positions per pallet (top part of the pallet = 15 cm below the top of a pallet, middle part of the pallet = 1.04 m above pallet base and bottom of the pallet = 15 cm above pallet base).

Relative humidity (RH) inside the reefer was monitored throughout the experiment using four sensors that were positioned 2.5 m apart along the length of the reefer (all in the top layer of the pallets). Temperature and relative humidity were monitored using T-type thermocouples with a 34970A data acquisition unit (± 0.1 °C; Agilent Technologies, Santa Clara CA 95051, USA) and tiny tag sensor (Tinytag TV- 4500, Hastings Data Loggers, Australia), respectively.

Stellenbosch University https://scholar.sun.ac.za

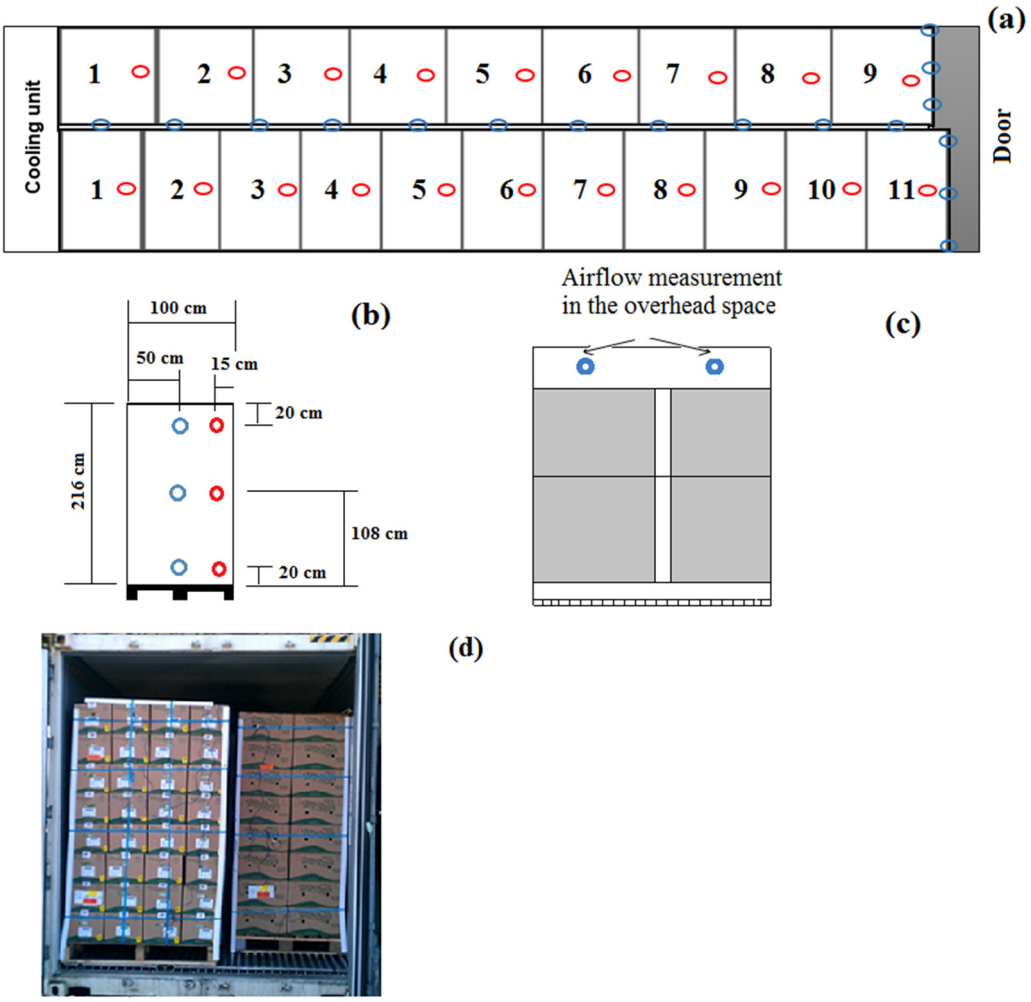

Figure 4-4: Schematics of the position of pulp temperature sensors (red circle) and air velocity sensors (blue circle). (a) Showing the positions of the temperature and air velocity sensors as seen from top, (b) position of temperature and air velocity sensors as seen from side of a pallet, (c) position of airflow sensors in the overhead space and, (d) a snapshot (door side) of a fully packed reefer wired with the sensors.

4.2.7. Model equations

Assumptions

The volume averaging technique (Hassani-zadeh and Gray, 1979; Nakayama and Kuwahara, 1999; Quintard and Whitaker, 2005) was used to develop a single-phase porous medium CFD model of the air flow and heat transfer. The model assumptions are discussed below.

Stellenbosch University https://scholar.sun.ac.za

- The region occupied by the stack pallets inside the reefer were modeled as four porous zones (two per row, one on top of the other accounting the top and bottom halves of a pallet). Splitting the top and bottom part of the pallet was necessary to different stacking configuration used in the two halves to ensure stability. The bottom half incorporated the vertical airflow resistance effect of the wooden pallet.
- The flow resistance characteristics of the four porous zones were estimated from a wind tunnel experiment that provides the pressure drop vs. velocity data of the two halves of a pallet.
- Porosity and resistance characteristics of the porous domains were assumed constant in space and time.
- The physical properties of air and apple fruit were assumed constant within the temperature range of the application. Density and thermal conductivity of apple were taken as 898 kg m^{-3} and 3829 J kg^{-1} K^{-1} (Lisowa et al., 2002).
- Evaporation/condensation of moisture inside the reefer was assumed negligible in the model.
- Heat generation due to produce respiration was calculated as a function of temperature only. In actual case, the heat generation is a function of temperature and gas conditions inside the reefer (O_2 and CO_2 concentration) (Hertog et al., 1998; Ho et al., 2013).
- Heat conduction through the walls, floor, door and ceiling was calculated based on an average outside air temperature of 10 °C. The composite walls (insulation) of the reefer were taken into account in the calculation of overall heat transfer coefficient at the boundaries based on properties major construction material (ASHRAE, 2010).
- Since the air circulation fans were positioned upstream of the evaporator coil (a blow-through configuration), the fan heat was assumed totally removed directly by the evaporator coil.
-

Stellenbosch University https://scholar.sun.ac.za

Governing equations

The airflow inside the reefer was modelled using three-dimensional Reynolds-averaged Navier Stokes (RANS) equations for incompressible fluid (Eqn. 4.1) and Eqn. (4.2).

$$\nabla \cdot \mathbf{V} = 0 \tag{4.1}$$

$$\frac{\partial \mathbf{V}}{\partial t} + \nabla \cdot \left((\mathbf{V} \times \mathbf{V}^{\mathbf{T}}) \right) - \nabla \cdot \left(\frac{\mu_{eff}}{\rho} \nabla \mathbf{V} \right) = \mathbf{M_V} - \frac{1}{\rho} \nabla p \tag{4.2}$$

$$\mathbf{M}_{V_i} = -\frac{\mu}{\kappa} V_i - \beta \rho |V_i| V_i \tag{4.3}$$

Where, **V** is the air velocity (m s^{-1}), *t* is time(s), μ is the dynamic viscosity of air (kg $m^{-1}s^{-1}$), $\mu_{eff} (= \mu + \mu_t)$ is the effective viscosity (sum the dynamic viscosity and turbulent viscosity) (kg $m^{-1}s^{-1}$), p is pressure (Pa) and $\mathbf{M}_V$ (m s^{-2}) is the momentum source term. Inside the porous domain, $\mathbf{M}_V$, accounts for the pressure loss as given in the Darcy-Forchheimer equation (Eqn. (4.3)) (van der Sman, 2002; Verboven et al., 2006), *i* stands for direction in the Cartesian coordinate system (*x, y or z*). β (m^{-1}), $1/\kappa (m^{-2})$ are the viscous and inertial resistance coefficients, respectively. These coefficients were determined using a dedicated wind tunnel experiment from the resulting pressure drop as a function of airflow. The calculated viscous and inertial resistance coefficients are summarized in Table 4.1.

Stellenbosch University https://scholar.sun.ac.za

Table 4-1 Pressure drop characteristics of a pallet. Values were calculated from curve fitting of the pressure drop vs. velocity data to the Darcy-Fochhaimer equation which describes the permeability and resistance of the pallet.

Flow direction	$1/\kappa(m^{-2})$	β (m^{-1})
X- direction	6×10^{5}	41438
Y-Top half	3.1×10^{6}	77072
Y-Bottom half	6.6×10^{7}	113174
Z-direction	1.7×10^{6}	2110

By assuming local thermal equilibrium between the solid and the cooling air (Nield, & Bejan, 2006), the heat transfer inside the reefer was modelled by Eqn. 4.4.

$$(\rho C)_{\mathrm{m}} \frac{\partial T}{\partial t} + (\rho C)_f \boldsymbol{V} \cdot \nabla T = \nabla \cdot (k_m \nabla T) + Q_m \qquad 4.4$$

$$k_m = (1 - \phi) k_p + \phi k_f \qquad 4.5$$

$$(\rho C)_{\mathrm{m}} = (1 - \phi)(\rho C)_{\mathrm{p}} + \phi(\rho C)_{\mathrm{f}} \qquad 4.6$$

Where,$(\rho C)_{\mathrm{f}}$ and $(\rho C)_{\mathrm{p}}$ (KJ $\mathrm{kg}^{-1}\,{}^{\circ}\mathrm{C}^{-1}$) are heat capacities per unit volume of fluid phase (air) and solid phase (fruit), respectively and ϕ is porosity, k_m, k_f and k_p (W $\mathrm{m}^{-1}{}^{\circ}\mathrm{C}^{-1}$) are thermal conductivities of porous medium (effective), air and produce, respectively. Porosity of the stack was estimated from the void space obtained by subtracting the volume of solids (fruits and packaging materials) from the total volume of a stack. Dividing the void space by the total volume of the stack gives the porosity ($\approx$ 0.6). The model assumed a spatially and temporarily uniform porosity. In actual case, porosity vary spatially and porosity in the interstice region of the stack, in the space above fruit in a box and between stacks differ considerably (Verboven et al., 2004; Zou et al., 2006a). However, the computational cost to consider all the detail is not practical; therefore, air and fruit are assumed to be uniformly distributed in the pallets.

Stellenbosch University https://scholar.sun.ac.za

The heat generation per unit volume of produce (Q_m) due to respiration was calculated using equation 4.7 (Becker et al., 1996) at the produce temperature T (°C).

$$Q_m = 10.7f \times \left(\frac{9T}{5} + 32\right)^g \quad 4.7$$

Where, f and g are produce respiration coefficients for apple fruit (5.6871×10^{-4} and 2.5977, respectively).

4.2.8. Geometry, boundary and initial conditions

Figure 4.5 depicts the model geometry and the boundary conditions. The pallets arranged in two rows form the porous domains and the free region around and above the rows form the fluid domain. Accordingly, fluid-porous interface (between the porous domain and fluid domain) was explicitly defined as a conservative interface flux boundary for the momentum and scalar transports. The cooling unit was modelled by specifying temperature, pressure, velocity and turbulence intensity at exit and outlet of the cooling unit. In all the models, the internal walls of the reefer were set to a no slip walls. The heat exchange with the environment has been incorporated as heat fluxes on the walls, ceiling, floor and the door as given by Eqn. (4.8).

$$q_w = U(T_\infty - T_W) \quad 4.8$$

Where, q_w is the heat flux (W m^{-2}), U (W m^{-2} °C^{-1}) is equivalent heat transfer coefficient of composite wall (including polyurethane insulation) calculated from the thermo-physical properties of wall, ceiling, floor and door (Table 3.1). The calculated equivalent heat transfer coefficient of the composite wall, ceiling, floor and the door were 0.28, 0.22, 0.20 and 0.28 W m^{-2} °C^{-1}, respectively. Ambient temperature (T_∞) is assumed to be constant (10 °C), and T_w is wall temperature.

Stellenbosch University https://scholar.sun.ac.za

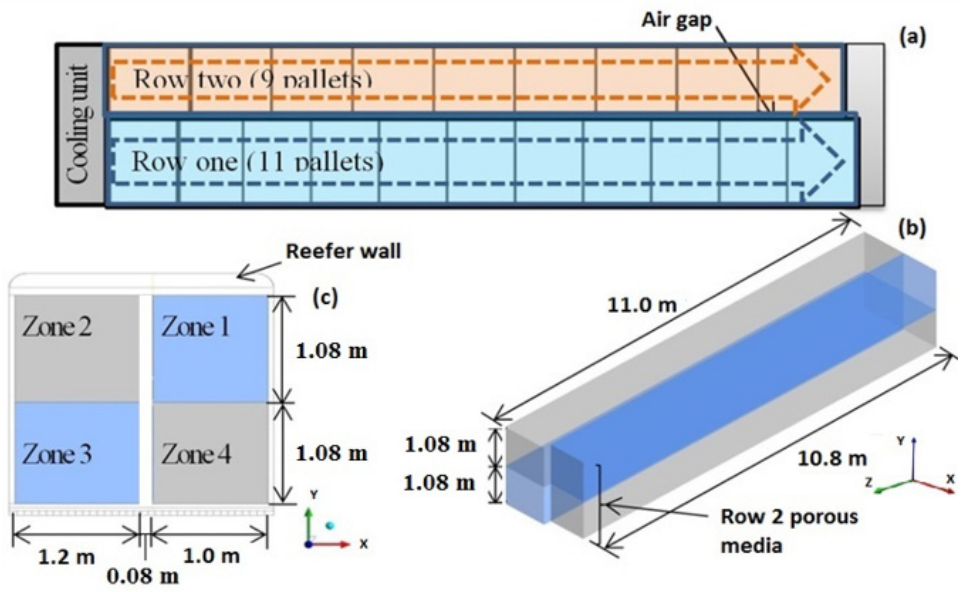

Figure 4-5: Pallet arrangement and porous media zonal representation of packed pallets inside a fully loaded reefer. Top view (a), dimensions of the stack shown on isomeric view of the porous pallet zones and, front view of the porous zones from the door side of the reefer (c).

4.2.9. Simulation procedure

Model geometry was developed using ANSYS® DesignModeler™ Release 16.0 (ANSYS, Canonsburg, PA, USA). Meshing was conducted based on the flow characteristics and structure of the geometry. Fine mesh was applied in the regions where large velocity gradient was expected and on narrow structures such as air inlet/outlet and T-bar floor structures. Discretization of the domain was on ANSYS® Meshing™ Release 16.0 and the problem setup and simulation was on ANSYS® Fluent™ Release 16.0 (ANSYS, Canonsburg, PA, USA). Value of mass fluxes and heat fluxes across the boundary of the porous domain were simulated with grid size of 8×10^6, 16×10^6 and 18×10^6 elements and the average discretization error was estimated by calculating an extrapolated, more accurate, value of the fluxes using the Richardson extrapolation (Roache, 1994; Franke et al., 2007). The simulations were undertaken using mesh elements of $\approx 16 \times 10^6$ which

Stellenbosch University https://scholar.sun.ac.za

has an average discretization error of 2 and 5 % in estimating mass fluxes and heat fluxes, respectively.

Steady state airflow simulation was first conducted and the result was used as initial condition to perform the transient heat transfer calculation. Turbulence was calculated using k-ω SST model. SIMPLE discretization scheme was used for pressure-velocity coupling and Second Order Upwind discretization was used for momentum, specific dissipation rate and energy calculations. A number of time step sizes (360 s, 180 s, 72 s, 36 s) were assessed. Based on accuracy and computational time, time step size of 180 s with maximum 20 iterations per time step, was used. Dell Precision computer (dual Intel Xeon processor@3.30 GHz with 40 GB Ram) was used.

Error calculation and cooling uniformity

Numerical and experimental results were compared to evaluate the accuracy of the model. Average errors obtained in air velocity and fruit temperature were calculated using equation 4.9 and 4.10:

$$\overline{E}_{CFD} = \frac{1}{n}\sum_{i=1}^{n}\frac{\left||V|^{i}_{CFD} - |V|^{i}_{EXP}\right|}{|V|^{i}_{EXP}} \times 100 \qquad 4.9$$

$$\overline{E}_{CFD} = \frac{1}{n}\sum_{i=1}^{n}\frac{\left||T|^{i}_{CFD} - |T|^{i}_{EXP}\right|}{|T|^{i}_{EXP}} \times 100 \qquad 4.10$$

4.3. Result and discussion

4.3.1. Pallet pressure drop characterization

Figure 4.6 summarizes the experimental airflow vs. pressure drop data for airflow horizontally (across the length and width) and vertically along the Y-axis through the bottom-half and top-half of a pallet. Clearly, the airflow resistance in the vertical direction was the highest and across the width was the list. The only path accessible for vertical airflow could be crevices between side by side boxes.

Stellenbosch University https://scholar.sun.ac.za

The pressure drop with respect to airflow characteristics have direct relationship with the vent-hole ratio of the sides of the packaging box (Delele et al., 2013ab). Absence of vent hole on the bottom side of the Econo-D box caused high airflow resistance in the vertical direction, whereas vent holes of 1.09 % (on long side) and 1.8 % (on short side) lead to intermediate and list resistance to airflow across the length and width of the pallet, respectively. It was observed that vertical airflow resistance was higher for the bottom half of the pallet compared to the top half. This confirms the added flow resistance due to wooden pallet.

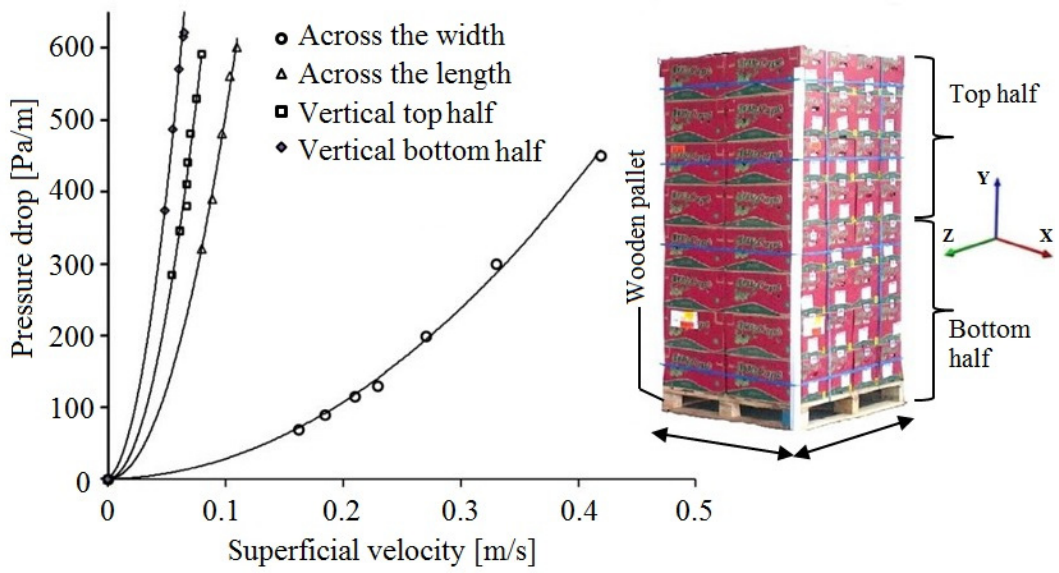

Figure 4-6: Experimental pressure drop versus superficial air velocity plot for air flow horizontally and vertically through half a pallet (see Figure 4.3). The vertical airflow for the bottom half included the flow resistance of the wooden pallet.

Curve fitting of the data points to the Darcy-Fochhaimer equation (Eqn. (4.4)) gives the viscous (β) and inertial ($1/k$) resistance coefficients of the four porous zones in the CFD model. These parameters are summarized in Table 4.1.

Stellenbosch University https://scholar.sun.ac.za

4.3.2. Model validations

Airflow pattern

Figure 4.7 show measured and simulated air velocities in the free regions between the two rows (Figure 4.7a) and top of the stack (under the ceiling) (Figure 4.7b). The corresponding velocity sampling points are shown in Figure 4.4. Air velocity ranges from 0.1 to 1.6 m s^{-1} in the free region between the two rows with high airflows near inlet region and low airflows near the door of the reefer. Airflow monotonously decreases going from the inlet side to the door side, dropping by 50 % between pallet 1 and pallet 5, and by 42 % between pallet 6 and pallet 10. When going from bottom to top, velocity decreases first and then increases, influenced by the return airflow under the ceiling. The region at the top of the stack (under the ceiling) acts as a channel for the return airflow. In this region measured velocities ranges between 0.2 to 1.5 m s^{-1} with a steep increase when going from the door side to the outlet (refrigeration unit inlet) (Figure 4.7b). Other studies also confirmed high velocity gradient inside a similar enclosure, however with top air delivery system (Moureh et al., 2009b).

The model captured the velocity profiles very well with an average prediction error of 26 ± 2 %. Velocity prediction near the inlet region was less accurate. The inlet region is a high velocity and high turbulence region that accuracy of measurements and predictions are normally difficult (Hoang et al., 2015). The average error of air velocity prediction at the bottom, middle and top regions were 30, 26 and 25 %, respectively. Previous studies also reported nearly the same levels of errors: Hoang et al. (2000), for apple fruit loaded cold store reported a 28.5 % accuracy and Moureh et al. (2009a) reported error range of 3-30% for air velocity prediction in a slot-ventilated enclosure.

Stellenbosch University https://scholar.sun.ac.za

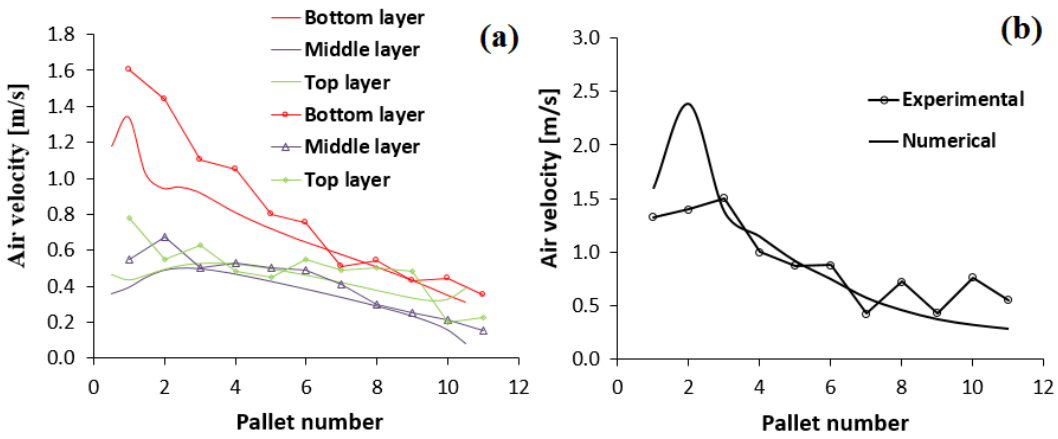

Figure 4-7 Measured and simulated air velocities in the free region between the two rows inside reefer (a) and in the region above the pallet (in the region between stack and the reefer ceiling) (b).

Simulated air flow profiles are shown using streamline and contour plots in Figure 4.8. Air leaves the cooling unit at an average velocity of 9.5 m s^{-1} and flows horizontally under the pallets through the T-bar structure. The model clearly shows the dominant airflow through the air gap between the two rows (Figure 4.8 b). Through this gap air directly flow to the overhead free space and return back to the refrigerator. This is undesirable short-circuit in the supply air path causing cold air to bypass the stack and return directly to the refrigeration unit unused, which leaves the door side of the reefer with low level of ventilation (air velocity < 0.4 m s^{-1}). Short-circuiting of air in such a way has been considered the main cause of cooling non uniformity. Moureh and Flick (2004) applied air duct that channel the air supply from the front side of refrigerated truck (loaded with 32 pallets) to the rear part of the truck and reported air velocity of 1 m s^{-1} (with air duct) instead of 0.1 m s^{-1} (without air duct).

Stellenbosch University https://scholar.sun.ac.za

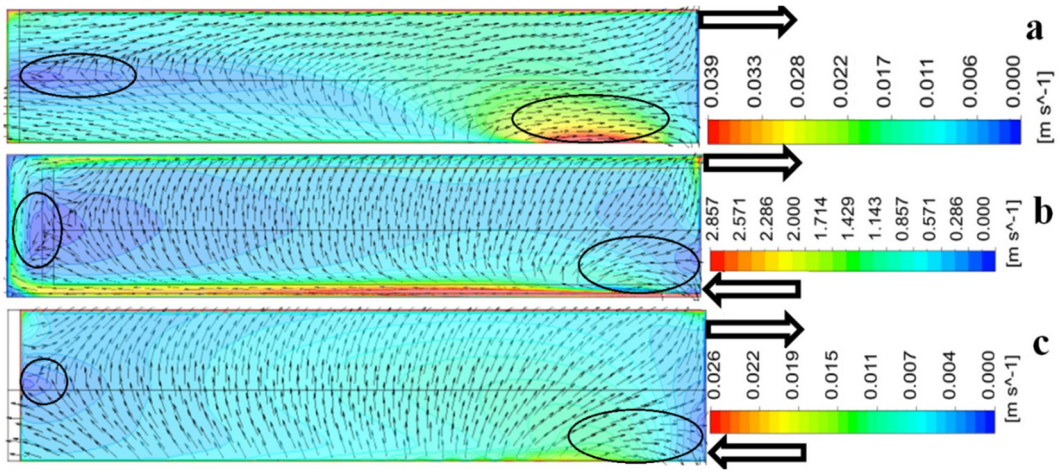

Figure 4-8 Simulated profile of airflow inside a fully loaded reefer. Colour contours show magnitude of air velocity and arrows (vector) show the local airflow direction on vertical plane bisecting pallets in row 1 (a), the air gap between the two rows (b) and pallets in row 2 (c).

Fruit cooling characteristics

Figure 4.9 shows the simulated and measured time history of average pulp temperatures inside the reefer. The reefer was initially equilibrated to cooling air temperature (-1 °C) before loading. By the time loading was finished (simultaneously sensors were installed), average pulp temperature inside the reefer was 9.5 °C. The cooling rate clearly differ between pallets. The front of the reefer (pallet 1 and pallet 2) of both rows cool the slowest, particularly the top half of the pallets due to the warm returning air through these pallets. Pallets in middle of the reefer (pallet 3 to 7) cools faster than the pallets in the front and the rear region since this region was with better level of vertical airflow (Figure 4.8b). The rear part of the reefer, particularly pallet 10 (row 1) and pallet 8 (row 2) cooled slowest. On the other hand, pallet 11 (row 1) and 9 (row 2) which share one more boundary with the pure air zone than the other pallets cooled faster than the adjacent pallets (Figure 4.9 c & f). Similarly, in the experimental study of citrus ambient loading in a reefer, Defraeye et al. (2016) reported that the bottom of first pallet reached the SECT almost half a day after the last pallet (door side). Overall, simulated produce

Stellenbosch University https://scholar.sun.ac.za

temperature agrees well with experimental data. The error of pulp temperature predictions was on average 18 %.

Temperature at half-cooling time (HCT) and seven-eighth cooling time (SECT) are marked by horizontal lines in Figure 4.9. The half cooling time (HCT) and the seven-eighths cooling time (SECT) are the times required to reduce the temperature difference between the fruit and the cooling air by half and seven eighth, respectively. SECT is mainly important in cooling operations because this temperature is adequately close to the temperature at which produce should be stored. Afterwards, the cooling unit of the reefer can be operated at lower efficiency (less energy cost) to remove the remaining heat load (Brosnan and Sun, 2001). Figure 4.10 depicts the row average pulp temperatures in time. It can be seen that in average the cooling rate of the two rows were different confirming effect of pallet orientation inside the reefer. Table 4.2 summarizes the HCT and SECT of the pallets inside the reefer obtained from the time history data.

Table 4-2 Summary of HCT and SECT of each pallet inside the reefer

	HCT (h)		SECT (h)	
Pallet	Row 1	Row 2	Row 1	Row 2
P1	32	25	>72	>72
P2	14	10.5	60	46
P3	10.7	8.7	51	40
P4	9.6	9	47	41
P5	9.5	10	47	45
P6	10	10.5	48.5	50
P7	11	12	54.5	57
P8	12.2	13.5	62	68
P9	13.5	15.4	72	61
P10	15.5	-	71.5	-
P11	12	-	45	-
Avg.	13.4	12.4	>58.6	>53.3

Stellenbosch University https://scholar.sun.ac.za

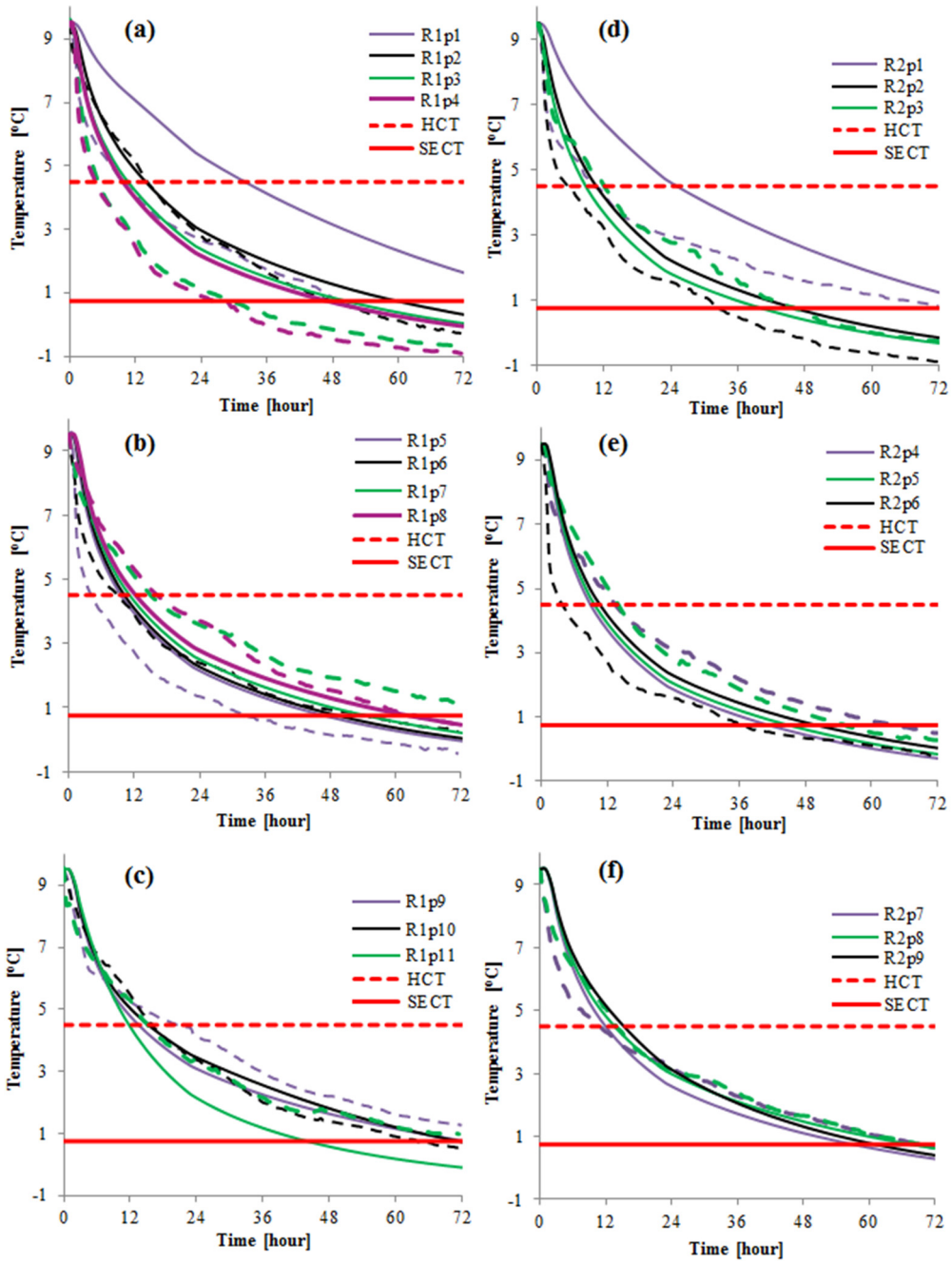

Figure 4-9 Measured (dashed line) and simulated (solid lines) evolution of pulp temperatures (pallet averages) inside a fully loaded reefer. Pallets(p) in row one (R1) p1 to p4 (a), p5 to 9(b) and (c) p9 to p11and, Pallets(p) in row two (R2) p1 to p3 (d) p4 to p6(e) and p7 to p9(f). The reefer was loaded with 15 tons of fruit (twenty pallets each holding 768 kg apple fruit). The reefer was operating at cooling flow rate of 5400 $m^3 h^{-1}$

Stellenbosch University https://scholar.sun.ac.za

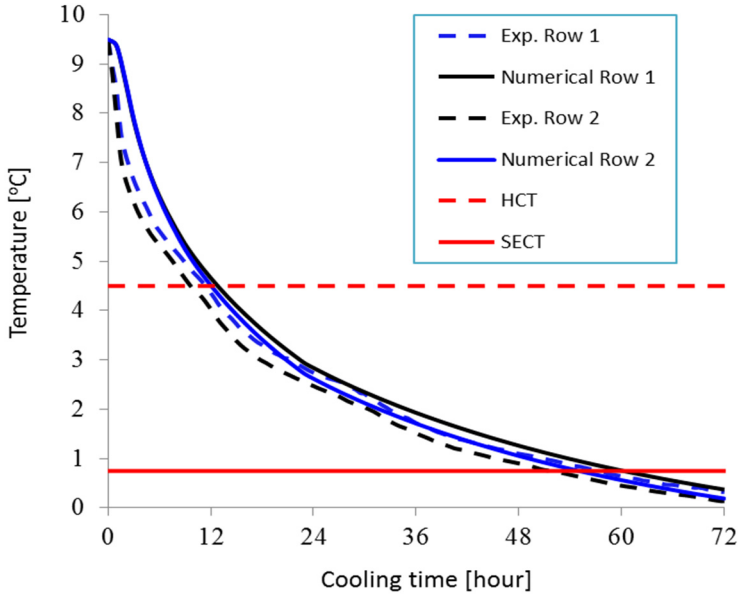

Figure 4-10: Average cooling rate of fruit in row 1 (blue) and row 2 (black). The dashed line curves show the measured (experimental) fruit temperature evolution and the solid line curves show the numerical predictions. The horizontal lines show half cooling times (dashed lines) and 7/8th cooling time (solid line)

Figure 4.11 illustrates simulated contours of temperature at 24 hours on vertical planes bisecting each row and Figure 4.12 shows the corresponding experimental and numerical pallet average temperatures. Vertical lines (error bars) in Figure 4.12 show the standard deviations calculated based on temperatures at bottom, middle and top of a pallet. Cooling within a pallet in the reefer varies primarily because the bottom layer of the pallets cooled much faster than the middle and top layer. Pallet 9 and pallet 4 in row 1 were with the highest and lowest temperature heterogeneity, respectively. Overall, the standard deviation of pulp temperature inside the reefer was 1.70 °C (exp.) and 2.32 °C (numerical). The design of the Econo-D box used in this study is for pre-cooling and cold room operations where airflow is dominantly horizontal. However, cooling in a reefer is mainly dependent on vertical airflow. The Econo-D box, which has no vent-hole on its bottom side, considerably suppressed vertical airflow inside the reefer. Both model and measurement confirmed this fact (Figure 4-12 a&b). Previous studies in

Stellenbosch University https://scholar.sun.ac.za

different cold chain systems have also shown the importance of uniform airflow for uniform temperature distribution (Chourassia and Goswami, 2007; Moureh et al., 2009a; Dehghannya et al., 2011; Jedermann et al., 2014).

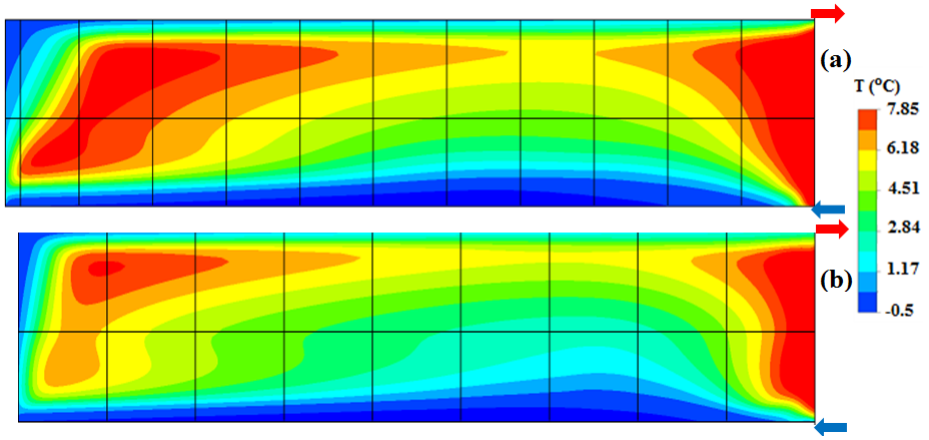

Figure 4-11 Simulated profile of produce temperature at 24 hour on vertical plane (YZ-plane) bisecting row 1 (a) and row 2 (2) inside reefer.

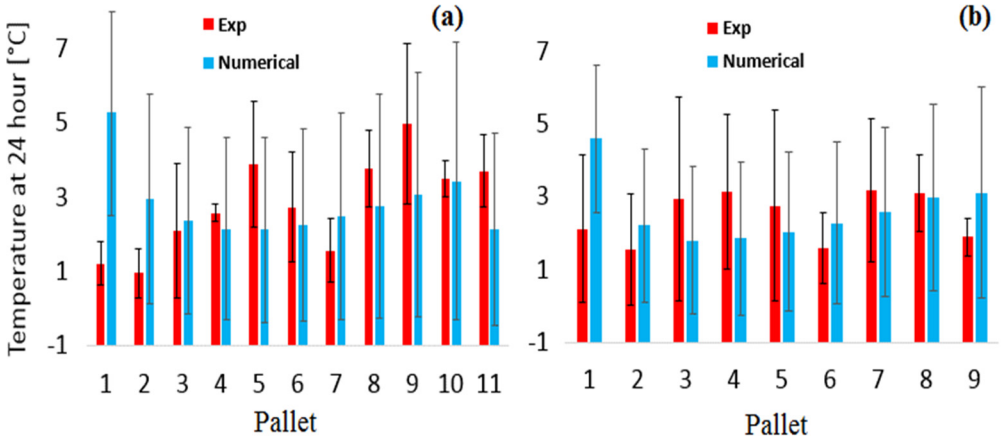

Figure 4-12: Experimental (red) and numerical (blue) average pallet temperatures at 24 hours of cooling. (a) Pallets in row 1 and, (b) pallets in row 2. Vertical lines in Figure 4.12 show standard deviations calculated based on temperatures at bottom, middle and top of a pallet.

Stellenbosch University https://scholar.sun.ac.za

4.4. Conclusion

In this study, wind tunnel experiment was used to characterize airflow resistances of stacked fruit on a standard pallet. The acquired pressure drop vs. velocity data were used to develop zonal porous media CFD model of airflow and heat transfers inside a fully loaded reefer. Airflow resistance of wooden pallet and the detail structure of T-bar floor were included in the model.

The simulation successfully reproduced the airflow and temperature profiles inside the reefer, high and low airflow and cooling regions were identified. The airflow and temperature distribution inside the reefer were visualized and quantified using vector and contour plots. The model was validated against air velocity and temperature experimental data from a full scale reefer packed with apple. Considering the complexity of the system, a reasonable agreement between the experimental and predicted air velocity and fruit temperature evolution was obtained.

The simulation showed high cooling non-uniformity inside the reefer as confirmed by experimental data. The design of the packaging box used in this study may contribute considerably to the observed cooling non-uniformity because it has no vent holes in its bottom side to help vertical airflow inside the reefer. To assess this, detailed investigation of apple packaging boxes with respect to vertical ventilation (vertical airflow resistance) parameters has been conducted in Part II of this research.

Stellenbosch University https://scholar.sun.ac.za

Chapter 5

5. Numerical evaluation of airflow, heat transfer, and effects of vertical flow inside apple packed refrigerated shipping container fruit packed inside commonly used packaging designs‡

Abstract

In the previous Chapter, a 3-D computational fluid dynamics (CFD) model of airflow and heat transfer inside a refrigerated shipping container (reefer) packed with apple was developed using porous media approach and validated. In this work, the performances of commonly used package boxes used in refrigerated apple containers were investigate. First, the study computes the aerodynamic and thermodynamic characteristics of three package designs. This confirmed the effect of vertical airflow on the rate and uniformity of cooling inside the reefer. Then, the effects of vertical flow resistance on the rate and uniformity of cooling was further investigated. Adding vent-holes on the bottom face of the package reduces the vertical airflow resistance, which leads to significant reduction in fruit cooling time.

‡ Samuel Getahun, Alemayehu Ambaw, Mulugeta Delele, Chris J. Meyer, Umezuruike Linus Opara. 2016. Airflow and heat transfer inside refrigerated shipping container packed with stacked load of apples: Part II – Evaluation of apple packaging designs and vertical flow resistance. Journal of Food Engineering (Submitted).

Stellenbosch University https://scholar.sun.ac.za

Adding a 3.5% vent area in the bottom side of a package reduced the seven-eighth ($7/8^{th}$) cooling time by 27 % (from 55 to 40 h) compared to a package with no vent-hole at its bottom. The study demonstrated the significance of vent-holes on the bottom face of packaging boxes and quantified the energy saving achievable through package design in refrigerated transport systems.

5.1. Introduction

Achieving uniform and rapid cooling during postharvest handling of produce remains a challenge. Several studies showed that non uniform cooling during forced-air cooling, cold storages and refrigerated transportation is caused by a heterogeneous airflow distribution within the fruit stack (Alvarez and Flick, 1999; Delele et al., 2013b; Zou et al., 2006 a,b). The airflow distribution depends on the operation of the cooling system and on how the produce is packed and stacked inside the cooling system (Ambaw et al., 2013; Opara, 2011; Ngcobo et al., 2012; Delele et al., 2013b). The main function of packaging is maintaining the quality of fruits during postharvest handling and storage by providing mechanical protection against injuries, minimizing produce moisture loss and retarding microbial growth (Opara, 2011; Ngcobo et al., 2012). However, packaging boxes are also the major cause of airflow resistance (Delele et al., 2013b).

Vent-holes are provided on packaging boxes to allow cold air to flow within and around the packed produce and warm air to evacuate. The size, shape and location of vent-holes should be in consideration of the mechanical integrity of the box (Pathare et al., 2012) and of the stack formed from the produce-loaded boxes. Hence, optimizing package design has been an area of interest for many researchers. Researchers recommended different optimal packaging designs for horizontal cooling operations (Castro et al., 2004a,b; Castro and Vigneault, 2005; Castro et al., 2005; Hui et al., 2008). Delele et al. (2013b) studied the effect of vent design parameters (vent area ratio, vent shape and number, vent position) on airflow uniformity and cooling rate. The authors showed vent area increment from 7% to 11% only decreased $7/8^{th}$ cooling time by only 5.44% during forced horizontal air

Stellenbosch University https://scholar.sun.ac.za

cooling processes. Castro et al. (2004a, b) also reported increasing vent area above 8% did not show a significant increase in produce cooling rate. In addition to the basic design of the packaging box, wooden pallets used during palletization block available vent areas at the bottom of the pallet. Misalignment of vent-holes during pallet stacking, pallet loading and vent hole obstruction by internal packaging accessories like plastic liners, trays and carry bags, can significantly reduce the cooling air circulation and uniformity of cooling. (Castro et al., 2005; Castro and Vigneault, 2005; Chourasia and Goswami, 2009; Vigneault, 2009). These previous studies mainly focussed on analysing the package designs with respect to horizontal airflow, which is the primary direction of airflow in cold storage rooms and pre cooling systems. The effect of package design with respect to the reefer configurations has not been properly addressed.

Fresh fruit export market uses different design of packaging that have different geometrical configurations and sizes. Display and Telescopic type corrugated fibreboard packaging boxes are the frequently used box types for apple fruit (Berry et al., 2015). In refrigerated shipping container (reefer) with bottom air delivery system the cooling air primarily flows from bottom to the top through packed produce. For this reason, vertical airflow is crucial for the proper handling of the produce inside reefers. Defraeye et al. (2015a, b) reported that airflow resistance contributed by fruit packing boxes becomes worse in a reefer due to the absence of appropriate box designs for vertical airflow in the system and the blockage of the vents. Hui et al. (2008) studied the effect of pallet configuration and bracing patterns on airflow distribution in refrigerated semi-trailers and the results obtained from 20 field tests varied greatly within each category. Although no firm conclusion was drawn, the authors reported that arranging pallets in a pinwheel pattern tends to assist air circulation better than an offset pattern. The aforementioned packaging boxes, if are not designed, stacked and palletized in consideration of reefers, can significantly limit the rate and uniformity of the cooling. Hence, it is important to study the suitability of these packaging boxes in reefer containers.

Stellenbosch University https://scholar.sun.ac.za

Study of cooling operation in a system as large and complex as a reefer can be approached experimentally by measuring the spatio-temporal temperature dynamics. Data obtained from the measurement is processed to estimate cooling coefficients, $7/8^{th}$ cooling times and cooling uniformities to perform a comparative assessment of designs (Akdemir and Arin, 2006). However, experimental approach alone is not convenient to perform an exhaustive investigation. It is economically expensive and time consuming. By combining experimental measurements with mathematical models, a more comprehensive analysis can be made (Ambaw et al., 2013, Dehghannya et al., 2010; Defraeye et al., 2015c; Verboven et al., 2006). Due to its powerful visualization capabilities and acceptable accuracy of its numerical predictions, computational fluid dynamics (CFD) is the primary method of choice to model mass and heat transfer processes in the postharvest cold chain (Norton and Sun Da-Wen, 2006; Smale et al., 2006). It has been effectively applied to study, optimize and design processes that are related to horticultural produce precooling (Defraeye et al., 2013; Ferrua and Singh, 2009a, b; Zou et al., 2006a, b), storage (Ambaw et al., 2016; Delele et al., 2009ab; Hoang et al., 2015; Nahor et al., 2005) and transportation (Menia et al., 2002; Alvarez et al., 2003; Defraeye et al., 2015b; Moureh and Flick, 2004; Tapsoba et al., 2007).

The aim of the present work is to examine the aerodynamic and thermodynamic performances of three different package designs commonly used in apples fruit cold chain while used in reefers. To accomplish this, a validated CFD model of the airflow and temperature distribution inside a fully loaded reefer was used. Additionally, the effects of vertical flow-resistance on the rate and uniformity of cooling was investigated using the CFD model.

5.2. Materials and methods

5.2.1. Packaging boxes

In this study three corrugated fibre carton (CFC) packaging boxes that are commonly used in apple fruit storage were examined. Figure 5.1 depicts the shape of the Econo-D, Mark9 (Mk9) and Mark6 (Mk6) boxes with their corresponding

Stellenbosch University https://scholar.sun.ac.za

bottom surface ventilation area. The Econo-D box has an outer (L × H × W) dimension of 49.0 cm × 26.0 cm × 29.0 cm and is 3 mm thick (Figure 5.1a). The short side has two horizontally oriented rectangular vent holes at the bottom region and one larger horizontally oriented rectangular vent hole (is also the handle) on the top middle region. Notice that the bottom vent hole is not accessible as an airflow path because during stacking this vent hole would be blocked. The long side has two circular vent holes positioned in the middle. The Econo-D contains 8 clusters of apple fruit in plastic bag. Each bag contains approximately 1.5 kg of apple. Hence, Econo-D carries a total of 12 kg apple fruit.

The Mk9 has outer (L×H×W) dimensions of 60.0 cm ×13.2 cm × 38.8 cm and is 3 mm thick (Figure 5.1b). This box has one vent at the bottom of the short sides and two rectangular holes at the bottom of the long sides. However, these holes are meant for socketing during stacking and hence would not be fully accessible as a flow path. The box also has a rectangular cut out at the top rime of the long side. Mk9 contains 7 bags of apple clusters, each 1.5 kg. Hence, a total of 10.5 kg of apple are contained in Mk9 packaging box.

Stellenbosch University https://scholar.sun.ac.za

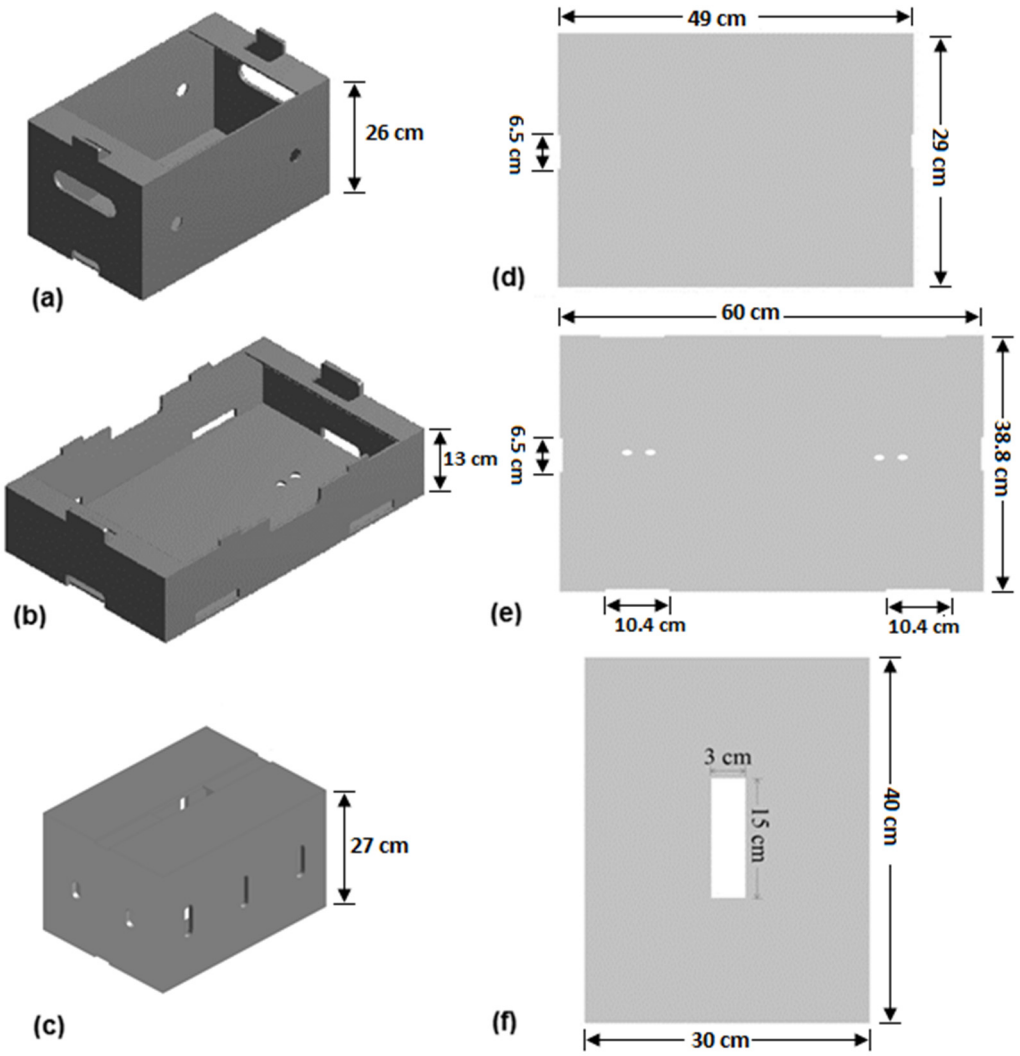

Figure 5-1: Schematics of the three package designs examined in this study. Isometric view of Econo D (a), double layer display carton box (Mk9) (b) and Telescopic packaging box (Mk6) (c). The right column depicts the bottom side of the Econo D (d), Mk9 (e) and Mk6 (f) boxes. Sizes shown correspond to the external dimensions.

The Mk6 has a Telescopic design with outer (L×H×W) dimensions of 40.0 cm× 30.0 cm × 27.0 cm (Figure 5.1c). It is 6 mm thick except the top and bottom where the thickness is 3 mm thick. It has two vents on the short side of the box and three vents on the long side. One rectangular shaped opening is placed at the top and bottom. Mk6 packaging box contains 9 kg of apple clustered in six bags,

Stellenbosch University https://scholar.sun.ac.za

each weigh 1.5 kg. Table 5.1 summarizes the loading capacities and vent hole characteristics of the boxes.

Table 5-1 Ventilation area ratio (VAR), loading characteristics of the Econo-D, Mk9 and Mk6 boxes

Box design	**Dimension, cm (L×H×W)**	**Apples/box**	**Capacity (kg)**	**Ventilation area ratios (%)**		
				Bottom side	**Long side**	**Short side**
Econo-D	49.0 ×26.0 × 29.0	88	12.0	0.00	1.09	1.80
Mark 9	60.0 ×13.0 × 38.8	70	10.5	0.25	3.07	4.00
Mark 6	40.0 ×27.0× 30.0	66	9.0	3.50	4.80	2.60

During cooling operation in a reefer, the ventilation area at the bottom side of the boxes is crucial. The Mk6 box has the highest bottom side vent-hole ratio and is expected to perform better in the cooling process compared to the Econo-D and Mark9 boxes.

Econo-D, Mk9 and Mk6 are stacked on a pallet in different patterns. The Econo-D Pallet contains 8 layers with each layer having 10 boxes arranged in a pattern as shown in Figure 5.2 a & b. Hence, this pallet contains a total of 64 boxes each containing 12 kg of apple fruit. The Mk9 pallet has 16 layers and each layer contains 5 boxes. Hence, a total of 80 boxes are in Mk9 pallet each containing 10.5 kg of apple (Figure 5.2 b & d). The Mk6 contains 8 layers with each layer having 10 boxes arranged in a pattern as shown in (Figure 5.2 e&f). Hence, this pallet contains a total of 80 boxes each containing 9 kg of apple fruit. Table 5.2 summarizes the details of palletization and stacking for each box design.

Stellenbosch University https://scholar.sun.ac.za

Table 5-2 Palletization and stacking of the three packaging boxes inside a reefer

Pallet	Pallet Dimension, cm (L×H×W)	Number of box per pallet	Mass of apple per pallet (kg)	Total load in reefer (kg)
Econo-D	120×2.08×100	64	768	15360
Mark 6	120×2.16×100	80	720	14400
Mark 9	120×2.08×100	80	840	16800

The Econo-D and Mk9 boxes have an interlocking mechanism that contributes for stability of the pallet. Therefore, stacking of these two designs takes place with identical layers from bottom to top of the pallet. However, Mk 6 and several other Telescopic packaging boxes has no such interlocking mechanism and hence the pallet of this box design has a staggered pattern to ensure stability (Defraeye et al., 2015 b) (Figure 5.2 c).

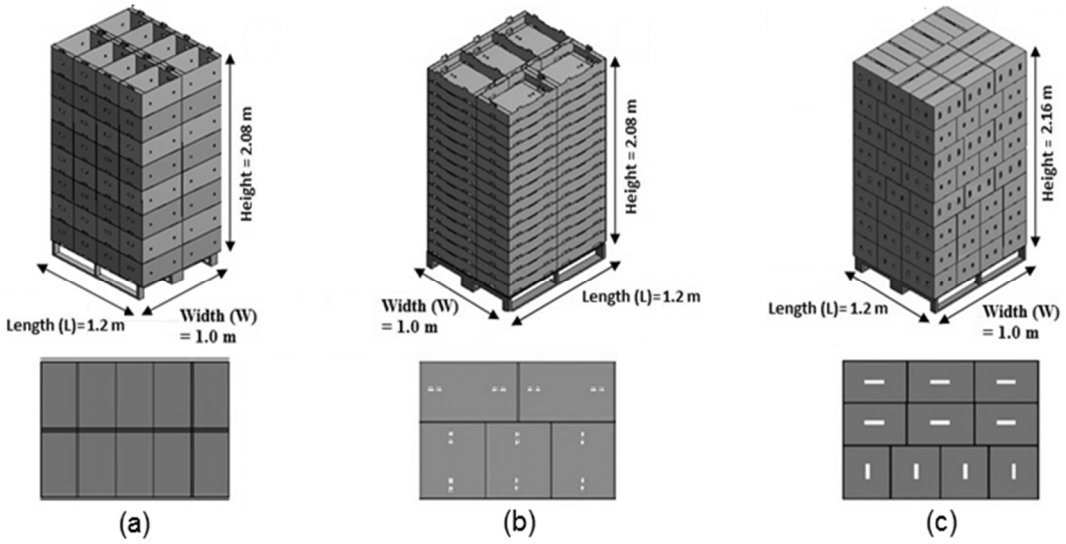

Figure 5-2: Stacking of the packaging boxes in to a pallet. The top row shows the palletized Econo-D (a) Mk9 (b) and Mk6 (c) packaging designs. The bottom row shows the corresponding box arrangement of an individual layer forming the pallet. Notice that pallet of the Mk6 packaging box is stacked in a staggered manner in the top half to ensure stability

Stellenbosch University https://scholar.sun.ac.za

Three reefers that were loaded with 20 pallets of apple packed using Mk 6, Mk9 and Econo-D packaging boxes are considered in this study. The arrangement of the pallets inside the reefers was in two rows. Row 1 contains 11 pallets while row 2 contains nine. The two rows have different pallet orientation.

5.2.2. Wind-tunnel experiment

Characterization of the airflow resistances of pallets of the three package designs were by use of a wind tunnel experiment. The test was conducted for the bottom and top half of the pallets. The bottom half of a pallet stacked with Mk6 and Mk9 consist a wooden pallet in addition to 4 and 8 layer of boxes, respectively. To represent apple fruit water filled plastic balls with a diameter of 8 cm were used. The airflow resistance in each flow direction (X-direction (across the length=1.2 m (L)), Y- direction (vertical= 1.08 m (V)), (Z- direction (across the width=1 m (W). For the vertical flow direction, the test was conducted with and without the wooden pallet to represent bottom half (V-B) and the top half (V-T) of a pallet using the experimental set up described in the previous chapter.

5.3. Mathematical modelling

5.3.1. Governing equations

The current study is built on our previous chapter which describes the porous medium formulation. In the approach, the palletized fruit inside the reefer consisting of the packaging boxes, stacked apples and air gaps between apples form a continuous and homogeneous porous medium. This method avoids the small details of the stack geometry such that the airflow, temperature and gas distributions were solved using a volume-averaged Reynolds Averaged Navier-Stokes equation.

The present study extends the investigation by addressing the performance of two additional fruit packaging boxes, commonly used in apple storage. The developed and validated model employed for a further investigation of vent areas (on the bottom side of a box) on airflow, temperature distribution and cooling performances of reefers.

Stellenbosch University https://scholar.sun.ac.za

5.3.2. Model parameters

The model parameters of the porous domain were calculated taking into account the proportion of fruit, package materials and the air entrained inside the apple packages. This was accomplished by using average material properties based on the volume proportion of each part in the porous domain. Resistance of airflow through the pallets was obtained from a measured pressure drop vs. airflow data in a wind tunnel experiment. The resistance values were then used to characterize the porous medium in the CFD model. Table 5.3 summarizes the resistance terms.

5.3.3. Boundary and initial condition

The reefer was in thermal contact with the ambient air with the door, walls, ceiling and floor as its boundaries. Inside these boundaries we have the porous domain consisting of all fruit loaded boxes and the remaining region which is the free air stream is defined as fluid domain. The cooling unit was represented by specifying temperature and velocity boundary condition at exit from the cooling system. In all the models, the internal walls of the reefer were set to a no slip walls and the heat exchange with the environment has been incorporated.

5.3.4. Simulation setups

The domains of each model were discretized using tetrahedral elements. For every model, the level of grid independence was evaluated using Richardson extrapolation method (Ambaw et al., 2016; Franke et al., 2007; Roache 1994). The transport equations were numerically solved using the finite volume method in ANSYS-Fluent-16 (ANSYS, Canonsburg, PA, USA). Turbulence was calculated using k-ω SST model. SIMPLE discretization scheme was used for pressure-velocity coupling and second order upwind discretization was used for momentum, specific dissipation rate and energy calculations. Time step size of 180 s with maximum 20 iterations per time step, was used. For each porous medium model, a steady state calculation was performed to obtain a converged solution of the airflow. The steady state solutions were used as the initial value for the subsequent transient heat transfer calculation. Under the selected optimum solver format, a single full

Stellenbosch University https://scholar.sun.ac.za

simulation took 40 to 60 h on a 64-bit, Dell Precision T3600, Intel Xeon CPU E5-1660 0 @3.30 GHz 3.30 GHz and 40GB Ram, Windows 7 PC.

5.3.5. Simulations

First, to investigate the airflow and temperature distributions inside a reefer containing apple fruit stacked with commonly used apple packaging boxes, namely Mk6 and Mk9 were simulated. For these simulations previously the validated model in which fruit was packed in Econo-D packaging box was used. Then, three separate simulations were conducted to assess the effect of bottom vent area variation on the airflow distribution and cooling uniformity, keeping all other factors constant. For this task, the validated porous medium CFD model corresponding to the Econo-D pallet was taken as a base model (VAR on the bottom side is zero) and its vertical airflow resistance was virtually reduced by 25 % (Ec-25), 50 % (Ec-50) and 75 % (Ec-75).

Stellenbosch University https://scholar.sun.ac.za

Table 5-3 Experimentally determined coefficients of the Darcy-Forchheimer equation of the three different pallets and for the modified Econo-D boxes.

	Packaging Design	Direction	$\frac{1}{K}(m^{-2})$	$\beta(m^{-1})$
Commonly used apple packaging boxes	Mk 6	X- direction	3.3×10^{6}	3717
		Y-Top half	2.4×10^{5}	8077
		Y-Bottom half	4.8×10^{5}	10456
		Z-direction	2.0×10^{8}	3023
	Mk 9	X- direction	147.0	7320
		Y-Top half	7.5×10^{7}	1158
		Y-Bottom half	9.6×10^{7}	1474
		Z-direction	134.0	11600
	Econo-D	X- direction	6×10^{5}	41438
		Y-Top half	3.1×10^{6}	77072
		Y-Bottom half	6.6×10^{7}	113174
		Z-direction	1.7×10^{6}	2110
Modified Econo-D	Ec-25	X- direction	6.0×10^{5}	41438
		Y-Top half	1.8×10^{6}	36387
		Y-Bottom half	9.4×10^{6}	9238
		Z-direction	1.7×10^{6}	2110
	Ec-50	X- direction	6.2×10^{5}	41438
		Y-Top half	1.0×10^{6}	17126
		Y-Bottom half	2.2×10^{7}	25150
		Z-direction	1.7×10^{6}	2110
	Ec-75	X- direction	6.2×10^{5}	41438
		Y-Top half	4.4×10^{5}	6291
		Y-Bottom half	4.4×10^{7}	43893
		Z-direction	1.7×10^{6}	2110

5.4. Result and discussion

5.4.1. Characterizing the airflow resistances

Figure 5.3 shows the result of the pressure drop vs flow rate data obtained from the wind tunnel experiment. Curve fitting of the data points to the Darcy-

Stellenbosch University https://scholar.sun.ac.za

Forchheimer equation characterizes the airflow resistances of the pallets. Table 5.3 summarizes the viscous (K-(m^{-2})) and inertial coefficients (β–(m^{-1})).

The lowest airflow resistance was observed for the Mk9 box at a horizontal airflow perpendicular to the width of the pallet (Mk9-L). However, Mk9 also has a very high airflow resistance against a horizontal airflow perpendicular to the length of the pallet (Mk9-W). Interestingly, even though the size of the width (1 m) is less than the length (1.2 m) the airflow resistance was much higher. This was mainly due to the interlocking feature of the Mk9 boxes that has blocked most of the vents on the pallet face perpendicular to the airflow direction. The only airflow path was the crevices/gaps between the boxes. The airflow resistance in this direction was similar to what was found for the vertical airflow resistance in the bottom half which include the wooden pallet. This showed the severity of the airflow resistance across the length.

The effect of the wooden pallet on the vertical airflow was clearly visible in both Mk6 and Mk9 stacked pallets. In Mk6 stacked pallet the layers in the top half were arranged in staggered manner but due to the effect of the wooden pallet the vertical airflow resistance in the bottom half was higher. As reported in previous chapter of the authors the wooden pallets block 70 % of the vents in the bottom layer of Mk6 stacked pallets. The vertical airflow resistance was high in the bottom half of the pallets in both Mk6 and Mk9. Better airflow (the least airflow resistance) was found for the airflow across the width in both pallets due to more direct airflow characteristics that was facilitated by alignment of the vents. Similar characteristics were observed by Ngcobo et al. (2012) plastic liners and carry bag (similar to carry bag used for apple) used for table grape fruit contribute over 80 % and 30 %, respectively, of the total pressure drop in Mk9 box.

Stellenbosch University https://scholar.sun.ac.za

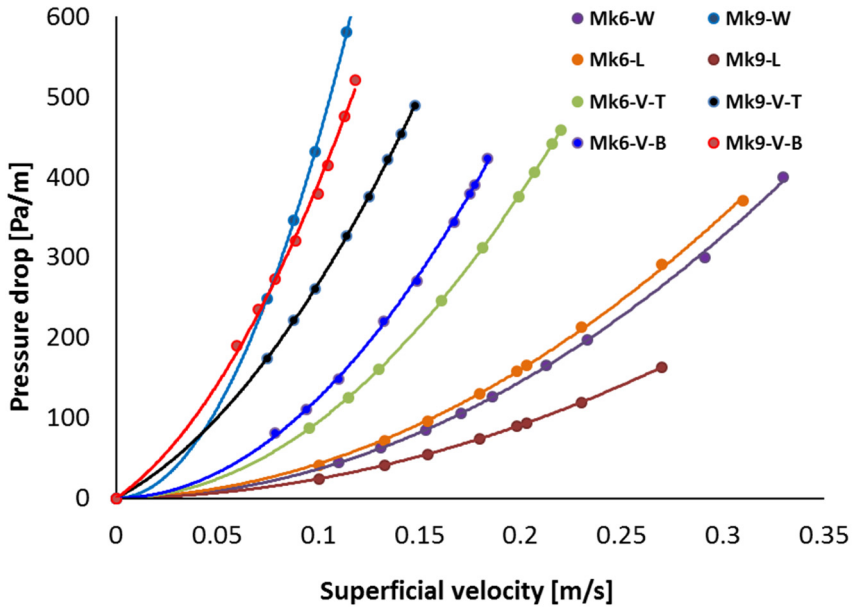

Figure 5-3: Experimentally obtained pressure loss vs. flow rate profiles of palletized Mk6 and Mk9 boxes. Pressure loss profiles for horizontal airflow perpendicular to the width (Mk6-L and Mk9-L) and, perpendicular to the length (Mk6-W and Mk9-W). The profiles of the pressure loss along the vertical direction were obtained for the bottom half of the pallet (Mk6-V-B and Mk9-V-B) and for the top half of the pallet (Mk6-V-T and Mk9-V-T). The bottom half incorporated the airflow resistance due the wooden pallets. Results for Econo-D (Figure 4-6).

To assess the effect of bottom vent area variation whilst keeping other factors constant one packaging box design (Econo-D) was chosen. For this study pallet stacked with the Econo-D box design was evaluated by varying it's the vertical flow resistance by 25 % (Ec-25), 50 % (Ec-50) and 75 % (Ec-75). Its 75 % flow resistance variation per unit length was almost the same as that of the flow resistance per unit length calculated for the Mk 6 box design which has 3. 5 % bottom vent area (Figure5.1). Therefore, two vertical flow resistances (Econo-D and Mk 6) were set as references for the worst case and the best-case scenarios to make sure the evaluation represents the reality, fairly.

5.4.2. Analysis of the airflow distribution inside the reefer

Profile of vertical airflow inside the reefer

Stellenbosch University https://scholar.sun.ac.za

The range of the vertical air velocity magnitude varies from one load to the other depending on the packaging design used for the fruit and the amount of fruit loaded. The amount of air reaching the fruit in the stacked load depends on the airflow resistances, which in turn dependents on the packaging design, amount of fruit, pallet stacking, and pallet orientation. Figure 5.4 depicts the magnitude of the vertical component of the air velocity (V_v) across each pallet of the row 1 and row 2 inside the reefer. The magnitude of the vertical airflow ranges from 0-0.026 m s^{-1} to 0-0.037 m s^{-1} in pallet row 1 and row 2, respectively. Notice that the airflow distribution in the reefer with Mk6 was more uniform and relatively higher in magnitude than the other box designs (Figure 5a&b). This box design is the one with the highest vent area ratio at the bottom side compared to the others. The result in part confirms the importance of vent holes on the bottom side of fruit packaging box.

Stellenbosch University https://scholar.sun.ac.za

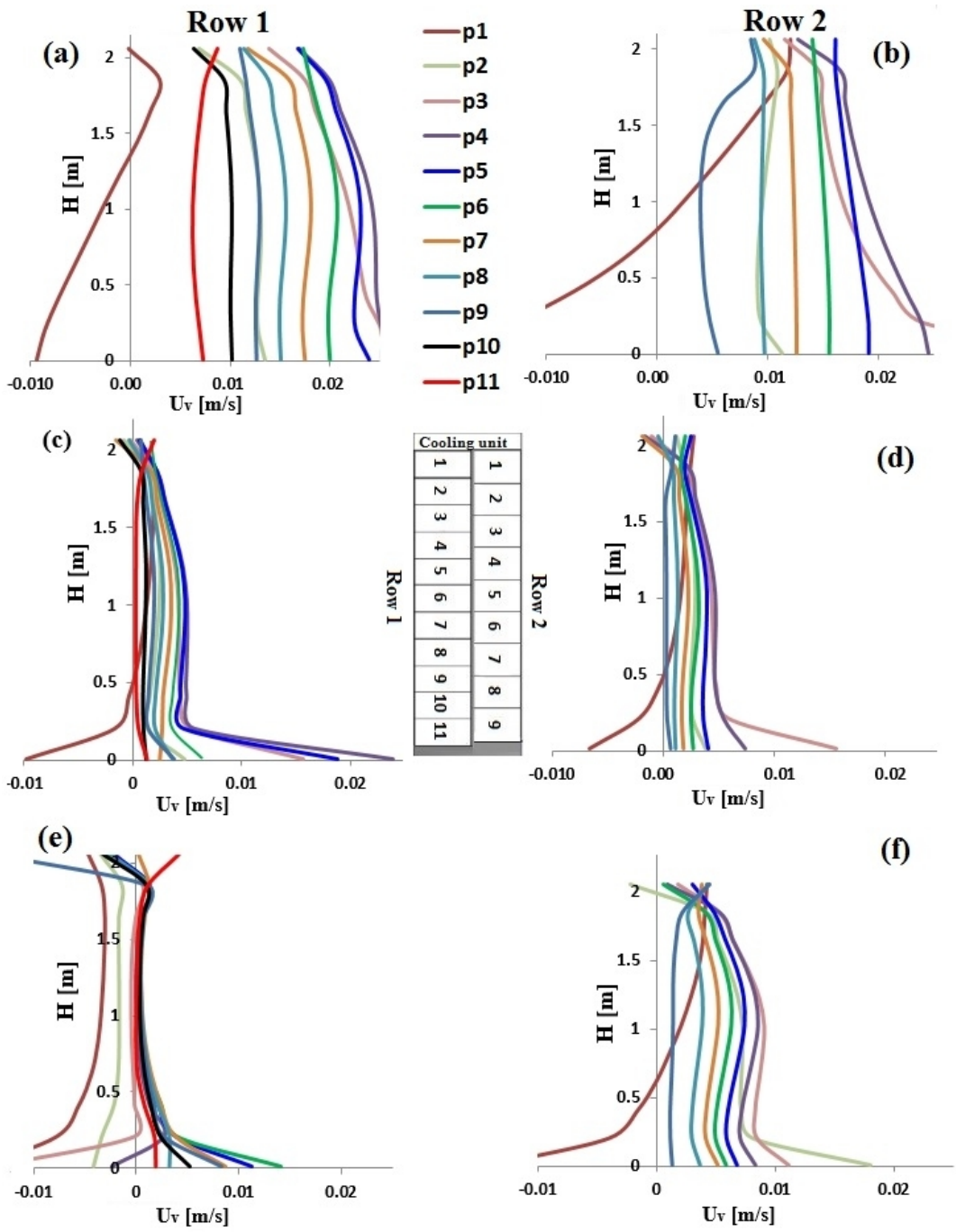

Figure 5-4: Predicted vertical airflow velocity profiles in the pallets configured in row 1 and row 2 inside a reefer with the Mk 6 (a)(b), Mk9 (c)(d) and, Econo-D (e)(f). The simulations correspond to a reefer working at an inlet airflow and temperature of 5400 $m^3 h^{-1}$ and -1 °C.

Stellenbosch University https://scholar.sun.ac.za

Pallet 1 and pallets closer to the reefers door (8, 9, 10, 11) showed a relatively low vertical airflow profiles. Pallet 1(p1) of both row 1 and row 2 are at low vertical airflow. This is due to the fact that the direction of airflow near the inlet region is mainly horizontal and Coanda effect further suppresses vertically directed flows in this region. Pallets 8, 9, 10, 11 are in the region where recirculation is dominant (Figure 5.4). The vertical air velocities in the pallets 3, 4, 5, 6 in each row were above average vertical velocity in their respective rows for the Mk6 and Mk9 designs. In the reefer packed with Econo-D packaging design the vertical airflow was very low in row 1, this could be due to the pallet orientation.

In row 1 the average vertical air velocity of Mk9 stacked pallets was 8-fold of Econo-D box stacked pallets (Figure 5.4c and Figure 5.4e, respectively). In row 2 the average vertical air velocity of Econo-D box stacked pallets was 2-fold of Mk9 stacked pallets (Figure 5.4 f & d, respectively). The ratio of fruit per pallet for the Econo-D and Mk9 stacked pallets was 1.1:1. This implies higher cooling air to fruit ratio was in effect for the Mk9 stacked fruit in both pallet rows. The average specific flow rate (L (s kg) $^{-1}$) in the two pallet rows inside the Econo-D, Mk9 and Mk6 containing reefers were (1.97×10^{-4},1.69×10^{-4}); (3.30×10^{-3}, 2.90×10^{-3}) and (2.40×10^{-2}, 2.00×10^{-2}), respectively. Specific airflow rate for a typical reefer normally ranges between ≈0.02 and 0.06 L (s kg)$^{-1}$ of fruit (Defraeye et al., 2015b,c). Notice that it is only the reefer packed with fruit in Mk6 box design that has fallen in the anticipated range at the normal inlet airflow rate of the reefer (1500 L s^{-1} or 5400 m^3 h^{-1}). This could be due to the circumstance that amount of air that can reach the fruit stacked in a pallet mainly dependant on the flow resistance of pallets. Of course, it is possible to increase the specific flow rate by increasing the flow rate of incoming air but it will increase operating costs. The other option is decreasing the airflow resistance in a pallet by optimizing packaging designs with respect to the cooling system for which they intended to be used.

Stellenbosch University https://scholar.sun.ac.za

Profile of horizontal airflow inside the reefer

Figure 5.5 shows the result of the horizontal airflow analysis inside the reefers corresponding to the three box designs. There is a clear difference in the airflow distribution between the box designs. Since the pallet orientations are different in the two rows inside a reefer, the horizontal airflow profiles of the two rows were also noticeably different. Hence, airflow profile inside a reefer varies in all spatial direction. The horizontal air velocity magnitude increase from zero to reach a maximum and decrease to reach a relatively steady air velocity after the first four meters for all the reefers. The fluctuation in the first four meters was a result of the recirculating flow of the incoming air in the region and has an opposite flow direction. The horizontal airflow velocity in the reefers ranges between 0 and 0.019 m s^{-1}.

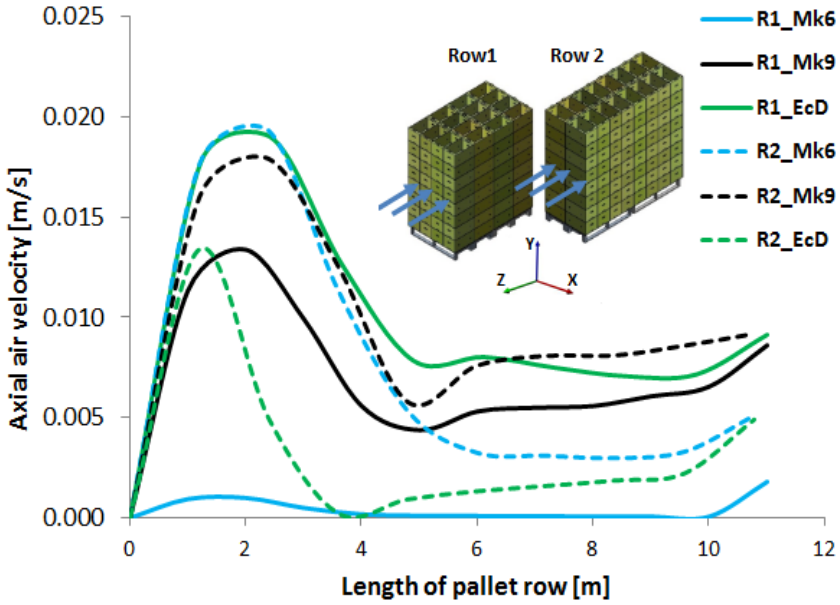

Figure 5-5: Average horizontal airflow magnitudes through row1 and row2 inside a reefer along the Z-axis. Pallets in row 1 and row 2 were configured with horizontal airflow (Z-direction) across the width and length of the pallets, respectively. The simulations correspond to a reefer working at an inlet airflow and temperature of 5400 m^3 h^{-1} and -1 °C.

Stellenbosch University https://scholar.sun.ac.za

For the pallets in row 1 and row 2 horizontal airflow was across the width and the length of pallets, respectively. Airflow in a reefer is a complex three dimensional flow (Defraeye et al. 2015b), the airflow characteristics in one direction is not only a result of an airflow resistance in the given direction but also the airflow characteristics in the other directions. This was reflected in the reefer with Mk6 packaging design. The horizontal airflow in row 1 (flow across the width or X-direction) was much lower than row 2 (flow across the length or Z-direction) despite the higher airflow resistance across the length (similar to row 2 configuration) than across the width (similar to row 1 configuration) (Figure 5.3). It was also found that average vertical airflow in row 1 was 15 % higher than in row 2. From this it can be concluded that the horizontal and vertical airflow in the two pallet rows were inversely related. This was consistent with all the rows of Econo-D, Mk9 and Mk6 stacked fruit pallets. The average horizontal air velocity was higher in row 2 than in row 1 for Mk6 and Mk9 packed reefers. And in the Econo-D packed reefer horizontal air velocity was higher in row 1 than in row 2. In contrast, vertical air velocity was higher in row 1 than in row 2 for Mk6 and Mk9, whereas it was higher in row 2 for Econo-D packed reefer.

Mk9 stacked reefers the magnitude of horizontal airflow velocity was higher in row 2 than in row 1. This was consistent with the airflow resistance characteristics of the Mk9 pallet for flows across the width and the length (Figure 5.3). For Econo-D higher horizontal airflow was found in pallet row 1(across the width), in which the lowest airflow resistance was recorded across the Econo-D pallet width.

Horizontal airflow magnitude comparison with respect to pallet orientation (row 1 and row 2) showed the airflow characteristics depend on the packaging design and how the pallet is configured in a reefer. It was also shown that the display type packaging boxes (Mk9 and Econo-D) have higher horizontal airflow (row 1 and 2 for Mk9; row 1 for Econo-D) compared with Telescopic Mk6 packaging design, particularly after the recirculating flow was settled down (from 5 m to

Stellenbosch University https://scholar.sun.ac.za

11 m). This could be due to the limited ventilation on the bottom (vertical airflow resistance) which resulted in an increase in horizontal airflow.

5.4.3. Analysis of the temperature distribution and the cooling rate

Figure 5.6 shows simulated contours of produce temperature profile on horizontal plane (perpendicular to the Y-axis) bisecting the reefer (all the pallets) in the horizontal direction. The contour corresponds to the instantaneous temperature distribution inside the reefers at 24, 48 and 72 hours of cooling. Clearly the temperature distributions are still highly non uniform even after 24 hours of cooling. Temperatures profile inside the reefers with the Mk6, Mk9 and Econo-D boxes was between -0.5 ℃ and 7.85 ℃.

Notice that the high temperature regions were close to the reefer walls and at the corners of the pallet rows. This was due to the lack of space between the reefer wall and the load which confines the removal of heat from the fruit in the region and heat from the environment. Mk6 packaging box provided the highest cooling rate as expected from its superior performance with respect to vertical airflow profile.

In all the cases, the pallet near the cooling air entrance and those at the rear of the reefer are relatively warmer. The reefers with the Mk9 and Econo-D boxes are characterized by a colder central region and warmer periphery. The reefer with the Mk6 box was distinct. It is colder than the reefers with the Mk9 and Econo-D boxes. This goes in accordance to its low airflow resistance in the vertical direction which provided better ventilation of the packed fruit.

Temperature heterogeneity within a single pallet was also significant. For example, in the reefer with the Mk9 and Econo-D boxes, produce adjacent to the central air gap (between row1 and row2) would be cooler than produce adjacent to the reefer wall. This was because heat from fruit in the boxes adjacent to the air gap was removed easier than the wall side which faces the reefer wall that restricts the removal of heat from the fruit into the free air.

Stellenbosch University https://scholar.sun.ac.za

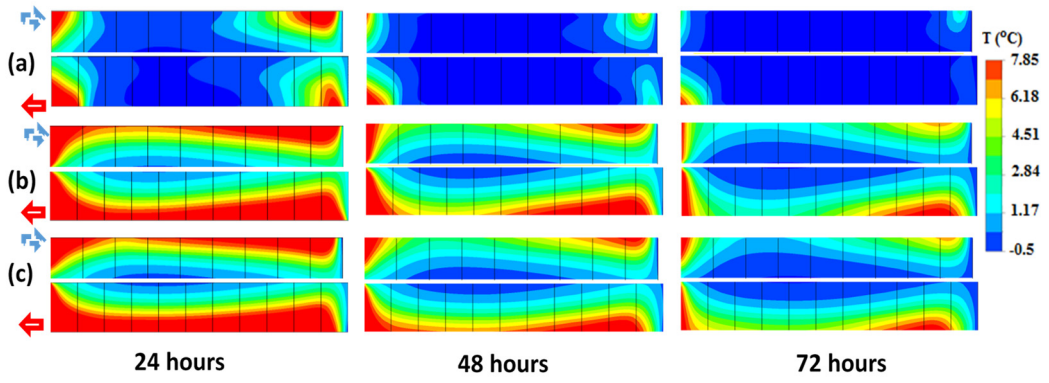

Figure 5-6: Temperature contour in time on a horizontal (ZX) plan bisecting the reefer with the Mk6 (a), Mk9 (b) and Econo-D (c) packaging boxes.

This shows the importance of air gap between pallets (Jedermann et al., 2013). Defraeye et al., (2015b) also showed the influence of air gaps between boxes in a pallet. Figure 5.7 shows simulated contours of produce temperature profiles on vertical planes (perpendicular to the X-axis) bisecting the two rows inside the reefers at 72 hours. Standard deviation (SD) was used to evaluate temperature uniformity in the reefers by considering temperature in 3 layers per pallet (bottom, middle and top layer temperature). The overall temperature SD in the reefers packed with Mk6, Econo-D and Mk9 were 0.43, 0.86 and 1.34 ℃, respectively. From this it can be established that after 72 hours (3 days) of cooling reefer packed with fruit in Mk6 packaging design gives a much better uniformity in the domain followed by Econo-D and Mk9 packaging designs. Temperature uniformity also varies with respect to pallet orientation in a reefer. The SD of Mk6, Econo-D and Mk9 reefers were 0.49, 0.94, 1.50 ℃ in pallet row 1 and, 0.36, 0.76, 1.10 ℃ in pallet row 2, respectively. In both pallet rows more homogenous cooling was obtained for Mk6 packaging design with less than 2 ℃ difference between maximum and minimum temperatures in the pallets. In all the packaging designs pallets configured in row 2 showed a better uniformity and, fast cooling was observed in pallets in row 2 for Mk9 and Econo-D packaging designs. This was also mirrored in the decreased size of hot regions in the models.

Stellenbosch University https://scholar.sun.ac.za

Produce in p2 to p6 of row 1 and p2 to p5 in row 2 were relatively colder than that of the other pallets (Figure 5.7). This goes in accordance to the cooling air distribution inside the reefer as discussed in the airflow distribution (sec 3.2.1). The magnitudes of vertical airflow in these pallets were above average (Figure 5.4). Although the vertical airflow of the supply cooling air is critical, the returning air also played a minor role in the cooling operation. This can be clearly observed in the Mk9 and Econo-D packed reefers' temperature profiles. The top of the pallets (parallel to the return air flow region) and the top half of last pallet that reached the desired temperature (Figure 5.7 b&c).

Figure 5.8 depicted the average temperature history in row 1 and row 2 of the three reefers. Thermal heterogeneity of fruit is not only generated due to insufficient flow rate of the cooling air, but also by a non-uniform distribution of cooling air within the palletized structure (Alvarez and Flick, 1999). As shown in Figure 5-4 vertical air velocity is almost three times higher near the bottom of the pallets than the in the middle particularly, in the reefers packed with Econo-D and Mk9 packaging designs. Although higher velocity that seem to be more beneficial for fast cooling, local higher cooling rates are actually not desired since they introduce higher cooling heterogeneity of fruit within a container (Defraeye et al., 2014). The HCT and SECT differ between rows inside a reefer and between package designs. Table 5.4 summarizes the HCT and SECT per reefer. There was a 2, 6 and 9-hour difference between the SECT of row1 and row2 inside the reefer containing the Econo-D, Mk6 and Mk9 boxes, respectively. The cooling rate was more uniform inside the reefer packed with the Mk6 box. This box has the highest vent area ratio on its bottom face which resulted better vertical airflow in the pallets as compared to Mk9 and Econo-D packed pallets (section 3.2.1). In addition, the total fruit mass in Mk6 containing reefer was lower than Econo-D and Mk9 containing reefers by 6.6 % and 16.67 %, respectively. Hence, Mk6 is characterized by its fast cooling performance and worst space utilization. However, fruit industries are more interested on maximizing the amount of fruit loaded in a reefer by employing large packaging boxes to minimize the space used by the packaging

Stellenbosch University https://scholar.sun.ac.za

boxes. The larger the packaging boxes the better is the space utilization. However, large weight (>18 kg) is inconvenient for manual labour (Berry et al., 2015). Mk9 and Econo-D packaging box designs carry 10.5 and 12 kg per box, respectively, which is manageable but the cooling performance of these boxes were not good. By carefully providing vent-holes in the bottom sides of these two boxes it is possible to improve their cooling performance. Further assessment of this aspect is made by virtually modifying the Econo-D box. The result of this modification is discussed in the section below.

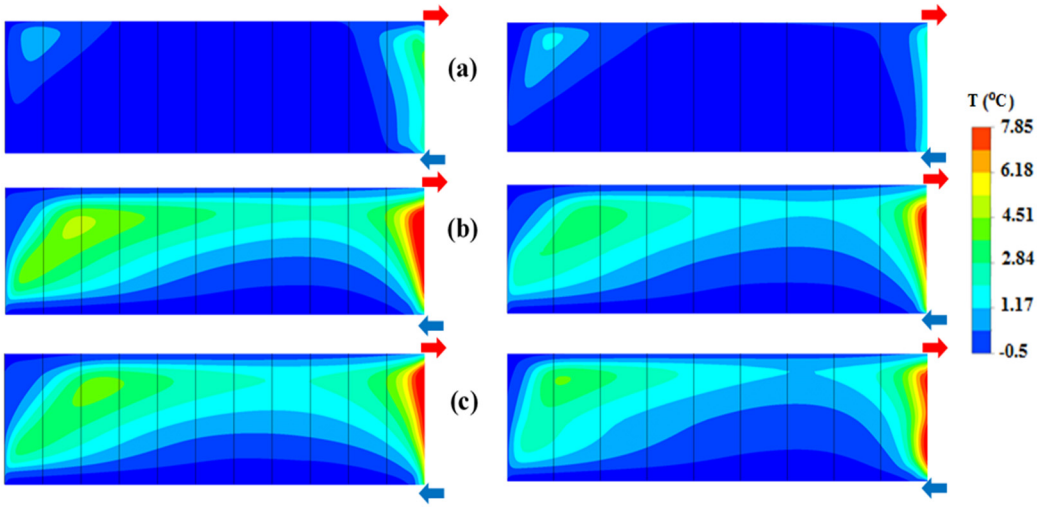

Figure 5-7: Temperature contour at 72 h on vertical (YZ) planes bisecting row 1(left) and row 2 (right) of the reefer with the Mk6 (a), Mk9 (b) and Econo-D (c) packaging boxes.

Stellenbosch University https://scholar.sun.ac.za

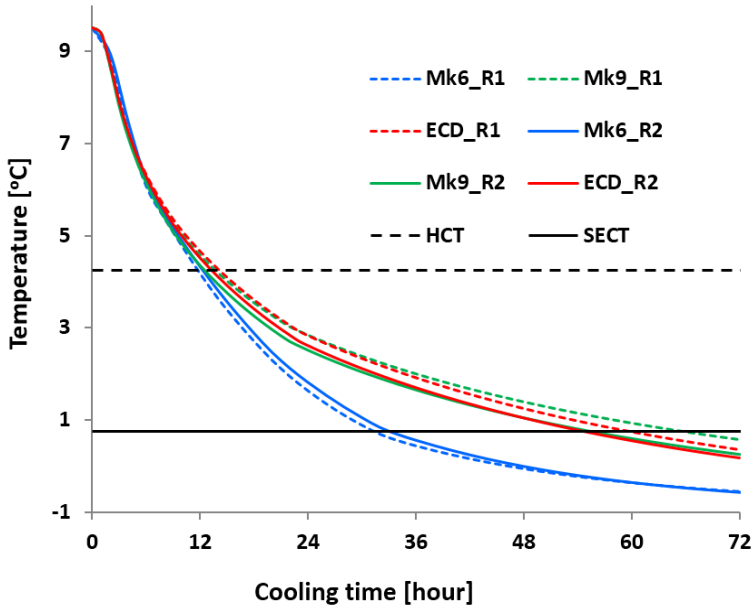

Figure 5-8: The produce temperature history (average) in row 1 (broken lines) and row 2 (solid lines) inside reefer with Mk6 (Blue), Mk9 (green) and Econo-D (red) boxes. The half cooling time and the 7/8th cooling time are marked with horizontal broken and solid lines, respectively.

Table 5-4 Average HCT and SECT of the different packaging designs in the two pallet rows

Packaging design	Fruit in reefer (tonne)	HCT (Hour)		SECT (Hour)	
		row 1	row 2	row 1	row 2
Mk9	16.8	14	13	66	55
Econo-D	15.36	13	12	60	54
Mk6	14.4	6	6	32	34

5.4.4. Influence of the vertical airflow resistance

To emulate the effect of bottom side vent-holes on the airflow distribution and the cooling performance, the vertical airflow resistances of the Econo-D box was reduced by 25 % (Ec-25), 50 % (Ec-50) and 75 % (Ec-75) from the experimentally obtained values. Hence, simulations were performed to calculate the airflow and temperature distribution in reefers packed with fruit in these modified Econo-D boxes. Figure 5.9 depicts the result of the analysis on the magnitude of air velocities along the vertical direction. Reducing the airflow resistance generally increases the vertical airflow magnitudes in both row1 and row2 inside the reefer.

Stellenbosch University https://scholar.sun.ac.za

The vertical air velocity in row1 of the Ec-25, Ec-50 and Ec-75 were 6, 10 and 20 fold of that of the original Econo-D box, respectively. Since the average vertical air velocity in row1 was very low (0.001 m s^{-1}) in the original Econo-D box the increments as the resistance reduced were more prominent than in row2. In row2 vertical air velocity increased by 1.10 fold, 1.12 fold and 2.50 fold were found for Ec-25, Ec-50 and Ec-75, respectively.

The specific flow rate (L $(s\ kg)^{-1}$) in the two pallet rows (R1&R2) of reefer models, 75% (Ec-75), 50% (Ec-50) and 25% (Ec-25), were 1.97×10^{-4} (R1) &1.69×10^{-4}(R2), 2.7×10^{-4}(R1) & 2.7×10^{-4}(R2), 1.97×10^{-4}(R1) & 1.94×10^{-4}(R2) and 1.64×10^{-4}(R1) & 1.54×10^{-4} (R2), respectively. The average specific airflow rate showed a 35% and 62 % increase in row1 and row2, respectively, as vertical airflow resistance decrease from the base model to Ec-75. This shows the prospect of increasing supply air to fruit ratio in the pallets by improving the bottom ventilation of the packaging boxes during cooling operation in a reefer.

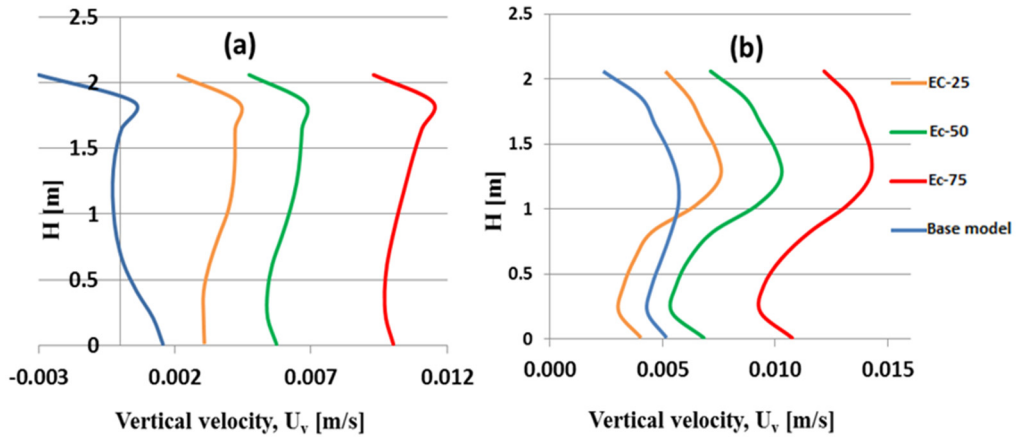

Figure 5-9: Average vertical airflow distribution as vertical airflow resistance in the pallets vary from the base model (100%) (Apple fruit packed in Econo-D) packaging box. Pallet row 1 (a) and, pallets row 2 (b)

Changing the vertical airflow resistance had an effect on the horizontal airflow as well. Figure 5.10 depicts the horizontal air velocity (U_w) magnitude in each row (calculated from averaged horizontal flow at bottom, middle and top

Stellenbosch University https://scholar.sun.ac.za

layers of the pallets in the respective row) for Ec-25, Ec-50 and Ec-75 models. The magnitudes for each model were compared with the base model (Figure 10 a&b). The result showed that as the vertical airflow resistance decrease the horizontal airflow decreased. The horizontal airflow magnitude in the first 4 to 5 meters was a result of flow recirculation (had negative value) in the region. This flow recirculation diminishes uniform distribution of cooling air in a reefer. The magnitude of recirculation estimated based on its horizontal velocity component showed different characteristics in row 1 and row 2. The recirculating flow magnitude has increased by 20 % in row 1 and decreased by 40 % in row 2 as the flow resistance was reduced by 75% (Ec-75) from the base model. In addition, the recirculation has reduced from row 1 to row 2 for all the models. This implies by configuring the pallets in such a way the recirculating flow can be reduced by 46 %, 63 %, 67 % and 74 % for the base model, Ec-25, Ec-50 and Ec-75 models, respectively.

Stellenbosch University https://scholar.sun.ac.za

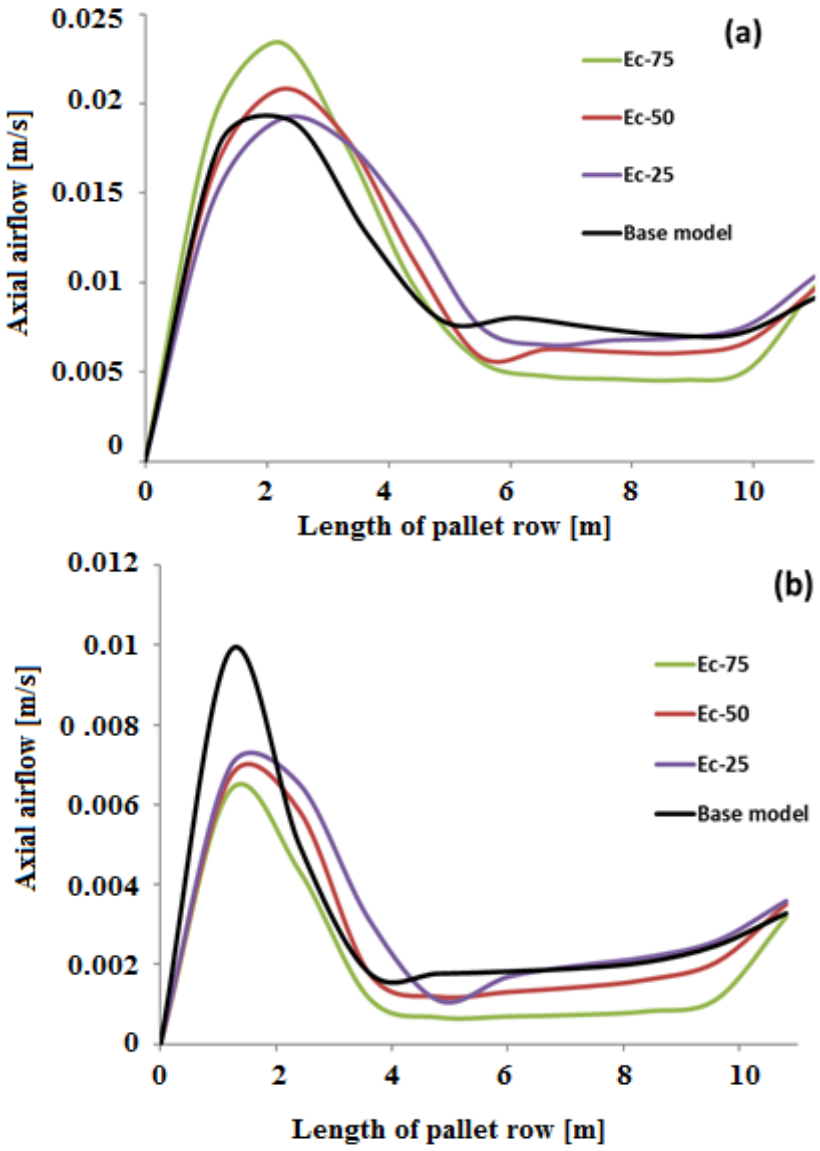

Figure 5-10: Average horizontal airflow magnitude in Ec-25, Ec-50, Ec-75 models. The horizontal airflow magnitude was calculated from averaged magnitudes at bottom, middle and top layers of the pallets in the respective row in the three models. These were compared with that of the result found for the base model in pallet row 1 (a) and pallet row 2 (b)

5.4.5. Cooling rate and temperature profile

Figure 5.11 depicts the result of the investigation on the effect of vertical airflow resistance on the cooling rate. The half-cooling time (HCT) and the 7/8th (SECT) cooling time are marked with horizontal lines in Figure 5.11. The effect of

Stellenbosch University https://scholar.sun.ac.za

the vertical airflow resistance on the cooling rate is clear. Reduction of the vertical airflow resistance decreases the cooling time. The Ec-75, which is the Econo-D with a 75% reduction of the airflow vertical resistance, gives the highest decrease in the cooling time. With this modification, the 7/8th cooling time was reduced from 55 h to 40 h. Notice that, the vertical airflow resistance characteristics of the Ec-75 is identical with that of the Mk6, which has a 3.5% Vent-hole area ratio at its bottom side. This means, by adding a 3.5 % vent area at the bottom side of the Econo-D box, it is possible to reduce the cooling time by 27 %. Similarly, the Ec-50 and Ec-25 resulted in a 13 % and 5 % reduction of the SECT, respectively. In a related study, Castro et al. (2004b) reported increasing vent area by 6 % increased cooling rate and uniformity however, increasing vent area more than 8 % did not improve cooling rate significantly (Castro et al. (2004a). However, it is important to take into account the mechanical stability of the package while designing vent-holes. Normally vent area ratio exceeding 6 % may impose mechanical instability and needs a dedicated analysis (Castro et al., 2004b; Singh et al., 2008; Pathare et al., 2012; Delele et al., 2013b). It has been reported by several authors that ventilated packaging box designs with increased ventilation area would decrease resistance to airflow of the packaging and thus improve cooling performance and energy efficiency during forced air cooling (Castro et al., 2004b; Delele et al., 20013b; Ngcobo, 2013; Berry et al., 2016). In this study by decreasing the vertical airflow resistance (increasing the bottom ventilation area) in the pallet domain by 75% (Ec-75) it was possible to increase the vertical airflow velocity by tenfold (Figure 5.9) and this in turn decreased the SECT of the fruit in the reefer by 27 % (Figure 5.11).

Stellenbosch University https://scholar.sun.ac.za

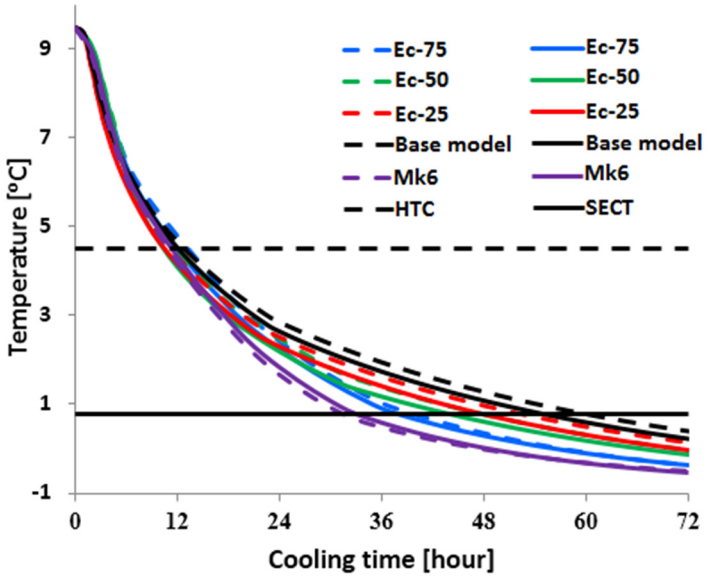

Figure 5-11: Average cooling rate of the produce in pallet row 1(broken curves) and pallet row 2 (full curves) of the reefers palletised with the normal Econo-D box (black curve), Econo-D with vertical airflow resistance reduced by 25% (blue curve-Ec-25), 50% (green curve-Ec-50) and 75% (red curve-Ec-75). The broken and full horizontal lines mark the half cooling time and the 7/8th cooling time, respectively.

In addition, the temporal temperature evolution (cooling uniformity) of fruit in row 1 and row 2 has shown an improvement as the vertical airflow resistance reduced. In EC-75 model the cooling rate of fruit in row 1 and row 2 were relatively the same. The average SECT difference between row 1 and row 2 was 6 hours for the base model. This implies the effect of pallet configuration on fruit cooling using Econo-D box design in a reefer can be reduced by increasing bottom ventilation.

Figure 5.12 shows the spatiotemporal temperature profile inside the reefers for selected pallets (pallet 2, 5, 8 and 11in row 1 and pallet 1, 2, 4, 6 and 8 in row 2). Produce cooling rate clearly increased as the pallets' vertical airflow resistance was reduced from the original Econo-D box (base model). In the reefer with the Ec-75, the minimum and maximum SECT reductions were 13 % (pallet 1 and 8) and 44% (pallet 4 in row 2 and 5 in row 1), respectively, compared to the reefer with

Stellenbosch University https://scholar.sun.ac.za

the base model. Generally, pallet 1 and pallet 8 cools gradually for all the cases (Figure 5.12c). In pallet 1 the vertical airflow was found to be very small due to two reasons; 1st incoming air has a jet property which flows in the axial direction (majority of the cooling air bypass the region) and, 2nd the vertical flow was limited due to the baffle plate at the inlet (on which the first pallets are partial placed on) which facilitates the forward flow of the cooling air and deters vertical airflow. Experimental study of the base model scenario reported in the previous paper also showed that the cooling rate of fruit the first pallets was actually slower than some of the pallets in the middle of the reefer. In general, the spatiotemporal temperature profile showed cooling rate improvement in the pallets located in the middle of the domain (from pallet 3 to pallet 6 in row 2) as the vertical airflow resistance reduced from the base model.

Stellenbosch University https://scholar.sun.ac.za

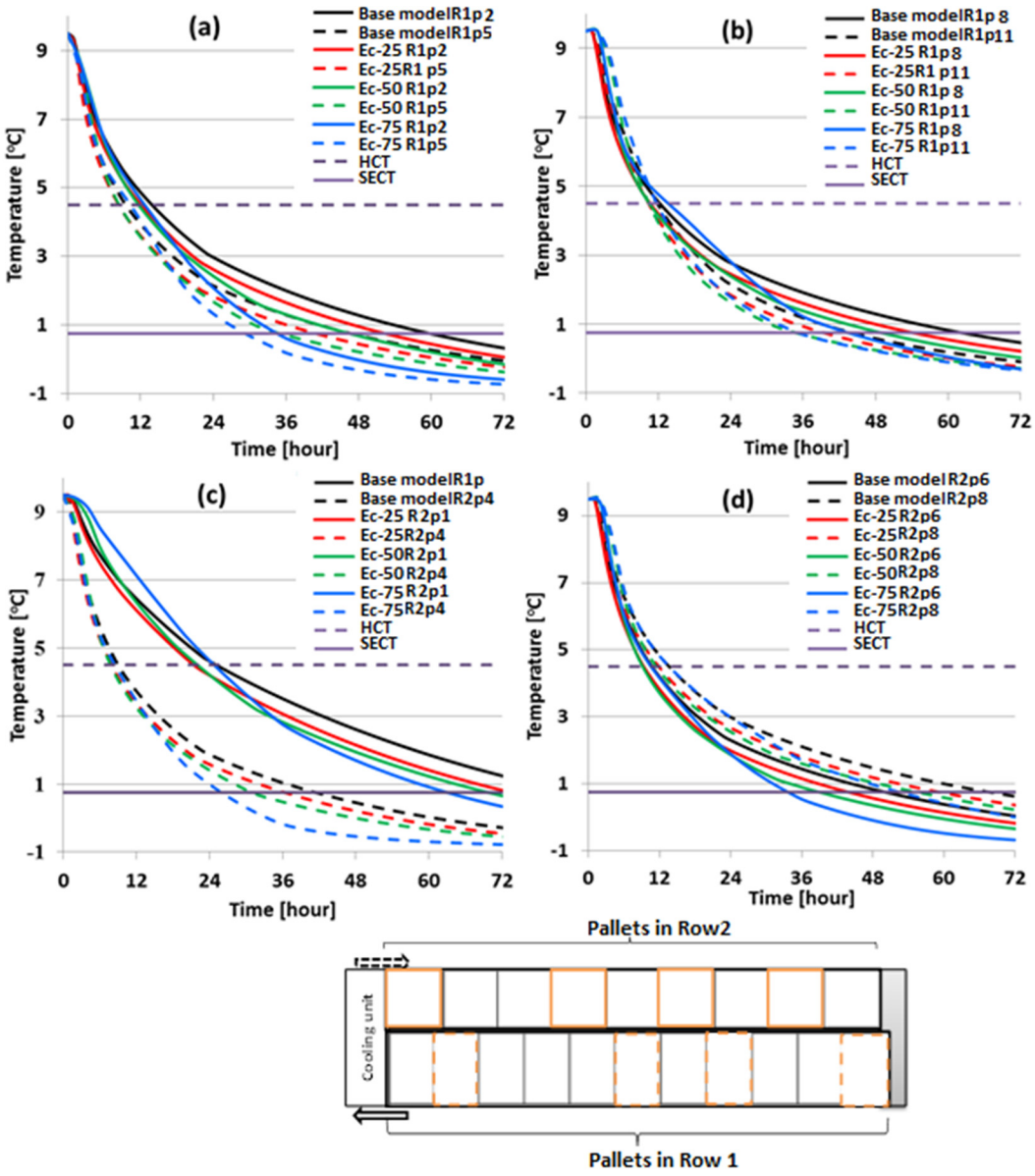

Figure 5-12: Simulated results showing the effect of the vertical airflow resistance on the cooling rate inside reefer. The spatial and temporal temperature evolution of apple fruit in a packed reefer as the vertical airflow resistance was set 25 % (Ec-25), 50 % (Ec-50) and 75 % (Ec-75) of the base model (No bottom vent packaging design-Econo-D box). Representative pallets (p) from row 1(R1) a) p2 & p5 b) p8 & p11 and, from row 2(R2) c) p1& p4 and d) p6& p8

Contours of produce temperatures on vertical planes (YZ) bisecting the pallets in row 1 and row 2 along the reefer length are shown for the EC-25, Ec-50,

Stellenbosch University https://scholar.sun.ac.za

Ec-75 and the Econo-D (base model)) (Figure 5.13). The uniformity of fruit temperature has shown improvement as the vertical airflow resistance decreased from the base model (Figure 5.13a) to Ec-75 (Figure 5.13d). More uniform temperature profile was obtained inside the Ec-75 reefer. This model represents higher ventilation area ratio on the bottom of Econo-D packaging box which resulted better vertical airflow in the pallets (section 3.4.1). The overall temperature SD of the reefers at 72 hours were 0.86, 0.78, 0.71 and 0.61 ℃ for the base model, Ec-25, Ec-50 and, Ec-75, respectively. It is interesting to point out that by adding vent hole area amounting to 3.5 % on the bottom side of the Econo-D box it is possible to achieve a performance comparable to that obtained with the Mk6 box which accommodates 6.6 % less fruit. This was mainly due to the stacking structure of the two boxes on pallets. The Econo-D box due to their interlocking designs all the layers are set on a pallet in the same pattern, where as in Mk6 boxes for stability of the pallets the layers were staggered which caused misalignment of vents for vertical airflow. This implies the interlocking packing designs can perform a lot better in reefers than the Telescopic boxes if their ventilation on the bottom is optimized.

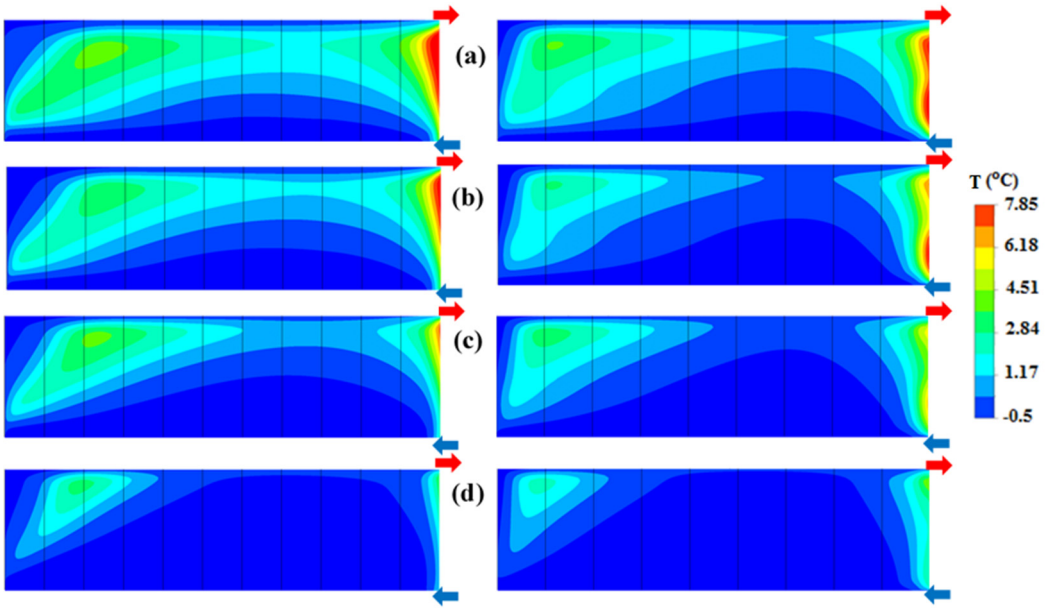

Figure 5-13: Simulated temperature contours on vertical plans (Z-Y planes) bisecting pallets in row 1(left) and row 2 (right). The contours correspond the instantaneous

Stellenbosch University https://scholar.sun.ac.za

temperature distribution inside the reefer after cooling the load for 72 hours from initial temperature of 9.5 ℃ with cooling air supply at -1 ℃ (5400 $m^3 h^{-1}$). (a) Base model (b) Ec-25 (c)Ec-50 and, Ec-75 (d)

5.5. Conclusion

A validated 3-D CFD model of an apple fruit packed reefer was applied to study the performance of commonly used apple packaging box designs and the effect of vertical airflow resistance on cooling operation. The evaluation of commonly used apple packaging box designs with respect to airflow distribution and fruit cooling revealed the unsuitability of the designs for cooling operation conditions in reefer. In addition, orientation/configuration of pallets was found to be important in airflow distribution, cooling rate and temperature uniformity in a reefer. This was due to their effect on networking and channelling air within a pallet and from pallet to pallet.

Cooling operation in a reefer has challenges mainly due to limited cooling air to produce contact. On this regard vertical flow resistance in the pallets of a fruits packed reefer was found to be the main limiting parameter in the cooling operation. Keeping the resistance of the fruits constant the design of the other factors should be reconsidered for a better performance of the reefer and to maintain the quality of fruit during long transportation. Reducing the vertical airflow resistance by 75 % from the base model to emulate increase in ventilation area at the bottom of packaging box resulted up to 62 % specific flow rate of the cooling air increase. The average cooling time of the fruits in the reefer has decreased by 27 %. The result demonstrated clearly the crucial role of bottom ventilation of packaging designs for vertical cooling operation in reefers. In addition, the result showed the potential energy saving opportunities for optimization of produce cooling in reefers in order to maximize fruit cooling rate and temperature uniformity.

Stellenbosch University https://scholar.sun.ac.za

Chapter 6

6. Numerical and experimental study of energy consumption in apple packed reefers

Abstract

A validated computational fluid dynamics (CFD) model of a fully loaded refrigerated shipping container (reefer) was used to investigate the energy consumption of apple packed reefers during shipping. The total energy consumption of a reefer packed with apple fruit and components of the refrigeration system were measured. Comparison of the measured and numerically calculated total energy consumption showed less than 10 % error. The performance of apple packaging designs in a reefer was evaluated with respect to energy consumption. These confirmed the influence of ventilation area, particularity on the bottom side, on energy use. Adding vent-holes (3.5 % vent area) on the bottom face of the Econo-D packaging box reduced vertical airflow resistance, which in turn reduced the reefer total power consumption by 12 % compared to with no bottom vent-holes a package. The effect of evaporator fan on energy consumption was studied by simulating fruit packed reefers operating at low, medium, high and variable evaporator fan speeds. The results demonstrated the potential of variable speed fan operation to reduce energy consumption.

Stellenbosch University https://scholar.sun.ac.za

6.1. Introduction

The world market for refrigerated containers has been estimated to grow by 10 % annually. The estimated number of 20 ft (6 m) reefers in 2000 was around 20 million (Jolly et al., 2000). Reefers are used to transport different varieties of goods that are temperature sensitive and perishable. Beside their benefits, reefers have a high-energy consumption following retail display and kitchen refrigeration (James S.J. & James C., 2010). Numerous papers have been written on energy utilization of reefers, cold storage facilities and cooling systems and mostly they are based on the information available at the facility's documentation (Ambaw et al., 2016; Castro et al., 2005; Evans, 2007; Wild et al., 2008; Fitzgerald et al., 2011; Goswami, 2009; Thompson et al., 2010; Wild et al., 1999; Wang & Muller, 2000). The electrical consumption is rising in cold chain facilities (Evans, 2007; Goswami, 2009), possibly due to higher volume of product being cooled than before. Energy efficiency of a cooling system is determined by design, operation and management of the cooling process. Efficiency would be lower if product is entering storage hotter,air infiltrate into the inside environment, doors open more often and, insulation is not sufficient (Ahmed et al., 2010; Billiard and Gautherin, 1993; Defraeye et al., 2015c; Gosney, 1975; Thompson et al., 2010).

Factors that affect energy consumption in the cold chain can be categorised into operational and design parameters for convenience. Operational parameters include fruit packaging design, produce property, fork lift heat load, stacking and pallets configuration. Design parameters include thermal infiltration, insulation, evaporator fan operation (such as QUEST (QUality and Energy in Storage and Transport) and non-QUEST or "Normal") and efficiency of refrigeration system (Defraeye et al., 2016; Lukasse et al., 2011). QUEST is a program based a fixed protocol designed to reduce the energy consumption of the unit, when operating in the interval -1 ℃ to 30 ℃ by avoiding inefficient part-load compressor operation and optimizing evaporator fan speed with heat load, without impairing produce quality (Lukasse et al., 2011). The main function of packaging materials is maintaining the quality of fruits during postharvest handling and

Stellenbosch University https://scholar.sun.ac.za

storage by providing mechanical protection against injuries, minimizing produce moisture loss and retarding microbial growth (Opara, 2011), however they are the main operational parameter that affects energy consumption (Defraeye et al., 2014; Thompson et al., 2010). Fruit packaging boxes are usually designed with consideration of one cooling method (cooling with horizontal airflow), however during transportation cooling is mainly by using vertical airflow (from bottom to top in reefers or from top to bottom in trailers/refrigerated trucks) (ASHRAE, 2010; Defraeye et al., 2015a, b; Moureh et al., 2009a, b). In addition, alignment of vents with adjacent cartons on a pallet (Castro et al., 2005; Castro et al., 2004; Delele et al., 2013a,b; Goswami, 2009) and pallet configuration (Defraeye et al., 2015c; Thompson et al., 2010) affect the airflow through a stack. Thermal heterogeneity of fruit is not only generated due to insufficient flow rate of the cooling air, but also by a non-uniform distribution of cooling air within the palletized structure (Alvarez and Flick, 1999). The uniformity of cooling air flow is greatly affected by the packaging design which consequently affects energy consumption of the system.

Evaporator fan is designed to deliver cooling air to meet the design maximum refrigeration load. However, most of the time, evaporators operate in conditions requiring much less than maximum refrigeration capacity (Thompson et al., 2010). In addition, since most cold chain facilities do not change operational set points between summer and winter time due to lack of seasonal control in cold chain systems (Ambaw et al. 2016), unnecessary energy is wasted, for example by continuously running fans (East et al., 2013). Thompson et al. (2010) also noted that peak airflow rates are not needed during the entire cooling period (Thompson et al., 2010). The large heat release from evaporator fans throughout the day, due to their continuous operation, and the fruit respiration heat load further increase the total required refrigeration load of the refrigerated container. Produce respiration heat load is less relevant for forced air cooling, due to the large cooling capacity. However, during long-term storage it can have an important effect on power consumption (Tanner et al., 2002a, b). Fan power consumption is proportional to the cube of the flow rate. This means of the airflow rate of the fan is reduced to

Stellenbosch University https://scholar.sun.ac.za

80 %, flow it only uses 50 % power. According to British Frozen Food Federation (2009), if one reduces flow further to 50 %, the power usage falls to 12.5 %. Therefore, the largest energy savings in refrigerated containers are expected to lie in optimizing fan operation (Defraeye et al., 2015c; GDV, 2014). Tassou et al. (2009) reported that the Coefficient of Performance (COP) of transport refrigeration systems was low, ranging from 0.5 to 1.7. Teitel et al. (2008) compared ON-OFF and variable frequency drive (VFD) systems on the energy consumption and resulting microclimate within greenhouses and poultry houses and reported much more significant power consumption reduction in VFD than ON-OFF operation.

The objective of this study is to evaluate energy saving options of an apple packed reefer by assessing operational and design parameters. In this study, the refrigeration load during cold handling of apple fruit in a reefer was estimated using a validated CFD model. Corresponding to this the total and component electricity usage of the cooling unit of the reefer were experimentally measured. In addition, the effect of operational parameters (packaging designs, and pallet vertical airflow resistance) and design parameter (evaporator fan speed) on energy consumption were numerically evaluated.

6.2. Materials and methods

6.2.1. Reefer

The Starcool reefer unit, models SCI-40 was used for this study. This reefer has internal and external Length / Width / Depth of 11.59 m × 2.29 m × 2.54 m and 12.19 m × 2.44 m × 2.90 m, respectively. The reefer is an electric powered picture frame, cooling and heating units operating on refrigerant tetrafluorethane (R134a). The cooling system of the unit is equipped with a two–stage compressor, electrically driven through a FC (frequency converter), which is designed to operate on a nominal 410/450 V AC, 3 phase, 50/60 Hz, primary power source (ISO 1496-2). The refrigeration system of the reefer mainly comprises a compressor, evaporator, and condenser. Each component of the cooling unit has a power supply, where the operational conditions are all controlled centrally. The compressor was

Stellenbosch University https://scholar.sun.ac.za

semi-hermetic two-stage reciprocating compressor with variable speed FC (frequency converter, 15-110 Hz, 450-3300 rpm) and 5.5 kW nominal powers. The evaporator has two axial fans driven by a 3–phase (410/450 V) 50/60 Hz motor. The fans can run at two speed, 3460 and 2850 RPM (voltage dependent, 60/50 Hz) and 1760/1425 RPM, with nominal power of 0.45 kW at 460V/60 Hz (Table 6.1). Condenser fan motor was a 3phase (400/460 V), 50/60 Hz, dual speed (1760/1460 RPM (60/50 Hz) and 870/730 RPM (60/50 Hz)) with nominal power of 0.25 kW at 460V/60 Hz and 0.3/0.08 kW at 460V/60 Hz. The airflow control system has two options, based on the evaporator fan performance RPM. In the QUEST control option, the evaporator fan can operate at high or low RPM. The other is the "Normal" control option, during which the evaporator fan operates at high RPM. The "Normal" control mode is used when the reefer is loaded with chilled produce (Lukasse et al., 2011).

Table 6-1 Nominal power of refrigeration unit motors

Motor	**No. of components**	**Nominal power**
Evaporator fan	2	0.45 kW at 460V/60 Hz
Condenser fan	1	0.25 kW at 460V/60 Hz
Compressor	1	5.5 kW

6.2.2. Packaging boxes

In this study the energy usage of a reefer was evaluated with respect to three different packaging box designs, namely, Econo-D, Mark9 (Mk9) and Mark6 (Mk6) (Figure 6.1). The Econo-D, Mk9 and Mk6 boxes have outer (L × H × W) dimensions of 49.0 cm × 26.0 cm × 29.0 cm, 60.0 cm ×13.2 cm × 38.8 cm and, 40.0 cm× 30.0 cm × 27.0 cm. Econo-D has ventilation area of 1.8 %, 1.09 % and 0 % on the short side, long side and bottom side respectively. Similarly, Mk9 and Mk6 have ventilation areas of 4 %, 3.07 % and 0.25 % and 3.8, 4.8 and 2.6 % on the short side, long side and bottom side, respectively.

Stellenbosch University https://scholar.sun.ac.za

The Econo-D, Mk9 and Mk6 boxes contain 12, 10.5 and 9 kg of apple fruit. The corresponding pallet stacks of these box designs contain 768kg, 720 kg and 840 kg of apple, respectively. The total weight of apple loaded per reefer using Econo-D, Mk6 and Mk9 was 15360 kg, 14400 kg and, 16800 kg, respectively.

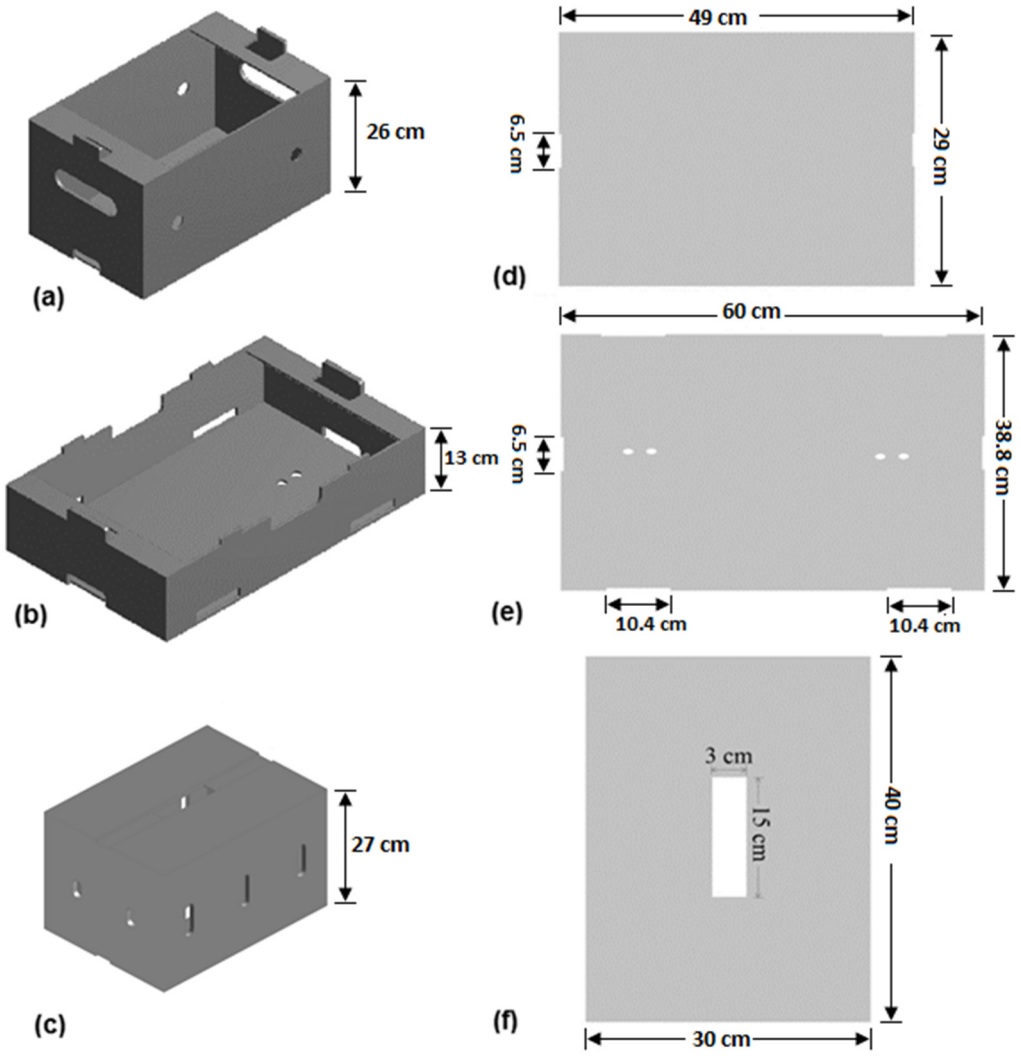

Figure 6-1: Schematics of the three package designs examined in this study. Isometric view of Econo D (a), double layer display carton box (Mk9) (b) and Telescopic packaging box (Mk6) (c). The right column depicts the bottom side of the Econo D (d), Mk9 (e) and Mk6 (f) boxes. Sizes shown correspond to the external dimensions.

Stellenbosch University https://scholar.sun.ac.za

6.2.3. Experimental study

6.2.4. Set-up and measurements

The reefer (Starcool SCI-40, Maersk reefer) was loaded with 20 pallets of apple fruit (9.5 ℃) (a total of 15.36 tons of fruit, 80 Econo-D boxes per pallet, each holding 12 kg apple fruit). Air circulation in the reefer was maintained by the evaporator fans. The returning warm air is forced through the evaporator coils and cooled to the required temperature and supplied to the load at a supply temperature (T_{sup}= -1 ℃) and after removing heat from the produce, returned back to the refrigeration unit at a return air temperature (T_{ret}).

The energy usages of the reefer, while operating under QUEST and non-QUEST (Normal) control modes were measured. For the QUEST control mode, the total power usage and the power usage of the compressor were measured. For the "Normal" control mode, the total power usage, the power consumption of the evaporator fans, condenser motors and compressor motors were measured. The actual power consumptions of the different components of the cooling unit of the reefer were measured for a 72 h period. The make-up air vent was closed during the experiments. Repeating an experiment was not possible due to technical and resource constraints.

Two PowerTrack instruments (Advanced Monitoring Solutions, Durbanville, South Africa) with ± 0.05 % reactive power uncertainty were used to monitor the total power consumption of reefer and compressor in the QUEST control mode. In case of the Normal control mode, four PowerTrack instruments were used to monitor the power consumptions of reefer total, compressor, evaporator fans and condenser motors, simultaneously (Figure 6.2). Data including the power use, power factor, current and voltage were logged by the PowerTrack data logger every 15 seconds.

Stellenbosch University https://scholar.sun.ac.za

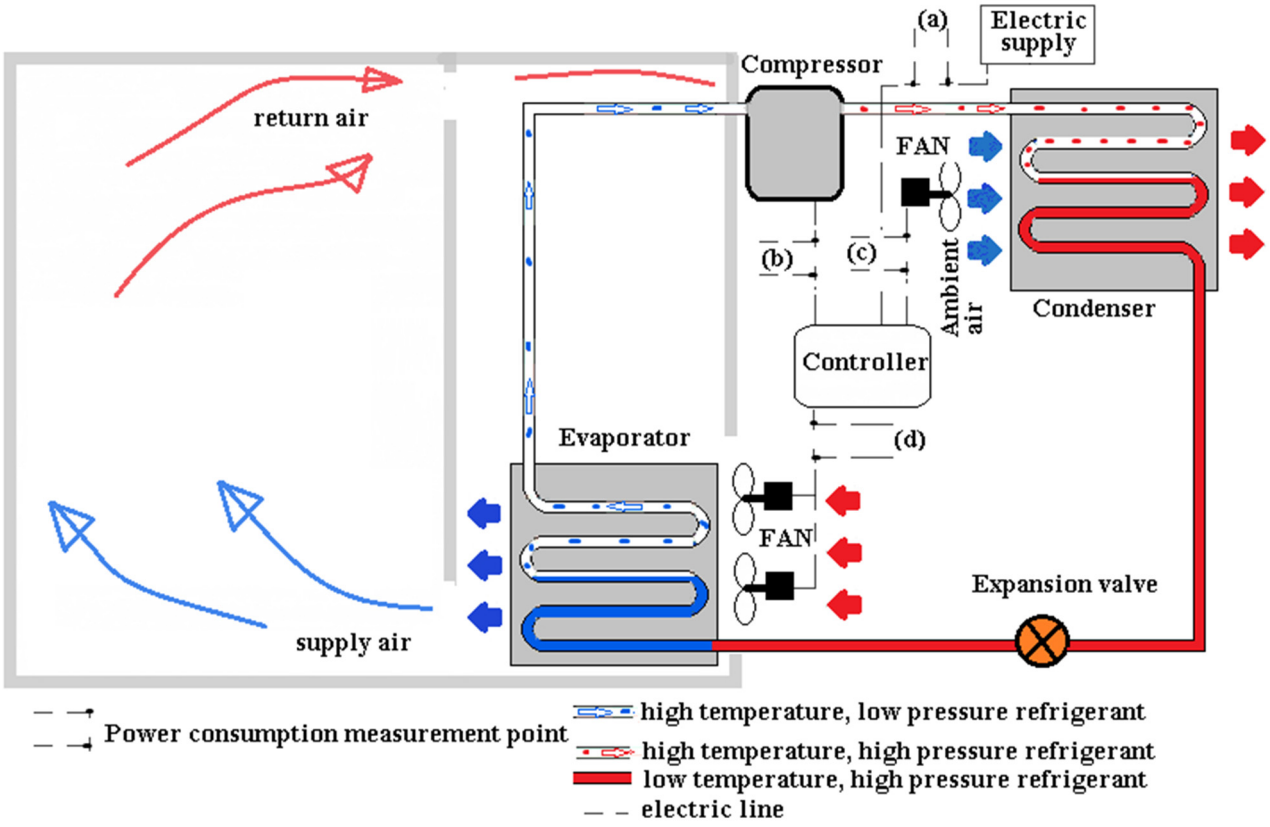

Figure 6-2: Simplified diagram of refrigeration system of a reefer and measurement points for power use of (a) total reefer, (b) compressor, (d) condenser motor and (d)evaporator motors

Stellenbosch University https://scholar.sun.ac.za

6.2.5. Model

In this study, simulations with a previously developed and validated CFD model were used to calculate refrigeration load (Chapter 6 section 6.4). In the model, since the air circulation fans were positioned upstream of the evaporator coil (a blow-through configuration), the fan heat was assumed totally removed by the evaporator coil. The model also assumed a completely airtight reefer domain, with the makeup air inlet closed (no infiltration heat load). Heat loads associated with condensation and evaporation of moisture inside the reefer and effect of defrost cycle were not considered. Navier-Stokes equations were applied as governing equation for mass, momentum and supplemented by energy conservation equation (chapter 4, Eqn. 4.1 to 4.6). The model allows the calculation of the refrigeration load, excluding fan heat, based on mass flow and temperatures of the return and supply air stream. The fan heat, which was assumed to be totally removed by the cooling unit, was separately calculated using the fan specifications. To this end, total refrigeration load can be described by equation 6.1. The model included heat transfer from the environment (Eqn. 6.2) and heat of respiration (Eqn. 6.3).

$$Q_T = M_o C_p \Delta T \tag{6.1}$$

$$Q_w = UA(T_\infty - T_W) \tag{6.2}$$

$$Q_m = 10.7 \rho_p f \times \left(\frac{9T_p}{5} + 32\right)^g \tag{6.3}$$

Where, Q_T and Q_{fan} (W) are total refrigeration and fan heat loads, M_o(kg s^{-1}) is mass flow rate of the returning air, C_p(1006.12 J (kg K)$^{-1}$) is specific heat capacity of air, ΔT (K) = T_0-T_i, Δt is time step size (sec). T_p (°C) is produce temperature, Q_w(W) is conduction heat load, U (W K^{-1} m^{-2}) is the overall heat transfer of the reefer's composite wall, A (m^2) is area, T_∞(K) is ambient temperature outside of the container and, T_W (K) is the container wall temperature. Q_m (W m^{-3}) is heat of respiration, ρ_p is density of produce (kg m^{-3}), f and g are

Stellenbosch University https://scholar.sun.ac.za

produce respiration coefficients for apple fruit (5.6871×10^{-4} and 2.5977, respectively) (Becker et al., 1996).

Fan heat (Q_{fan}) contributes a significant amount of heat load and should be included in the cooling load calculation (Thomson et al. 2002). Fans can be located upstream (blow-through), downstream (draw-through) or parallel (rooftop penthouse) to the evaporator coil (Figure 6.3). In reefers, a blow-through configuration (ASHRAE, 2010) is used to drive the returned warm air over the cooling coil as shown in Figure 6.3a. Hence, the heat from the fan motor is removed by the evaporator coil before entering the reefer. For this configuration the heat load from the evaporator fan motor can be calculated using Eqn. 6.4 (Evans et al., 2014).

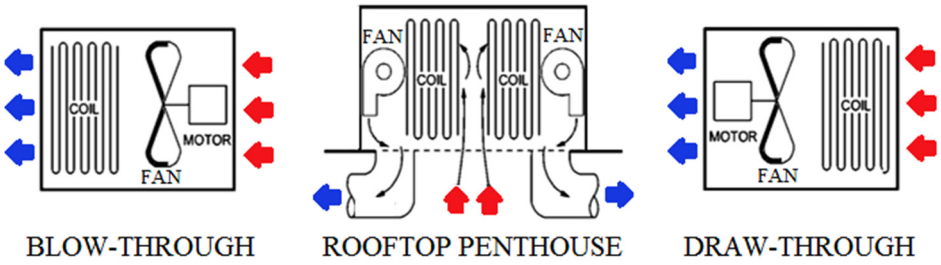

Figure 6-3: Configuration of fan motor and evaporator coils (ASHRAE, 2010).

$$Q_{fan} = \frac{N_m P_m}{\eta_{mot}} \qquad 6.4$$

Where, N_m is number of motors, η_{mot} is motor efficiency and, P_m is motor power. The two fans have nominal power of 0.45 kW. Motors rated at 0.45 kW have a 66 % motor efficiency at full load, which results in a heat load of 1364 W (ASHRAE 2010).

Stellenbosch University https://scholar.sun.ac.za

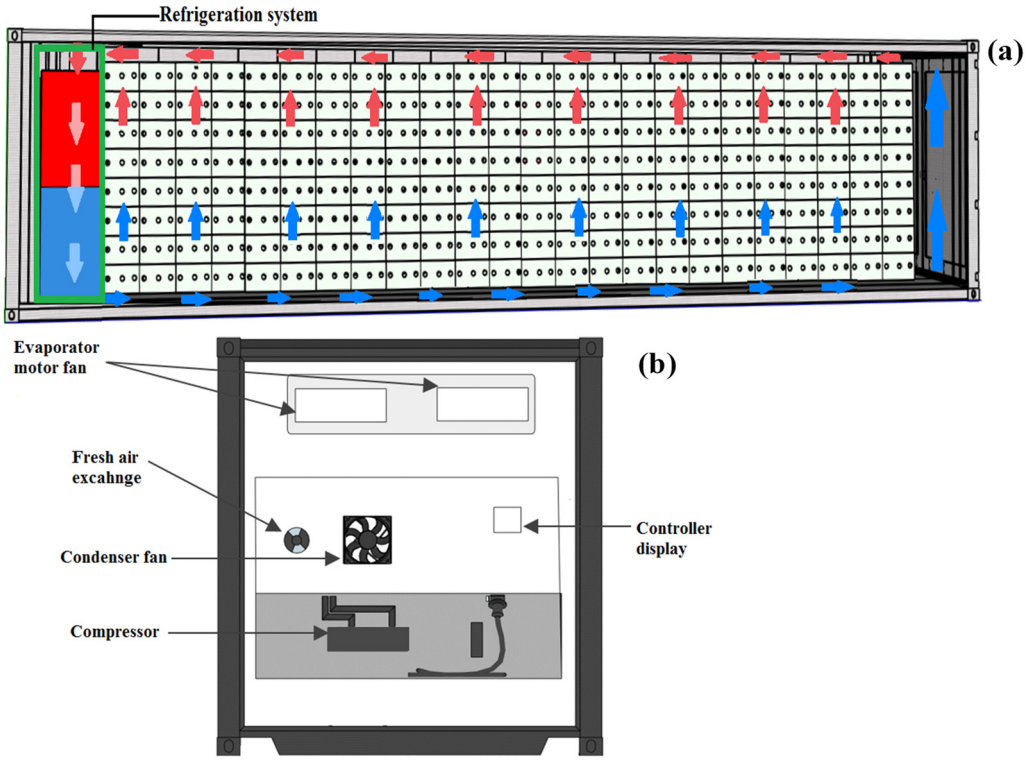

Figure 6-4: Representation of airflow path inside a fully packed reefer (a) and, components of the refrigeration unit of a reefer (b)

The refrigeration system of a reefer consist compressor, evaporator and condenser (Figure 6.4b). Total electric power consumption (E_{tot}) is the sum of all the loads by refrigeration system components (Eqn. 6.5). The total and component poser usages were measured in this study. The CFD model provides the corresponding total refrigeration load (Q_T) and its components, which are otherwise difficult to quantify experimentally. Then, by using these, the coefficient of performance (COP) of the reefer was estimated to quantify the efficiency of the refrigeration system. COP is a dimensionless number defined as the ratio of the amount of cooling provided to the work required. There are different theoretical approaches to calculate coefficient of performance (COP) of an ideal vapour-compression machine operating on the reverse Carnot cycle (Evans et al., 2009). In this study, the COP of the refrigeration system calculated using equation 6.6. It is

Stellenbosch University https://scholar.sun.ac.za

the ratio of the total refrigeration load ($Q_T\ (kW)$) and the total power consumed by the reefer ($E_{tot}(kW)$).

$$E_{tot} = E_{comp} + E_{Evap} + E_{Cond} + E_{control\ systems} \quad 6.5$$

$$COP = \frac{Q_T}{E_{tot}} \quad 6.6$$

6.2.6. Simulation

The airflow and heat transfer inside the reefer was simulated using ANSYS-Fluent-16 (ANSYS, Canonsburg, PA, USA). Turbulence was calculated using k-ω SST model. The fruit (15.36 tonnes) was initially at ≈ 9.5 ℃ and under 10 ℃ ambient temperature condition and while stationary (wind speed = 0.2 ms^{-1}). First, cooling under "Normal" control mode fruit packed with Econo-D, Mk6 and Mk9, packaging design was simulated and compared experimental result. Second, to study the effect of vertical airflow resistance the pressure drop of pallet stacked with Econo-D packaging design was virtually reduced by 25 % (Ec-25), 50 % (Ec-50) and 75 % (Ec-75). Then, in order to evaluate the effect of variable speed fan on the energy consumptions, simulations under high (8100 $m^3\ h^{-1}$), medium (5400 $m^3\ h^{-1}$) and low (2700 $m^3\ h^{-1}$) evaporator fans speeds were conducted. In all the simulations the cooling air temperature was -1 ℃ and duration of simulation was 72 h. Total refrigeration heat load, based on the supply and return air temperature, was calculated. In addition, the time history of field heat removed from the fruit, the respiration heat load and heat conducted from the environment during the cooling process were individually computed. The simulation results at the three cooling airflow rates (fan speeds) were used to investigate the effect of variable speed fan on energy consumption.

Stellenbosch University https://scholar.sun.ac.za

6.3. Result and discussion

6.3.1. Total and component-specific electricity usage of the refrigeration system

Figure 6.5 shows the measured total power consumption and component-specific power consumption of the reefer while operating in "Normal" and QUEST control modes. For the "Normal" control mode, the power consumption by the reefer (total), compressor, evaporator and condenser were monitored. For the QUEST control mode the total and compressor power consumptions were monitored (Figure 6.5b). After 72 h of cooling, the cumulative total energy consumed by the reefers operating in "Normal" and QUEST control mode were 148 and 120 kWh, respectively. The reefer operating in QUEST control mode, which is made to save energy, consumed 20 % less power compared to the "Normal" control mode, which can be attributed to the controller which adjust the fan speed between off, half and maximum with respect to the return air temperature of the reefer. The small spikes in the measurement data were internal voltage surges due to power transitions in large equipment hooked up on the same power line (Paul, 2001), such as the compressor, which should be frequently throttled to regulate the evaporator. High magnitude, longer (>30 minute) and more frequent spikes were found in the reefer operating in the "Normal" than QUEST control mode. These voltage surges affect the reading of the power usage. On the other hand, in the QUEST control mode, the average of supply and return temperature are used to control set point instead of just controlling supply temperature to the set point. Thereby, the throttling, which causes increase the power consumption was avoided (Lukasse et al., 2011). The algorithm (Maersk QUEST I) adjusts evaporator fan speed to the heat load, avoids inefficient throttled part-load compressor operation, and indirectly controls cargo temperature instead of just the supply temperature.

The reefer's energy consumption reduced from 65 kWh (day 1) to 37 (day 3) and from 47 (day 1) to 38 kWh (day 3), in "Normal" and QUEST mode, respectively (Table 6.2). The reason was that the field heat of the fruit that needed to be removed reduced, and thereby also the required cooling load. The decrease in

Stellenbosch University https://scholar.sun.ac.za

the energy consumption of the reefers from day 1 to day 2 and day 2 to day 3 was 30 % and 18 % for the reefer operating in “Normal” mode and 24 and -7 % for the reefer operating in QUEST mode, respectively. The reefer operating in QUEST mode consumed power in a relatively uniform pattern from day 1 to day 3, 39, 30 and 32 % of the total consumption.

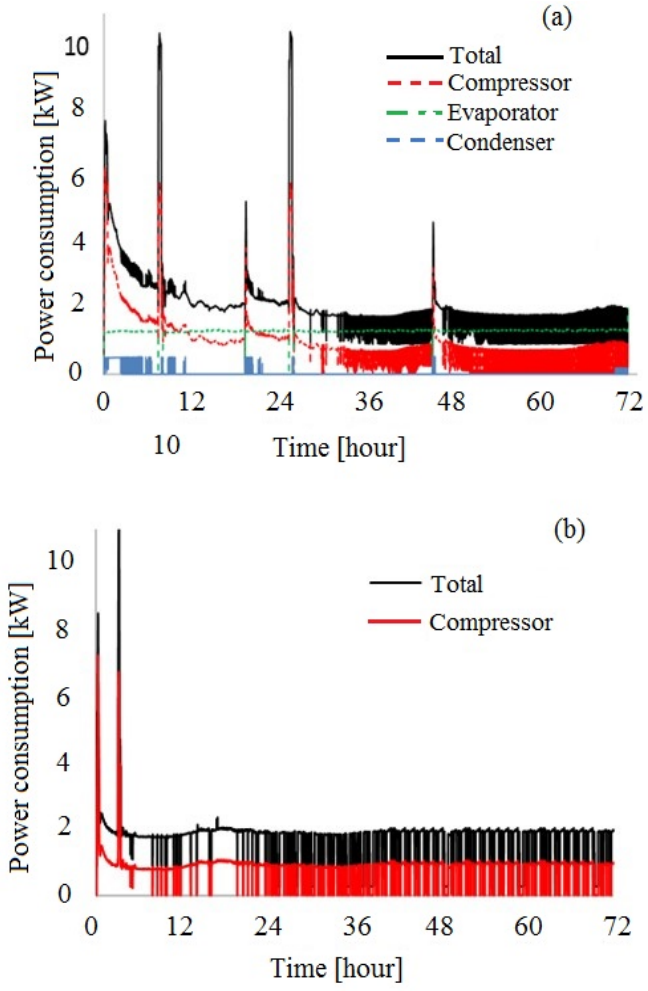

Figure 6-5: Measured power consumption of reefer operating in “Normal” control mode (a) and, QUEST control mode (b) during the 72 h cooling period. Reefer loaded with 15.36 tonnes apple fruit (in Econo-D box) at 9.5 °C initial produce temperature. Cooling air at 5400 $m^3 h^{-1}$ and -1 °C was supplied.

Stellenbosch University https://scholar.sun.ac.za

Table 6-2: Daily total energy consumption of reefers operating in "Normal" and QUEST control mode. For the reefer operating in "Normal" mode energy use of refrigeration sub units was measured

	Total-Normal (kWh)	**Compressor-Normal (kWh)**	**Evaporator-Normal (kWh)**	**Condenser-Normal (kWh)**	**Total-QUEST (kWh)**	**Compressor-QUEST (kWh)**
Day 1	65	38	20	2.3	47	22
Day 2	46	21	20	0.1	35	14
Day 3	37	13	20	0.2	38	16
Total	148	72	61	3	120	52
%		49	41	2		43

Power factor (ranges between −1 to 1) is the ratio of the actual electrical power dissipated by an AC circuit to the product of the RMS (root mean square) values of current and voltage. An electric load with a low power factor draws more current than a load with a high power factor for the same amount of useful power transferred. The power factor of the compressor, evaporator and condenser were, 0.97, 0.67 and 0.66 respectively and the corresponding share of these component towards the total energy consumption of the reefer were 49, 41 and 2 %, respectively (Table 6.2). Energy consumed by the three components makes up ≈ 92 % (136 kWh) of the total, while the remaining ≈ 8 % (12 kWh) can be assumed to be used by, the control systems of the refrigeration unit, display control board and wasted due to inefficiency of the system.

The power usage of the compressor decreased from 6 kW to 0.8 kW in 24 hours. On the other hand, the power consumption of the two evaporator fans was relatively constant for the "Normal" control mode (1.26 kW) for the entire cooling period. The high power consumption by the compressor during the first 24 hours was due to the high initial heat of the produce. During this period the compressor should work at high capacity. The condenser of the refrigeration system operates in on/off mode and its power consumption was 2 %. For the Quest mode, the power

Stellenbosch University https://scholar.sun.ac.za

consumption of the fans could not be measured, but will not be constant (Lukasse et al., 2011).

The numerical model was used to quantify total refrigeration heat load of the reefer. In addition, the heat removed from the fruit, the fan heat production, heat conduction from the environment through the container wall and the heat load due to respiration were quantified. Figure 6.6 depicts the contribution of the heat loads from different entities in the reefer to the total refrigeration load of the reefer. The fruit field heat together with the respiration heat load are basic (unavoidable) heat loads, contribute 57 % to the total required refrigeration load of the reefer (Figure 6.6a). Similarly, by the end of the cooling period, heat conduction from the environment and fan heat loads (Figure 6.6b) contributed 43 % to the total refrigeration load. Due to the cold ambient temperatures used in the calculation, the effect of conduction from the environment was lower compared to the fan heat load. This can be marked as a potential option to reduce the heat load by improving the insulation material and fan operation. The two fans have a nominal power of 0.45 kW and with a 66 % motor efficiency, this results 1364 W heat load (Evans et al., 2014). Total energy consumption by the refrigeration system is the result of the work done to remove the heat loads from all the heat load sources discussed.

Stellenbosch University https://scholar.sun.ac.za

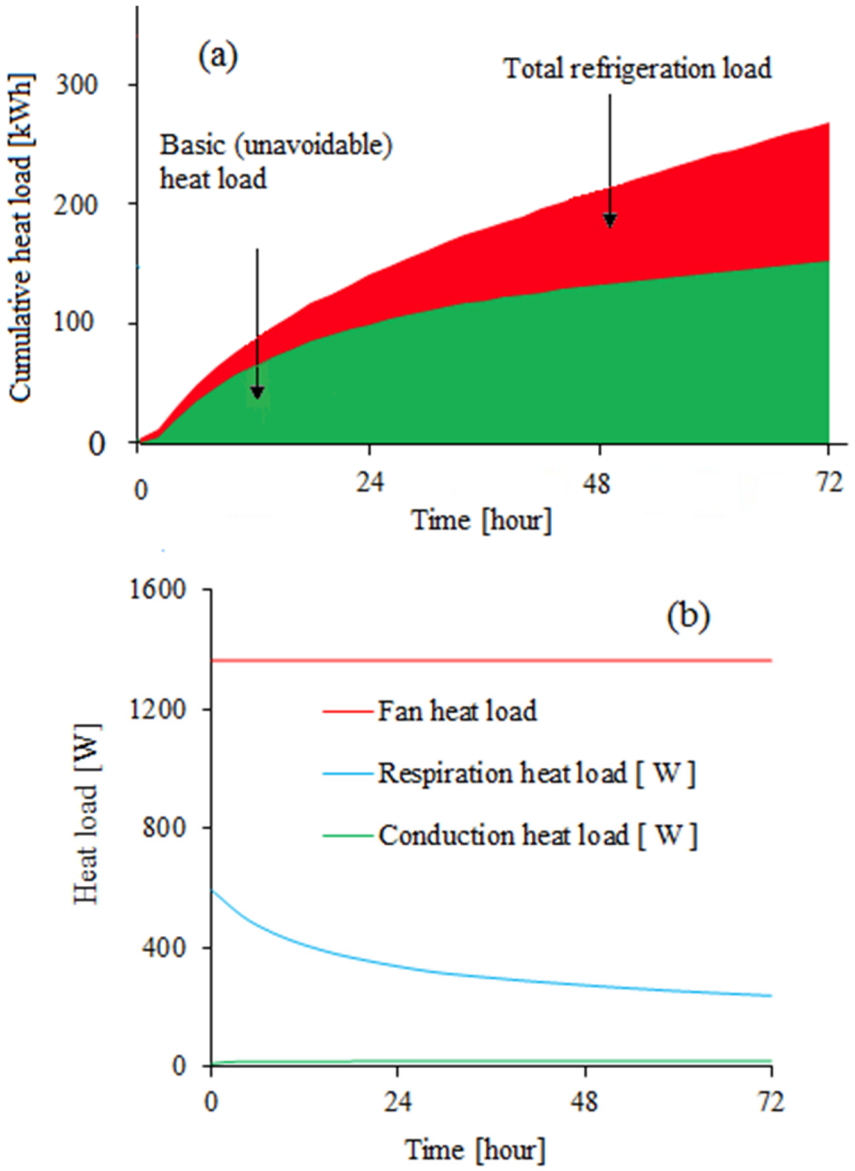

Figure 6-6: Cumulative heat load of the reefer packed with apple fruit in Econo-D packaging boxes (a) and, heat load due evaporator fan, respiration and, conduction from the environment (b).

Obtaining the total refrigeration heat load from the CFD model enables the calculation of the coefficient of performance (COP) of the reefer as the ratio of cumulative refrigeration heat load removed by the system (244 kWh) and the total power consumed during the cooling period (148 kWh). Once the COP (1.7) was obtained, the time – energy-usage curve was generated (Figure 6.7) for the reefer packed with apple fruit inside Econo-D box. The total energy consumption from

Stellenbosch University https://scholar.sun.ac.za

the numerical study of the packed reefer resulted 135 kWh and was 8 % less than the measured value (148 kWh). The performance of refrigeration system varies depending on the temperature difference between the supply and the return air (Tassou et al., 2009). Therefore, the difference between the numerical and measured energy consumption results could be due to the constant supply air temperature equal to the set temperature in the model. In the actual reefer it took 2 and ½ hours for the supply air to reach the set temperature and this temperature was fluctuating (±0.5 ℃) during the entire cooling operation. In addition, the model did not predict the voltage surge in the system which increased the power consumption in the system as described in the previous section (section 3.1). In general, the model predicted the total power consumption of the reefer quite accurately during the three-day cooling experiment.

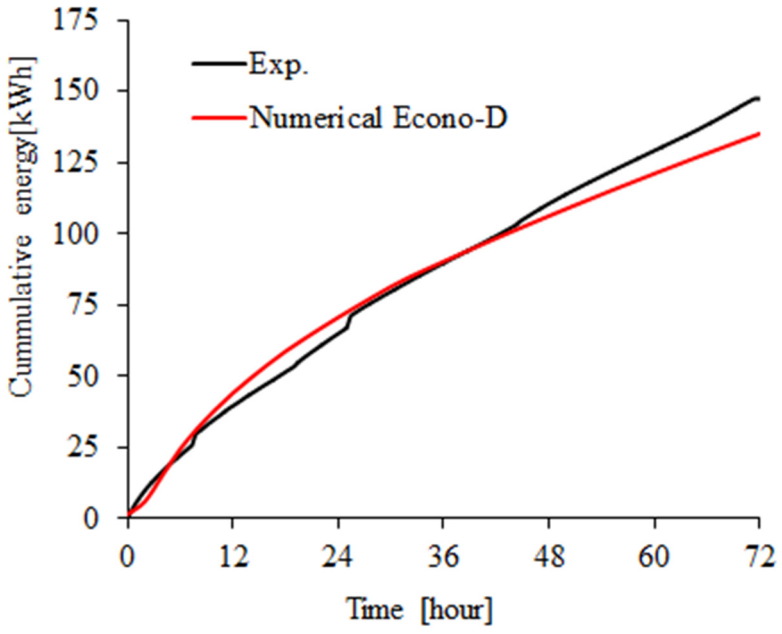

Figure 6-7: Measured and predicted energy consumption of the reefer packed with apple fruit in Econo-D box design during the 72 hours cooling operation.

Stellenbosch University https://scholar.sun.ac.za

6.3.2. Ventilated packaging design

Electric energy consumption of the reefers packed with Mk6 and Mk9 packaging designs were estimated from the total refrigeration load (Q_{Tot}) and coefficient of performance (COP). COP (1.7) calculated in the previous section was used. The total power consumption (calculated from simulation result of refrigeration load) of reefers packed with apple in Econo-D, Mk6 and Mk9 packaging design during the 72 hour cooling period showed a considerable difference (Figure 6.8a). The reefer packed with Mk6 packaging design (3.5 % bottom ventilation area) consumed the highest power during the initial stages but achieved faster fruit cooling than with the other packaging designs (SECT ≈ 34 h). This was due to its high ventilation area that facilitated high fruit cooling rate but imposed high refrigeration load in a short period. The reefer packed with Mk9 box design contains the highest amount of fruit load (16.8 tonnes) and has lower fruit cooling rate (SECT≈ 62 h). This resulted in a lower power (low refrigeration load) in the first 34 h compared to the reefer packed with Mk6 box, however took 28 h more to reach SECT (Figure 6.8a). Similarly, the reefer packed with fruit inside Econo-D (SECT≈ 58 h) packaging resulted slightly lower energy consumption per unit time during these period followed by a relatively constant (1.26 kW) power consumption in the remaining cooling period.

Stellenbosch University https://scholar.sun.ac.za

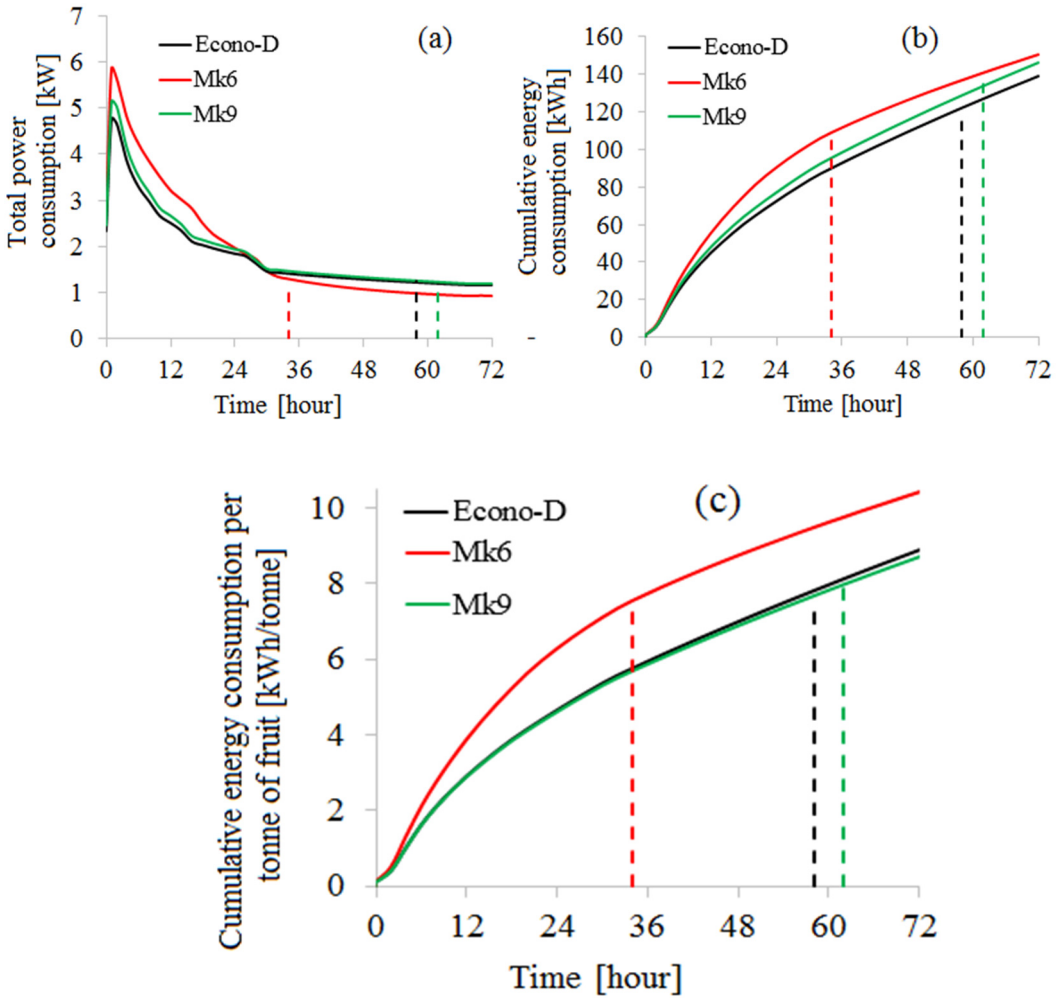

Figure 6-8: Energy consumption of reefers loaded with apple fruits inside Econo-D packaging box, Mk6 and, Mk9 packaging boxes in a reefer operating in "Normal" control mode. (a) Transient power use by each reefer, (b) cumulative energy consumption of each reefer and, (c) energy consumption per tonne of apple fruit. Solid lines show the power consumption of the reefers and, broken lines show the SECT of fruit in each reefer.

In principle, the boxes are designed to pack and transport fruit safely, however, particular attention must be paid to the design of these boxes. When designing ventilated packaging, their use in a reefer should be considered in order to ensure adequate ventilation to the fruit load (Defraeye et al., 2015; 2016). The maximum energy was consumed by the reefer for the Mk9 packaging design which used 139 kWh to cool 16.8 tonnes of apple to the SECT in (62 hours) (Figure 6.8b).

Stellenbosch University https://scholar.sun.ac.za

The reefer packed with Mk6 packaging design, on the other hand, consumed 22 % less energy (106 kWh) to cool 14.4 tonnes of fruit to SECT (34 hours). On the other hand, the reefer packed with Econo-D packaging design consumed 12 % less energy compared to Mk9 packaging design and cooled 8.6 % less fruit in 58 hours. The energy consumed (per tonne of apple fruit), to cool fruit to the SECT, in the reefers packed with Mk6, Econo-D and Mk9 packaging designs were 7.6, 7.8 and, 8.3 kWh tonne^{-1}, respectively (Figure 6.8c). These results show that Mk6 packaging design saves 0.7 kWh per tonne of fruit until SECT is reached. However, employing such a packaging design, that provides lower fruit density per reefer (14.4 tonnes), compared with Mk9 (16.8 tonnes), increases the cost per kg of fruit for long distance transportation. Although the three reefers contain different amount of fruit, it can be seen that better cooling performance and lower energy use have a strong relationship with the ventilation area of the bottom of the packaging as the cooling air flows primarily from bottom to top. In the following section this was further investigated using a pallet stacked with Econo-D packaging design (no bottom ventilation area) as a reference.

6.3.3. Vertical airflow resistance

The vertical airflow resistance (bottom to top of the pallet) of a pallet stacked with Econo-D packaging design was reduced by 25, 50 and 75 % resulting in pallets Ec-25, Ec-50 and Ec-75, respectively to emulate increase in ventilation area on the bottom of packaging (Chapter 5). Econo-D is the reference packaging design with no vent on the bottom side, whereas Ec-75 has a resistance equivalent to a packaging design with a 3.5 % bottom side ventilation area (Chapter 5, section 5.5.1). The initial basic heat load (field heat and respiration heat load) of the reefers packed with Econo-D, Ec-25, Ec-50 and Ec-75 packaging designs was the same at time zero. Due to the difference in the vertical airflow resistance of the pallets stacked with these packaging designs in the respective reefers, both airflow distribution and rate of heat removal varied and that resulted in SECTs ranging from 40 hours for Ec-75 (lowest vertical airflow resistance) to 58 hours for Econo-D (highest vertical airflow resistance). The rate of heat removal from the Ec-75

Stellenbosch University https://scholar.sun.ac.za

packed reefer was higher due to lower vertical resistance and the SECT was reduced by 27 % compared to the base model. This resulted in a 12 % reduction in total energy consumption or 0.91 kWh per tonne of fruit load or ≈14 kWh per reefer until SECT is reached (Table 6.3). Similarly, the energy consumption was reduced by 9.6 and 10.9 % for Ec-25 and Ec-50, respectively.

Table 6-3 Energy required to pull down fruit temperatures to the SECT temperature using different apple packaging designs (apple fruit load of 15.36 tonnes per each reefer)

Packaging design	SECT [hour]	Energy consumption [kWh]	Energy consumption per tonne [kWh/tonne]
Econo-D	58	119	7.8
Ec-25	52	107	6.9
Ec-50	47	106	6.8
Ec-75	40	104	6.7
Mk6	34	106	7.6
Mk9	62	139	8.3

Although the energy consumption of reefers packed with different packaging designs varies when the fruit load is due to the difference in SECT of the fruit, after the field heat of fruit is removed and during extended land and marine transportation of reefer, energy use of these reefers is basically the same despite packaging design. This is because the reefer operates at the same operating condition: evaporator fans are running constantly and energy is used to remove heat load from the fans (≈1.4 kW), heat conducted from the environment and, fruit respiration heat load. However, the energy consumed is beyond what is required. In the following section, an alternative energy saving strategy for a reefer is evaluated with respect to reefer design parameter (evaporator fan operation) (section 6.3.4).

Stellenbosch University https://scholar.sun.ac.za

6.3.4. Evaporator fan speed

Cooling of apple (15.36 tonnes) packed in reefers working at (8100$m^3 h^{-1}$), medium (5400 $m^3 h^{-1}$) and low (2700 $m^3 h^{-1}$) airflow supply evaporator fan were simulated. The heat load in the fruit packed reefer was removed faster at high fan speed operation (Figure 6.9a) than the medium and low fan speed operations in the first 40 hours. During this period convective heat transfer mechanism is dominant. After 40 hours, the cooling capacity of the high speed operation was matched by the low speed fan operation. Similarly, the refrigeration load of medium speed operation was also matched by low speed operation at 55 hours (Figure 6.9b). The fruit average temperature inside the reefers operating at high, medium and low fan speed reached SECT at 47, 58 and 122 hours, respectively. As shown in Figure 6.9a the refrigeration load of high, medium and low fan speeds narrows down as temperature gradient between the fruit load the cooling air was sufficiently low. This is due to the shift in heat transfer mechanism from convective dominated to conduction dominated cooling. A simulation result of a reefer operating with a variable speed showed that sufficient cooling rate can be maintained by changing the speed of the fans (Figure 6.9b). The reefer was operating at high fan speed for the first 40 hours, followed by medium speed fan operation from 40 to 55 hour, and at low fan speed for the last 17 hours. The SECT of the fruit load inside this reefer was reached at 55 hour. After the fruit reached the SECT the reefer operating at low fan speed was managed to maintain the fruit at the desired temperature. Hence, operating the reefer at a constant speed during the entire cooling period is not compulsory.

Stellenbosch University https://scholar.sun.ac.za

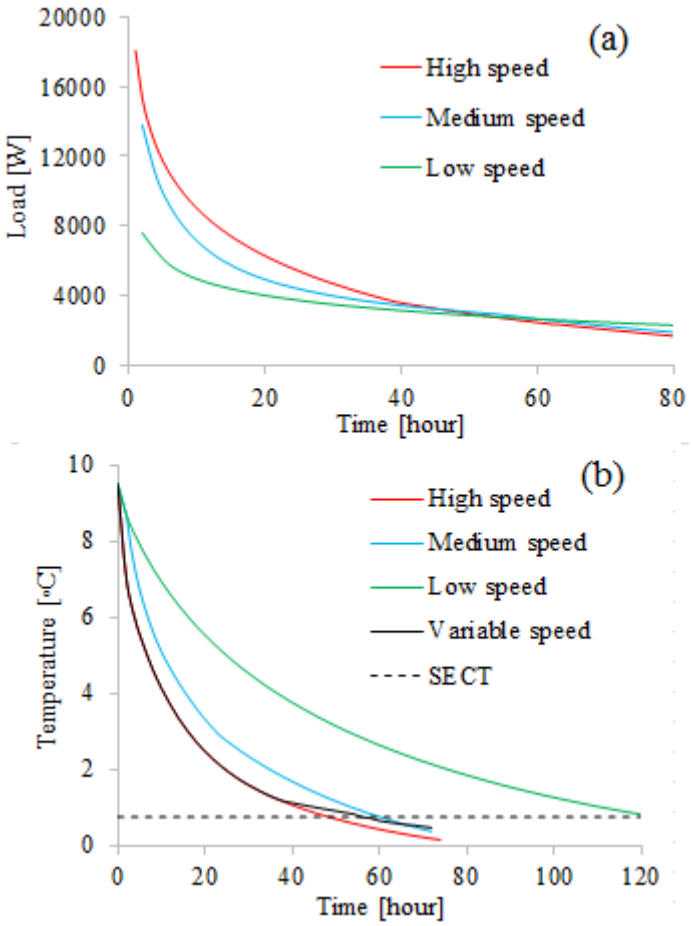

Figure 6-9: Reefers operating at high, medium and low fan speeds. (a) Refrigeration heat load and, (b) average temperature evolution during high, medium, low and variable speed fan. Variable speed used high speed – 8100 $m^3 h^{-1}$ (0-40 hours), medium speed – 5400 $m^3 h^{-1}$ (40-55 hours) and, low speed - 2700 $m^3 h^{-1}$ (55-72 hours)

The reefers consume power to run fan motor. In addition energy is consumed by the reefer to remove the heat generated by the fan during operation due to the blow-through fans arrangement. Energy consumed for fan operation during high, medium and low speed fan operation was compared with variable speed operation (Figure 6.10) considering a five day operation. The reefers operating at constant fan speeds of high, medium and low consumed 222, 154 and 77 kWh, respectively. On the other hand, the energy consumption with the variable speed fan configuration was 116 kWh. This implies application of the variable speed fan configuration can reduce the energy consumption by 47 and 17 % compared to high and medium speed fan operations, respectively. The application

Stellenbosch University https://scholar.sun.ac.za

of variable speed have a more distinct effect on energy consumption, particularly during long distance transportation since the reefer operates at low fan speed once the fruit load reached the desired temperature (Figure 6.10). Optimal fan operation will not only save fan power consumption but also save the compressor power needed to remove heat generated by the fan motor (Thompson et al., 2010). To this end, it is clear that application of variable speed fan configuration delivers better energy efficiency, compared to fan operation at a constant speed.

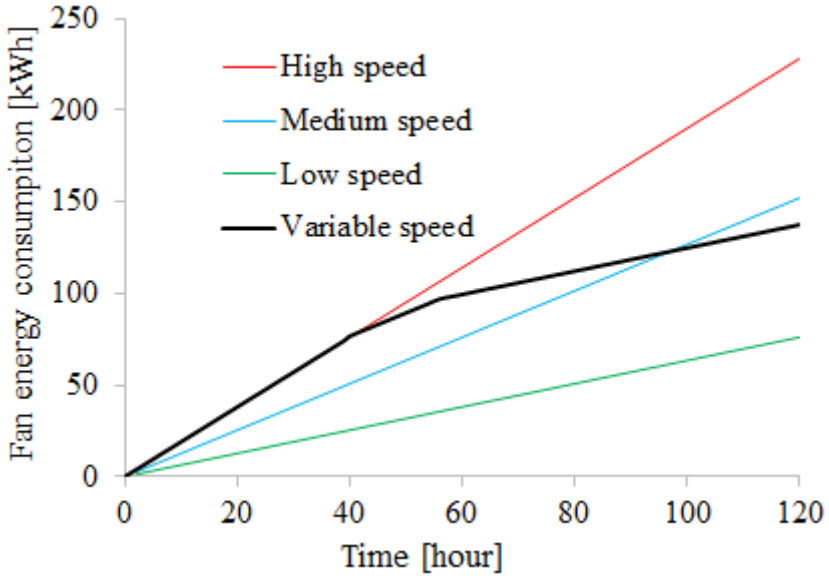

Figure 6-10: Energy consumption associated with evaporator fan of the reefers operating at high, medium, low and variable fan speeds. High speed – 8100 $m^3 h^{-1}$ (0-40 hours), medium speed – 5400 $m^3 h^{-1}$ (40-55 hours) and, low speed–2700 $m^3 h^{-1}$ (55-72 hours)

6.4. Conclusion

Energy consumption of reefers, that are used to transport fresh produce, was studied in relation to packaging designs and evaporator fan operations using

Stellenbosch University https://scholar.sun.ac.za

numerical method and experimental measurement. In the experimental study, the total electrical power consumption and the power use of major refrigeration system components were monitored. The numerical study successfully unveiled the effect of packaging designs on the total energy consumption of reefers, particularly by reducing the cooling period. The maximum energy consumption (139 kWh) was recorded by the reefer packed with Mk9 packaging design to cool 16.8 tonnes of apple to SECT in 62 hours, whereas the reefer packed with Mk6 packaging design consumed 21.73 % less energy to cool 14.4 tonnes of fruit to the SECT in 34 hours. On the other hand, evaluation of the vertical airflow resistance of the pallets stacked with Econo-D, Ec-25, Ec-50 and, Ec-75 packaging designs, that contain the same amount of fruit, a 12 % reduction in reefer total energy consumption. Similarly, the energy consumption was reduced by 9.6 and 10.9 % for Ec-25 and Ec-50, respectively. This was mainly due to a 27 % reduction in the SECT from due to better ventilation of Ec-75 (≈ 3.5 % bottom ventilation area) compared to Econo-D (no bottom vent hole).

Simulation results of reefers operating at high, medium, low and variable speed evaporator fan operation demonstrated the potential energy saving that can be achieved by using variable speed fan operation, particularly over extended transportation period. Application of the variable speed fan configuration reduced the energy consumption by 47 and 17 % compared to high and low speed fan operations after 120 hours, respectively. Operating the fan at with respect to the refrigeration load not only save energy but could also reduce CO_2 emission as electric energy for the reefers is generated by diesel combustion on board vessels using engines.

Stellenbosch University https://scholar.sun.ac.za

Chapter 7

7. Effects of climatic conditions on cooling characteristics and energy consumption of apple packed reefer during marine transport

Abstract

During long marine transportation periods fruit packed reefers are exposed to a wide range of climatic conditions that can compromise the quality of fruit load and affect reefer energy utilization. In this study, a validated computational fluid dynamics (CFD) model of a fully loaded refrigerated shipping container (reefer) was used to evaluate the impact of climate (0, 20 and 40 ℃ ambient temperatures and 7.2 m s^{-1} wind speed) on fruit cooling and energy consumption. The numerical study successfully unveiled the effect of climatic conditions on fruit cooling, temperature distribution and energy consumption of reefers. Heat transfer through the walls increased temperature of the fruits near the side walls by 4 ℃, particularity under 40 ℃ environment. The maximum energy (159 kWh) was used by the reefer operating in 40℃ region climatic condition. The reefer under adiabatic condition and 0 ℃ region consumed the minimum energy (109 KWh). In addition, the reefer passing through climatic zones with 20, 40 and 0 ℃ ambient temperatures and 7.2 m s^{-1} wind speed consumed 397 kWh energy in 9-day. The reefer consumed 42 % of the total energy in 40 ℃ ambient temperature region.

7.1. Introduction

Refrigerated shipping containers (reefers) carry out a highly demanding routine to transport different varieties of goods that have a desired temperature

Stellenbosch University https://scholar.sun.ac.za

ranging from -30 to +20 ℃ under a wide range of climatic conditions with an ambient temperature range of -40 to +50 °C. Efficient temperature control in the reefer is critical, particularly for temperature sensitive perishable produce load in a chilled mode. Poor thermal insulation and air infiltration into a reefer and cold storage contribute to poor control of storage conditions and energy loss (Foster et al., 2003; Gosney, 1975).

Cold storage must be insulated in such a way that heat in-leak should not increase beyond 6 – 8 W/m^2 (Tridib, 2009). Ahmed et al. (2010) studied the heat transfer across the insulated walls of refrigerated truck trailers experimentally. The authors adapted well proved phase change material (PCM) from its successful practical result in building walls and structural insulated panel(SIP) by (Zhang et al., 2005; Medina et al., 2008). Integration of PCMs in regular building walls resulted in 11–20 % peak heat transfer rate reduction with a PCM concentration of 10 %. A lower capital investment with an inferior quality and thinner insulation leads to a larger heat in-leak. A larger compressor with more power consumption is required to make up for the additional cooling load. It is therefore obvious that when the energy cost has already increased and set to increase further, the quality and thickness of insulation has to improve further. It is however not so in practice.

The primary factor for heat transfer from the environment is the airflow and ambient temperature around reefer on open space, such as on shipping vessels during marine transport. Airflow during marine transportation has a forced nature and the convective heat transfer coefficient on the exterior of a reefer is seriously influenced. Several experimental and numerical studies have shown that flow over a flat plate, similar to that of walls of a reefer, is affected by, temperature, humidity and wind speed (Xiao et al., 2011). James et al. (2006) emphasised the far less coverage of refrigerated transport compared to other refrigeration processes with respect to modelling. The authors also recommended further study of heat transfer between the container walls and the outside air and heat transfer to the produce load from the container walls.

Stellenbosch University https://scholar.sun.ac.za

The objective of this study was to evaluate the effects of environmental conditions on fruit packed reefers during transportation. Three ambient temperatures (0, 20 and 40 ℃) were evaluated using a numerical model to emulate various climatic conditions across Atlantic fruit transport in reefers.

7.2. Materials and methods

7.2.1. Reefer and fruit load

A state-of-the-art reefer (Starcool SCI-40, Maersk reefer) with internal and external length / width / depth of 11.59 m × 2.29 m × 2.54 m and 12.19 m × 2.44 m × 2.90 m, respectively was used to evaluate environmental conditions on fruit handling during shipping. The walls of the reefer are mainly composed of three different layers of materials. Polyurethane insulation is used in the middle (ASHRAE, 2010). The materials and thicknesses used per side of the reefer are summarised in chapter 3 (Table 3.1). The reefer has a bottom air delivery unit in which cold air from the refrigeration unit enters into the reefer from the bottom and the returning air leaves the reefer at the top to the refrigeration unit. Totally, 15 tons of apple fruit are loaded into the reefer on 20 pallets (each holding 768 kg apple fruit) that were arranged in two rows. One of the rows contains 11 pallets with the shortest side of the pallets against the side wall whilst the second one contains 9 pallets with the longest side against the side wall.

During transportation the reefers on are exposed to different ambient temperatures and various wind speed conditions that affect the of quality fruit load due to heat transfer through the walls. As shown in Figure 7a&b, reefers on vessel can be exposed to a wide range of ambient temperature (0 to 40 ℃) and wind speeds ranging 0 to 39 knots or 0 to 20 m s^{-1} (Figure 7.1c). In addition to that vessels also have sailing speed ranging 16 to 21 knots (Wang and Meng, 2012).

Stellenbosch University https://scholar.sun.ac.za

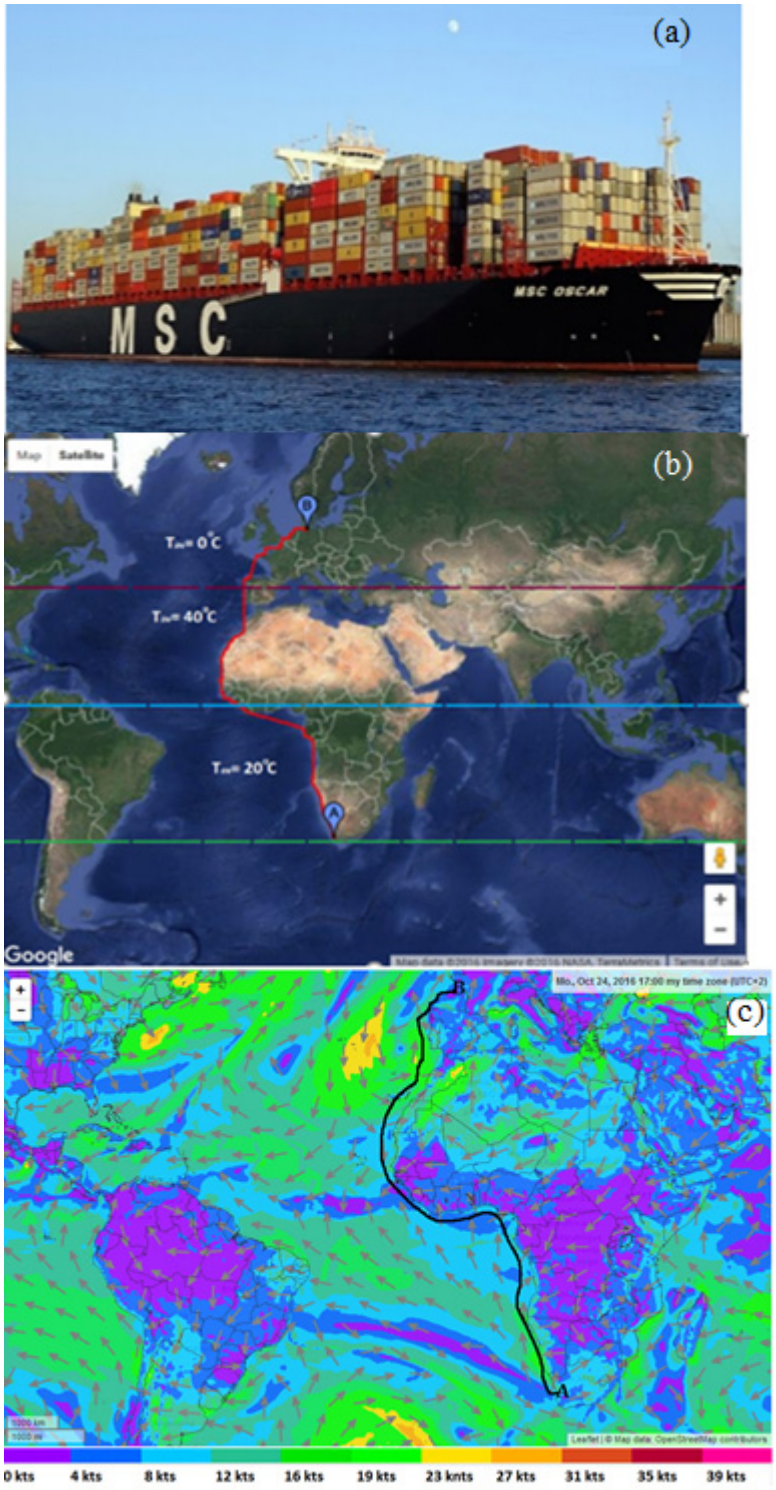

Figure 7-1: (a) Reefer container ship on route, (b) apple export route from South Africa to Europe and, (c) annual average wind speed map(www.windfinder.com)

Stellenbosch University https://scholar.sun.ac.za

7.2.2. Numerical model and assumptions

For this study a previously validated numerical model of apple packed reefer was used to study the effect of ambient conditions. Placement of the stacked pallets against the side walls provides support during transportation and limits the removal of heat conducted from the environment. The pallets were modelled as two rows of porous domains and there is a free air region below and above the pallet rows that make up the rest of the domain. Fluid-porous interface (between the porous domain and fluid domain) was explicitly defined as a conservative interface flux boundary for the momentum and scalar transports. The cooling unit was modelled by specifying temperature, pressure, and velocity and turbulence intensity at inlet. The refrigeration unit was operating at cooling flow rate of 5400 $m^3 h^{-1}$ (at an air exchange rate of ≈ 80 h^{-1}). The environmental conditions were represented by the ambient temperature and setting the overall convective heat transfer coefficient of the wall, ceiling, floor and door. Navier-Stokes equations were applied as governing equation for mass, momentum and supplemented by energy conservation equation (Eqn. 4.1 to 4.6). The heat generation per unit volume of produce due to respiration was calculated using equation 4.7 at the produce temperature.

Some assumptions were made to simplify the model. (1) heat load due to moisture evaporation from the fruit load was assumed negligible as the fruits are packed in bagged in plastic and packed in packaging boxes, (2) wind speed used to calculate convective heat transfer coefficient on the outside was assumed to be constant during reefer transportation and, (3) the release of heat due to condensation of water on the surface and defrost cycle of the reefer was not considered. In addition, the following basic assumptions were made during the model formulation.

- A constant ambient air temperature was assumed for the outside environment, pressure of 101 kPa and relative humidity of 80 %.
- Thermal radiation exchange between the exterior surface and the surroundings was neglected since the outer surfaces of the walls of the reefer were painted white (low emissivity).

Stellenbosch University https://scholar.sun.ac.za

- The physical properties of air were assumed constant for the given ambient temperature.
- Since the air circulation fans were positioned upstream of the evaporator coil (a blow-through configuration), the fan heat was assumed totally removed directly by the evaporator coil (Figure 6.3a).

7.2.3. Numerical simulation

Discretization of the domain was on ANSYS® Meshing™ Release 16.0 and the problem setup and simulation was on ANSYS® Fluent™ Release 16.0 (ANSYS, Canonsburg, PA, USA). Airflow simulation was conducted at steady state and the result was used as initial condition for the transient heat transfer calculation. Turbulence was calculated using k-ω SST model. SIMPLE discretization scheme was used for pressure-velocity coupling and Second Order Upwind discretization was used for momentum, specific dissipation rate and energy calculations. A time step size of 180 s with maximum 20 iterations per time step, was used. Dell Precision computer (dual Intel Xeon processor@3.30 GHz with 40 GB Ram) was used. Cooling operation inside four reefers loaded with precooled fruit loads (≈0.75 ℃) were simulated. Three of them were under climatic conditions (20, 40 and 0 ℃ ambient temperature and 14-knot (7.2 m s^{-1}) wind speed) and an adiabatic condition (no interaction with the environment). In addition, a loaded reefer traveling (9 days) through 20, 40 and 0 ℃ ambient temperature regions in the given sequence was simulated.

7.2.4. Initial and boundary conditions

In all the models, the internal walls of the reefer were set to a no slip conditions. Initially the average fruit temperature in the domain was assumed to be at 0.75 ℃. Convective heat transfer coefficient of the composite walls of the reefer were calculated based on the physical properties of air at the film temperature for ambient temperatures of 0, 20 and 40 ℃ under consideration. The heat fluxes at the container walls, floor and door were calculated using Fourier's Law (Eqn. 7.1).

Stellenbosch University https://scholar.sun.ac.za

$$Q_w = U\,(T_\infty - T_W) = U\,\Delta T \qquad 7.1$$

$$U = \frac{1}{\frac{2\Delta x_1}{k_1 A_1} + \frac{\Delta x_2}{k_2 A_2} + \frac{1}{h_o A_o}} \qquad 7.2$$

Where, k_1 (W m^{-1} K^{-1}) is thermal conductivity of the outer and inner wall material, k_2 (W m^{-1}°C^{-1}) is thermal conductivity of polyurethane which is sandwiched between the outer and inner wall, h_o (W m^{-2} K^{-1}) is the convective heat transfer coefficient between the outside surface and ambient air, A_1 (m^2) is the area of the inner surface of a wall, A_2 (m^2) is the area of the middle (polyurethane) layer of a wall and A_0 (m^2) is the area of the outer surface of a wall. U (W K^{-1} m^{-2}) is the overall heat transfer coefficient of composite wall, A (m^2), T_∞(K) is ambient temperature and, T_W (K) wall temperature. Q_m (J m^{-3}) is heat of respiration. The convective heat transfer coefficient, h_o (W K^{-1} m^{-2}) was calculated assuming turbulent flow over a flat plate (Eqn. 7.3) (Bird, 2002).

$$\mathrm{Nu} = 0.037\mathrm{Re}^{0.8}\mathrm{Pr}^{1/3} \qquad 7.3$$

Where Nu is the Nusselt number, Re is the Reynold's number and Pr is the Prandtle number. Air velocity near the wall was taken as 7.2 m s^{-1} (14 knots), which is the average annual wind speed in Atlantic Ocean (Reference). For the three ambient conditions, properties of air (Pr, μ, C_p, ρ and k) at the film temperatures 272.9, 282.9 and, 292.9 K were used to calculate overall heat transfer coefficient of the composite side wall, ceiling, floor and the door. Assuming $A_1 = A_2 = A_0 = A$, an overall heat transfer coefficient U can be used to simplify Eqn. 7.2. The heat exchange with the environment has been incorporated as heat fluxes on the walls, ceiling, floor and door and the corresponding heat transfer coefficients are given in Table 7.1.

Stellenbosch University https://scholar.sun.ac.za

Table 7-1 Calculated overall heat transfer coefficients of the walls of the reefer at three ambient temperatures

Ambient temperature, T_∞ (□)	Overall heat transfer coefficient (W $m^{-2}°C^{-1}$)			
	Wall	Door	Ceiling	Floor
0	0.28	0.27	0.27	0.26
20	0.34	0.32	0.32	0.31
40	0.37	0.34	0.34	0.34

Heat load from the fruit (sensible and respiration heat) and heat conduction from the environment were monitored during simulation. Transient total refrigeration heat load was calculated based on the temperature difference between the supply and return air temperature and evaporator fan heat load using equation (7.4).

$$Q_T = M_o C_p \Delta T \tag{7.4}$$

$$Q_w = UA(T_\infty - T_W) \tag{7.5}$$

Where, Q_T is total refrigeration and fan heat loads, M_o(kg s^{-1}) is mass flow rate of the returning air at the outlet, C_p(1006.12 J kg^{-1} K^{-1}) is specific heat capacity of air, ΔT (K) = T_0-T_i, ΔT_p (K) = $T_{P,t-1}$-$T_{p,t}$, Q_w (kW), U (W K^{-1} m^{-2}) is the overall heat transfer coefficient of composite wall, A (m^2), T_∞(K) is ambient temperature and, T_W (K) wall temperature. Fan heat (Q_{fan}) contributes a significant amount of heat load and should be included in the cooling load calculation (Thomson et al. 2002) and calculated using equation 7.6 (Evans et al., 2014).

$$Q_{fan} = \frac{N_m P_m}{\eta_{mot}} \tag{7.6}$$

Stellenbosch University https://scholar.sun.ac.za

Where, N_m is number of motors, η_{mot} is motor efficiency and, $P_m$is motor power. The two fans have nominal power of 0.45 kW. Motors rated 0.45 kW at 66 % motor efficiency contribute heat loads of 1363.6 W.

7.3. Result and discussion

7.3.1. Fruit cooling characteristic and temperature profile

The cooling performance of apple packed reefer was investigated by taking into account ambient climatic conditions that are close to the reality. Figure 7.2a depicts apple fruit load average temperature evolution inside a reefer. Each reefer was traveling through regions with 20, 40 and 0 ℃ ambient temperatures and 14-knot (7.2 m s^{-1}) wind speed climatic conditions. After 72 hours, the fruit load temperatures inside reefers in 20 and 0 ℃ ambient conditions cooled to 0.36 and 0.09 ℃, respectively. The cooling performance of the reefer in 0 ℃ region was almost the same as that of the reefer in adiabatic condition (0.1 ℃). Compared to the cooling performance of the reefer in adiabatic condition, the reefer in 20 ℃ region achieved 45 % less fruit temperature pull down. It was also noticed the fruit load inside the reefer under 20 ℃ condition reached its minimum temperature, 0.32 ℃, after 24 hours of cooling (day 4), however it slightly increased to 0.36 ℃ after another 48 hours (day 6) (Figure 7.2a). This could be due to cumulative impact of the heat conduction from the environment. In contrast to the other reefers, fruit average temperature inside the reefer in 40 ℃ region increased by 45.33 % (1.09 ℃) compared with the reefer in adiabatic condition.

The performance of apple packed reefer and its interaction with the environment were studied as it travels through three climatic regions. Figure 7.2b showed evolution of fruit average temperature inside a reefer when exposed to 20, and to 40 and then to a 0 ℃ ambient temperature regions with wind speed of 14 knot (7.2 m s^{-1}), consecutively. The effect of each climatic zone was markedly different. The fruit load exposed to ambient temperature of 40 ℃ showed reefers packed with apple fruit load at a temperature of 0.75 ℃. This was mainly due to the high heat conducted from the environment (458 W).

Stellenbosch University https://scholar.sun.ac.za

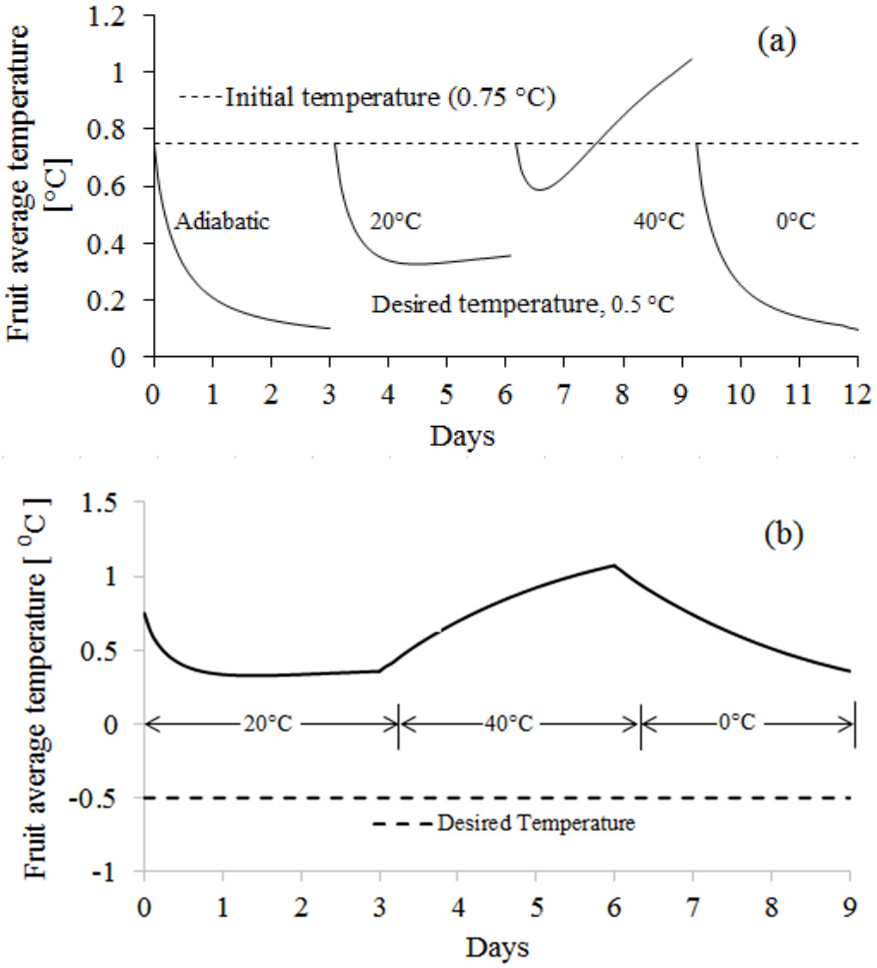

Figure 7-2: Effects of climatic conditions on fruit temperature inside a reefer. (a) Reefers in different climatic conditions (20, 40, 0 ℃ and 7.2 m s^{-1} wind speed) and adiabatic condition. (b) Fruit temperature evolution in a reefer during nine days of marine transportation through successive climatic conditions (20, 40 and 0 ℃ and 7.2 m s^{-1} wind speed)

The impact of climatic condition on spatio-temporal fruit temperature distribution in a reefer is shown in Figure 7.3. The impact was mainly on the fruits near the side walls of the reefer. Figure 7.3 (a,b & c) show this effect on a plane bisecting the reefer horizontally at the middle of the reefer (between the cooling unit and the door). At the end of a 3-day period in 20 ℃ ambient temperature zone 25 % of the fruit load was found to be above the initial temperature (0.75 ℃) and 3 % of the load reached ≈4 ℃ (Figure 3a). After another 3 days in 40 ℃ ambient

Stellenbosch University https://scholar.sun.ac.za

temperature zone, the amount of fruit above 0.75 ℃ increased to 42 %, and 11 % of the fruit load was greater than or equal to 4 ℃. However, in the final 3 days in 0 ℃ ambient temperature region the size of warm regions in the fruit load near the side walls diminished, less than 3 % of the load was ≈4 ℃.

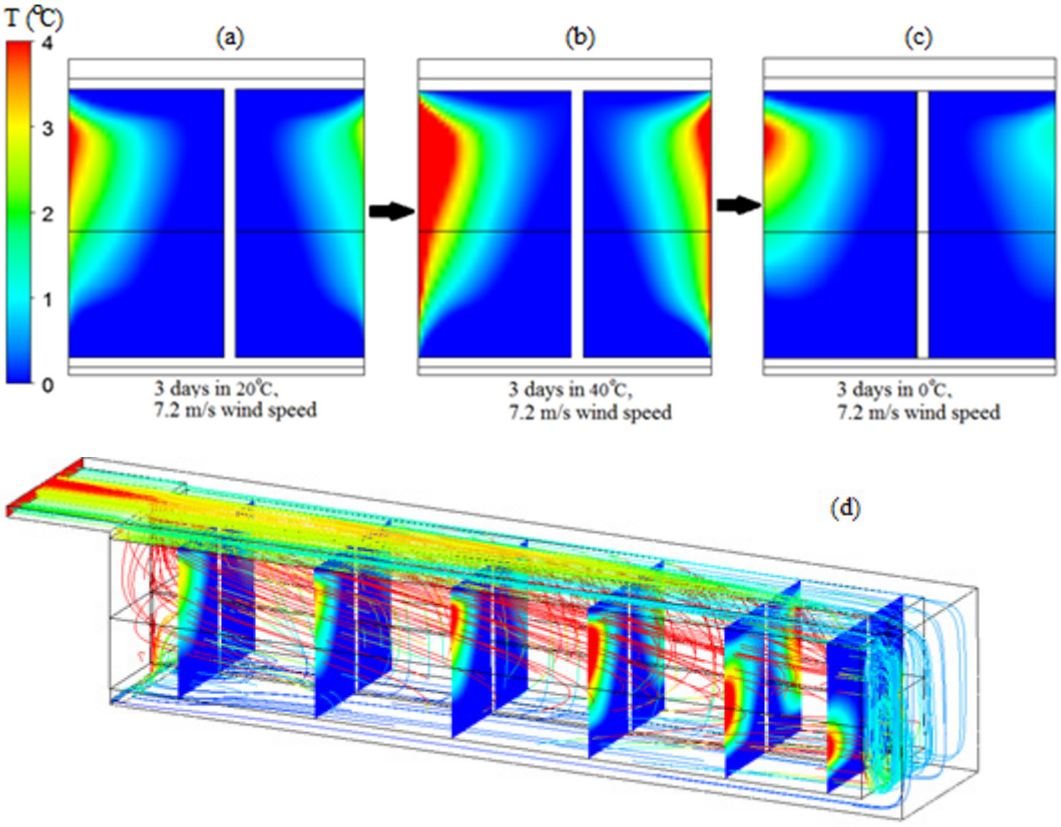

Figure 7-3: Effects of heat conduction through the walls of the reefer on fruit load adjacent the side walls of the reefer. Temperature profile on a plane bisecting the reefer horizontally at the middle (5.8 m from cooling unit) of the reefer after 3 days in (a) 20, (b) 40 and, (c) 0 ℃ ambient temperature zones. (d) Spatial temperature variation along the length of the reefer and airflow streamlines coloured by temperature (coloured by temperature from -1 to 0 ℃).

The temperature profile of the fruit load showed spatial variation across the width and the length of the reefer. Across the width of the refer, fruit loads in the pallet row 1 (left side) were more affected than in the pallets on the right side due to the arrangement of the pallets. The pallets in row 1 were arranged with the longest

Stellenbosch University https://scholar.sun.ac.za

side (1.2 m deep) perpendicular to the side wall, whereas pallets on the right are arranged with the shortest side perpendicular to the walls (1.0 m deep). Higher depth imposed higher confinement and airflow resistance, which obstructed the removal of heat conducted from the environment.

The temperature profile along the length of the reefer also varies. Figure 7.3d shows distinct pattern of temperature profile along the reefer length (1, 3, 5, 7, 9, and 10.5 m from the cooling unit). The warm regions near the side walls were wider in the middle of the reefer and were more concentrated in the middle of the pallets (Figure 7.3d). On the other hand, the warm regions on the pallets near the cooling unit and the door side were concentrated near the top and bottom of the pallets, respectively. This was mainly due to the cooling air distribution in the domain. As shown in the airflow streamlines (coloured by temperature from -1 to 0 ℃), near the cooling unit, air at lower temperature flows into the pallets from the bottom and air (returning air) at higher temperature flows over the pallets. For the pallets in the rear part of the reefer (near the door side), vertical airflow through the bottom of the pallets was low (discussed in chapter 4 section 4.4). However, the space between the last pallets and the door allowed higher airflow recirculation, which might have facilitated heat removal near the sidewalls, in the top of the pallets.

7.3.2. Heat load and environmental effect

In the previous study it has been shown that majority of refrigeration heat load was contributed by field heat of the fruit when the initial temperature was 9.5 ℃ (Chapter 6 section 6.4.1). In this case, precooled fruit (0.75 ℃) was loaded and the initial total fruit heat load was 73516.8 kJ for all the reefers. At the end of the cooling period (day 3) the field heat of the fruit loads in reefers under adiabatic condition, 0 and 20 ℃ ambient temperature decreased by 51.8, 52.8 and, 32 %, respectively. In contrast, heat load of the fruit load in the reefer under 40 ℃ ambient temperature increased by 23.2 % due to heat transfer from the environment by conduction and fruit respiration heat. Heat conduction into the reefers operating

Stellenbosch University https://scholar.sun.ac.za

under adiabatic condition, 0, 20 and 40 ℃ ambient temperature regions were 0, 0.3, 127 and 458 W, respectively (Figure 7.4a). In the previous study, of fruit packed reefer conduction heat load of 18 W was recorded under 10 ℃ ambient temperature while the reefer was stationary (0.2 m s^{-1} wind speed) (Chapter 6 section 6.4.1). High ambient temperature combined with high wind speed (annual average wind speed on Atlantic Ocean ≈7.2 m s^{-1}) on the outer surface of the reefers resulted in higher heat conduction into the reefers. Similarly, respiration heat from fruit in 40 ℃ region was 13 % higher compared to fruit load in adiabatic condition (Figure 7.4b).

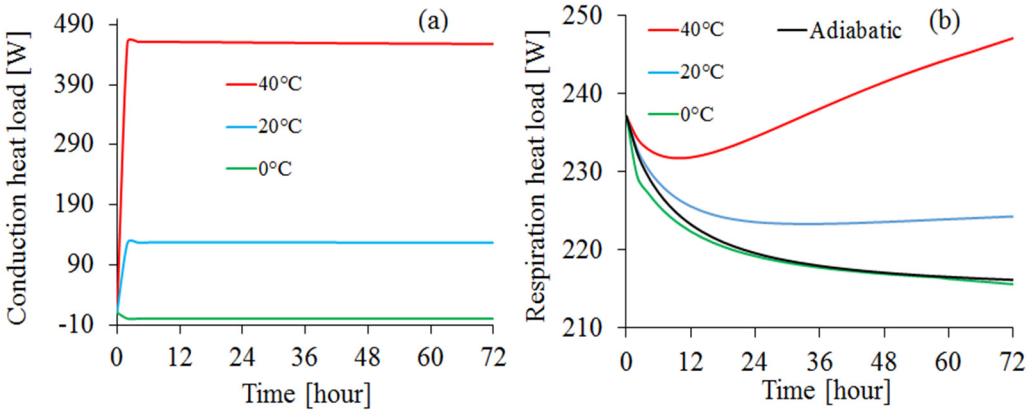

Figure 7-4: Heat load due to to respiration (a) and conduction from the environemt (b) in the reeefers that were exposed to three ambient temperatuers and one under adiabatic condition.

7.3.3. Energy consumption

The reefer in 40 ℃ region consumed the highest energy (159 kWh) in 72 hours (Figure 7.5). The reefers in 0 ℃ region and adiabatic condition consumed almost the same amount of energy (109 kWh) as the conduction heat through the walls was low (0.3 W) for the reefer in 0 ℃ region. The resulting total energy consumption of reefers in adiabatic condition and 0 ℃ region could have been much lower. As it was discussed in the previous chapter (section 6.4.5), due to low temperature gradient (1.25 ℃) between fruit and cooling air heat transfer mechanism is primarily by conduction and operation of evaporator fans at

Stellenbosch University https://scholar.sun.ac.za

maximum cooling air supply rate is not needed. The reefer operating in 20 ℃ region consumed 11.9 % (13 kWh) more energy in 72 hours compared to the reefer in adiabatic condition. Considering identical initial and operating conditions set for all the reefers, the amount of extra energy consumed by the reefers in the 40 ℃ (50 kWh) and 20 ℃ (13 kWh) regions clearly shows the impact of climatic conditions on energy consumption.

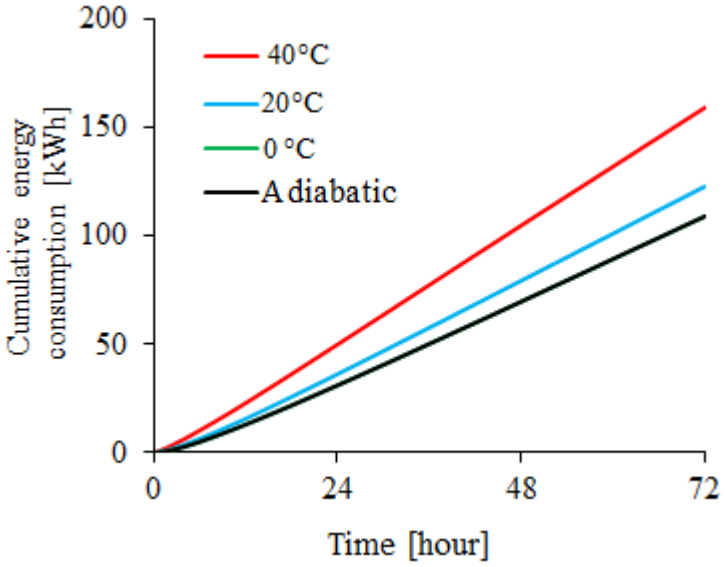

Figure 7-5: Cumulative energy consumption of fruit packed reefer under three climatic conditions with 20 (blue), 40 (red) and 0 ℃ (green) temperatures and 7.2 m s^{-1} wind speed. Fruit load initial temperature was 0.75 ℃.

The reefer passing through climatic zones with 20, 40 and 0 ℃ temperatures and 7.2 m s^{-1} wind speed consumed 396.65 kWh by the end of the 9-day voyage (Figure 7.6). The reefer consumed 42 % of the total energy in 40 ℃ ambient temperature region. The maximum and minimum energy consumptions were recorded in the regions with 40 ℃ (166 kWh) and 0 ℃ (108 kWh) ambient temperature, respectively. The main factor for this difference was the higher refrigeration load on the reefer due to heat conduction through the walls and heat generated by respiration, combined. The cumulative heat load due to heat conduction from the environment and respiration combined were 25.11, 49.36,

Stellenbosch University https://scholar.sun.ac.za

15.85 kWh in the 20, 40 and 0 ℃. As a result, the energy consumption of the reefer in the 40 ℃ region increased by 58 kWh compared to that of in 0 ℃ region.

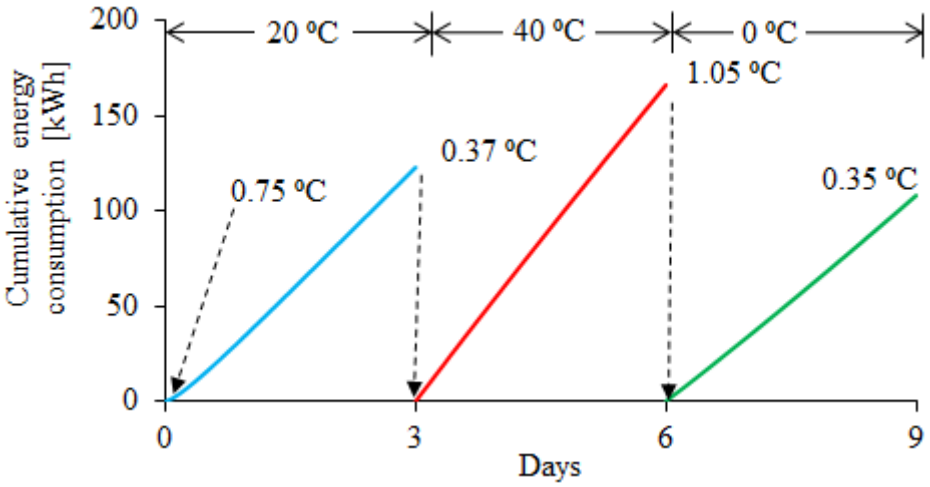

Figure 7-6: Reefer cumulative energy consumption of a reefer passing through climatic conditions of 20 (blue), 40 (red) and 0 ℃ (green) temperatures and 7.2 m s^{-1} wind speed. Initially, the fruit load was at 0.75 ℃ entering 20 ℃ ambient temperature region

7.4. Conclusion

During long marine transportation fruit packed reefers are exposed to a wide range of climatic conditions that can compromise the quality of fruit load and affect reefer energy utilization. The numerical study successfully unveiled the effect of climatic conditions on fruit cooling, temperature distribution and energy consumption of reefers. Heat conduction through the walls raised temperature of the fruit near the side walls by 4.5 ℃ above the desired temperature, particularity under 40 ℃ conditions. The maximum energy (159 kWh) was used by the reefer operating in 40 ℃ region climatic condition. The reefer under adiabatic condition and 0 ℃ region consumed the minimum energy (109 kWh). The results indicate appropriate measures should be taken to minimize the potential damages on fruit load and energy consumption during transportation, particularly in high temperature ambient climates.

Stellenbosch University https://scholar.sun.ac.za

Chapter 8

8. General summary and conclusions

8.1. Summary and conclusions

Cold chain systems are the most important postharvest technologies that are applied to maintain the quality during handling, storage and transportation of horticultural produces. Refrigerated shipping containers (reefers) are important part of this cold chain system to deliver fresh fruit that meets standard quality parameters in the global (export) and local market (domestic use). On the other hand, energy use for product refrigeration is raising anxiety as the primary energy sources are depleting and their impact on environment. The main aim of this study is to develop and validate a computational fluid dynamic (CFD) model applicable to reefers that is capable of predicting the total energy consumption of the system and then apply the validated model for improving the operation and design of reefers.

The effect of reefer design and operational conditions on the airflow distribution was studied using CFD modelling and reported in chapter 3. In this study, the airflow and temperature distribution inside T-bar and flat floor type reefers, operating at high and low evaporator performances, were investigated. The CFD model was validated with experimental study conducted in a full-scale reefer, and good agreement was found between measured and predicted values of air velocities and temperatures. Airflow distribution in the two container designs was markedly different. The reefer with T-bar floor design exhibited a noticeable reduction of air recirculation zone and enhanced vertical air movement compared to the reefer with flat floor design.

One of the controlling parameters for fruit quality is temperature and poor management of temperature in the reefer results in deterioration of fruit postharvest

Stellenbosch University https://scholar.sun.ac.za

quality and loss. Uniform distribution of air inside reefers is very important to ensure uniform cooling of the produce. A CFD model that is capable of predicting airflow and produce cooling inside a fully loaded reefer was developed using porous medium approach (Chapter 4). The model included the detailed structure of the reefer, aerodynamic characteristics of packed produce and stacked pallets. The model was validated by data obtained from a reefer fully loaded with stacks of apple fruit, and the model successfully reproduced the airflow and temperature profiles with an acceptable accuracy. Non-uniform airflow distribution leading to a highly heterogeneous cooling was found primarily due to the absence of vent-hole on the bottom face of the apple packaging box. The results demonstrated the importance of packaging design that takes into account the of airflow path inside reefers.

Further to investigate the effects of packaging designs, the performance of packaging designs, which are commonly used for handling apple fruit (Econo-D, Mark 6 (Mk6) and Mark 9 (Mk9)), and effect of vertical airflow resistance was studied using the validated model (Chapter 5). First, the study computes the aerodynamic and thermodynamic characteristics of three package designs. The packaging design that has higher bottom-ventilation area (Mk6) showed better cooling airflow distribution and faster fruit cooling compared to the other packaging designs, however, it offers less fruit load per reefer. On the other hand, the study of vertical airflow resistance for the same packaging design (Econo-D) confirmed the effect of vertical airflow on the rate and uniformity of cooling inside the reefer. Adding vent-holes (3.5 % vent area) on the bottom face of the package reduced vertical airflow resistance, and reduced the seven-eighth cooling time by 27 % compared to a package with no bottom vent-holes.

Refrigerated transport systems are one of the highest energy consuming food refrigeration systems. In Chapter 6 the energy consumption reefers were also studied with respect to operational and design parameters during apple cooling. The performance of apple packaging designs in a reefer with respect to energy consumption confirmed the influence of ventilation area, particularity on the bottom side, and the trade-off between the energy savings that can be achieved by

Stellenbosch University https://scholar.sun.ac.za

employing packaging designs with low (Mk6) and high (Mk9) fruit packing density. To this end, adding vent-holes (3.5 % vent area) on the bottom face of the Econo-D packaging box reduced the reefer total energy consumption by 12 % compared to packaging designs with no bottom vent-holes. The effect of evaporator fan operation on energy consumption was studied by simulating reefers operating at low, medium, high and variable fan speeds. The simulation result confirmed fans operating at constant speed were performing over or under with respect to the refrigeration load, which caused high energy consumption or slow cooling. On the other hand, a simulation result of a reefer with the variable speed fan configuration matched the refrigeration load throughout the cooling period. Energy consumption obtained for a reefer operating with the variable speed fan configuration was 47 and 17 % less compared to reefers operating at high and low fan speed, respectively, during a 120-hour operation. The results established application of variable speed fan operation can reduce energy consumption of reefers without compromising the cooling operation.

Lastly, (chapter 7) is presented regarding the impact of ambient conditions during transportation of apple fruit. The heat conduction through the walls of the reefer can damage fruit quality during freight shipping. Reefers loaded with precooled apple (0.75 ℃) operating in three climatic conditions (0, 20 and 40 ℃ ambient temperatures and 7.2 m s^{-1} wind speed) were studied using a validated model. In addition, a reefer on crossing through three climatic conditions 20, 40 and 0 ℃ ambient temperatures (7.2 m s^{-1} wind speed), consecutively, was studied. Heat conduction through the side walls of the reefer increased the temperature of fruit load (≈11 % of the total load) to 4 ℃ near the side walls inside the reefer operating in the 40 ℃ zone. The maximum (159 kWh) and minimum (109 KWh) energy were used by the reefers operating in 40, and 0 ℃ zones. The reefer crossing the three climatic zones consumed 42 % of the total energy (397 kWh) in the 40 ℃ ambient temperature region during 9-days journey (3 days in each zone). It is recommended there is space between the walls of the reefer and the pallets so that heat from the environment can be removed easily.

Stellenbosch University https://scholar.sun.ac.za

8.2. Future prospects

The study presented in this dissertation has touched on and contributed to various topics that affect the performance of reefers during fresh fruit handling. The results could be used to study quality parameters of perishable products at different stages during extended transportation period and in various climatic conditions. This could be done by relating the spatio-temporal data of produce temperature with the physical (such as weight loss), biological (such as enzymatic activities) and, chemical (such as total soluble solid) activities of the perishable produce.

During long distance fruit transportation, from countries such as South Africa to Europe, the shipment has to pass through various climatic conditions; from the very cold (near the poles) to hot regions (equator). Despite the availability of integrated refrigeration systems, the incidence of cold chain breaks happen and inadequate fruit handling environment may occur and the possible scenarios should be known to make informed decisions to minimize losses and subsequent claims associated with fruit quality and energy use. Some of the breaks take place primarily due to a power failure at ports as the reefers are in line to be loaded onto a vessel, when refrigeration systems are switched off as a strategy to save electricity consumption and when refrigeration systems malfunction. More comprehensive research on cooling mode strategies is important to minimize energy consumption without compromising the quality of produce.

Stellenbosch University https://scholar.sun.ac.za

References

Adre, N., & Albright, L. D., 1994. Criterion for establishing similar air flow patterns (isothermal) in slotted-inlet ventilated enclosures. *Transactions of the ASAE*, *37*(1), 235-250.

Akdemir, S., & Arin, S., 2006. Spatial variability of ambient temperature, relative humidity and air velocity in a cold store. *Journal of Central European Agriculture*, *7*(1), 101-110.

Alvare, G., Bournet, P. E., & Flick, D., 2003. Two-dimensional simulation of turbulent flow and heat transfer through stacked spheres. *International Journal of Heat and Mass Transfer*, *46*(13), 2459-2469.

Ambaw, A., Delele, M. A., Defraeye, T., Ho, Q. T., Opara, L. U., Nicolai, B. M., & Verboven, P., and 2013.The use of CFD to characterize and design post-harvest storage facilities: Past, present future. *Computers and Electronics in Agriculture*, *93*, 184-194.

Ambaw, A., Bessemans, N., Gruyters, W., Gwanpua, S.G., Schenk, A., De Roeck, A., Delele, M.A., Verboven, P. and Nicolai, B.M., 2016. Analysis of the spatiotemporal temperature fluctuations inside an apple cool store in response to energy use concerns. *International Journal of Refrigeration*, *66*, 156-168.

ASHRAE., 2010. ASHRAE handbook OF refrigeration: Systems and applications (SI ed.). (Atlanta).

Becker, B. R., Misra, A., & Fricke, B. A., 1996. Bulk refrigeration of fruits and vegetables Part I: theoretical considerations of heat and mass transfer. *HVAC&R Research*, *2*(2), 122-134.

Berry, T., Delele, M. A., Griessel, H., & Opara, U. L., 2015. Geometric design characterisation of ventilated multi-scale packaging used in the South African pome fruit industry. *Agricultural Mechanization in Asia, Africa, and Latin America*, *46*(3), 34-42.

Stellenbosch University https://scholar.sun.ac.za

Berry, T.M., Defraeye, T., Nicolai, B.M. and Opara, U.L., 2016. Multiparameter analysis of cooling efficiency of ventilated fruit cartons using CFD: impact of vent hole design and internal packaging. *Food and Bioprocess Technology*, 1-13.

Bird, R. B., 2002. Transport phenomena. *Applied Mechanics Reviews*, *55*(1), R1-R4.

Brosnan, T., & Sun, D. W., 2001. Precooling techniques and applications for horticultural products—a review. *International Journal of Refrigeration*, *24*(2), 154-170.

Castro (de), L. R., Vigneault, C., & Cortez, L. A., 2004a. Container opening design for horticultural produce cooling efficiency. *Journal of Food, Agriculture and Environment*, *2*, 135-140.

Castro (de), L. R., & Vigneault, C., 2004b. Effect of container opening area on air distribution during precooling of horticultural produce. *Transactions of the ASAE*, *47*(6), 2033.

Castro (de), L. R., & Vigneault, C., 2005. Effect of container openings and airflow rate on energy required for forced-air cooling of horticultural produce. *Canadian Biosystems Engineering, 47,* 1-9.

Chourasia, M. K., & Goswami, T. K., 2007. Steady state CFD modelling of airflow, heat transfer and moisture loss in a commercial potato cold store. *International Journal of Refrigeration*, *30*(4), 672-689.

Chourasia, M. K., & Goswami, T. K., 2009. Efficient design, operation, maintenance and management of cold storage compressor. *eJournal of Biological Sciences*, 1(1), 2076-9954.

Defraeye, T., Verboven, P., & Nicolai, B., 2013. CFD modelling of flow and scalar exchange of spherical food products: Turbulence and boundary-layer modelling. *Journal of Food Engineering*, *114*(4), 495-504.

Defraeye, T., Lambrecht, R., Delele, M.A., Tsige, A.A., Opara, U.L., Cronjé, P., Verboven, P. and Nicolai, B., 2014. Forced-convective cooling of citrus fruit: cooling conditions and energy consumption in relation to package design. *Journal of Food Engineering*, 121,118-127.

Stellenbosch University https://scholar.sun.ac.za

Defraeye, T., Cronje, P., Verboven, P., Opara, U. L., & Nicolai, B., 2015a. Exploring ambient loading of citrus fruit into reefer containers for cooling during marine transport using computational fluid dynamics. *Postharvest Biology and Technology*, *108*, 91-101.

Defraeye, T., Verboven, P., Opara, U. L., Nicolai, B., & Cronjé, P., 2015b. Feasibility of ambient loading of citrus fruit into refrigerated containers for cooling during marine transport. *Biosystems Engineering*, *134*, 20-30.

Defraeye, T., Cronje, P., Berry, T., Opara, U. L., East, A., Hertog, M., Verboven, P., & Nicolai, B., 2015c. Towards integrated performance evaluation of future packaging for fresh produce in the cold chain. *Trends in Food Science & Technology*, *44*(2), 201-225.

Defraeye, T., Nicolai, B., Kirkman, W., Moore, S., van Niekerk, S., Verboven, P. and Cronjé, P., 2016. Integral performance evaluation of the fresh-produce cold chain: A case study for ambient loading of citrus in refrigerated containers. *Postharvest Biology and Technology*, *112*,.1-13.

Dehghannya, J., Ngadi, M., & Vigneault, C., 2010. Mathematical modeling procedures for airflow, heat and mass transfer during forced convection cooling of produce: a review. *Food Engineering Reviews*, *2*(4), 227-243.

Dehghannya, J., Ngadi, M., Vigneault, C., 2011. Mathematical modeling of airflow and heat transfer during forced convection cooling of produce considering various package vent areas. *Food Control 22* (8), 1393–1399.

Dehghannya, J., Ngadi, M., & Vigneault, C., 2011. Mathematical modelling of airflow and heat transfer during forced convection cooling of produce considering various package vent areas. *Food Control*, *22*(8), 1393-1399.

Delele, M. A., Tijskens, E., Atalay, Y. T., Ho, Q. T., Ramon, H., Nicolai, B. M., & Verboven, P., 2008. Combined discrete element and CFD modelling of airflow through random stacking of horticultural products in vented boxes. *Journal of Food Engineering*, *89*(1), 33-41.

Delele, M.A., Schenk, A., Tijskens, E., Ramon, H., Nicolai, B.M., Verboven, P., 2009a. Optimization of the humidification of cold stores by pressurized

Stellenbosch University https://scholar.sun.ac.za

water atomizers based on a multiscale CFD model. *Journal of Food Engineering*, 91, 228–239.

Delele, M.A., Schenk, A., Ramon, H., Nicolai, B.M., Verboven, P., 2009b. Evaluation of a chicory root cold store humidification system using computational fluid dynamics. *Journal of Food Engineering* 94, 110–121.

Delele, M. A., Ngcobo, M. E. K., Getahun, S. T., Chen, L., Mellmann, J., & Opara, U. L., 2013a. Studying airflow and heat transfer characteristics of a horticultural produce packaging system using a 3-D CFD model. Part I: Model development and validation. *Postharvest Biology and Technology*, *86*, 536-545.

Delele, M. A., Ngcobo, M. E. K., Getahun, S. T., Chen, L., Mellmann, J., & Opara, U. L., 2013b. Studying airflow and heat transfer characteristics of a horticultural produce packaging system using a 3-D CFD model. Part II: Effect of package design. *Postharvest Biology and Technology*, *86*, 546-555.

Evans, J.A., Foster, A.M., Huet, J.M., Reinholdt, L., Fikiin, K., Zilio, C., Houska, M., Landfeld, A., Bond, C., Scheurs, M. and van Sambeeck, T.W.M., 2014. Specific energy consumption values for various refrigerated food cold stores. Energy and Buildings, 74, 141-151.

Ferrua, M. J., & Singh, R. P., 2009a. Modeling the forced-air cooling process of fresh strawberry packages, Part I: Numerical model. *International Journal of Refrigeration*, *32*(2), 335-348.

Ferrua, M. J., & Singh, R. P., 2009b. Modeling the forced-air cooling process of fresh strawberry packages, Part II: Experimental validation of the flow model. *International Journal of Refrigeration*, *32*(2), 349-358.

Finn, D. P., & Brennan, S. L., 2003. Sensitivity analysis using CFD of air distribution in transport refrigeration containers. *In Proc. 21st IIR International Congress of Refrigeration,* Washington DC, 17-22 August 2003.

Stellenbosch University https://scholar.sun.ac.za

Fitzgerald, W. B., Howitt, O. J., Smith, I. J., & Hume, A., 2011. Energy use of integral refrigerated containers in maritime transportation. *Energy Policy*, *39*(4), 1885-1896.

Flórez-Orrego, D., Arias, W., López, D., & Velásquez, H., 2012. Experimental and CFD study of a single phase cone-shaped helical coiled heat exchanger: an empirical correlation. In *Proceedings of ECOS 2012-The 25th International Conference on Efficiency, Cost, Optimization, Simulation and Environmental Impact of Energy Systems*, 375-394.

Franke, J., Hellsten, A., Schlünzen, H., Carissimo, B., 2007. Best practice guideline for the CFD simulation of flows in the urban environment. COST Action 732: Quality assurance and improvement of microscale meteorological models, Hamburg, Germany.

Foster, A. M., Barrett, R., James, S. J., & Swain, M. J. 2002. Measurement and prediction of air movement through doorways in refrigerated rooms. *International Journal of Refrigeration*, *25*(8), 1102-1109.

Foster, A.M., Swain, M.J., Barrett, R., D'Agaro, P., Ketteringham, L.P. and James, S.J., 2007. Three-dimensional effects of an air curtain used to restrict cold room infiltration. *Applied Mathematical Modelling*, 31(6),1109-1123.

Gonçalves, J.C., Costa, J.J., Figueiredo, A.R. and Lopes, A.M.G., 2012. CFD modelling of aerodynamic sealing by vertical and horizontal air curtains. *Energy and Buildings*, *52*, 153-160.

Hassanizadeh, M. and Gray, W.G., 1979. General conservation equations for multi-phasesystems: 1. Averaging procedure. *Advances in Water Resources*, *2*, 131-144.

Hertog, M.L.A.T.M., Peppelenbos, H.W., Evelo, R.G. and Tijskens, L.M.M., 1998. A dynamic and generic model of gas exchange of respiring produce: the effects of oxygen, carbon dioxide and temperature. *Postharvest Biology and Technology*, *14*(3), 335-349.

Ho, Q.T., Verboven, P., Verlinden, B.E., Schenk, A. and Nicolai, B.M., 2013. Controlled atmosphere storage may lead to local ATP deficiency in apple. *Postharvest Biology and Technology*, *78*,103-112.

Stellenbosch University https://scholar.sun.ac.za

Hoang, M.L., Verboven, P., De Baerdemaeker, J., Nicolai, B.M., 2000.Analysis of the air flow in a cold store by means of computational fluid dynamics. *International Journal of Refrigeration* 23, 127–140.

Hoang, M. H., Laguerre, O., Moureh, J., & Flick, D., 2012. Heat transfer modelling in a ventilated cavity loaded with food product: Application to a refrigerated vehicle. *Journal of Food Engineering*, *113*(3), 389-398.

Hoang, H. M., Duret, S., Flick, D., & Laguerre, O., 2015. Preliminary study of airflow and heat transfer in a cold room filled with apple pallets: Comparison between two modelling approaches and experimental results. *Applied Thermal Engineering*, *76*, 367-381.

Hui, K. C., Vigneault, C., Sotocinal, S. A., de Castro, L. R., & Raghavan, G. V., 2008. Effects of loading and air bag bracing patterns on correlated relative air distribution inside refrigerated semi-trailers transporting fresh horticultural produce. *Canadian Biosystems Engineering*, *50*(3), 27-35.

ISO 1496-2 Series 1 Freight containers – specification and testing, Part 2:thermal containers, 3rd ed., 1988.

Jedermann, R., Geyer, M., Praeger, U., & Lang, W., 2013. Sea transport of bananas in containers–Parameter identification for a temperature model. *Journal of Food Engineering*, *115*(3), 330-338.

Jedermann, R., Praeger, U., Geyer, M., & Lang, W., 2014. Remote quality monitoring in the banana chain. *Philosophical Transactions of the Royal Society of London A: Mathematical, Physical and Engineering Sciences*, *372*(2017), 20130303.

James, S.J., James, C. and Evans, J.A., 2006. Modelling of food transportation systems–a review. *International Journal of Refrigeration*, *29*(6), 947-957.

James, S.J. and James, C., 2010. The food cold-chain and climate change. *Food Research International*, *43*(7), 1944-1956.

Karimipanah, M. T., 1998. Deflection of wall-jets in ventilated enclosures described by pressure distribution. *Building and Environment*, *34*(3), 329-333.

Stellenbosch University https://scholar.sun.ac.za

Laguerre, O., Aissa, M.B. and Flick, D., 2008. Methodology of temperature prediction in an insulated container equipped with PCM. *International Journal of Refrigeration*, 31(6), 1063-1072.

Laguerre, O., Hoang, M. H., & Flick, D., 2012. Heat transfer modelling in a refrigerated display cabinet: the influence of operating conditions. *Journal of Food Engineering*, *108*(2), 353-364.

Laguerre, O., Hoang, H. M., & Flick, D., 2013. Experimental investigation and modelling in the food cold chain: Thermal and quality evolution. *Trends in Food Science & Technology*, *29*(2), 87-97.

Lisowa, H., Wujec, M., & Lis, T., 2002. Influence of temperature and variety on the thermal properties of apples. *International Agrophysics*, *16*(1), 43-52.

Liu, S. and Masliyah, J.H., 2005. Dispersion in porous media. *Handbook of porous media*, 110.

Lukasse, L.J.S., Baerentz, M.B., Kramer-Cuppen, J.E.D., 2011. Quest II: Reduction of CO_2 emissions of reefer containers, in: 23rd *IIR International Congress of Refrigeration*. Prague, 3203-3210.

McMillan, G.K. and Considine, D.M., 1999. *Process/industrial instruments and controls handbook* (Vol. 7). McGraw Hill.

Maersk, 2014.URL www.mcicontainers.com/Pages/default.aspx, Accessed (11.10.2016)

Ménia Z, N., Moureh, J., & Flick, D., 2002. Modélisation simplifiée des coulements d'air dans un véhicule frigorifique. *International Journal of Refrigeration*, *25*(5), 660-672.

Moureh, J., Menia, N., & Flick, D., 2002. Numerical and experimental study of airflow in a typical refrigerated truck configuration loaded with pallets. *Computers and Electronics in Agriculture*, *34*(1), 25-42.

Moureh, J., & Flick, D., 2004. Airflow pattern and temperature distribution in a typical refrigerated truck configuration loaded with pallets. *International Journal of Refrigeration*, 27(5), 464-474.

Stellenbosch University https://scholar.sun.ac.za

Moureh, J., Tapsoba, S., Derens, E., Flick, D., 2009a. Airflow in a slot-ventilated enclosure partially filled with porous boxes: Part I – measurements and simulations in the clear region. *Computers & Fluids* 38, 194–205.

Moureh, J., Tapsoba, S., Derens, E., Flick, D., 2009b. Airflow in a slot-ventilated enclosure partially filled with porous boxes: Part II – measurements and simulations within porous boxes. *Computers & Fluids* 38, 206–220.

Nakayama, A., & Kuwahara, F., 1999. A macroscopic turbulence model for flow in a porous medium. *Journal of Fluids Engineering*, *121*(2), 427-433.

Ngcobo, M. E., Delele, M. A., Opara, U. L., Zietsman, C. J., & Meyer, C. J., 2012. Resistance to airflow and cooling patterns through multi-scale packaging of table grapes. *International Journal of Refrigeration*, *35*(2), 445-452.

Nield, D.A. and Bejan, A., 2006. Convection in porous media. Springer Science & Business Media.

Norton, T. and Sun, D.W., 2006. Computational fluid dynamics (CFD)–an effective and efficient design and analysis tool for the food industry: a review. *Trends in Food Science & Technology*, *17*(11), .600-620.

Opara, U. L., 2011. *From hand holes to vent holes: what's next in innovative horticultural packaging? (Inaugural Lecture, Faculty of AfriSciences*), South Africa: Stellenbosch University, 1-24.

Pathare, P. B., Opara, U. L., Vigneault, C., Delele, M. A., & Al-Said, F. A. J., 2012. Design of packaging vents for cooling fresh horticultural produce. *Food and Bioprocess Technology*, *5*(6), 2031-2045.

Paul, D., 2001. Low-voltage power system surge overvoltage protection. *IEEE Transactions on Industry Applications*, *37*(1), 223-229.

Quintard, M. and Whitaker, S., 2005. Coupled, nonlinear mass transfer and heterogeneous reaction in porous media. In: Kambiz, Vafai (Ed.). *Handbook of porous media*, Taylor & Francis Group, LLC, 3-37, second ed.

Redding, G.P., Yang, A., Shim, Y.M., Olatunji, J. and East, A., 2016. A review of the use and design of produce simulators for horticultural forced-air cooling studies. *Journal of Food Engineering*, 190, 80-93.

Stellenbosch University https://scholar.sun.ac.za

Roache, P. J., 1994. Perspective: a method for uniform reporting of grid refinement studies. *Journal of Fluids Engineering*, *116*(3), 405-413.

South African Department of Agriculture, Forestry and Fishery annual report, 2014

Singh, J., Olsen, E., Singh, S.P., Manley, J. and Wallace, F., 2008. The effect of ventilation and hand holes on loss of compression strength in corrugated boxes. *Journal of Applied Packaging Research*, *2*(4), 227-238.

Rodríguez-Bermejo, J., Barreiro, P., Robla, J. I., & Ruiz-García, L., 2007. Thermal study of a transport container. *Journal of Food Engineering*, *80*(2), 517-527.

Smale, N. J., 2004. Mathematical modelling of airflow in shipping systems: model development and testing. PhD thesis. *Massey University, Palmerston North, New Zealand*.

Smale, N.J., Moureh, J. and Cortella, G., 2006. A review of numerical models of airflow in refrigerated food applications. *International Journal of Refrigeration*, *29*(6), 911-930.

Tanner, D. J., Cleland, A. C., Opara, L. U., & Robertson, T. R., 2002a. A generalised mathematical modelling methodology for design of horticultural food packages exposed to refrigerated conditions: Part 1, Formulation. *International Journal of Refrigeration*, *25*(1), 33-42.

Tanner, D. J., Cleland, A. C., & Opara, L. U., 2002b. A generalised mathematical modelling methodology for the design of horticultural food packages exposed to refrigerated conditions Part 2. Heat transfer modelling and testing. *International Journal of Refrigeration, 25*(1), 43-53.

Tanner, D. J., & Amos, N. D., 2003. Heat and mass transfer -temperature variability during shipment of fresh produce. Acta Horticulturae 599, 193–204.

Tapsoba, M., Moureh, J. and Flick, D., 2006. Airflow patterns in an enclosure loaded with slotted pallets. International Journal of Refrigeration, 29(6), 899-910.

Stellenbosch University https://scholar.sun.ac.za

Tapsoba, M., Moureh, J., & Flick, D., 2007. Airflow patterns in a slot-ventilated enclosure partially loaded with empty slotted boxes. *International Journal of Heat and Fluid Flow*, *28*(5), 963-977.

Tassou, S.A., De-Lille, G. and Ge, Y.T., 2009. Food transport refrigeration–Approaches to reduce energy consumption and environmental impacts of road transport. *Applied Thermal Engineering*, *29*(8), 1467-1477.

Thompson, J.F., Mejia, D.C. and Singh, R.P., 2010. Energy use of commercial forced-air coolers for fruit. *Applied Engineering in Agriculture*, *26*(5), 919-924.

Verboven, P., Hoang, M.L., Baelmans, M., and B.M. Nicolai., 2004. Airflow through beds of apples and chicory roots. *Biosystems Engineering* 88: 117–125.

Verboven, P., Flick, D., Nicolai, B.M., Alvarez, G., 2006. Modelling transport phenomena in refrigerated food bulks, packages and stacks: basics and advances. *International Journal of Refrigeration*, 29 (6), 985–997.

Versteeg, H.K. and Malalasekera, W., 2007. An introduction to computational fluid dynamics: the finite volume method, second ed., Pearson Education, New York.

Van der Sman, R. G. M., 2002. Prediction of airflow through a vented box by the Darcy–Forchheimer equation. *Journal of Food Engineering*, *55*(1), 49-57.

Vigneault, C., Thompson, J., Wu, S., Hui, K. P. C., & LeBlanc, D. L., 2009. Transportation of fresh horticultural produce. In N. Benkeblia (Ed.), *Postharvest Technologies for Horticultural Crops* (2), 1–24, Kerale, India: Research Signpost

Wang, H. and Touber, S., 1990. Distributed dynamic modelling of a refrigerated room. *International Journal of Refrigeration*, *13*(4), 214-222.

Wang, D. G., & Muller, P. K., 2000. Improving cooling efficiency by increasing fan power usage. *Microelectronics Journal,* 31(9-10), 765–771

Wild, Y., Kraus, A.N.D.R.E.A.S. and Horn, R., 1999. Transport of refrigerated containers in cargo holds. In *Proceedings of the 20th International Congress of Refrigeration, Sydney, Australia*.

Stellenbosch University https://scholar.sun.ac.za

Wild, Y., 2008. Proceedings of the Carbon Footprint Workshop. Environmental aspects of the transport of reefer containers, 3rd Reefer Logistic Conference. Antwerp, 26 June.

Xia, B., & Sun, D. W., 2002. Applications of computational fluid dynamics (CFD) in the food industry: a review. Computers and electronics in agriculture, 34(1), 5-24.

Xie, J., Qu, X. H., Shi, J. Y., & Sun, D. W., 2006. Effects of design parameters on flow and temperature fields of a cold store by CFD simulation. *Journal of Food Engineering*, *77*(2), 355-363.

Yu, H., & Hoff, S. J., 1999. Airflow pattern similarity criteria for ceiling slot-ventilated agricultural enclosures under isothermal conditions. *Transactions of the ASAE*, 42(2), 459.

Zhang, Z., Zhang, W., Zhai, Z. J., & Chen, Q. Y., 2007a. Evaluation of various turbulence models in predicting airflow and turbulence in enclosed environments by CFD: Part 1—Summary of prevalent turbulence models. *Hvac&R Research*, *13*(6), 853-870.

Zhang, Z., Zhang, W., Zhai, Z. J., & Chen, Q. Y., 2007b. Evaluation of various turbulence models in predicting airflow and turbulence in enclosed environments by CFD: Part 2—Comparison with experimental data from literature. *HVAC&R Research*, *13*(6), 871-886.

Zhao, F.Y., Liu, D. and Tang, G.F., 2008. Multiple steady fluid flows in a slot-ventilated enclosure. *International Journal of Heat and Fluid Flow*, *29*(5), 1295-1308.

Zhao, C.J., Han, J.W., Yang, X.T., Qian, J.P. and Fan, B.L., 2016. A review of computational fluid dynamics for forced-air cooling process. *Applied Energy*, *168*, 314-331.

Zou, Q.,Opara, L.U.,& McKibbin, R., 2006a. A CFD modelling system for airflow and heat transfer in ventilated packaging for fresh foods I: initial analysis and development of mathematical models. *Journal of Food Engineering*, 77(4), 1037–1047.

Stellenbosch University https://scholar.sun.ac.za

Zou, Q.,Opara, L.U.,& McKibbin, R., 2006b.A CFD modelling system for airflow and heat transfer in ventilated packaging for fresh foods II: computational solution, software development and model testing. *Journal of Food Engineering*, 77(4), 1048–1058.